

Laboratory Study and Numerical Modeling of Cement Stabilized Aalborg Gyttja

Master Thesis 30 ECTS

Martin Tanderup

Aalborg University

Structural and Civil Engineering

4th semester



**AALBORG
UNIVERSITY**

STUDENT REPORT

**THE FACULTY OF ENGINEERING AND
SCIENCE**

Study Board of the Built Environment

Thomas Manns Vej 23

9220 Aalborg East

<https://www.build.aau.dk/>

Title:

Laboratory Study and Numerical Modeling of Cement Stabilized Aalborg Gyttja

Project period:

From 01-02-2023 until 09-06-2023

Project type:

Master Thesis 30 ECTS

Author:

Martin Tanderup

Supervisor:

Lars Bo Ibsen

Number of pages: 209

Date of completion: 09-06-2023

Synopsis:

This thesis investigates the mechanical and physical effects of cement stabilizing Aalborg gyttja with respectively 150 kg/m³ and 30 kg/m³ FutureCem cement.

To investigate the effects of adding FutureCem cement to Aalborg gyttja several triaxial, bender element, and oedometer tests are performed on laboratory cast gyttja-cement specimens to quantify the strength and stiffness gain.

Based on the laboratory tests, soils in PLAXIS 2D are calibrated using the built-in SoilTest module. The numerical results are compared to the current analytical method. It is found that the analytical method estimates the settlement quite accurately in the drained case when using large amounts of cement. However, when using small amounts of cement the analytical methods significantly overestimate the settlements.

It is concluded that using small amounts of binder can be very beneficial for lowering the CO₂ emission when performing cement stabilization. However, the sensitivity of the stiffness of the stabilized columns increases. Hence, if small amounts of the binder are to be used to decrease the CO₂ emission, numerical modeling is necessary and the field installation can not deviate too much from the laboratory tests.

Preface

This 30 ECTS master thesis is written during the 4th semester of the M.Sc. Structural and Civil Engineering program at Aalborg University and conducted between February and June 2023.

The report is written under the supervision of Professor Lars Bo Ibsen, to whom a big thanks should be made. Furthermore, the project could not have been conducted without the facilities and equipment provided by Aalborg University as well as the laboratory assistance provided. Lastly, thanks should be made to my colleagues at COWI for sparring.

The thesis is a continuation of an internship at COWI during the 3rd semester of the M.Sc. Structural and Civil Engineering program (autumn 2022). During the internship, the sustainability (specifically CO₂ emission) of cement stabilization was investigated and compared to other Danish foundation methods by using analytical methods. The internship report is referred to as Tanderup [2022] and can be issued upon request with permission from COWI.

The thesis includes an advanced laboratory study covering various triaxial tests, oedometer tests, and bender element tests. Laboratory reports for each test can be found in Appendix E, F, or G. The laboratory tests solely used in the discussion in chapter 6 are not included in the Appendix. However, these can be issued upon request as well.

Aalborg Portland is acknowledged for supplying FutureCem cement used for testing.

The thesis should be printed in colors in order to obtain the correct understanding.

All dates are specified as DD-MM-YYY.

Contents

1	Introduction to soil stabilization	1
1.1	Untreated soil used	2
1.2	Binders used	3
1.3	Sustainability of cement stabilization	5
1.4	Usage of cement stabilization in Denmark	10
2	Scope of the thesis	11
2.1	Motivation	11
2.2	Objectives	12
2.3	Methodology	12
3	State-of-the-art review	15
3.1	Primary literature	15
3.2	Cementation effects	15
3.3	Casting in the laboratory	20
3.4	Strength and stiffness gain	22
3.5	Numerical modeling	23
4	Laboratory study	25
4.1	Casting and test methodology	25
4.2	Evaluation of standard triaxial tests	32
4.2.1	Specimens curing at 20 °C	32
4.2.2	Specimens curing at 8 °C	37
4.3	Evaluation of bender element tests	39
4.4	Evaluation of cyclic triaxial tests	41
4.5	Evaluation of oedometer tests	43
4.6	Evaluation of plasticity and pH changes	46
5	Numerical modeling	51
5.1	Scenarios investigated	51
5.2	Calibration of soil models	54
5.2.1	Calibration of undrained soils	55
5.2.2	Calibration of drained soils	57

5.3	Typical analytical procedure	58
5.3.1	Comparison between analytical and numerical model	60
5.4	Untreated scenario	62
5.4.1	Undrained case	62
5.4.2	Drained case	63
5.5	Cement stabilized base scenario	64
5.5.1	Effects of edge reinforcement	70
5.5.2	Effects of geonet reinforcement	72
5.5.3	Sensitivity of column and pavement stiffness	74
5.5.4	Sensitivity of surcharge load	76
6	Discussion	81
6.1	Triaxial test dimensions	81
6.2	Small versus large amounts of binder	83
6.3	The use of numerical models versus analytical	85
6.4	Sustainability evaluation	89
6.5	Further research	91
6.5.1	Laboratory correlations to the field	91
6.5.2	Curing periods beyond 28 days	91
6.5.3	Numerical modeling in 3D	92
6.5.4	Other types of soil	92
7	Conclusion	93
A	Boring profile for batch 1 gyttja	95
B	Life Cycle Assessments	97
B.1	Mass exchange	97
B.2	Piled foundation	98
B.3	Cement stabilization	99
C	Laboratory theory	101
C.1	Standard triaxial tests	101
C.2	Cyclic triaxial tests	104
C.3	Bender element tests	106
C.4	Oedometer tests	108
D	PLAXIS models	111
D.1	Material models investigated	111

D.2	Staged construction of PLAXIS models	113
D.3	Convergence analysis	115
D.4	Soil parameters used	116
D.5	Structure parameters used	119
E	In-situ experiments	121
E.1	Triaxial01: CU test depth 5.5-5.5 m	121
E.2	Triaxial02: CD test depth 1.5-2.0 m	123
E.3	Oedometer01: Depth 3.0-3.5 m	125
E.4	BenderElement01: Depth 3.0-3.5 m	129
F	Cement specimens 30 kg/m³	131
F.1	Triaxial03: CU test curing for 7 days at 20 °C	131
F.2	Triaxial04: CU test curing for 14 days at 20 °C	133
F.3	Triaxial05: CU test curing for 21 days at 20 °C	135
F.4	Triaxial06: CU test curing for 28 days at 20 °C	137
F.5	Triaxial07: CU test curing for 25 days at 8 °C	139
F.6	Triaxial08: CU test curing for 54 days at 8 °C	141
F.7	Triaxial09: CU test curing for 83 days at 8 °C	143
F.8	Triaxial10: CD test curing for 7 days at 20 °C	145
F.9	Triaxial11: CD test curing for 14 days at 20 °C	148
F.10	Triaxial12: CD test curing for 28 days at 20 °C	151
F.11	Triaxial13: Cyclic test curing for 28 days at 20 °C	154
F.12	Oedometer02: Curing for 28 days at 20 °C (Swell log)	157
F.13	BenderElement02: Curing for 28 days at 20 °C (V _s log)	163
G	Cement specimens 150 kg/m³	169
G.1	Triaxial14: CU test curing for 7 days at 20 °C	169
G.2	Triaxial15: CU test curing for 14 days at 20 °C	171
G.3	Triaxial16: CU test curing for 21 days at 20 °C	173
G.4	Triaxial17: CU test curing for 28 days at 20 °C	175
G.5	Triaxial18: CD test curing for 7 days at 20 °C	177
G.6	Triaxial19: CD test curing for 14 days at 20 °C	180
G.7	Triaxial20: CD test curing for 28 days at 20 °C	183
G.8	Triaxial21: Cyclic curing for 28 days at 20 °C	186
G.9	Oedometer03: Curing for 28 days at 20 °C (Swell log)	189
G.10	BenderElement03: Curing for 28 days at 20 °C (V _s log)	199

Bibliography

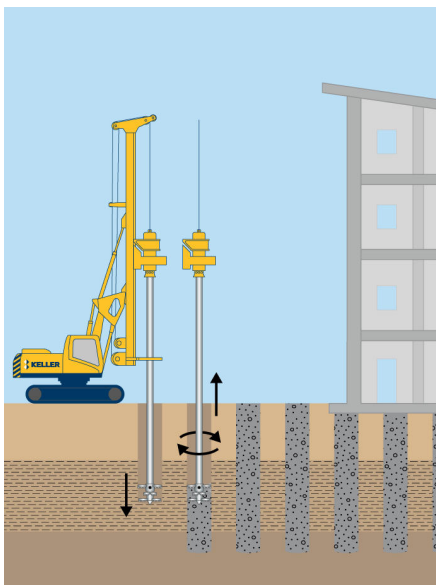
205

Introduction to soil stabilization

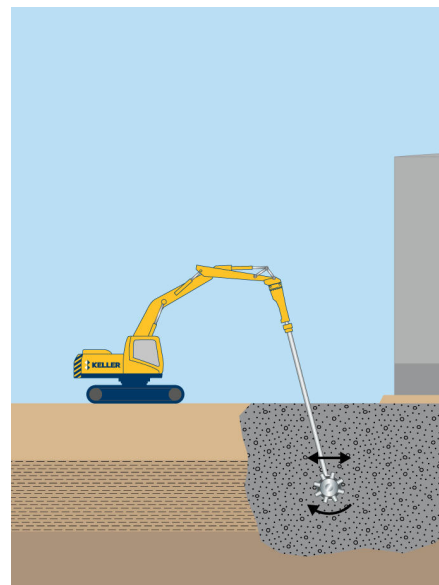
1

Deep soil mixing is a foundation technique used for decades in multiple Scandinavian countries to stabilize soft soils to improve strength and stiffness parameters. The technique usually involves the mechanical mixing of a dry binder (e.g. cement or quick lime) into the soft soil, where the binder reacts with the pore water and binds the soil particles together in a hydration process.

The equipment used to perform deep soil mixing is shown in Figure 1.1a. The equipment stabilizes the soil by constructing columns with a diameter of 0.6-1.0 m to a depth of a maximum of 25 m, to stabilize a ratio of the poor soft soil [Keller, 2018]. If the soils are especially poor and the equipment cant be placed on top of the soft soil, the equipment in Figure 1.1b can be used for shallow soft soil deposits. However, it is not as common to use this equipment.



(a) Deep Soil Mixing (DSM) [Keller, 2023a].



(b) Mass Soil Mixing (MSM) [Keller, 2023b].

Figure 1.1. Equipment used to perform soil stabilization.

The deep soil mixing method in Figure 1.1a is performed by driving a rod with a mixing tool into the ground. From the surface, until the design depth is reached the

soil is sheared to a remolded state, to prepare the meddling of the binder. When the mixing tool is withdrawn binder is expelled through the mixing tool. The radial paddles on the mixing tool are ensuring a satisfying mixture based on the specified amount of rotations and binder as well as the withdrawal speed.

The pattern of the columns installed by deep mixing techniques can vary depending on the given problem. Figure 1.2 highlights the most common installation patterns. Roads can e.g. be stabilized with either the grid, disc, or block pattern. Other uses of soil stabilization could be the stabilization of slopes, fillings, construction pits, or vibration damping from e.g. railways [Norwegian Geotechnical Society, 2012].

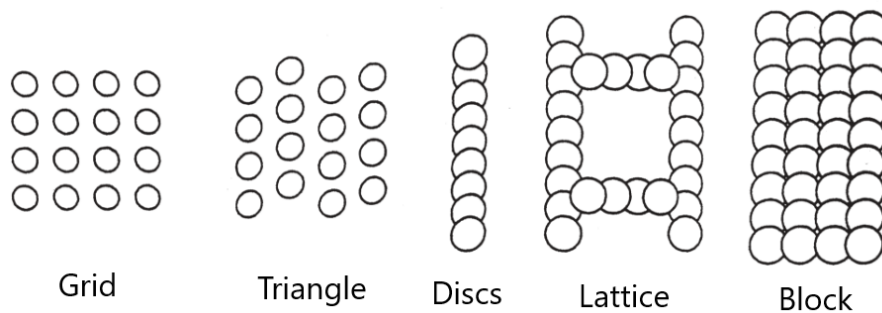


Figure 1.2. Deep Soil Mixing installation patterns [Larsson, 2006]*.

1.1 Untreated soil used

This thesis seeks to investigate the effect of adding small and large amounts of binder to Aalborg gyttja. The untreated soil is collected from two sites approximately 150 m apart. The coordinates for each soil batch collected are seen in Table 1.1. Batch 1 was collected during a geotechnical boring. The boring profile can be found in Appendix A. Batch 2 was collected by a manual hand boring in a depth of 3-5 m.

Table 1.1. UTM-32 coordinates for gyttja batches collected.

UTM-32 coordinates	Batch 1	Batch 2	Unit
X:	563057	563198	m
Y:	6322514	6322332	m

The soil parameters for the two batches collected are seen in Table 1.2. It is seen that batch 2 has a higher water content and exceeds the liquid limit, hence having a softer consistency in-situ. Batch 2 was also collected in a more marshy area, where the water table exceeded the ground level slightly. Batch 1 was collected in an area

where the groundwater table was 1-2 m below the surface. Intact specimens collected from the geotechnical boring were subjected to in-situ triaxial and oedometer tests to determine the strength and stiffness parameters. The unit weight for batch 1 and batch 2 is assumed similar in this thesis.

Table 1.2. Comparison between two soil batches collected.

Parameter	Batch 1	Batch 2	Unit
Water content	65.2	102.5	%
Organic content	6.3	7.4	%
Liquid Limit	72.1	93.9	%
Plastic Limit	29.9	31.0	%
Plasticity Index	42.2	71.5	%
pH	8.3	8.8	%
Unit weight	15.8	-	kN/m ³
Undrained shear strength	19.2	-	kPa
Friction angle	24.7	-	°
Oedometer modulus (80-160 kPa)	1.132	-	kPa
Hydraulic conductivity	1E-10	-	m/s

The particle size distribution for the two soil batches is seen in Figure 1.3. It is seen that batch two consists of a higher ratio of fines.

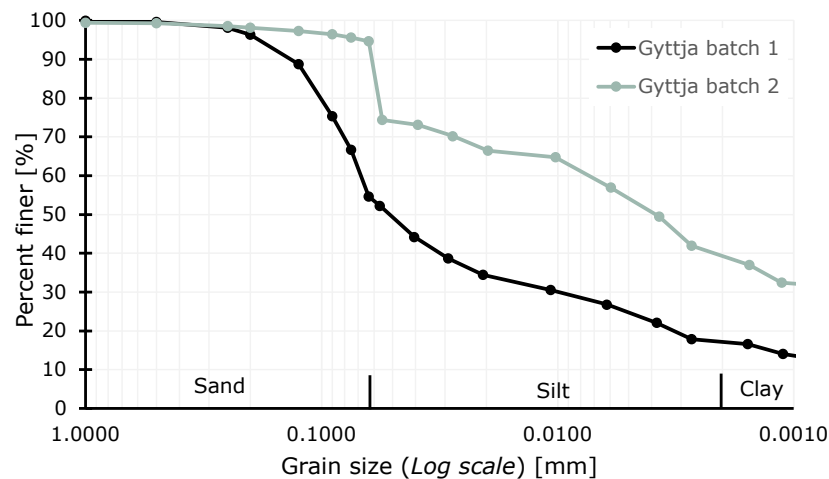


Figure 1.3. Comparison of the particle size distribution for two soil batches collected.

1.2 Binders used

The most common binders used for deep soil mixing are cement, quick lime, or a combination of both. The choice of binder can depend on several factors such

as project location, economy, and necessary strength/stiffness increase. Quick lime is usually not used as a stand-alone binder for deep mixing, due to the low strength increase. For this thesis, cement will be used as a stand-alone binder. The stabilization procedure will therefore be referred to as cement stabilization. In Åhnberg [2006] cement alone generally resulted in the lowest dispersion in undrained shear strength and had the most rapid early strength gain, compared to a mixture of cement and quick lime. However, in one case cement and quick lime resulted in a higher long-term strength (beyond 3 months). Another reason for choosing cement as a stand-alone binder is the emission during manufacturing compared to quick lime. Based on Environmental Product Declarations (EPDs) from manufacturers, the emission from cement is generally lower than for quick lime, as shown in Figure 1.4 [Aalborg Portland, 2023a] [Aalborg Portland, 2019] [Boral, 2022].

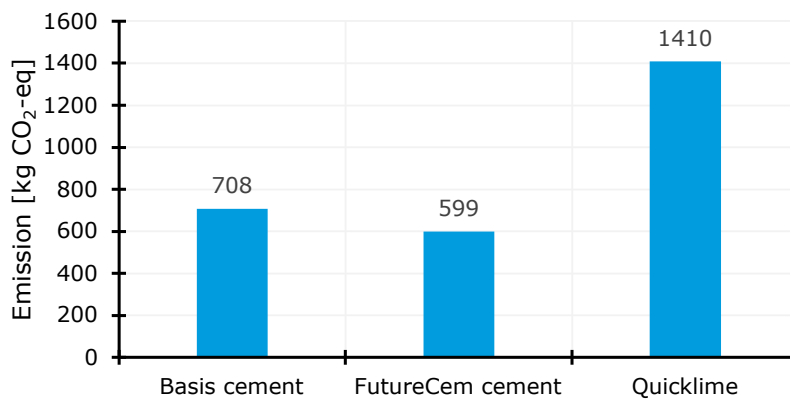


Figure 1.4. Emission during the production stage for 1.000 kg binder.

Based on the emission shown in Figure 1.4, the binder is set to be the recently launched CO₂ reduced FutureCem cement from Aalborg Portland. This cement is a composite cement of type CEM II/B-M (Q-LL) 52,5N (LA) with a CO₂ reduction of $\approx 15\%$ compared to their Basis cement. The reduction is based on the substitution of cement clinker with lime filler [Aalborg Portland, 2020]. The FutureCem product is seen in Figure 1.5.



Figure 1.5. FutureCem cement [Aalborg Portland, 2023b].

This thesis seeks to investigate the influence of using small and large amounts of binder on Danish Aalborg gyttja. The cement amounts used during this investigation are 150 kg/m³ and 30 kg/m³ FutureCem cement. The amount of binder used is occasionally informed in relation to the percentage-wise amount added according to Equation (1.1) [Al-Jabban, 2019].

$$A_w = \frac{m_b}{m_s} \quad (1.1)$$

A_w	Amount of additive [%]
m_b	Mass of binder [kg/m ³]
m_s	Mass of dry soil [kg/m ³]

The amount of cement added to the untreated gyttja based on Equation (1.1) is specified below. All specimens with 150 kg/m³ were cast with gyttja from batch 2. However, the specimens with 30 kg/m³ were cast with gyttja from both batches. All specimens except for the CD triaxial tests were cast with gyttja from batch 1, hence consisting of 3.1 % cement.

Cement percentage for 150 kg/m ³ specimens:	19.2 %
Cement percentage for 30 kg/m ³ specimens:	3.1-3.8 %

1.3 Sustainability of cement stabilization

In 2015 the United Nations adopted 17 Sustainable Development Goals (SDGs) as a call to action to end some of the greatest problems worldwide [United Nations Development Programme, 2023]. SDG 13 seeks to call to action on the current climate crisis. According to United Nations [2022] the CO₂ emission need to peak before 2025 to limit warming below 1.5 °C below pre-industrial levels. Furthermore, the emission must then decline 43 % by 2030 and reach net zero by 2050. The construction industry therefore also needs to lower the CO₂ emission to reach this goal. This can be done by performing Life Cycle Assessments (LCAs) to assess the emission of different foundation options. The emission should therefore also be in focus when developing/considering new foundation options.

When performing LCAs multiple stages in a structure or foundation's lifetime can be considered. These stages are shown in Figure 1.6 according to EN standards. Considering these stages when choosing a foundation can optimize the decision-making process since the emission from each possibility can be quantified.

Product Stage			Construction Process Stage		Use Stage							End-of-Life Stage				Benefits and loads beyond the system boundary		
Raw material supply	Transport	Manufacturing	Transport to building site	Installation into building	Use/application	Maintenance	Repair	Replacement	Refurbishment	Operational energy use	Operational water use	Deconstruction/demolition	Transport	Waste processing	Disposal	Reuse	Recovery	Recycling
A1	A2	A3	A4	A5	B1	B2	B3	B4	B5	B6	B7	C1	C2	C3	C4	D	D	D

Figure 1.6. Life Cycle Assessment stages [Castro et al., 2019] [The European Committee For Standardization, 2012].

In the following, the CO₂ emission from cement stabilization is compared to traditional Danish foundation options to evaluate the sustainability of DSM. The calculation method and assumptions can be found in Appendix B.

Cement stabilization compared to mass exchange

Mass exchange of poor soft soil with engineered fill/sand is a common foundation method used. Mass exchange is compared to a cement-stabilized grid and block pattern according to Figure 1.2. The coverage/stabilized ratio is determined according to Equation (1.2) for a grid pattern [Larsson, 2006].

$$a = \frac{A}{c^2} \quad (1.2)$$

A | Area of stabilized column with $d = 0.6$ m [m²]
 c | Center-to-center distance of the stabilized columns [m]

The grid and block pattern used to evaluate the CO₂ emission is shown in Figure 1.7. The first illustration in Figure 1.7 (a) represents a complete exchange of the soft gyttja with engineered fill. The other two illustrations (b) (c) represent the cement stabilized columns installed in the gyttja with respectively a center-to-center (C-C) distance of 1.00 m and 0.55 m.

The CO₂ emission from cement stabilization versus mass exchange for 1 m³ is compared in Figure 1.8. It is seen that a mass exchange is very sensitive to the transport distance since the curve is quite steep. This is due to transportation accounting for more than 90% of the emission for the mass exchange solution. Furthermore, it is seen that 3/4 of the cement stabilization solutions have a lower emission than mass exchange beyond a transport distance of 50 km. Based on a

preliminary study of cement stabilization in Tanderup [2022] all cement-stabilized solutions are expected to be viable options for this instance.

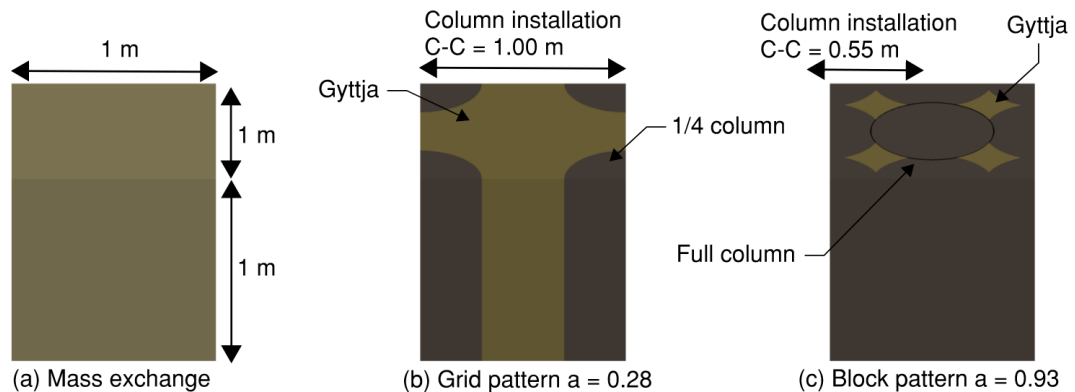


Figure 1.7. Principle illustration of mass exchange (a) and cement stabilized patterns (b)(c) used in the CO₂ emission comparison for 1 m³.

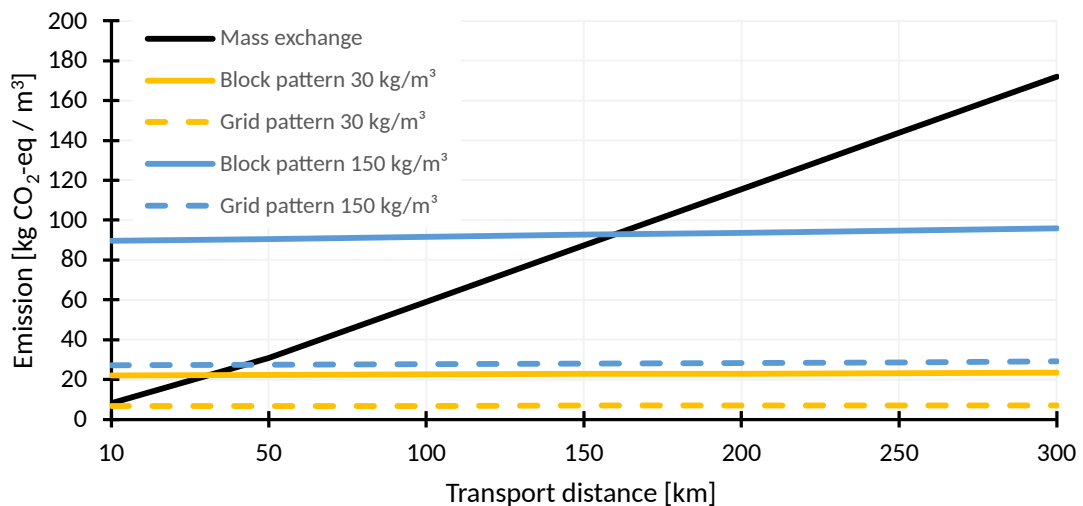


Figure 1.8. Emission from cement stabilization in a block pattern with $a = 0.93$ and grid pattern with $a = 0.28$ compared to a mass exchange for 1 m³ gyttja.

Another upside of using cement stabilization compared to a mass exchange is the reduced need for natural sand and gravel resources which are in shortage. This is due to a huge worldwide demand for these materials. According to Torres et al. [2017] sand and gravel are the most extracted group of materials worldwide, exceeding fossil fuels and biomass. According to Larsen et al. [2019] Denmark will also run out of sand gravel at some point. From 2016 until 2040 the usage of these materials is expected to increase by 64 %, whereas the usage will exceed the materials that are recovered from land by 9 million m³ [Larsen et al., 2019]. When exactly Denmark

will run out of these resources will depend greatly on national resource strategies and alternatives for the current and upcoming uses.

Cement stabilization compared to piled foundation

Deep-embedded reinforced concrete piles are another traditional solution when encountering soft soils. Cement stabilization is also expected to be a suitable replacement for these. However, the assessment of the emission is more complicated, since the center-to-center distance of both subjects as well as actions used to prevent arch effects are highly important. Arch effects are expected to be a potential issue for both solutions since the gap between the columns or piles is prone to deflect due to the stiffness of the upper structure (e.g. a pavement structure).

The cement stabilized column and the reinforced concrete pile used to evaluate the difference in emission are seen in Figure 1.9. In the CO₂ emission calculations no actions to prevent arch effects are included. Furthermore, actions to prevent the drag-down of the piles (bitumen cover in the upper part) are not included. This is usually incorporated into the pile design for soft soil areas.

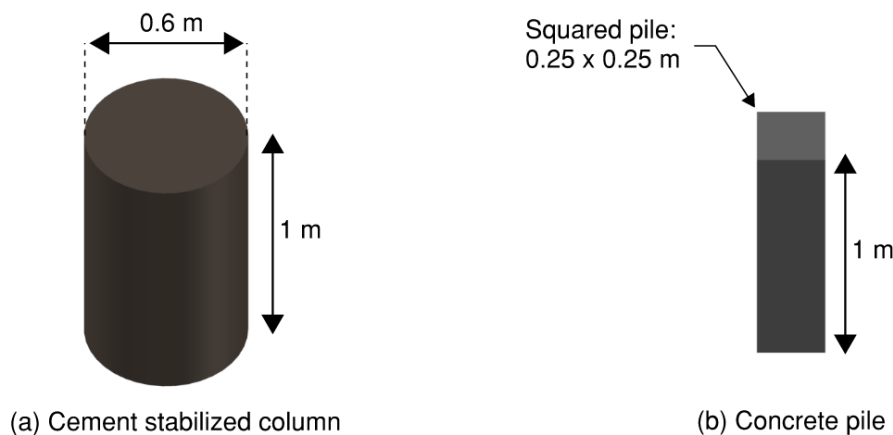


Figure 1.9. Illustration of cement stabilized column and reinforced concrete pile.

The emission from deep-embedded concrete piles is compared to cement-stabilized columns in Figure 1.10. The subjects are compared for 1 m versus 1 m for the sake of direct comparison. However, the piles are also compared as being 2.5 times longer, since this won't be unrealistic in Holocene deposits due to drag-down effects, hence a significant bearing capacity reduction. This will naturally depend on the soil deposits below the gyttja deposit as well. It is seen that both cement contents potentially can be a sustainable alternative to concrete piles in terms of

CO₂ emission. The reason for the 30 kg/m³ mixture only yielding $\approx 1/3$ of the CO₂ emission of the 150 kg/m³ is due to the highly emissive installation method.

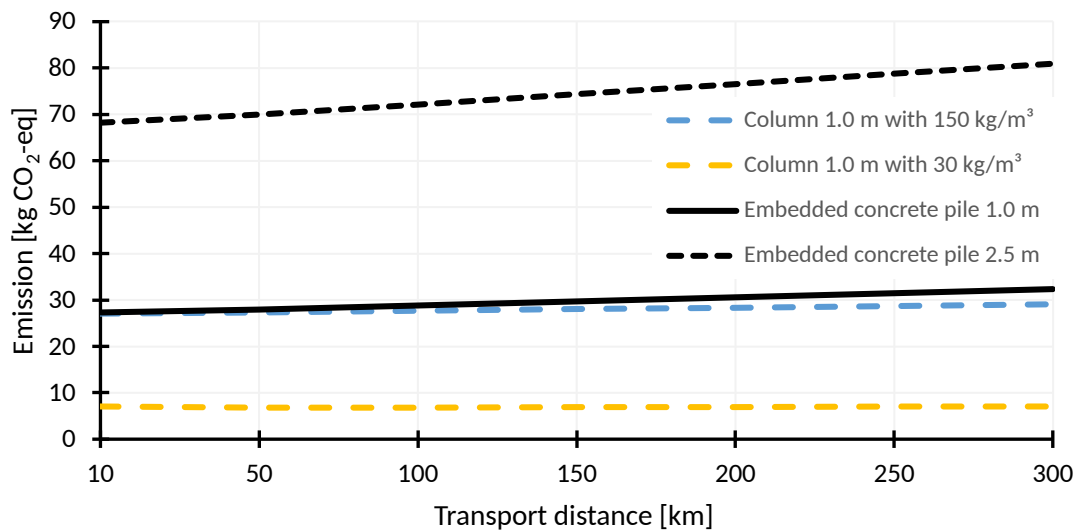


Figure 1.10. Emission of cement stabilization column compared to deep embedded concrete pile for a soft soil deposit of 1 m.

A further upside of using cement stabilized columns compared to reinforced concrete piles is the installation time. Based on the information used in Appendix B the cement stabilized columns are significantly faster to install compared to the piles.

Evaluation of sustainability of cement stabilization

Based on the calculated CO₂ emissions above cement stabilization can potentially be a sustainable alternative to mass exchanges and piled foundations. However, this is very dependent on the strength and stiffness gain of the cement stabilized columns. This thesis seeks to quantify the strength and stiffness gain for gyttja mixed with 150 kg/m³ and 30 kg/m³ FutureCem cement.

In the future cement stabilization can be even less CO₂ emissive if actions are taken. This could for instance be by incorporating carbon capture into the manufacturing process or reducing the highly emissive installation procedure. Some of the cement stabilized solutions revealed that the installation emission accounted for up to 32% of the total emission.

1.4 Usage of cement stabilization in Denmark

As of now, cement stabilization is not a common geotechnical method used in Denmark. However, few projects have been carried out using this technique.

The first project carried out in Denmark using cement stabilization was around 2011. In this project sludge deposits in Kolding Harbour were reinforced by stabilizing the surrounding soil using cement stabilized columns [COWI, 2011].

The next project using cement stabilization was carried out between 2013 and 2016. In this project, cement stabilization was used to stabilize soft soil in a marsh. This was deemed necessary to set up an excavation pit used for casting a concrete foundation for a highway bridge [Arkil, 2023].

Besides these two examples, cement stabilization does not appear to have been used.

Scope of the thesis 2

This chapter presents the objectives of this thesis, along with the methodology used to investigate them. This chapter is followed by a state-of-the-art review of cement stabilization and its effects.

2.1 Motivation

The motivation behind this thesis is the increasing focus on sustainability in the geotechnical society. Based on the sustainability evaluation in chapter 1 it was evident that cement stabilization could be significantly less CO₂ emissive compared to a mass exchange or a piled foundation.

To emphasize the potential of this foundation technique tests on different types of soil need to be carried out. Generally, the literature does not present lots of testing on gyttja compared to different clay types. However, in Denmark, gyttja is one of the most challenging soil deposits to handle during a foundation design. This is generally also a challenging deposit to stabilize with binders since the organics can lead to a significant strength reduction [Al-Jabban, 2019].

The reason for testing two amounts of binder (30 kg/m³ and 150 kg/m³) is to quantify the effects of using a high and low cement content. Recommendations for stabilizing very soft generally recommend a significant cement amount. But is a high cement content really necessary or is it redundant? And could it be more beneficial to reduce the cement amount and increase the stabilization ratio instead?

According to [Al-Jabban, 2019] only a limited number of studies have covered the effect of using below 7% binder. Using 30 kg/m³ FutureCem is, therefore, a highly interesting area to investigate. Especially considering this mixture could reduce the environmental footprint and construction costs significantly.

2.2 Objectives

This thesis will focus on answering and investigating the following three objectives:

- "What is the effect of adding FutureCem cement to gyttja and how do the two gyttja-cement mixtures (30 kg/m^3 and 150 kg/m^3) manage in relation to one other?"
- "What is the effect of using PLAXIS 2D to evaluate cement stabilization compared to analytical methods and does the usage of advanced soil models, based on advanced laboratory tests, yield value to a design?"
- "Is it beneficial to use low cement contents compared to high cement contents, in terms of CO_2 emission?"

2.3 Methodology

Firstly a state-of-the-art review of the current literature is conducted. This is performed to evaluate the current knowledge of cement stabilization. This involves a review of the general cementation effects and the laboratory methods used to cast the cement-stabilized specimens as well as models used to assess the strength gain.

After the state-of-the-art review, the laboratory study is presented. This involves a description of the tests performed and their results. To assess the effects of cement stabilizing Aalborg gyttja, multiple advanced laboratory tests are conducted. Consolidated undrained and drained triaxial tests are performed to monitor the development of undrained and drained strength based on the curing period. This also yields the development in undrained and drained stiffness parameters.

Cyclic triaxial tests are combined with bender element tests to evaluate the increase in small strain stiffness and the cyclic degradation of the shear modulus. Furthermore, oedometer tests are performed to evaluate the change in quasi-pre-consolidation stress and oedometer modulus at different load steps. The oedometer tests are compared to the drained triaxial tests to assess the validity of using oedometer tests for cement stabilized soils. The two cement contents are compared to one another and their behavior is discussed.

After the laboratory study, the numerical study is presented. This involves a comparison of the current analytical methods used to assess the serviceability and ultimate limit state of cement stabilization compared to a numerical PLAXIS 2D

model designed to reflect the analytical conditions. The numerical study investigates the Linear Elastic, Mohr-Coulomb, Hardening Soil, and Hardening Soil with Small Strains material models. The soils will be calibrated with the material models based on the laboratory tests performed.

The numerical study in PLAXIS 2D also covers an investigation of different effects when cement stabilizing e.g. the effects of different center-to-center distances, the use of geotextile, and the effects of using calibrated soil with a good fit compared to a lesser good fit. Sensitivity analyses are also carried out to evaluate the effects of reaching a higher or lower stiffness than expected in the field. All of the investigations are carried out or evaluated in the undrained and drained cases.

After the numerical study, a discussion is carried out. The discussion evaluates the findings in the thesis with emphasis on the objectives stated in section 2.1. An evaluation of the methods used and their plausibility is also carried out. Furthermore, further research on cement stabilization is discussed.

Finally, a conclusion of the thesis is presented.

This chapter presents a state-of-the-art review of the literature on cement stabilization. The review is performed to obtain general knowledge about the cementitious processes taking place and the effects observed based on the curing period. Furthermore, the procedure used to cast the gyttja-cement specimens will be presented.

3.1 Primary literature

The primary literature used during the literature review is stated in Table 3.1. These articles are used to assess the effects observed when adding different amounts and types of binder into soft soils. Furthermore, a recently published method on how the cast soil stabilized specimens for laboratory purposes.

Table 3.1. Primary literature used in the state-of-the-art review.

Source	Description
[Al-Jabban, 2019]	Swedish PhD thesis investigating modifications in stabilized soils based on different binders. The thesis includes a review of the effects observed in stabilized soils over the last decades.
[Åhnberg, 2006]	Swedish PhD thesis investigating the strengths of stabilized clays and organic soils by uniaxial and triaxial tests.
[Helle et al., 2021]	Norwegian article describing a new laboratory procedure used to cast stabilized soil specimens.

3.2 Cementation effects

Cement stabilization utilizes chemical reactions to alter the physical and engineering properties of soft soils. In this section, the general effects of adding cement to soft soils are reviewed.

Chemical reactions

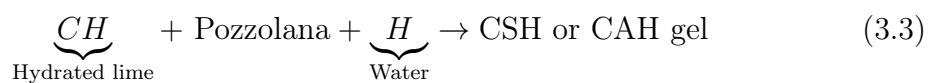
When cement is mixed with water hydration and pozzolanic reactions result in the altering of the soil. The hydration process starts immediately after mixing cement with water and results in a reduction in the initial water content. This water content is decreased further with time since the chemical reactions result in a drying effect due to the usage of pore water over time. [Al-Jabban, 2019]

During the hydration process, the cement clinkers' reaction with the pore water produces three primary cementitious materials. Firstly the two cementitious gels calcium-silicate-hydrate (CSH) and calcium-aluminate-hydrate (CAH). These products bind the soil particles together and result in a strong and stiff stabilized soil with time [Al-Jabban, 2019]. The main contributor to the strength gain is the CSH gel, whilst the CAH gel only yields minor contributions.

The main four cement clinkers in cement are two silica (S) clinkers and two aluminate (A) clinkers [Aalborg Portland, 1999]. The hydration reactions from the silica cement clinker, which accounts for the strongest bonds, are seen in Equation (3.1) and (3.2) [Al-Jabban, 2019]. The general chemical concrete designations are used to describe the hydration process.



The third cementitious material, hydrated lime (CH), is produced from the same chemical reactions, see Equation (3.1) and (3.2). The production of CH leads to the release of calcium ions, thereby raising the pH value of the soil [Al-Jabban, 2019]. The increase in pH increases the solubility of the clay minerals containing alumina and silica, hence resulting in the possibility of pozzolanic CH and alumina-silica reactions producing further CSH and CAH gels. The slower pozzolanic is seen in Equation (3.3) [Al-Jabban, 2019].



Another phenomenon occurring that strengthens the soil is cation exchange resulting in the structure of soft soils becoming more flocculated, compared to the dispersed

nature of clay particles. This is due to the positive ions released from the chemical reactions being attracted to the negative clay particles like magnets. A schematic overview of the chemical hydration process in a cement stabilized soil is seen in Figure 3.1.

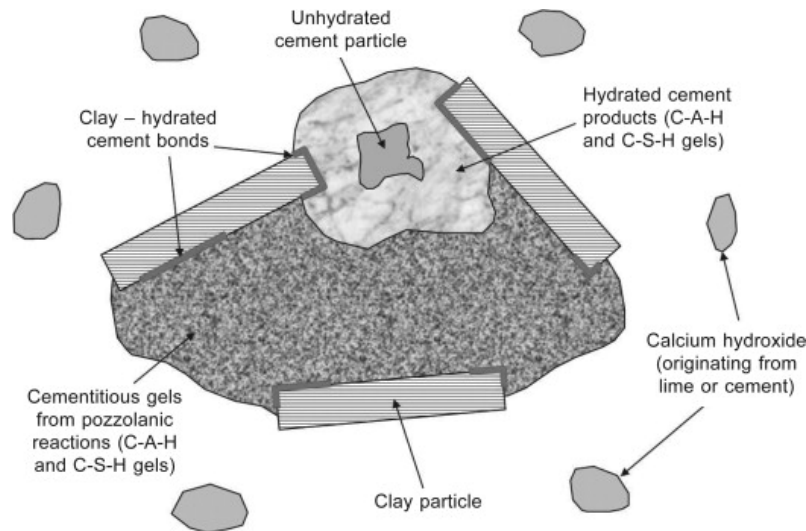


Figure 3.1. Schematic overview of chemical reactions in cement stabilization [Pacheco-Torgal et al., 2014].

Plasticity change

In terms of Atterberg Limits/ soil consistency limits adding cement to soft soils increases the Plastic Limit (PL) and increases or decreases the Liquid Limit (LL) based on its initial value. For soils with a LL less than 40 % the LL increased while soils with a LL above 40 % tended to decrease. The reduction in Plasticity Index (PI) increased as cement content and curing time increased. [Al-Jabban, 2019]

Particle size change

A general observation described in Al-Jabban [2019] was that the cementitious bonds increase the size of the soil particles. This generally means reducing the clay proportion and increasing the amount of silt and fine sand particles.

pH change

The release of calcium ions due to the chemical processes increases the pH value of the stabilized soil since the ions are attracted to the surface of the flocculated

particles due to cavity exchange. According to Al-Jabban [2019] studies from 1969-2012 have observed that a pH value higher than 10 increases the solubility of the clay minerals, hence increasing the production of CSH and CAH gels. However, it is emphasized that a pH value higher than 12 is recommended. This will ensure the development of long-time strength of the pozzolanic reactions since a decrease in pH has been observed long-term [Al-Jabban, 2019].

Strength and stiffness change

The strength and stiffness of cement-stabilized soils increase due to the cementitious bonds formed between the soil particles. Generally, the stiffness increases more than the strength [Åhnberg, 2006]. It was also observed in Åhnberg [2006] that the strain at failure decreased with the uniaxial compression strength. This is due to the soil starting to behave as overconsolidated and brittle compared to normal consolidated, hence starting to show dilative behavior instead of contractive. This means that the soil develops a peak and residual strength.

The dilative behavior is due to the cementitious bonds establishing a quasi-pre-consolidation pressure of the soil. In Åhnberg [2006] it was found that increasing the confining stress for drained triaxial tests showed a significant increase in the strain at failure. The change in the strain at failure was not observed for undrained tests.

The result of stress levels closer to the quasi-pre-consolidation pressure has also been discussed for oedometer tests in terms of compression modulus. Figure 3.2 shows the change in compression modulus based on the vertical stress. When the quasi-pre-consolidation pressure is surpassed the stiffness decreases significantly until M_{min} is reached. After the cementitious bonds have been broken, the compression modulus increases with the stress level like the unstabilized soil. Whether the soil acts at having low or high cementitious effects is e.g. dependent on the amount of binder used.

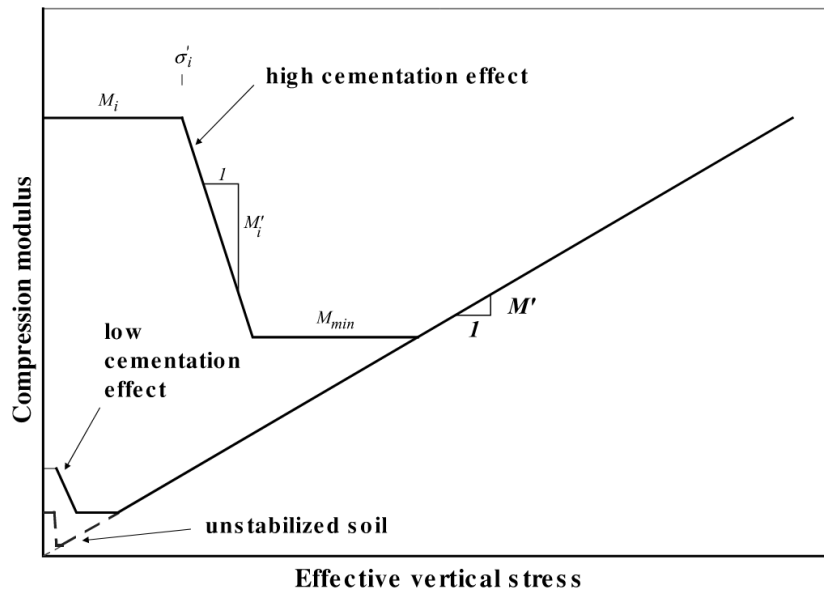


Figure 3.2. Change in compression modulus based on effective vertical stress for cemented soils [Åhnberg, 2006].

The quasi-pre-consolidation pressure can be estimated to be 1.3 times the uniaxial compressive strength based on [Åhnberg, 2006].

Small strain stiffness change

Like the strength and stiffness, the small strain stiffness has been observed to increase as well. In Lang et al. [2020] the small strain stiffness was recorded for a silty clay during curing. From curing day 3 until day 28 the small strain stiffness increased at least 25%. In Chaiprakaikeow et al. [2017] a relation between the shear wave velocity, generally used to determine the small strain stiffness, was correlated to the unconfined compressive strength of coarse-grained cement stabilized road structures. The possibility of using this as a quality control was therefore suggested. This was tested in Aslmand et al. [2022] on deep soil mixing where it was found that the shear wave velocity generally was about 20% larger in the field. However, the field strength was not tested.

Cyclic resistance change

The cyclic properties have primarily been tested on cemented coarse-grained soils. However, in Gebretsadik [2014] a clay with large amounts of binder was tested. It was found that the cement amount and curing period had a significant effect on the

strain magnitude and degradation of the material. A general observation was that the degradation of the material took place in the first 100 cycles.

Permeability change

In terms of permeability, both decreases and increases have been observed. It is expected that the permeability changes with time since the macro-structure of the soil changes [Åhnberg, 2006]. Generally, there will be an initial increase in permeability due to the flocculation and change in void ratio and water content. In time the permeability is generally decreasing since there is an indirect correlation between strength gain and permeability decrease. A rough estimate of the permeability can be made based on Equation (3.4).

$$\frac{k_{stab}}{k_{soil}} \approx 0.043 \cdot \exp\left[6 \cdot \frac{w}{w_0} - 0.004 \cdot q_c\right] \quad (3.4)$$

k_{stab}	Permeability of stabilized soil [m/s]
k_{soil}	Permeability for untreated soil [m/s]
w	Water content for stabilized soil [%]
w_0	Water content for untreated soil [%]
q_c	Unconfined compressive strength [kPa]

As a rule of thumb, the permeability in the laboratory is lower than the one found in the field. This could be due to a more inhomogeneous macro-structure [Åhnberg, 2006].

3.3 Casting in the laboratory

The casting procedure for replicating the field installation in the laboratory has varied throughout time. In 2021 a new laboratory procedure for preparing soil specimens was put forward by Helle et al. [2021]. The procedure is made for clay, however, in this thesis, it will be used on gyttja.

The procedure involves stirring in-situ soil to a remolded state in a kitchen machine. The binder is then added and stirred for 2 x 30 seconds. The mixture is then packed into metal cylinders where the curing occurs as described in Helle et al. [2021]. It has been shown that reducing the mixing time can reduce the compressive strength, hence the stirring guideline is followed closely for comparison sake [Al-Jabban, 2019].

According to Helle et al. [2021] the soil should be stomped into the metal cylinder in four layers. However, it was found in a preliminary study that this method resulted in the development of cracks between the stomped layers [Tanderup, 2022]. For this thesis the soil is therefore stopped carefully by hand, to avoid the development of clear distinctions between the stomped layers. The specimens are compacted with end plugs to ensure the correct volume.

The specimens are packed according to the in-situ density to avoid overestimating strength and stiffness parameters due to increased density [Helle et al., 2021]. It has been recorded multiple times that an increase in density increases the strength [Axelsson et al., 2000]. The cylinder with the specimen inside is stored in a zip-lock bag with a wet cloth to simulate 100 % humidity.

In Tanderup [2022] it was found that different cement types resulted in varying levels of swelling during curing. Stabilized peat in Åhnberg [2006] was also exposed to an initial load after curing, which influenced the strength significantly.

The cylinders are usually stored for 7, 14, or 28 days before the strength is evaluated by uniaxial compression tests. For research purposes, the curing period is sometimes increased. In this thesis, curing will take place for 7, 14, 21, and 28 days to evaluate the early strength gained with time. Furthermore, the strength will be evaluated with triaxial tests, where the consolidation phase is set to account for one of the curing days.

Temperature effects

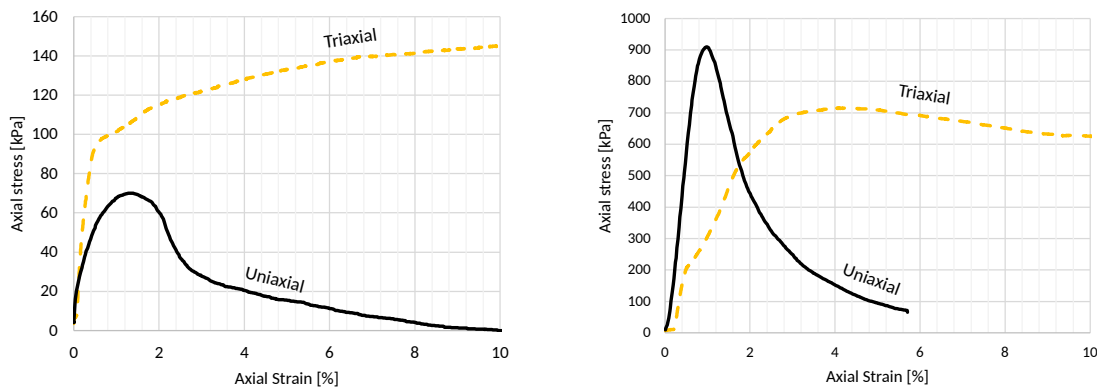
The curing temperature for binder-stabilized specimens is typically 20 °C in the laboratory, although soil temperature in the field is 6-8 °C. This is partly due to the faster reaction in the laboratory, hence lowering the curing period during preliminary designs. Furthermore, the temperature in installed field columns varies greatly depending on the installation pattern and the binder used. Columns with quick lime typically experience a larger temperature rise early on. If soils are stored at other temperatures than 20 °C the equivalent curing time to that of 20 °C is calculated based in Equation (3.5). For Swedish clay and silty clay, K is set to 0.5.

$$t_{eq} = \frac{(20 + K(T_C - 20))^4}{(20 + K(T_{ref} - 20))^4} \cdot t_c \quad (3.5)$$

t_{eq}	Equivalent curing time [days]
K	Curing coefficient [-]
T_C	Curing temperature [°C]
T_{ref}	Reference temperature of 20°C [°C]
t_c	Curing time at the curing temperature [kPa]

3.4 Strength and stiffness gain

As described in Helle et al. [2021] the strength is usually evaluated by the use of uniaxial compression tests. This has been the standard way of evaluating the increase in undrained shear strength (S_u) and secant stiffness (E_{50}) for a long time. For this thesis, the strength and stiffness are evaluated by Consolidated Undrained (CU) and Consolidated Drained (CD) triaxial tests. This is expected to yield more accurate results since these tests are a better replication of reality. Uniaxial compression tests have been observed to overestimate the strength [Al-Jabban, 2019] [Åhnberg, 2006]. In Tanderup [2022] it was observed that the uniaxial compression test underestimated the strength gain for low cement contents and overestimated the strength gain for high cement contents as shown in Figure 3.3. This was deemed to be based on a combination of the difference in column stability with $\sigma_3 = 0$ and the change in the strain at failure. Generally, the strain at failure decreases with increased curing and cement content [Al-Jabban, 2019].



(a) Cement content of 37.5 kg/m³.

(b) Cement content of 150 kg/m³.

Figure 3.3. Comparison of stress-strain curve for uniaxial and triaxial test for (a) low and (b) high cement contents [Tanderup, 2022].

It is not common practice to use oedometer tests to evaluate the stiffness gain for cement-stabilized soils. It was found in Tanderup [2022] that the oedometer behavior

was difficult to data process, due to large initial settlements and yielding very small consolidation and creep settlements.

The use of triaxial tests for this thesis complicates the comparison to empirically developed formulas for strength development. This is due to the strength usually being evaluated by uniaxial compression tests. An acknowledged normalized relationship between the strength gain and curing period is seen in Equation (3.6) [Helle et al., 2021] [Åhnberg, 2006].

$$\frac{C_{uUC}}{C_{uUC28}} = 0.3 \cdot \ln t_{eq} \quad (\text{Åhnberg, 2006}) \quad (3.6)$$

C_{uUC}	Undrained shear strength at time t_{eq} [kPa]
C_{uUC28}	Undrained shear strength after 28 days of curing [kPa]

Another expression for the gain in undrained shear strength is seen in Equation (3.7). This expression is based on various tests with cement amounts from 3% to 16% testes after a curing period of 28 days [Al-Jabban, 2019].

$$q_{u(d)} = q_{u(d_0)} + K \cdot \log \left(\frac{d}{d_0} \right) \quad (\text{Mitchell, 1976}) \quad (3.7)$$

C_{uUC}	Unconfined compressive strength after curing for d days [kPa]
$q_{u(d_0)}$	Unconfined compressive strength after curing for d_0 days [kPa]
K	Coefficient. Equal to $70 \cdot C$ where C equals the cement content in % [-]

Compared to a curing period of 28 days the 1-year strength for pure cement is 1.4-1.8 times the unconfined compressive strength Åhnberg [2006].

3.5 Numerical modeling

As of now the bearing capacity and serviceability of DSM are usually assessed by analytical formulas based on Larsson [2006].

In Koch et al. [2013] a 4 m high railway embankment was modeled in Plaxis 3D based on the undrained shear strengths and undrained elasticity modulus from laboratory tests on soft chalky silt. It was found that the diameter and spacing of the columns had a significant effect on the effectiveness of the settlement reduction. It was also found that unconfined compressive strengths beyond 400 kPa had little effect on the settlements, compared to the rapid reduction up to 400 kPa. Furthermore, it was found that mass stabilization can be very effective even with small unconfined compressive strengths ($q_u = 0.1$ MPa reduced the settlements to one-fourth).

Laboratory study 4

This chapter presents the laboratory study performed to evaluate the effects of adding different amounts of cement to gyttja. Firstly the casting procedure of the untreated gyttja meddled with cement is put forward. This includes the reasoning behind the dimensions of the specimens and the compaction method used when mixed, as well as the reasoning for using or not using a pre-load.

Secondly, the properties of the cured gyttja-cement specimens are presented. This involves the change in undrained shear strength, friction angle, different stiffness parameters, pH, plasticity, and particle size distribution. The main theory used to derive data from the triaxial tests (CU and CD), oedometer tests, cyclic tests, and bender element tests can be found in Appendix C.

4.1 Casting and test methodology

The casting procedure is based on the method reviewed in chapter 3 by Helle et al. [2021]. The first step involved in the gyttja-cement casting is shearing the soil to a remolded state. Untreated soil is stirred in a kitchen machine until the soil is deemed sufficiently remolded. According to Al-Jabban [2019] the stirring time of the untreated soil has not been observed to change the strength parameters after curing. The first step is shown in Figure 4.1.

The next step is to introduce the binder into the mixture, see Figure 4.2. The amount of binder is determined according to the mass of the untreated gyttja. When the binder is added the mixture is stirred for 2x30 seconds according to the laboratory procedure by Helle et al. [2021]. When the meddling is finished the gyttja-cement mixture is compacted into metal cylinders reflecting the triaxial test dimensions.



(a) Untreated soil in the mixing bowl.



(b) Untreated soil after remolding.

Figure 4.1. Remolding of the untreated soil to prepare for binder meddling.



(a) Adding cement to the remolded soil.



(b) Mixing of the gyttja-cement mixture.

Figure 4.2. Meddling of FutureCem cement into the untreated soil.

The dimensions of the triaxial tests are set to be 70 mm x 70 mm which is referred to as single-height triaxial specimens. Usually, double-height triaxial specimens are used, they are however associated with shear band failures due to the height/diameter (H/D) ratio being greater than one [Ibsen et al., 2012]. According to Ibsen et al. [2012] both compaction and dilation will occur in the shear band simultaneously, resulting in a water flow from contracting to dilating zones, resulting in a not truly undrained behavior, even though the volumetric strains are zero. To avoid this behavior and get a more homogeneous stress and strain field, the

specimens should therefore be single-height ($H/D = 1$) with smooth end plates as illustrated in Figure 4.3. The Santa Monica Bay sand used in the study showed a slightly lower peak strength and an extension of the stress-strain before failure [Ibsen et al., 2012].

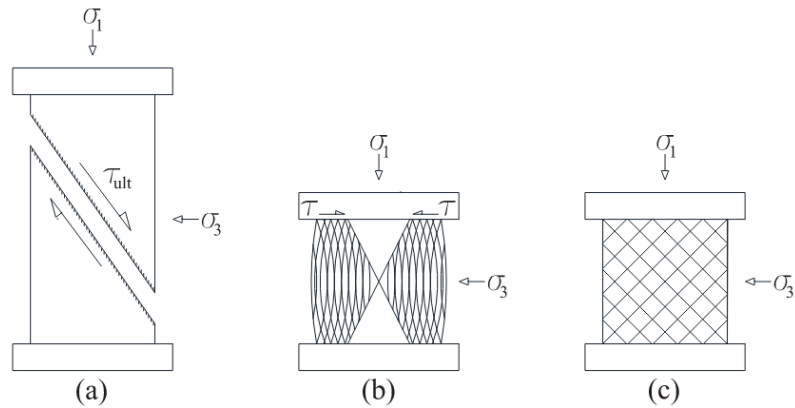


Figure 4.3. Failure mechanism for triaxial specimens. (a) Double-height ($H/D = 2$) with a shear band. (b) Single-height with rough end plates. (c) Single-height with smooth end plates [Ibsen et al., 2012].

The compaction of the gyttja-cement mixture in Figure 4.2 is shown in Figure 4.4. Firstly the soil is gently finger-stamped in non-horizontal layers to avoid the development of cracks between the stamped layers (1). The other end plug is then used to compact the specimen to the right height and density (2). Both end plugs are then removed and the longer end plug is used on the other end, to produce horizontal ends (3). The end plugs are then switched to the original position again to secure the volume is correct (4).

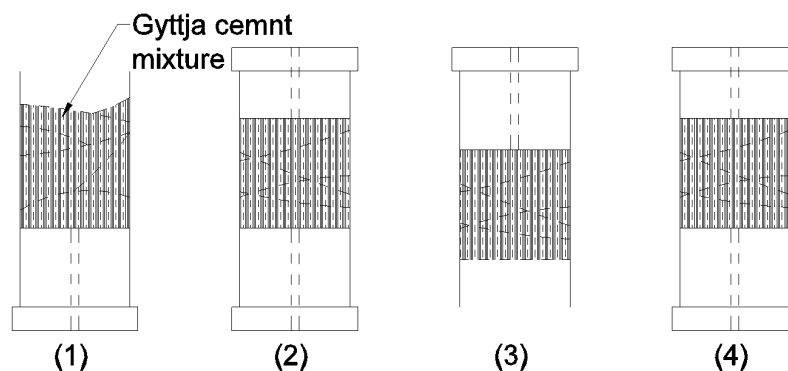


Figure 4.4. Compaction procedure for single-height triaxial specimens.

The equipment used to compact the specimens are shown in Figure 4.5. The metal cylinder has an inner diameter of 70 mm. The end plugs are made from nylon and have a small hole in the middle to allow air to escape during the compaction.

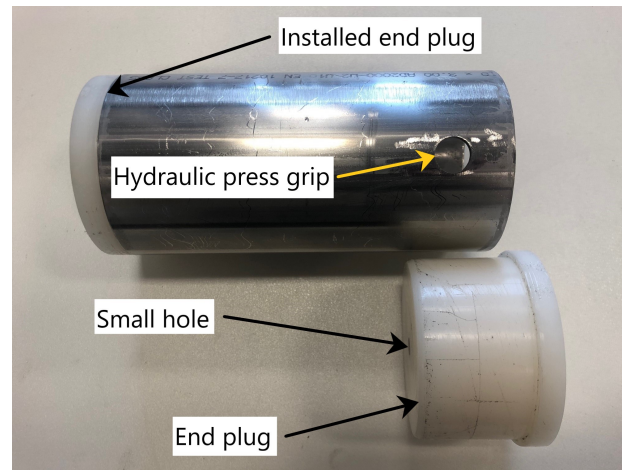


Figure 4.5. Equipment used for casting the gyttja-cement specimens.

Before the specimens were cast two swelling tests were performed. These were performed on gyttja-cement specimens cast in the oedometer ring according to the in-situ density. The results from the swelling tests are shown in Figure 4.6. It is seen that both specimens experienced shrinkage directly after casting. The specimen containing 150 kg/m^3 cement afterward experienced swellings. The specimens with 150 kg/m^3 will therefore be placed under a pre-load during curing to ensure that the specimen won't be able to swell beyond a height of 70 mm.

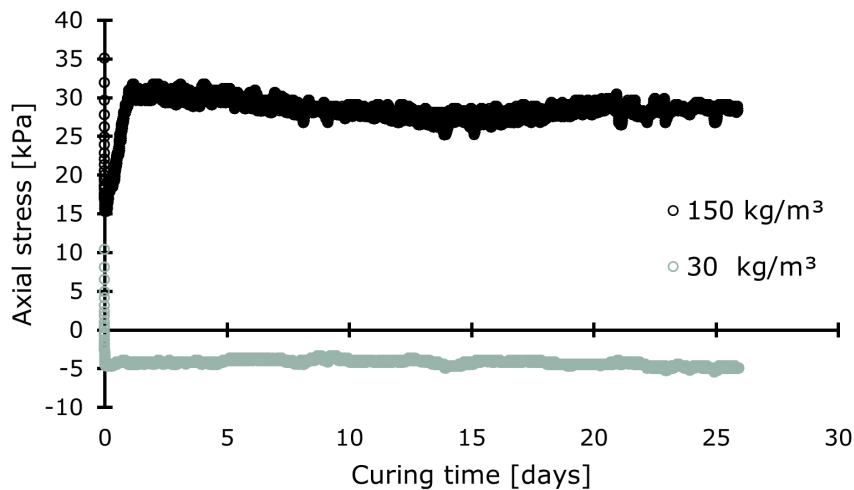


Figure 4.6. Swelling log for oedometer specimens.

The curing setup for specimens with different cement contents is shown in Figure 4.7. The specimens containing 150 kg/m^3 are subjected to a pre-load on the end plugs to avoid swellings. The specimens containing 30 kg/m^3 are not subjected to any pre-load, since the swelling test showed no swelling potential. All specimens were wrapped in plastic with a wet cloth to obtain 100% humidity.

Nearly all specimens were curing at 20°C except three specimens. Three of the specimens were cured at 8°C to investigate the maturity formula based on the equivalent temperature presented in Equation (3.5).



(a) Specimens containing 30 kg/m³.

(b) Specimens containing 150 kg/m³.

Figure 4.7. Curing setup for specimens with both cement contents.

After the curing period, the specimens were pressed out of the metal cylinder using a hydraulic press. The densities of the specimens after curing are shown in Figure 4.8. It is seen that density for the 150 kg/m³ specimens generally is a little lower than the cast in-situ density, presumably due to a water content loss while curing.

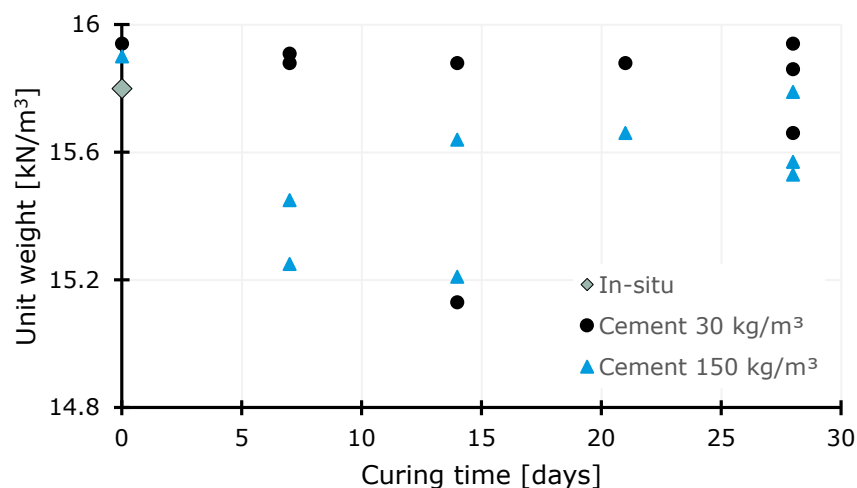
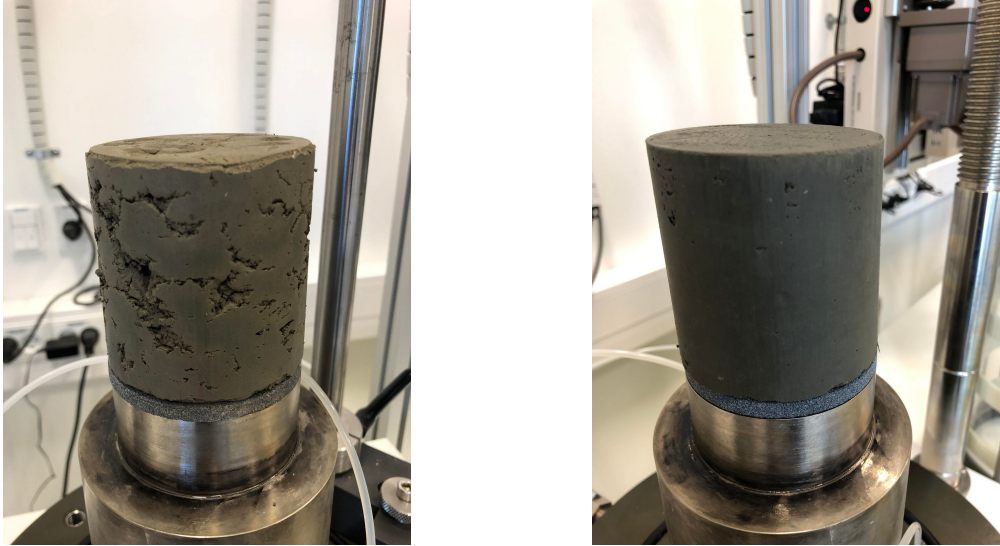


Figure 4.8. Density of gyttja-cement specimens after curing.

Specimens illustrating the general observation after curing are shown in Figure 4.9. The specimen containing 30 kg/m³ is characterized by several imperfections com-

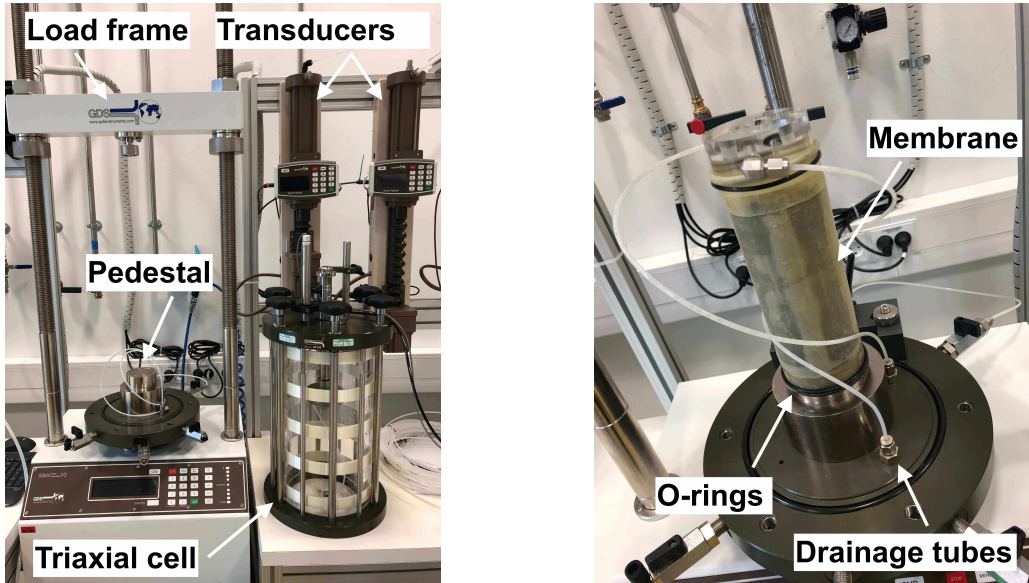
pared to the specimen containing 150 kg/m^3 . The difference in shrinkage/swelling potential is assumed to have had a major role in this since the swellings for the 150 kg/m^3 could have ensured fewer imperfections. However, the casting procedure is also expected to have had an influence.



(a) Specimen containing 30 kg/m^3 . (b) Specimen containing 150 kg/m^3 .

Figure 4.9. Appearance of specimens with different cement contents after curing.

After curing the specimens were primarily subjected to triaxial tests. The standard triaxial test setup is shown in Figure 4.10. The static tests were carried out using The GDS Triaxial Automated System (GDSTAS) and the dynamic tests were carried out using The GDS Advanced Dynamic Triaxial Testing System (DYNTTS).



(a) General setup of GDSTAS equipment. (b) Preparation of test specimen.

Figure 4.10. Static triaxial test setup for CU and CD tests.

Specimens illustrating the general observation after undergoing CU or CD tests are shown in Figure 4.11. It is seen that the apparent failure mechanism is similar to the uniform stress-strain conditions (c) shown in Figure 4.3. However, it can be argued whether the porous discs represent smooth end plates.



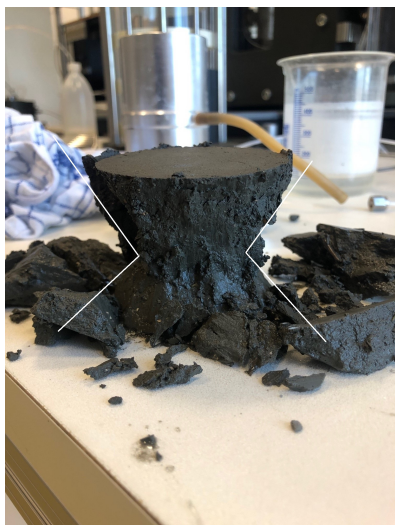
(a) Specimens containing 30 kg/m^3 .



(b) Specimens containing 150 kg/m^3 .

Figure 4.11. Appearance of specimens with different cement content after CU tests.

The failure mechanism for the specimens containing 150 kg/m^3 in 4.11 is seen in Figure 4.12a when investigated further. This was the failure mechanism observed for all specimens containing 150 kg/m^3 except the one, see Figure 4.12b. The failure mechanism for the specimens containing 30 kg/m^3 had a less brittle behavior, whereas the failure mechanism could not be observed for the majority of them.



(a) Failure mechanism (b) in Figure 4.3.



(b) Failure mechanism (a) in Figure 4.3.

Figure 4.12. Failure mechanism of specimens with 150 kg/m^3 after triaxial tests.

4.2 Evaluation of standard triaxial tests

The stiffness and strength parameters presented in this section are derived from Consolidated Undrained (CU) and Consolidated Drained (CD) triaxial tests. All specimens were subjected to an isotropic consolidation of $\sigma' = 30$ kPa. The specimens are divided based on the curing temperature. The majority of the specimens were cured at room temperature at 20 °C. However, three specimens were cured at 8 °C to investigate the effects of different curing temperatures. The formulas used to derive the presented parameters can be found in Appendix C. A short description of the standard triaxial tests can be found in the Appendix as well.

4.2.1 Specimens curing at 20 °C

The increase in undrained shear strength, C_u , based on the curing period for both cement contents is shown in Figure 4.13. The correlation coefficient, R^2 , represents the best fit with a logarithmic trendline. The development in undrained shear strength is usually correlated to a logarithmic development. The undrained shear strength for the untreated soil is 19.2 kPa based on a CU test, see Appendix E.

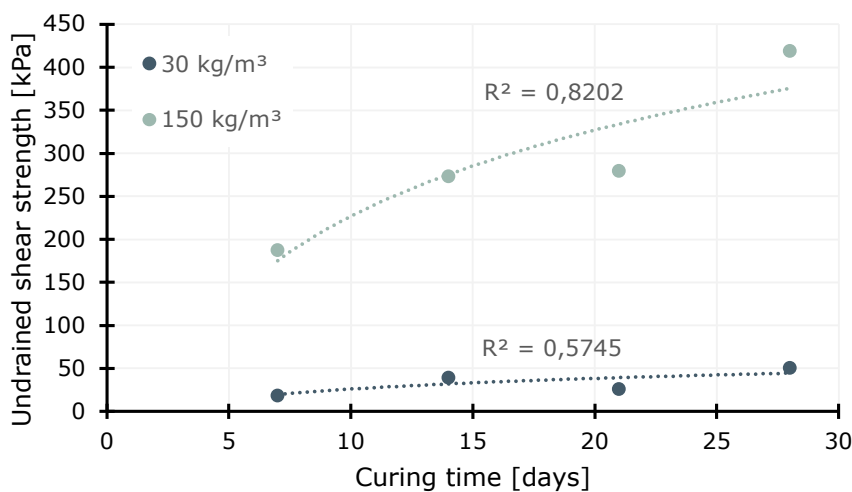


Figure 4.13. Undrained shear strength increase based on curing at 20 °C.

The development in undrained shear strength in Figure 4.13 is correlated to the strength development relationships presented in the state-of-the-art review, see Equation (4.1), (4.2) and (4.3). The modified Åhnberg equation projects the strength based on the 7-days strength instead of the 28-days strength. The modified

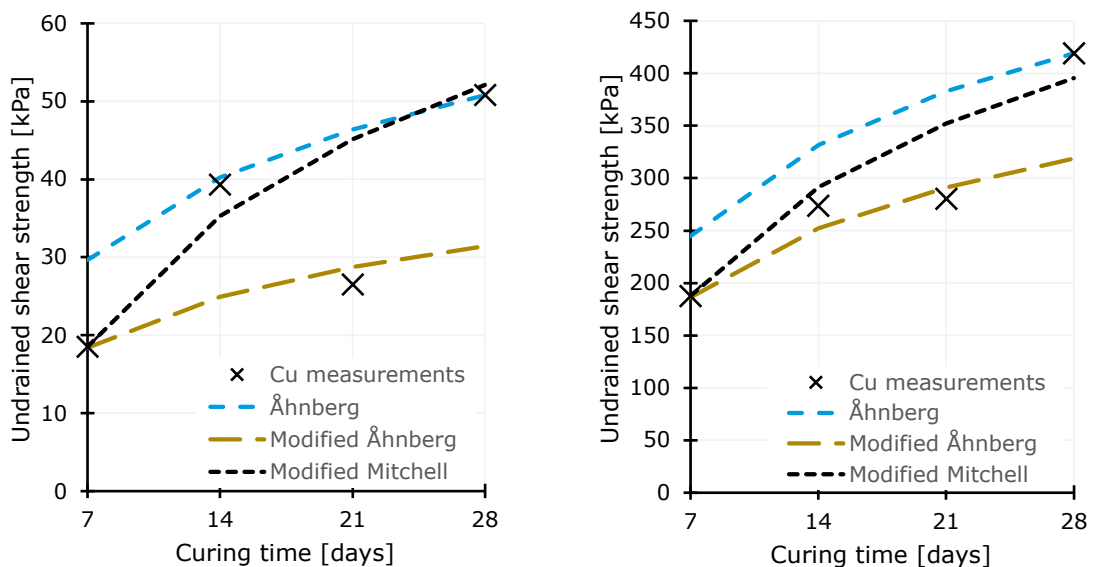
Mitchell equation describes the development in undrained shear strength where the K factor has been changed from $70 \cdot C$ to $18 \cdot C$. See chapter 3 for definitions.

$$C_u = 0.3 \cdot \ln(t_{eq}) \cdot C_{u28} \quad (\text{Åhnberg}) \quad (4.1)$$

$$C_u = 0.51 \cdot \ln(t_{eq}) \cdot C_{u7} \quad (\text{Modified Åhnberg}) \quad (4.2)$$

$$C_u = C_{u(d0)} + (18 \cdot C) \cdot \log\left(\frac{d}{d_0}\right) \quad (\text{Modified Mitchell}) \quad (4.3)$$

The correlation between the test data and the expressions in Equation (4.1), (4.2) and (4.3) is shown in Figure 4.14. The Modified Mitchell formula is found to be a good fit for both mixtures with 3.1 % and 19.2 % cement respectively. The specimen with 21 days of curing is an apparent outlier for both mixtures. The reason for the acknowledged Åhnberg formula not having a better fit with the test data could be due to deviations in the undrained shear strength.



(a) Specimens containing 30 kg/m³.

(b) Specimens containing 150 kg/m³.

Figure 4.14. Correlation between undrained shear strength and curing time.

Another observation for the CU tests was that the strain at failure decreased when the curing and cement content increased. This corresponds to what is expected, even though all specimens containing 150 kg/m³ were expected to reach failure before 10 % strain due to dilative behavior.

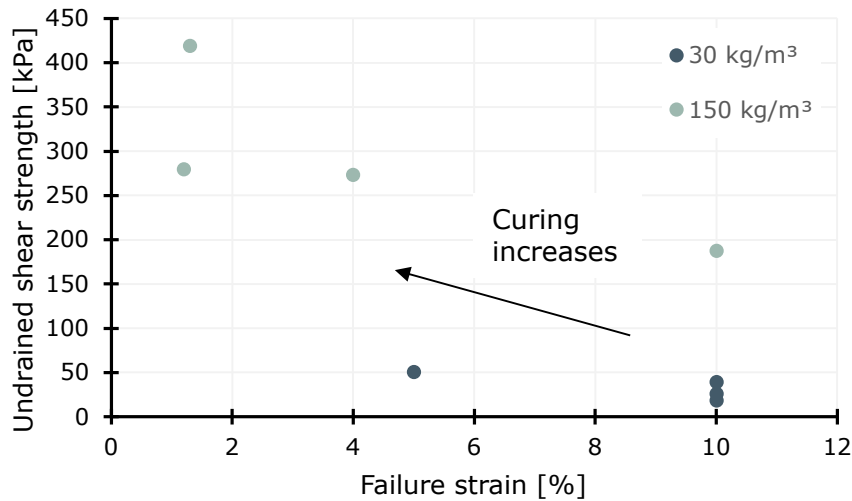


Figure 4.15. Failure strain versus undrained shear strength for CU tests.

The correlation between the undrained shear strength and the undrained secant stiffness, E_{u50} , is shown in Figure 4.16. It is seen that the lower cement content yields a higher stiffness as a function of the undrained shear strength compared to the high cement content. Furthermore, the correlation for the higher cement content could potentially lead to a larger overestimation of the stiffness, due to the data being more spread out. The errors in the linear regressions are primarily due to the deviation in development in undrained shear strength since the development in undrained secant stiffness has a nearly linear relationship with the curing period.

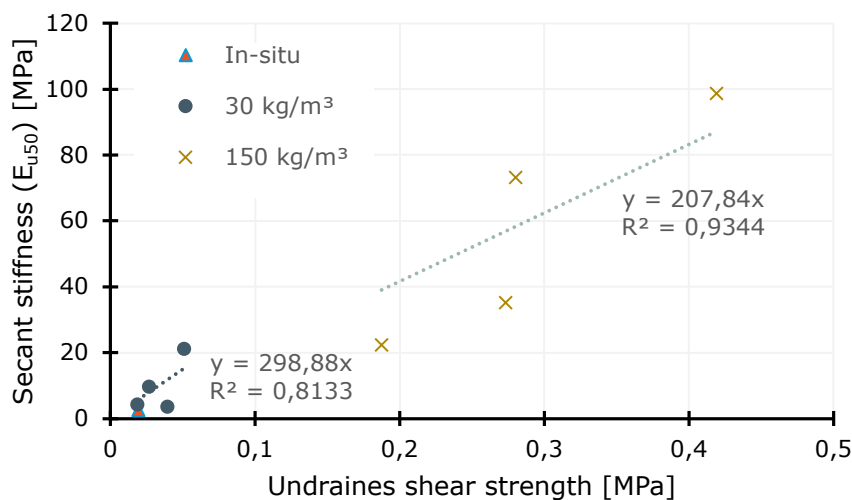


Figure 4.16. Correlation between undrained shear strength and undrained secant stiffness for CU tests.

The expressions used to estimate the undrained secant stiffness are shown in Equation (4.4) and (4.5). The relationship for the untreated gyttja is approximately 130 multiplied by the undrained shear strength.

$$E_{u50} \approx 300 \cdot C_u \quad (30 \text{ kg/m}^3) \quad (4.4)$$

$$E_{u50} \approx 210 \cdot C_u \quad (150 \text{ kg/m}^3) \quad (4.5)$$

Consolidated drained triaxial tests were performed to assess the change in drained parameters. However, only one test for each curing period and each cement type was performed. Hence the relationship between effective cohesion, c' , and friction angle, φ , could not be established. Therefore the effective cohesion is assumed to be equal to zero. The change in friction angle based on the curing period is seen in Figure 4.17. Curing periods of 21 days were not investigated. It is seen that the friction angle changes the most in the first 7 days since the friction angle for the untreated soil was 24.7° based on 3 CD tests [Tanderup, 2022].

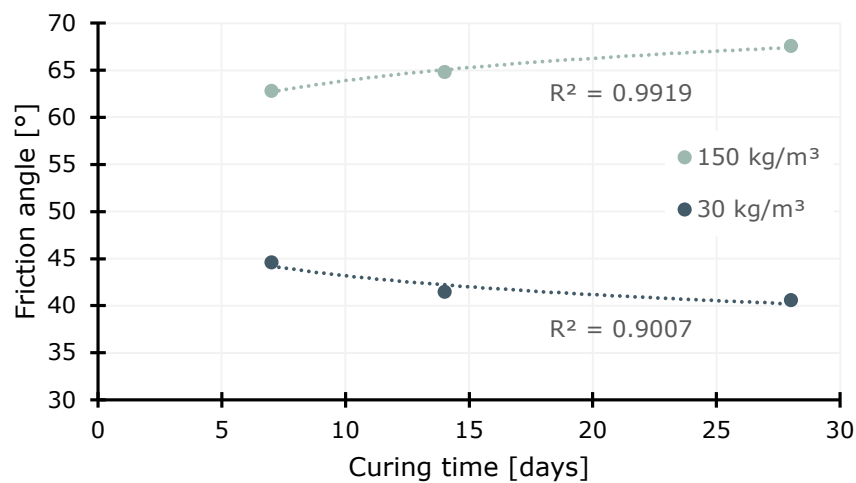


Figure 4.17. Friction angle based on curing time.

The correlation between the drained secant stiffness, E_{50} , and undrained secant stiffness, E_{u50} , is shown in Figure 4.18. The mixture containing 150 kg/m^3 yields a larger proportion of the undrained secant stiffness.

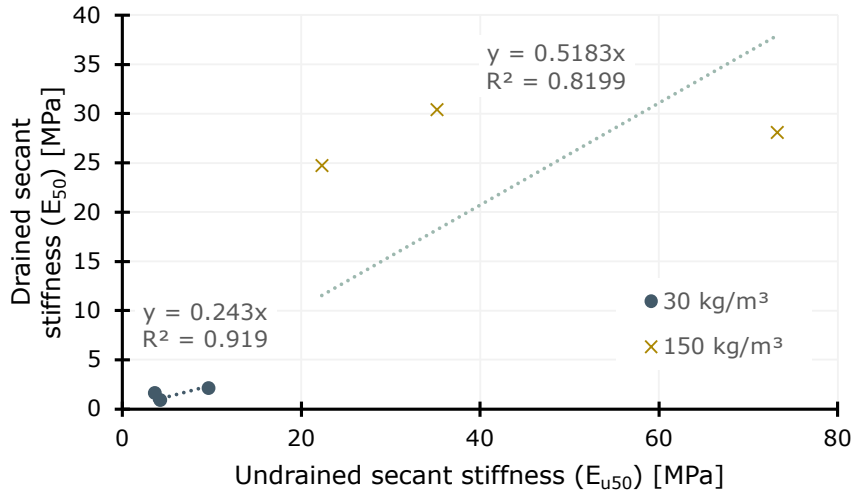


Figure 4.18. Correlation between drained and undrained secant stiffness.

The expressions used to estimate the drained secant stiffness based on the undrained secant stiffness are shown in Equation (4.6) and (4.7).

$$E_{50} \approx 0.24 \cdot E_{u50} \quad (30 \text{ kg/m}^3) \quad (4.6)$$

$$E_{50} \approx 0.52 \cdot E_{u50} \quad (150 \text{ kg/m}^3) \quad (4.7)$$

The drained secant stiffness can also be correlated to the undrained shear strength, see Figure 4.19. Compared to the fit in Figure 4.18 a correlation based on the undrained shear strength is a better fit for the mixture with 150 kg/m³.

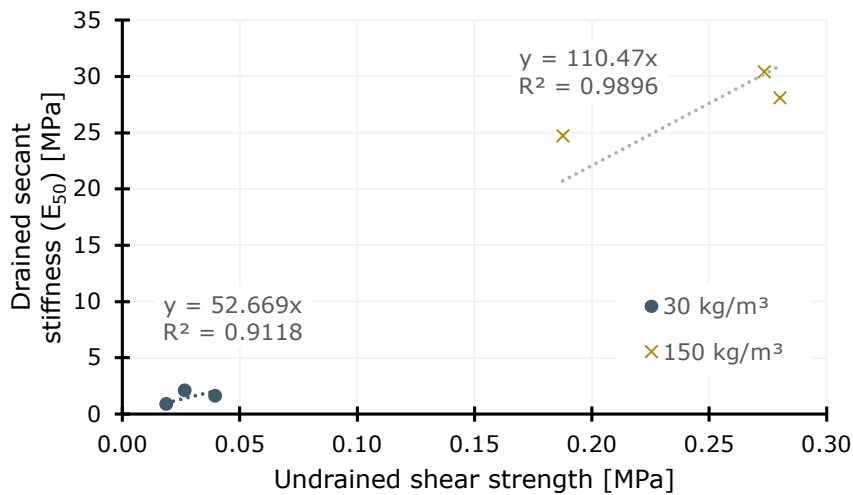


Figure 4.19. Correlation between drained secant stiffness and undrained shear strength.

The expressions used to estimate the drained secant stiffness based on the undrained shear strength are shown in Equation (4.8) and (4.9). If compared to Equation (4.6)

and (4.7) it is seen that the drained stiffness is significantly lower than the undrained.

$$E_{50} \approx 55 \cdot C_u \quad (30 \text{ kg/m}^3) \quad (4.8)$$

$$E_{50} \approx 110 \cdot C_u \quad (150 \text{ kg/m}^3) \quad (4.9)$$

The correlation between the unloading-reloading modulus and the drained secant stiffness is shown in Figure 4.20. It is seen that the R^2 value yields a quite good correlation between the data, even though the data are quite spread out. Lower bound correlations yields 5.3x for the 30 kg/m³ mixture and 2.5x for the 150 kg/m³ mixture.

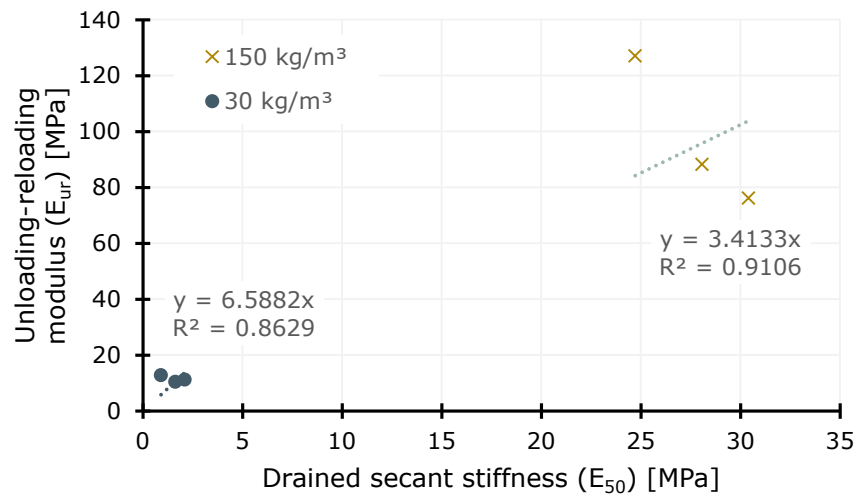


Figure 4.20. Correlation between unloading-reloading modulus and secant stiffness.

The expressions used to estimate the unloading-reloading modulus based on the secant stiffness are shown in Equation (4.10) and (4.11).

$$E_{ur} \approx 6.6 \cdot E_{50} \quad (30 \text{ kg/m}^3) \quad (4.10)$$

$$E_{ur} \approx 3.4 \cdot E_{50} \quad (150 \text{ kg/m}^3) \quad (4.11)$$

4.2.2 Specimens curing at 8 °C

To investigate how the temperature affects the undrained parameters based on the curing period, three specimens were subjected to curing at 8 °C. This is due to the field installations being subjected to a lower temperature than the general laboratory temperature of 20 °C.

The curing periods are based on Equation (4.12), where $K=0.5$ is assumed based on Helle et al. [2021]. The factor of +1 corresponds to the consolidation process in the triaxial apparatus. The $t_{eq} = 7$ days specimen at $8\text{ }^{\circ}\text{C}$ will therefore cure for $t_{eq} = 6$ days at $8\text{ }^{\circ}\text{C}$ and one day at $\approx 20\text{ }^{\circ}\text{C}$ during consolidation. The specimens curing at $20\text{ }^{\circ}\text{C}$ also had the last day of their curing period as consolidation of $\sigma' = 30\text{ kPa}$ in the triaxial apparatus. The equivalent curing time is aimed at 7, 14, and 21 days.

$$t_{eq} = \frac{(20 + K(T_C - 20))^4}{(20 + K(T_{ref} - 20))^4} \cdot t_c + 1 \quad (4.12)$$

The three specimens were subjected to 26 (25+1), 55 (54+1), and 84 (83+1) days of curing at $8\text{ }^{\circ}\text{C}$. The undrained shear strength obtained is seen in Figure 4.21. During the CU test for the specimen with a curing period of 55 days, the load cell showed abnormal behavior. The undrained shear strength was evaluated by a manual curve, see test the log in Appendix G for further clarification.

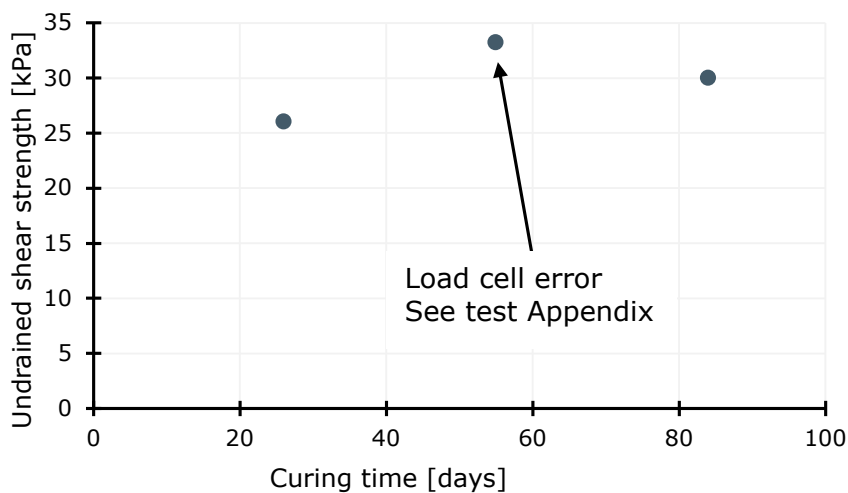


Figure 4.21. Correlation between undrained shear strength and curing at $8\text{ }^{\circ}\text{C}$.

The correlation between the undrained shear strength and equivalent curing time for different K values is seen in Figure 4.22. It is seen that the currently acknowledged $K = 0.5$ is a decent fit with the $20\text{ }^{\circ}\text{C}$ data. However, it is difficult to assess the K value based on the amount of data points and the low increase in undrained shear strength.

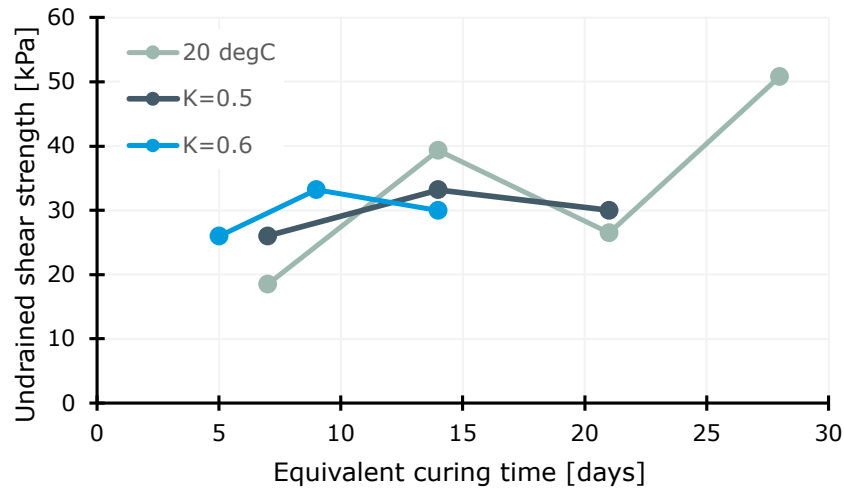


Figure 4.22. Comparison of undrained shear strength for 20 and 8 °C specimens.

The correlation between the undrained secant stiffness and the equivalent curing time is seen in Figure 4.23. Again $K = 0.5$ seems like a decent fit with the data available.

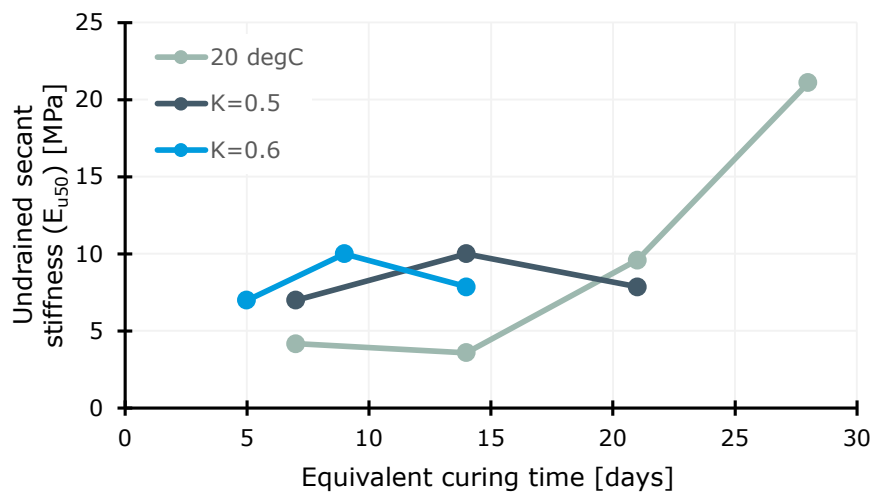


Figure 4.23. Comparison of undrained secant stiffness for 20 and 8 °C specimens.

4.3 Evaluation of bender element tests

The development in the shear wave velocity, V_s , and small strain shear modulus, G_{max} , was monitored by bender element tests. The shear wave velocity is of interest since studies correlating this to the undrained shear strength have been carried out in recent years. The shear wave velocity can therefore be used to evaluate the field development in undrained shear strength without using destructive CPT and shear

vane tests. Furthermore, the small strain shear modulus can be used in advanced numerical models to potentially yield a less costly design.

The development in shear wave velocity for both cement contents is shown in Figure 4.24. The shear wave velocity for the untreated gyttja is approximate 28 m/s.

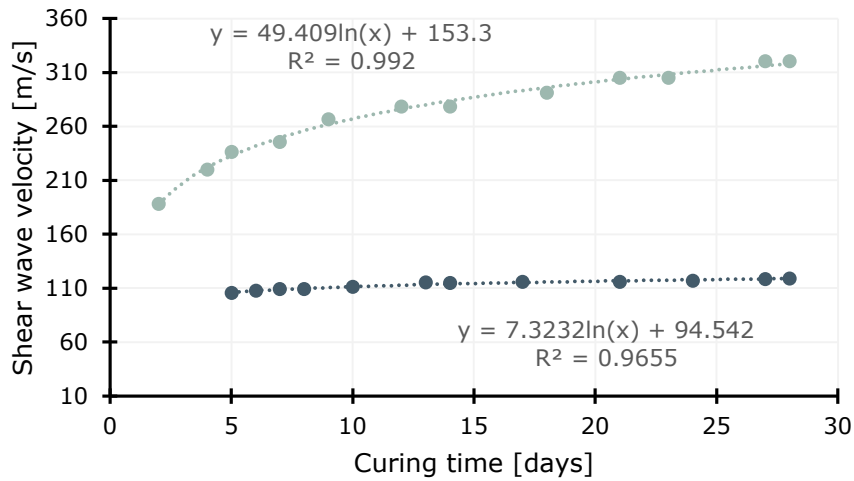
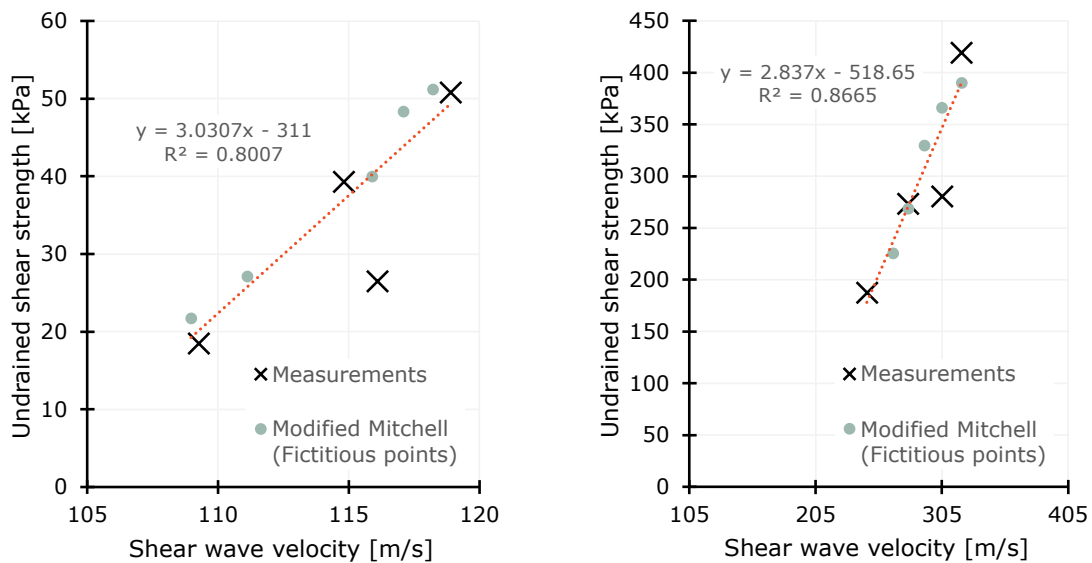


Figure 4.24. Shear wave velocity based on curing time.

The correlation between the undrained shear strength and shear wave velocity is shown in Figure 4.25. The Modified Mitchell formula is used to add additional fictitious points to the chart, see Equation (4.3). It is seen that the fit correlates well with the majority of the existing/ measured data points.



(a) Specimens containing 30 kg/m³.

(b) Specimens containing 150 kg/m³.

Figure 4.25. Correlation between undrained shear strength and shear wave velocity.

The expression used to determine the undrained shear strength based on the shear wave velocity is seen in Equation (4.13) and (4.14).

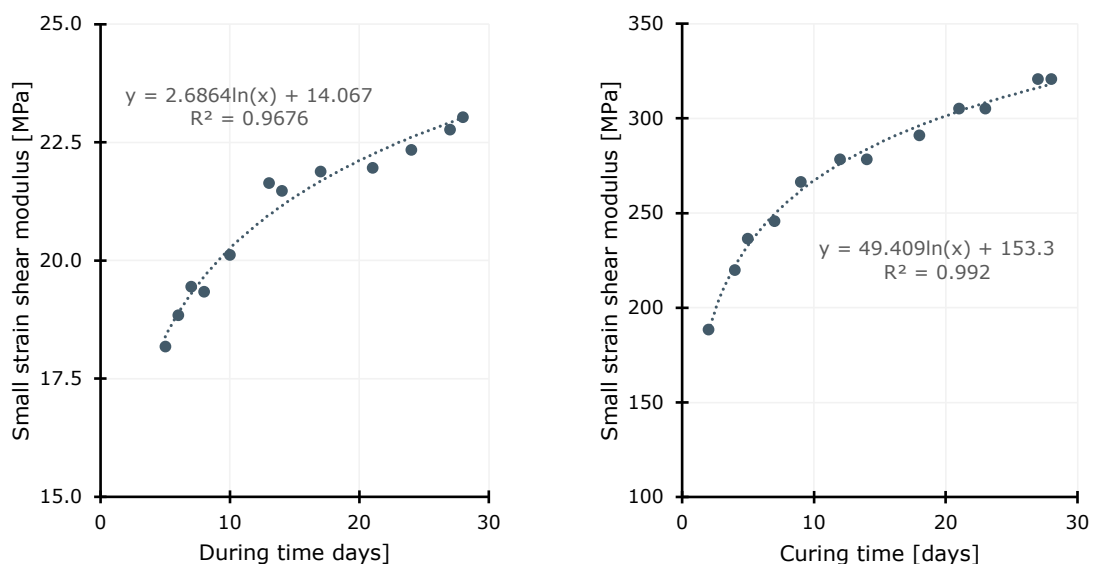
$$C_u \approx 3.03 \cdot V_s - 311 \quad (30 \text{ kg/m}^3) \quad (4.13)$$

$$C_u \approx 2.84 \cdot V_s - 519 \quad (150 \text{ kg/m}^3) \quad (4.14)$$

The small strain shear modulus can be derived on the basis of the bender element tests and the soil density, ρ . This is performed according to Equation (4.15).

$$G_{max} = \rho \cdot V_s^2 \quad (4.15)$$

The development of the small strain shear modulus is shown in Figure 4.26. The small strain shear modulus for the untreated gyttja is approximately 1.3 MPa.



(a) Specimens containing 30 kg/m³.

(b) Specimens containing 150 kg/m³.

Figure 4.26. Correlation between small strain shear modulus and curing time.

4.4 Evaluation of cyclic triaxial tests

The cyclic triaxial tests were primarily performed to investigate the degradation of the shear modulus. Two cyclic tests were performed on specimens with 30 kg/m³ and 150 kg/m³ both cured for 28 days. The system was set to conduct 10.000 stress-controlled cycles at 5 kPa with a frequency of 0.1 Hz. The load was chosen based on

the serviceability load for a road [Energi Styrelsen, 2013]. A cyclic triaxial test was not performed on the untreated gyttja.

The axial strain based on the number of cycles is shown in Figure 4.27. It is seen that the specimen containing 150 kg/m^3 undergoes a significantly lower accumulated strain, compared to the specimen containing 30 kg/m^3 .

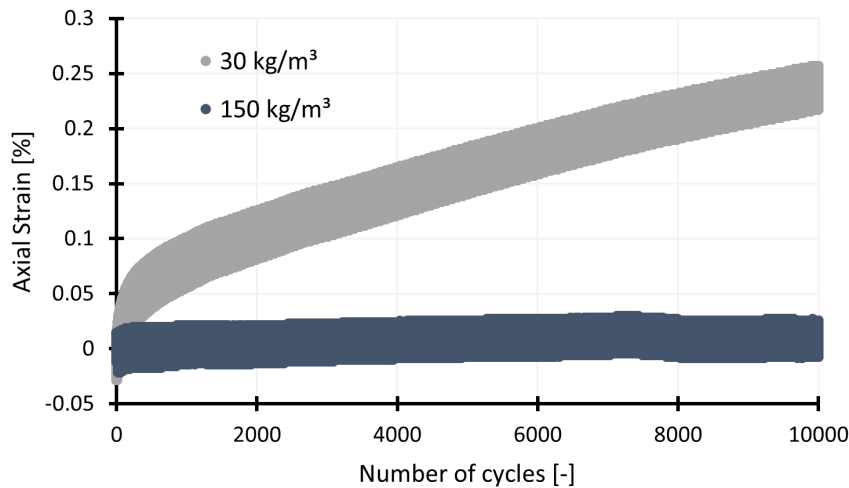


Figure 4.27. Strain increment for 10.000 load cycles.

The degradation in the shear modulus as the plastic strains increase is shown in Figure 4.28. It is seen that the shear modulus below 0.01% shear strain was not monitored. This was presumably due to the magnitude of the load. This is also the reason for the limited ranges of measurements for the mixture containing 150 kg/m^3 .

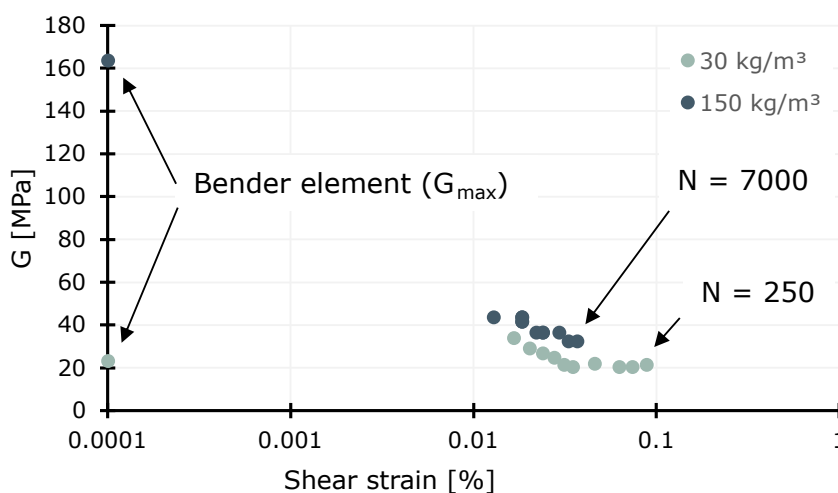


Figure 4.28. Shear modulus data from cyclic and bender element test.

The shear modulus is normalized in terms of the bender element test and the first

cycle extracted in Figure 4.29. For the 30 kg/m³ specimen, the bender element normalization yields a ratio above one, which should not be possible. This could be due to deviations between the two specimens or the disturbance of the bender element test. The normalization in terms of the first cycle, shows the best results, even though the degradation stops at a larger ratio than expected. When the results are normalized according to the bender element test for the 150 kg/m³ specimen, the cyclic shear modulus decreases significantly fast. The results when normalized according to the first cycle are expected to yield better results. After the 10.000 cycles at 5 kPa the stress should have been increased to obtain further knowledge of the stagnation point of the degradation.

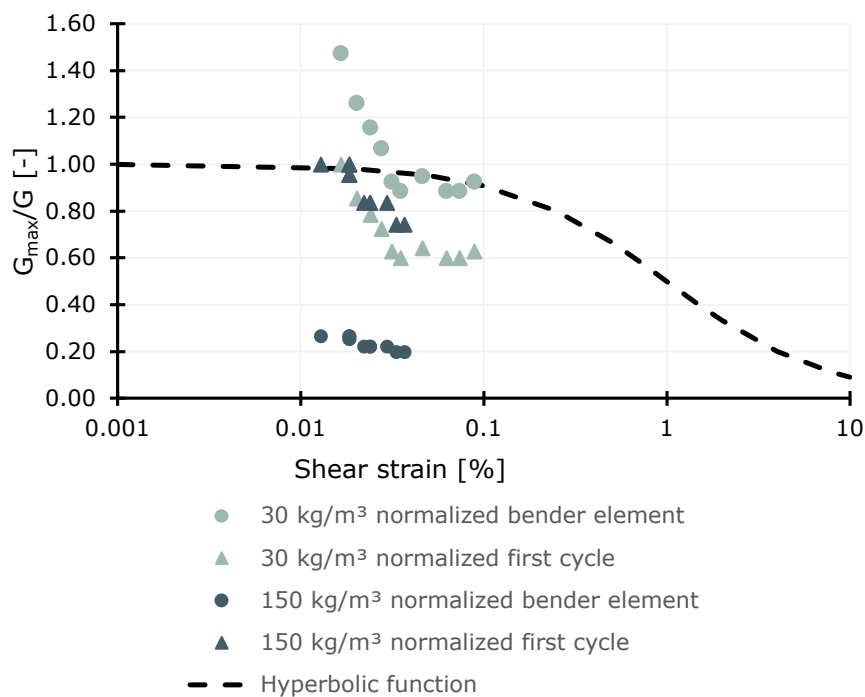


Figure 4.29. Shear modulus data from cyclic and bender element test.

A third test was conducted with varying stress levels for the cycles from 0.1 kPa to 15 kPa. However, due to the coarseness of the load cell data saves (0.001 kN), the results of the test were difficult to interpret. The test is therefore not included.

4.5 Evaluation of oedometer tests

The stiffness was evaluated by two oedometer tests with respectively the low and high cement content. The specimens were cast in the oedometer ring, whereas the

curing period was monitored by a swelling log. The swelling log was presented earlier in this chapter, see Figure 4.6.

The oedometer test results (stress-strain curves) are shown in Figure 4.30 and 4.31 for respectively a cement content of 150 kg/m^3 and 30 kg/m^3 . The initial settlements during the first 10 sections are marked due to being a significant proportion of the total settlements, especially for the specimen containing 150 kg/m^3 . For some of the load steps the initial settlements accounted for more than 50% of the total settlements. This is presumably due to a low saturation of the specimens.

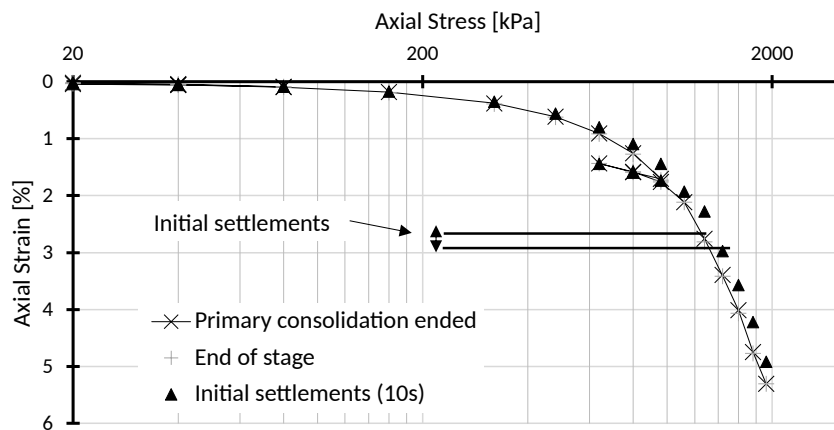


Figure 4.30. Stress-strain oedometer curve for mixture 150 kg/m^3 FutureCem.

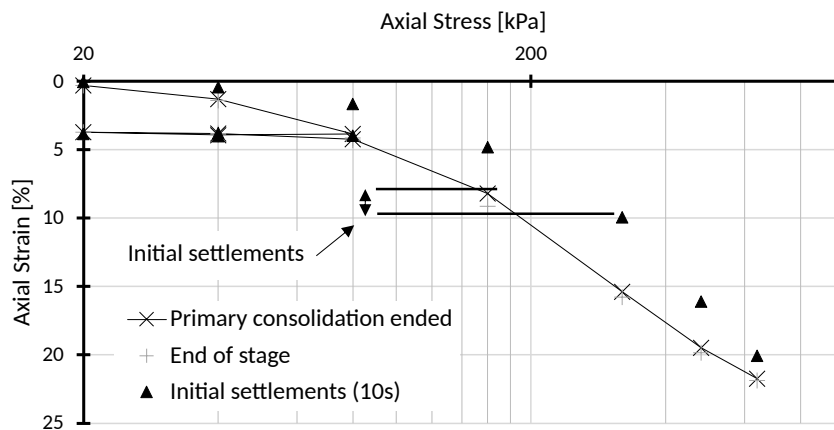


Figure 4.31. Stress-strain oedometer curve for mixture 30 kg/m^3 FutureCem.

The untreated oedometer curve is compared to the cement stabilized oedometer curves in Figure 4.32. The main difference between the untreated and 30 kg/m^3 mixture is the initial stiffness. However, the specimen with 150 kg/m^3 is significantly stiffer than the untreated gyttja.

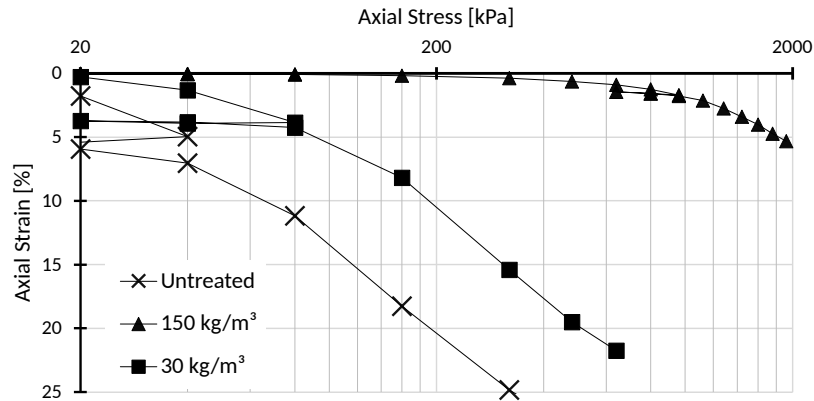


Figure 4.32. Comparison of untreated and cement stabilized oedometer curves.

The stress-strain curve from the oedometer test is compared to the stress-strain curve from the drained triaxial test in Figure 4.33 and 4.34. The oedometer and triaxial curve have a good correlation for the 30 kg/m³ mixture. However, for the mixture containing 150 kg/m³ the oedometer test is significantly stiffer.

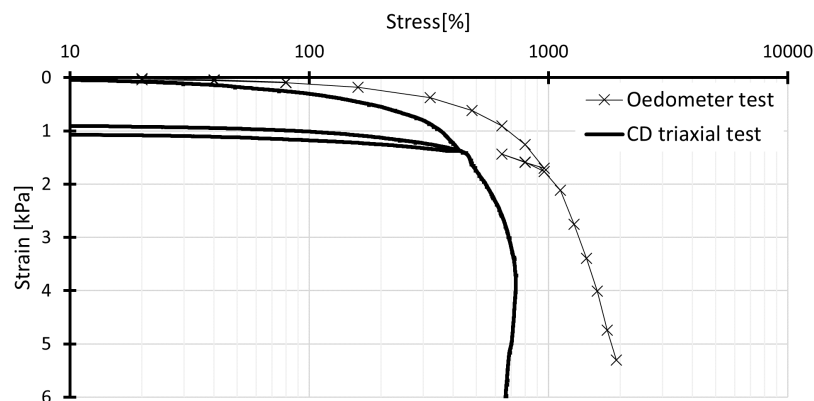


Figure 4.33. Stress strain curve comparison for 150 kg/m³.

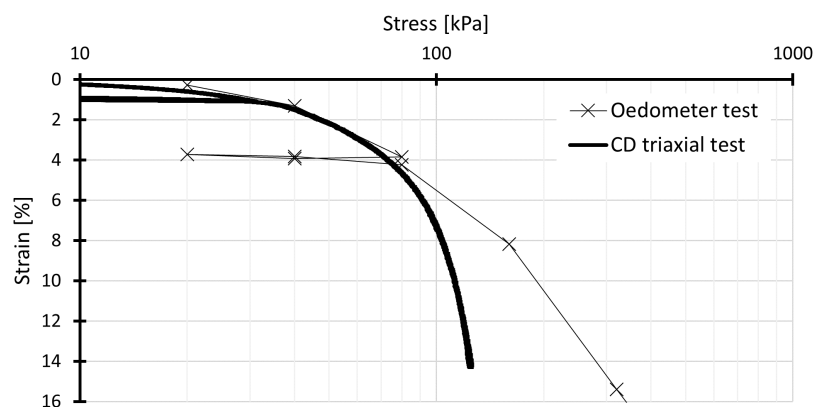


Figure 4.34. Stress strain curve comparison for 30 kg/m³.

The change in the oedometer modulus versus the axial stress is seen in Figure 4.35 and 4.36. It is seen that the cementitious bonds degrade until the stress of 1,000-1.200 kPa for the 150 kg/m³ specimen. The specimen containing 30 kg/m³ starts showing normal consolidated behavior beyond axial stress of 200 kPa.

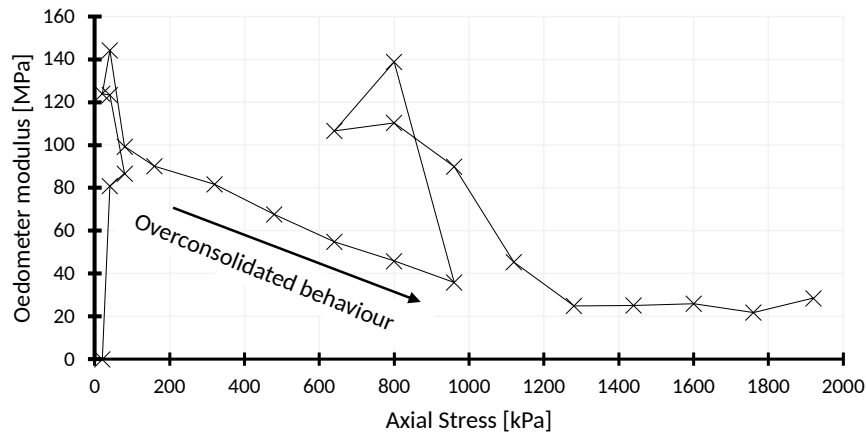


Figure 4.35. Oedometer modulus versus axial stress for 150 kg/m³.

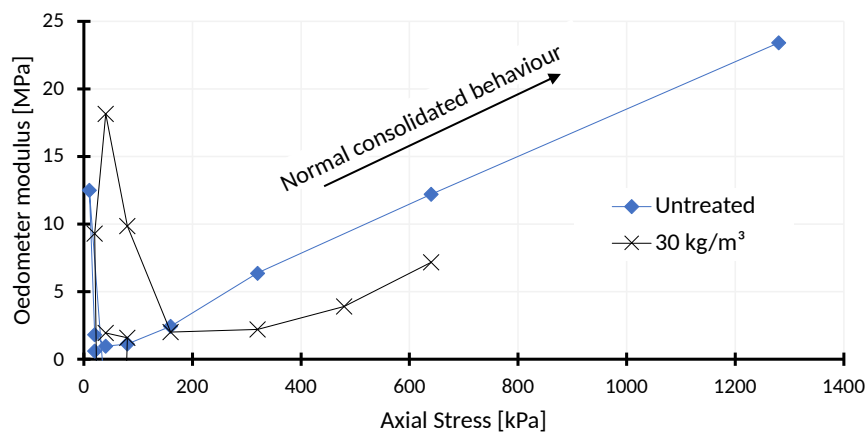
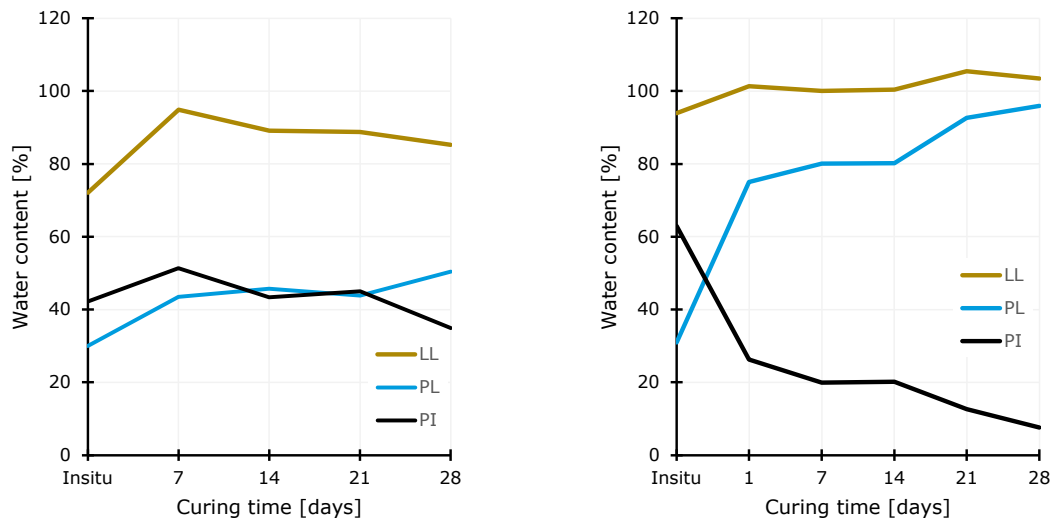


Figure 4.36. Oedometer modulus versus axial stress for 30 kg/m³ mixture compared to untreated intact specimen.

4.6 Evaluation of plasticity and pH changes

After the CU tests were conducted the pH value was measured and the plasticity limits were assessed. This only applied to the specimens curing at 20 °C. For the mixture containing 150 kg/m³ a separate sample was made to investigate the early development of the plastic properties. The changes in Liquid Limit (LL), Plastic Limit (PL), and Plasticity Index (PI) are shown in Figure 4.37. For the specimens

containing 30 kg/m^3 the plastic limit increases initially and decreases in time. For the specimens containing 150 kg/m^3 there is a significant change in the Plastic Limit from the beginning and they end up being nearly non-plastic.



(a) Specimens containing 30 kg/m^3 .

(b) Specimens containing 150 kg/m^3 .

Figure 4.37. Plasticity changes in gyttja-cement specimens after CU tests.

The Plasticity Index is calculated according to Equation (4.16) [Budhu, 2021].

$$PI = LL - PL \quad (4.16)$$

The cementitious bonds forming in the soil also change the size of the soil particles. The change in grain size is seen in Figure 4.38. There is a significant change for the specimens containing 150 kg/m^3 , where the grains generally become larger. However, not much change is seen for the mixture with 30 kg/m^3 .

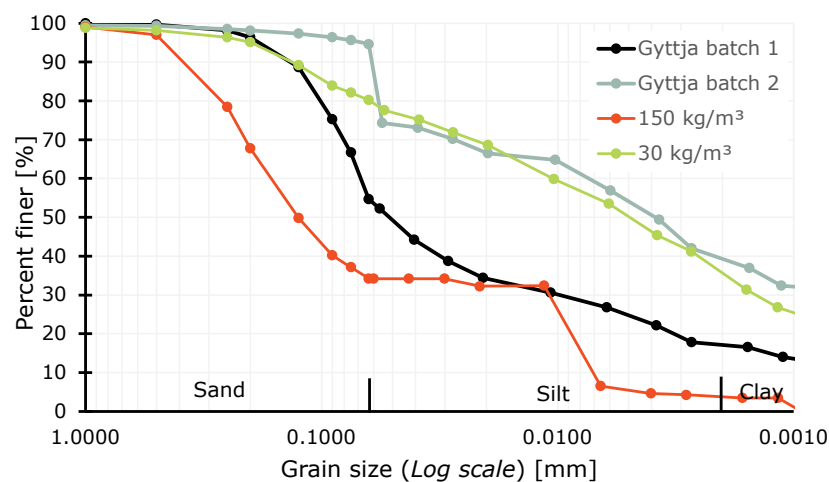


Figure 4.38. Comparison of the particle size distribution for untreated and cemented soils with 150 kg/m^3 and 30 kg/m^3 . Specimens curing beyond 45 days.

The chemical processes between the cement and pore water, result in a significant reduction in the water content of the cemented soils, compared to the untreated soil. If the decrease in water content is combined with the changes in plastic properties the soils become stiffer. The changes in Liquidity Index (LI) for the cemented specimens are shown in Figure 4.39. Generally, the soil changes from a softer consistency near the Liquid Limit to going beyond the Plastic Limit.

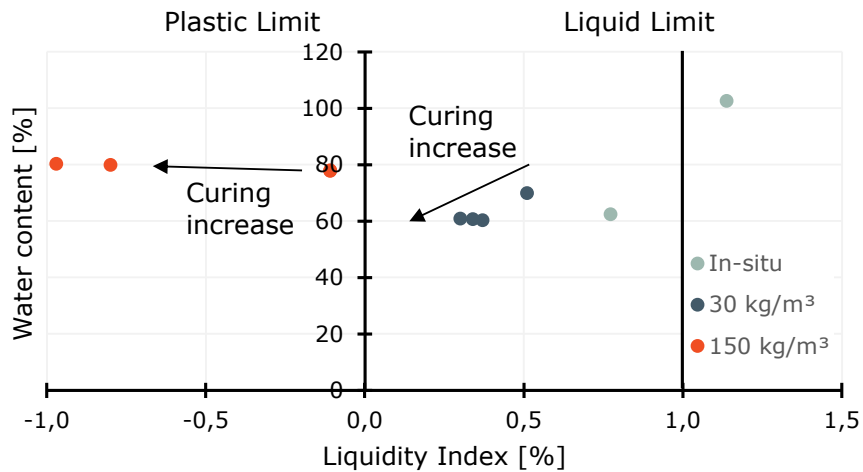


Figure 4.39. Liquidity Index versus soil water content.

The Liquidity Index is calculated according to Equation (4.17) [Budhu, 2021].

$$LI = \left(\frac{w - PL}{LL - PL} \right) \tag{4.17}$$

The structural changes from a soft to stiffer consistency can also be correlated to the increase in undrained shear strength, see Figure 4.40.

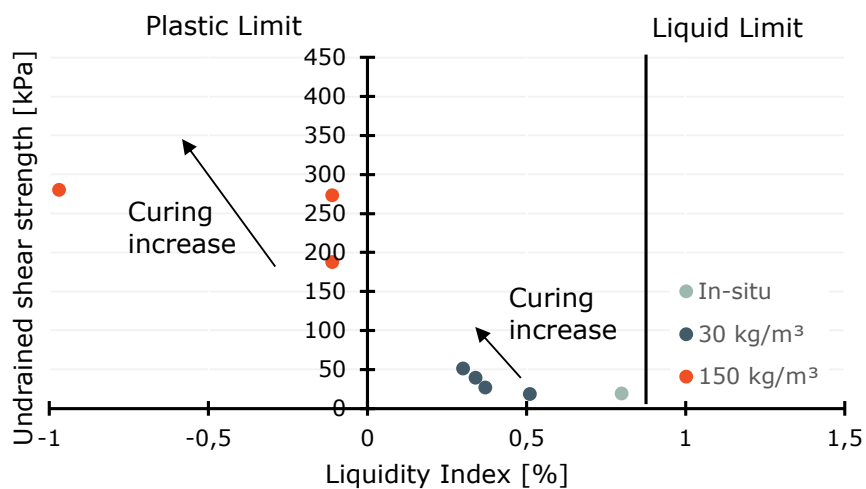


Figure 4.40. Correlation between Liquidity Index and shear strength.

According to Al-Jabban [2019] the pH changes could affect the long-term strength and stiffness development and the value should exceed 12 for proper long-term strength development. The pH measurements on the cemented specimens are shown in Figure 4.41. It is seen that the pH value increases significantly initially, whereas it decreases again as the curing time increases.

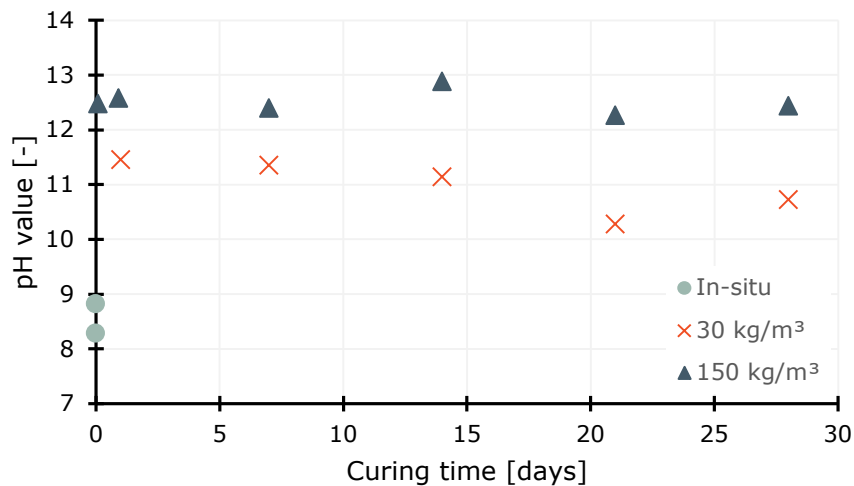


Figure 4.41. pH value based on curing.

One sample with 150 kg/m³ and 30 kg/m³ were stored for respectively 49 and 63 days. The pH value for the 150 kg/m³ specimen was 12.14 and the 30 kg/m³ was 9.38. It is therefore expected that the specimen with the low cement content has a low strength development at this point. However, since the pH value for the mixture with 150 kg/m³ exceeds 12, it is expected that this mixture has a proper long-term strength development.

This chapter investigates the influence of using numerical models to assess the feasibility of cement stabilization compared to analytical methods. The numerical models are created in PLAXIS 2D where the SoilTest module is used to calibrate different soil models based on the laboratory test presented in chapter 4. The soil models investigated are Linear Elastic (LE), Mohr-Coulomb (MC), Hardening Soil (HS), and Hardening Soil with Small Strains (HS-Small).

Firstly the different design scenarios are presented as well as the PLAXIS 2D SoilTest calibration of the CU and CD tests curing for 28 days with both 150 kg/m^3 and 30 kg/m^3 . The numerical study will investigate the influence of cement stabilization in undrained and drained cases. Next up is the presentation of the analytical procedure used to assess the effects of cement stabilization, where the effects of different soil models are discussed. Further, the different design scenarios are used to assess the effects of e.g. different center-to-center distances of the columns and the effects of geosynthetics.

5.1 Scenarios investigated

The numerical modeling is performed in PLAXIS 2D, hence plane strain effects are included. It will therefore not be possible to investigate the grid pattern presented in chapter 1. The patterns investigated due to plane strain effects are therefore the disc and block patterns. The disc pattern is investigated for different cement amounts of columns beneath a pavement structure of a road. The effects are primarily investigated by evaluating the change in settlements compared to the untreated scenario. However, the bearing capacity is also evaluated.

The pavement structure investigated is set to be 12 m wide. This reflects plausibly road widths in Danish practice. The center-to-center (C-C) distance of the columns is determined according to Equation (5.1). The 12 m are based on the road width

and the 0.6 m are based on the diameter of the columns installed.

$$\text{C-C} = \frac{(12.0 \text{ m} - 0.6 \text{ m})}{(x - 1)} \quad (5.1)$$

C-C | Center-to-center column distance [m]
 x | Amount of columns [-]

The different C-C distances investigated in this thesis are shown in Table 5.1. The design with 20 columns equals mass stabilization, where none of the untreated gyttja is left beneath the pavement structure.

Table 5.1. Stabilization ratio based on the amount of stabilized columns.

Amount of columns [-]	Center-to-centre distance [m]	Stabilized ratio [-]
20	0.60	1.00
10	1.27	0.50
8	1.63	0.40
6	2.28	0.30
4	3.80	0.20
3	5.70	0.15

The models used to evaluate the effects of cement stabilization and the different actions investigated to optimize the technique are presented below.

The first section investigated is used to evaluate the analytical solution versus the results obtained in PLAXIS 2D, see Figure 5.1. This section is only investigated with 4 columns. A stiff plate is placed on top of the stabilized area to ensure equal settlements in the untreated soil and the columns, which is an assumption in the analytical procedure.

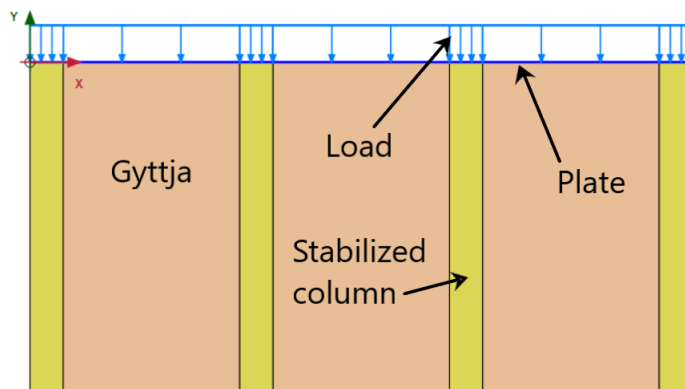


Figure 5.1. PLAXIS 2D model used to evaluate the analytical procedure.

To determine the settlements and bearing capacity for the untreated scenario the model shown in Figure 5.2 is used. The section solely consists of untreated gyttja

except for the pavement structure of 12 m. The gyttja layer below the pavement structure is assumed to be 6 m thick and to be placed on top of a stiff deposit with no settlement issues.

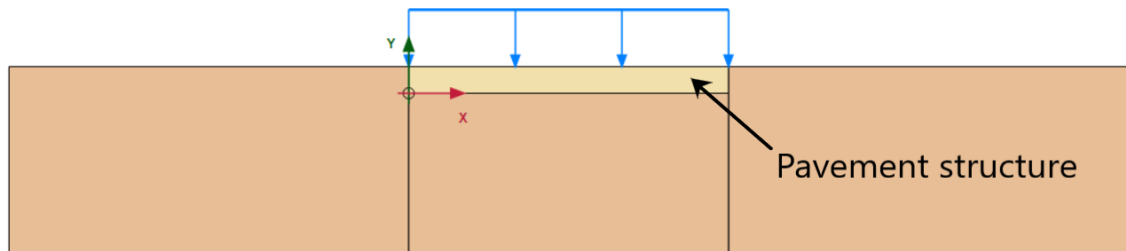


Figure 5.2. PLAXIS 2D model used to evaluate the untreated scenario.

The cement stabilized columns are to be installed below the pavement structure for the untreated section in Figure 5.2. An example of cement stabilization with 4 columns ($a = 0.2$) is shown in Figure 5.3. The columns are primarily evaluated by the CU and CD tests with 28 days of curing.

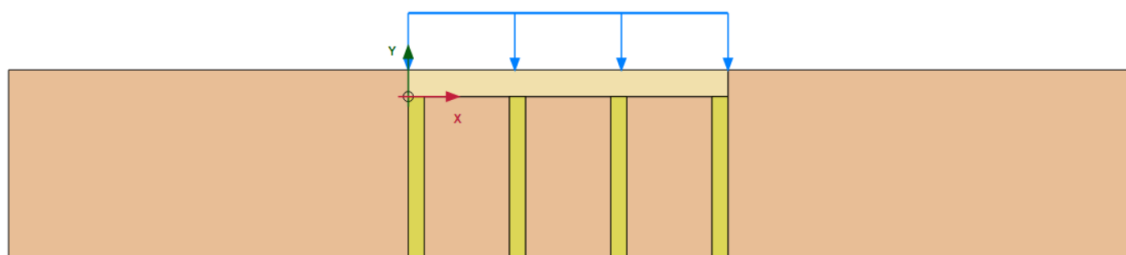


Figure 5.3. PLAXIS 2D model with 4 cement stabilized columns.

The basic model in Figure 5.3 is also investigated with reinforcement columns (double-columns) at the edges of the pavement structure, see Figure 5.4.

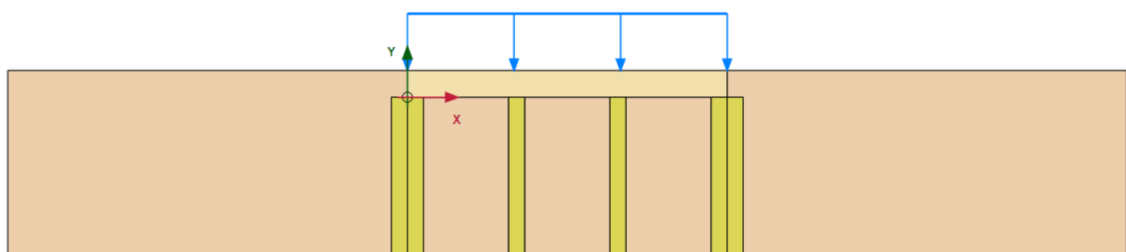


Figure 5.4. PLAXIS 2D model with 4 cement stabilized columns and reinforcement at the edges of the pavement structure.

The models are initially investigated without any geosynthetics included. However, a study is also performed with geonets to evaluate the effect based on the C-C

distance. The model with geonet included is shown in Figure 5.5. An interface is added to each geonet to simulate the interaction with the surrounding soil.

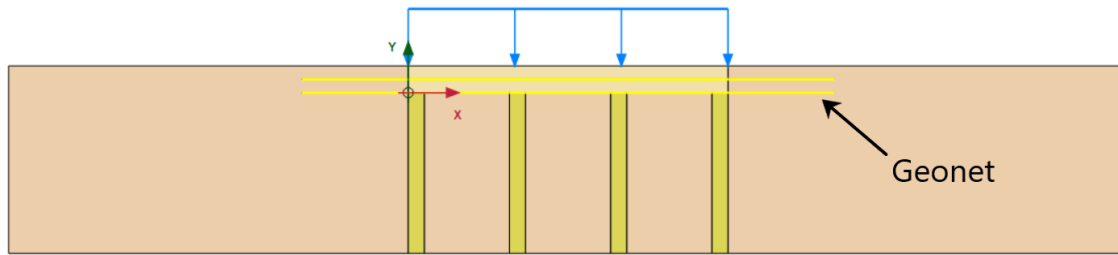


Figure 5.5. PLAXIS 2D model with four cement stabilized columns and geonet.

The models presented above are the ones primarily investigated in this thesis. Some of the main assumptions during the analysis are listed below unless otherwise specified. The load surcharge is based on the characteristic serviceability load for roads according to Energi Styrelsen [2013].

- The pavement structure has a stiffness of 22.3 MPa and a friction angle of 37°
- The ground water table is not included in the models
- The road width is set to 12 m and the surcharge load is set to 5 kPa
- The thickness of the pavement structure is set to 1 m
- The drainage type in PLAXIS for undrained modeling is Undrained B
- The gyttja deposit below the pavement structure is 6 m thick. The deposit below is assumed very stiff and yields no settlements, whereas a fixed boundary is assumed representative

5.2 Calibration of soil models

To investigate the effect of using numerical modeling compared to analytical formulas, different soil models are calibrated based on the laboratory tests performed in chapter 4. The different soil models used to simulate the soil behavior are stated in Table 5.2 with the laboratory tests potentially used for the calibration. The soil calibrations will be shown for the untreated soil and the gyttja-cement specimens with a curing period of 28 days.

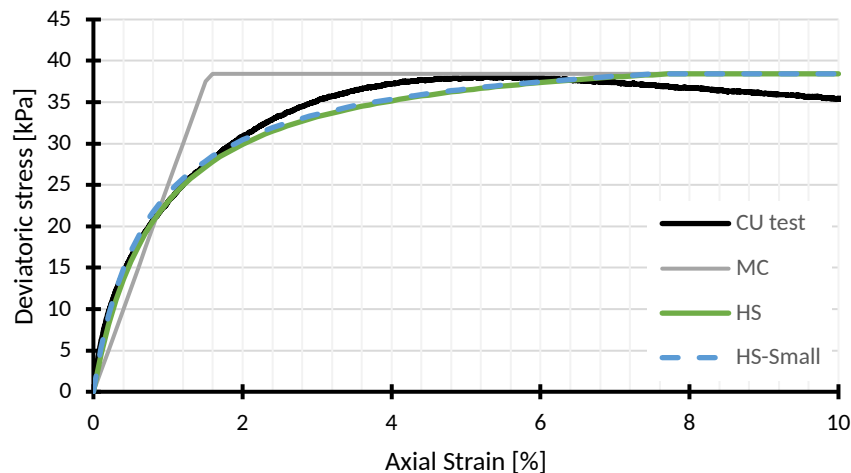
The calibration of the soil models will be partly based on PLAXIS guidelines. Some of the input parameters have general guidelines, due to possible errors if not followed. The guidelines for the correlation between the input parameters are discussed in Appendix D.

Table 5.2. Soil models investigated and laboratory tests used for calibration.

Material model	Laboratory tests used
Linear-Elastic (LE):	CU and CD triaxial tests (E_{u50} , E_{50})
Mohr-Coulomb (MC):	CU and CD triaxial tests (E_{u50} , E_{50} , C_u , φ)
Hardening Soil (HS):	CU and CD triaxial tests (E_{u50} , E_{50} , E_{ur} , C_u , φ) and oedometer tests (E_{oed})
Hardening Soil-Small (HS-Small):	CU and CD triaxial tests (E_{u50} , E_{50} , E_{ur} , C_u , φ), bender element tests (G_0), cyclic triaxial tests ($\gamma_{0.7}$) and oedometer tests (E_{oed})

5.2.1 Calibration of undrained soils

The calibration of the untreated gyttja is shown in Figure 5.6 for the undrained case. It is seen that the HS model generally is a better fit than the MC model. However, the difference between HS and HS-Small is visually insignificant.

**Figure 5.6.** PLAXIS SoilTest calibration fit with CU test for the untreated gyttja.

The undrained calibration for the gyttja-cement specimens curing for 28 days is shown in Figure 5.7 and 5.8. The main difference in the models is how the stress-strain curve is defined for the first $\approx 3\%$ strain. A further description of the optimized parameters and the soil models can be found in Appendix D.

The difference between the calibrated soil models at the beginning of the stress-strain curve is shown in Figure 5.9. For both specimens, HS and HS-Small yield a significantly stiffer soil in the beginning where MC is a better fit with the CU test. However, when the strains are increasing HS and HS-Small yield a less stiff soil compared to MC.

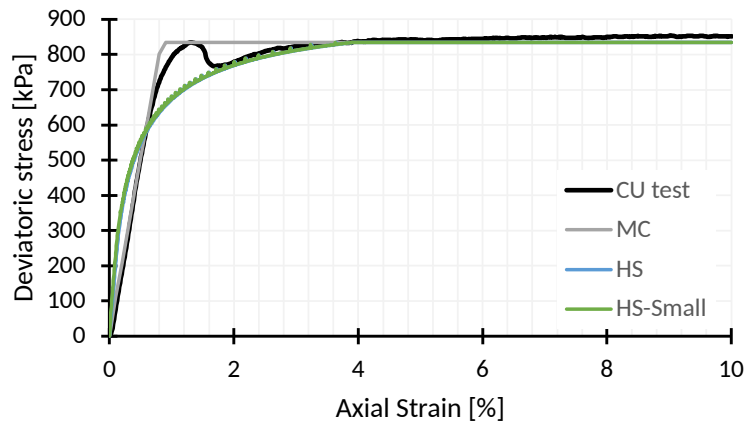


Figure 5.7. PLAXIS SoilTest fit with CU test for 150 kg/m³.

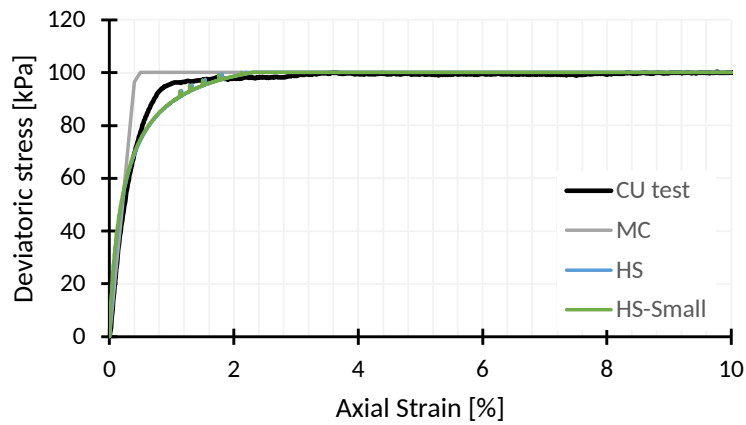
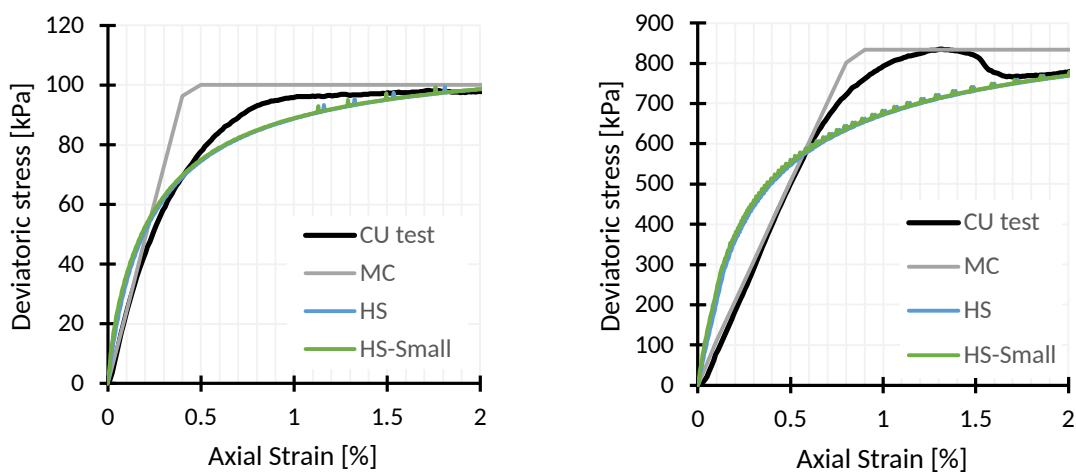


Figure 5.8. PLAXIS SoilTest fit with CU test for 30 kg/m³.



(a) Specimens containing 30 kg/m³.

(b) Specimens containing 150 kg/m³.

Figure 5.9. PLAXIS SoilTest fit for the first 2% strain.

5.2.2 Calibration of drained soils

The difference between the undrained and drained cases is investigated by calibrating the soils based on the CD tests performed.

The gyttja is expected to have a stiffness of 1.25 MPa and a friction angle of 24.7° based on CD tests performed in Tanderup [2022]. However, the HS parameters are calibrated to a stiffness of 1.5 MPa and a friction angle of 30° , see Figure 5.10.

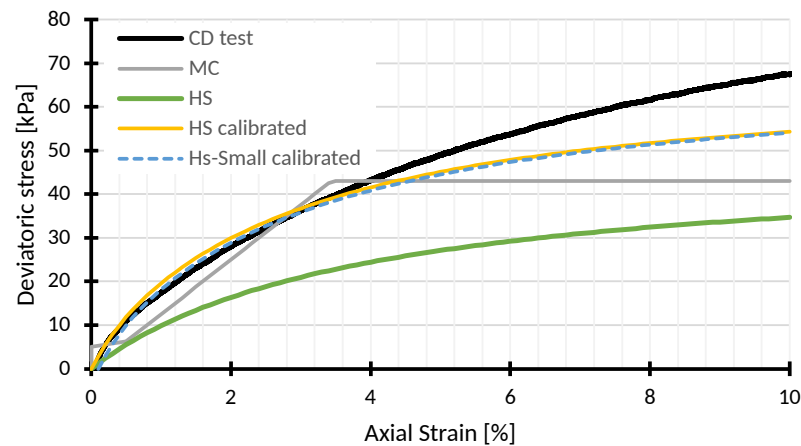


Figure 5.10. PLAXIS SoilTest fit with CD test for untreated gyttja.

The specimens curing for 28 days containing 150 kg/m^3 and 30 kg/m^3 are also calibrated for the drained case, see Figure 5.11 and 5.12. The HS model is the best fit for both cement contents at low strains. However, when the strains exceed 2% and 4% strains for respectively the 150 kg/m^3 and 30 kg/m^3 mixture the HS model yields larger settlements. For the majority of the analysis performed in this chapter, the HS model fit is deemed sufficient.

The HS-Small models with the raw data yielded unrealistic results, hence both models are calibrated to the HS curve. The small strain shear modulus is reduced from $\approx 160 \text{ MPa}$ to 40 MPa for the 150 kg/m^3 mixture and from 25 MPa to 5 MPa for the 30 kg/m^3 mixture. These were the minimum values allowed in PLAXIS.

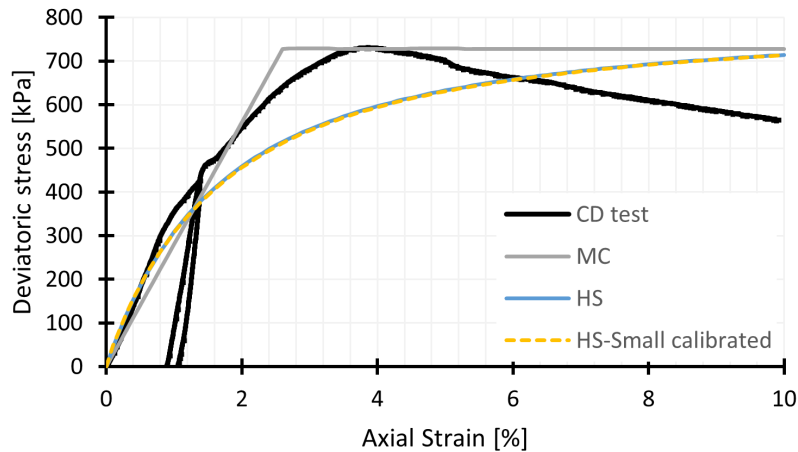


Figure 5.11. PLAXIS SoilTest fit with CD test for 150 kg/m^3 .

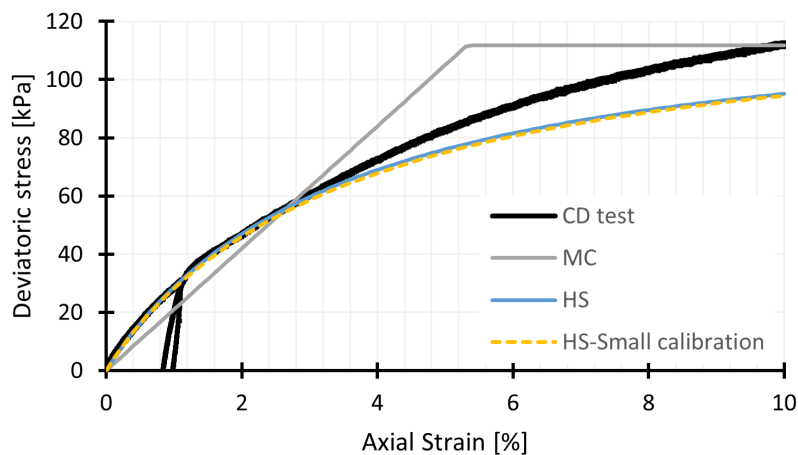


Figure 5.12. PLAXIS SoilTest fit with CD test for 30 kg/m^3 .

The calibrations shown above will be the basis for the numerical study. The input parameters and a description of their estimation can be found in Appendix D.

5.3 Typical analytical procedure

The current analytical method used to evaluate serviceability and bearing capacity is based on a linear elastic perfectly plastic model [Larsson, 2006]. The ultimate limit state is evaluated by the general bearing capacity formulas, with an increased undrained shear strength or friction angle due to the stabilization. The increased shear strength is determined according to Equation (5.2) [Larsson, 2006].

$$c_{u,area} = a \cdot c_{u,columns} + (1 - a) \cdot c_{u,gyttja} \quad (5.2)$$

$c_{u,area}$	Undrained shear strength for stabilized area [kPa]
$c_{u,columns}$	Undrained shear strength for stabilized columns [kPa]
$c_{u,gyttja}$	Undrained shear strength for the untreated soil [kPa]
a	Coverage ratio [-]

The ultimate limit state is evaluated by the general bearing capacity [Larsson, 2006]. The simplified general bearing capacity formula for the undrained case is shown in Equation (5.3) [Trafik, Bygge- og Boligstyrelsen, 2021]. The overburden pressure is not considered in this instance.

$$q_f = (2 + \pi) \cdot c_{u,area} \quad (5.3)$$

q_f	Bearing capacity [kN/m ²]
q	Total overburden pressure [kN/m ²]

The simplified formula general bearing capacity for the drained case is seen in Equation (5.4) [Trafik, Bygge- og Boligstyrelsen, 2021]. The overburden pressure is not considered in this instance either.

$$q_f = \frac{1}{2} \cdot \gamma' \cdot b' \cdot N_\gamma \quad (5.4)$$

γ'	Effective unit weight [kN/m ³]
b'	Effective width [m]
N_γ	Bearing capacity factor [-]

The bearing capacity factors are seen in equation (5.5) and (5.6) [Trafik, Bygge- og Boligstyrelsen, 2021]. The increased friction angle due to cement stabilization is determined similarly to Equation (5.2) with the friction angle substituted with the undrained shear strength [Larsson, 2006].

$$N_\gamma = \frac{1}{4} ((N_q - 1) \cdot \cos(\varphi_{area}))^{\frac{3}{2}} \quad (5.5)$$

$$N_q = \frac{1 + \sin(\varphi_{area})}{1 - \sin(\varphi_{area})} \cdot e^{\pi \cdot \tan(\varphi_{area})} \quad (5.6)$$

φ_{area}	Friction angle for stabilized area [°]
------------------	--

The serviceability limit state is evaluated by a linear elastic soil model. The stabilized columns take the majority of the load. The load distribution must fulfill

Equation (5.7).

$$q_{total} = q_{columns} \cdot a + q_{gyttja} \cdot (1 - a) \quad (5.7)$$

q_{total}	Total serviceability load [kPa]
$q_{columns}$	Stress in stabilized columns [kPa]
q_{gyttja}	Stress in untreated soil [kPa]

The stress in the untreated soil is based on the stress in the stabilized columns. This is based on an iterative process where the stress in the columns is set and the stress in the untreated soil is calculated according to Equation (5.8).

$$q_{gyttja} = \frac{q_{total} - a \cdot q_{columns}}{1 - a} \quad (5.8)$$

The settlements in the columns and the untreated soil are calculated according to Equation (5.9). To ensure the stabilized soil acts as a continuum, the settlements need to fulfill $s_{column} = s_{soil}$ [Larsson, 2006]. If the settlements are not equal the stress in the columns is changed and the procedure is repeated.

$$s_{column} = \Delta h \cdot \frac{q_{columns}}{E_{columns}} \quad s_{gyttja} = \Delta h \cdot \frac{q_{gyttja}}{E_{gyttja}} \quad (5.9)$$

$s_{columns}$	Settlements of the stabilized columns [m]
Δh	Thickness of the soil layer [m]
$E_{columns}$	Elasticity modulus for the stabilized columns [MPa]
s_{soil}	Settlements of the untreated soil [m]
E_{soil}	Elasticity modulus for the untreated soil [MPa]

5.3.1 Comparison between analytical and numerical model

The analytical solution is compared to the PLAXIS 2D model in Figure 5.1, where even settlements are ensured by a stiff plate. The results are seen in Figure 5.13 for the undrained case. The LE model is modeled in Undrained C and assumes $\nu = 0.495$ and $\gamma = 0$ to comply with the undrained behavior. The numerical model generally yields much smaller settlements compared to the analytical. This is expected to be due to the generation of excess pore water pressure for the undrained calculations. As expected the HS models yield smaller settlements than MC due to the increased early stiffness showcased in section 5.2.

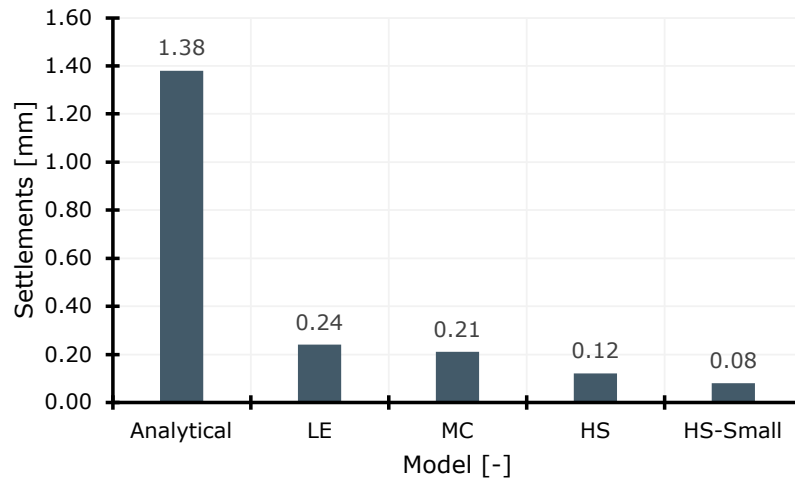


Figure 5.13. PLAXIS 2D serviceability comparison to analytical solution for the undrained case for 150 kg/m^3 .

The modeling of the drained case is seen in Figure 5.14. In this instance, the LE model is modeled as drained with $\nu = 0$ and $\gamma = 0$. It is seen that the analytical solution corresponds to the phase displacement of the LE PLAXIS model. The HS-Small model yields a reduction of the settlements compared to the traditional HS models as expected.

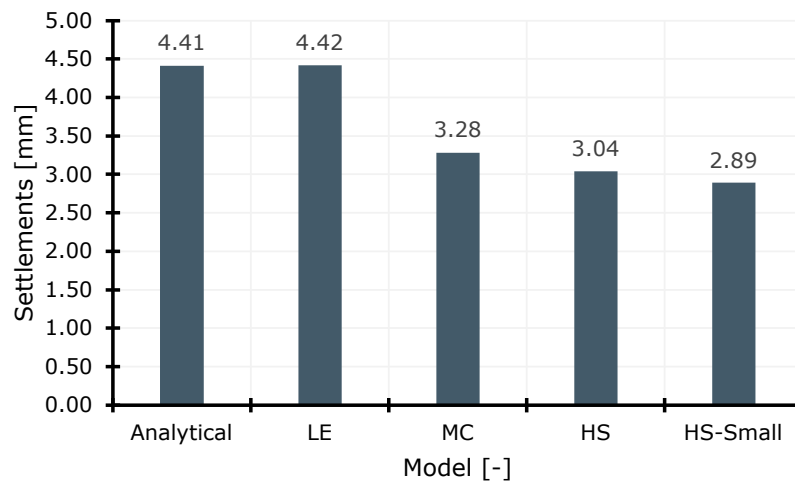


Figure 5.14. PLAXIS 2D serviceability comparison to analytical solution for the drained case for 150 kg/m^3 .

Based on the comparisons above it can be concluded that the numerical models yield smaller settlements than the analytical ones. For the drained HS case, which was deemed the best fit at low strains, the settlements are reduced by more than 30% compared to the analytical method.

5.4 Untreated scenario

This section covers the undrained and drained modeling of the untreated scenario in Figure 5.2. Throughout this chapter, the untreated scenario presented in this section will act as a baseline for the effects of cement stabilization.

5.4.1 Undrained case

The results from the serviceability (SLS) and ultimate limit state (ULS) for the untreated scenario are shown in Figure 5.15. It is seen that the settlements are very similar for HS and HS-Small, whereas MC yields significantly larger settlements as expected based on the SoilTest calibration. Furthermore, the analytical bearing capacity and the numerical bearing capacity are nearly identical. The analytical bearing capacity is evaluated by Equation (5.3) with the gyttja strength solely.

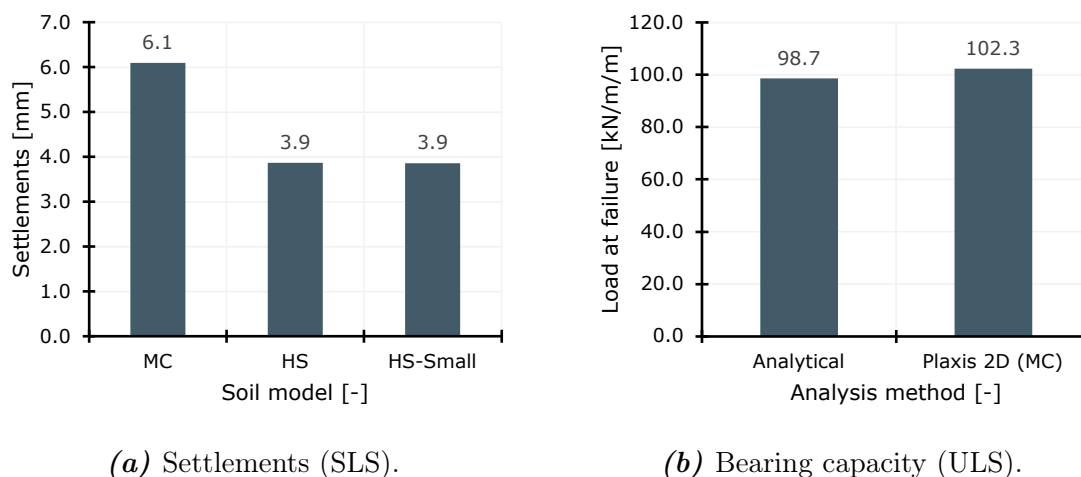


Figure 5.15. PLAXIS and analytical results from the untreated design scenario.

The failure mechanism obtained from PLAXIS is shown in Figure 5.16. The failure mechanism corresponds very well with what is expected for a shallow foundation.

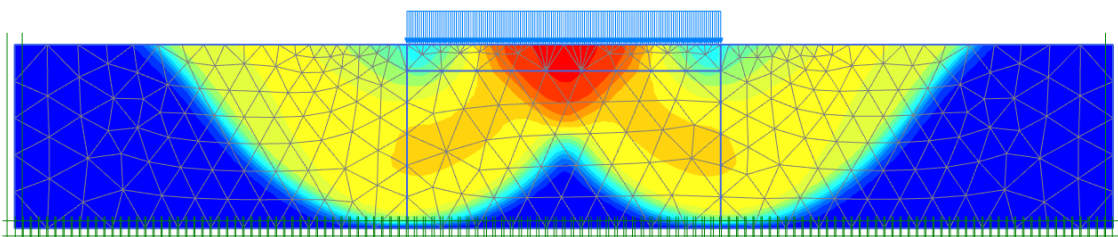


Figure 5.16. Undrained failure mechanism in PLAXIS for the untreated scenario.

5.4.2 Drained case

The results from the serviceability and ultimate limit state for the drained case are shown in Figure 5.17. The analytical settlements are based on a simple linear elastic settlement estimation by using Equation (5.9) with a gyttja stiffness of 1500 kPa. The numerical MC model yields the total settlements of the different numerical stages (e.g. installing the pavement structure) which is one reason for the MC model yielding larger settlements. If the phase displacements of the loading stage are considered the MC model yields 18.9 mm settlements, whereas the analytical formulas overestimate the settlements. The HS/HS-Small models are deemed the best fit for the calibrated CD test.

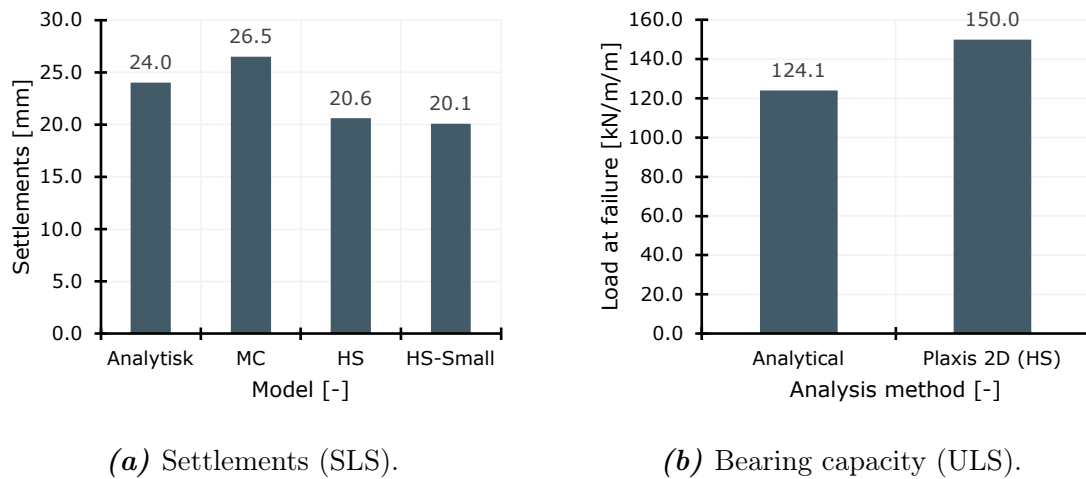


Figure 5.17. PLAXIS and analytical results from the untreated design scenario.

The failure mechanism obtained from PLAXIS is shown in Figure 5.18.

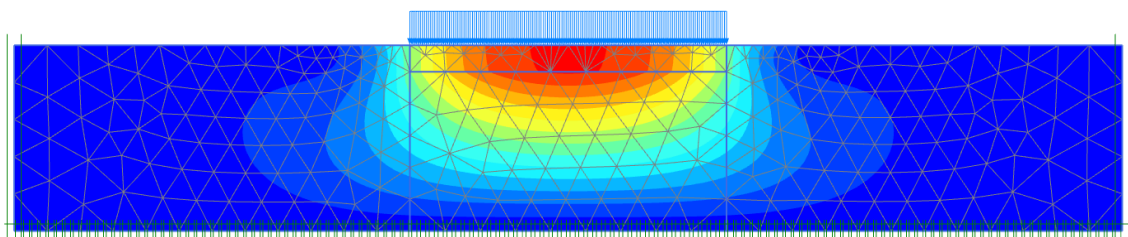


Figure 5.18. Drained failure mechanism in PLAXIS for the untreated scenario.

Based on the insignificant differences and uncertainties associated with the HS-Small model compared to the standard HS model in the previous analysis, the HS-Small model will not be considered further.

5.5 Cement stabilized base scenario

This section covers the effect of different C-C distances of the stabilized columns for the base model in Figure 5.3 and the effect of different reinforcements. Sensitivity analyses are performed on the columns and the pavement structure stiffness. The serviceability and ultimate limit state are investigated for 150 kg/m^3 and 30 kg/m^3 for the undrained and drained case. The C-C distances investigated are stated in Table 5.1.

Undrained case

The effect of the center-to-center distance on the settlements based on the material models used is shown in Figure 5.19 for the mixture containing 150 kg/m^3 . The mixed scenario with HS gyttja and MC columns is deemed to be the most reliable model since this model is based on the best calibration for both soils. Forward the mixed model will therefore be used to represent the undrained case with 150 kg/m^3 .

It is expected the constitutive modeling of the untreated soil is dominating in terms of the total settlements when only a few columns are present. This is due to the mixed model being closest to the full HS model at this point. If the gyttja is modeled as MC compared to HS the settlements increase by $\approx 50\%$.

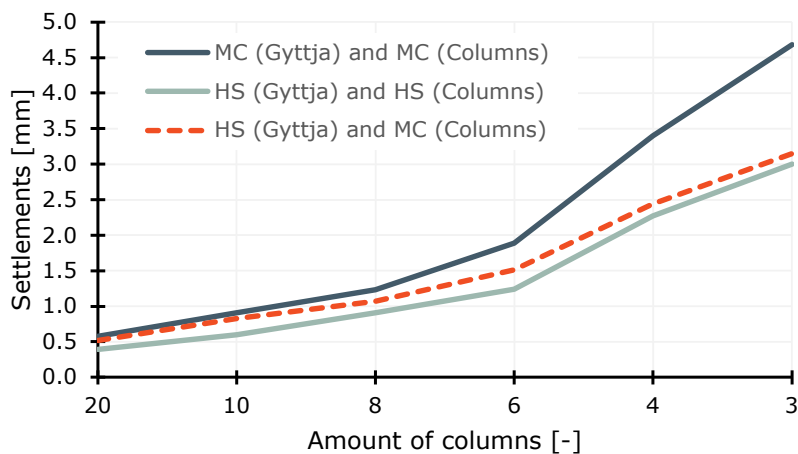


Figure 5.19. C-C effect on settlements for columns with 150 kg/m^3 . Undrained case.

The effect of the center-to-center distance of the columns on the settlements for the mixture containing 30 kg/m^3 is shown in Figure 5.20. The settlements are again very sensitive to how the soil is modeled. In this case, the mixed model is also deemed

the most reliable for the undrained case with 30 kg/m^3 , since this combination has the best fit with the CU test used for calibration.

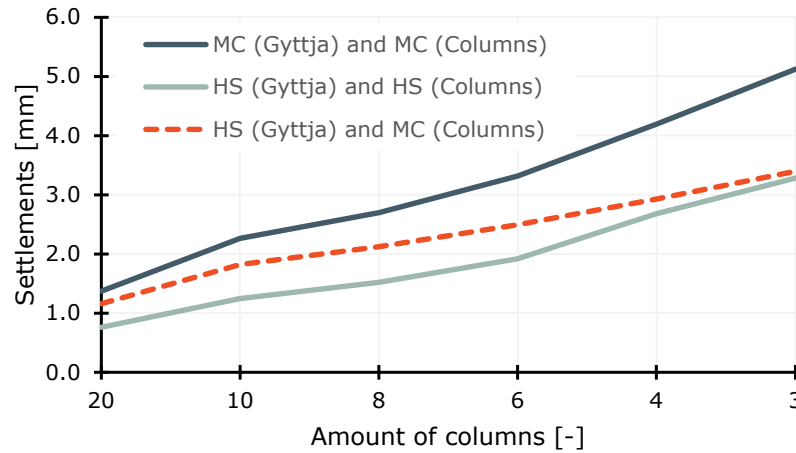


Figure 5.20. C-C effect on settlements for columns with 30 kg/m^3 . Undrained case.

The settlement reductions are evaluated according to Equation (5.10). The settlements will be compared to the untreated scenario modeled with the HS model.

$$SR = \left(1 - \frac{s_{stabilized}}{s_{untreated}} \right) \cdot 100 \quad (5.10)$$

SR	Settlement reduction [%]
$s_{stabilized}$	Stabilized scenario settlements [mm]
$s_{untreated}$	Untreated scenario settlements [mm]

The reduction in settlements compared to the untreated scenario is shown in Figure 5.21. It is seen that the mixture with 30 kg/m^3 reduces the settlements significantly compared to the 150 kg/m^3 if the cement usage is considered.

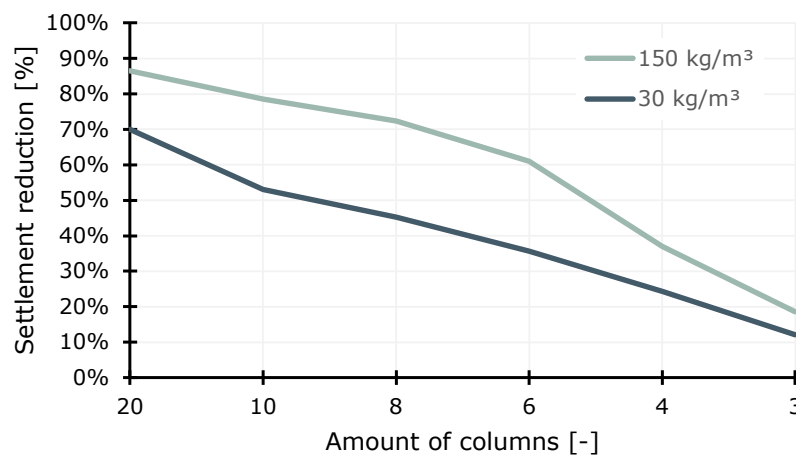


Figure 5.21. Settlement reduction in the undrained case based in the untreated HS scenario compared to mixed cement stabilized scenario.

The deformed mesh and failure mechanism for the base scenario with 6 columns is shown in Figure 5.22 and 5.23. It is seen that the failure is highly characterized by arch effects in between the stabilized columns.

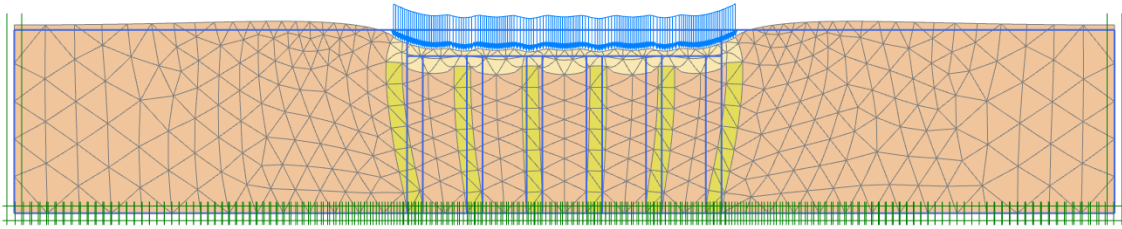


Figure 5.22. Deformed SLS mesh with 6 columns for 150 kg/m^3 (Scale x500).

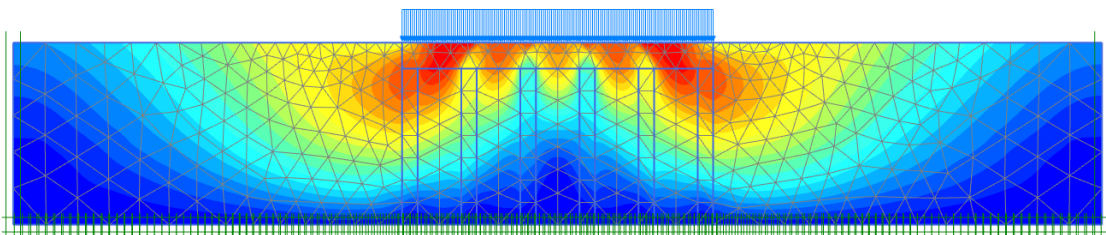


Figure 5.23. Deformation mechanism in Figure 5.22 with shading.

For the low cement content of 30 kg/m^3 it can be seen that the columns are softer, see Figure 5.24 and 5.25. In this instance, the arch effects between the columns are not quite as dominating due to a softer foundation.

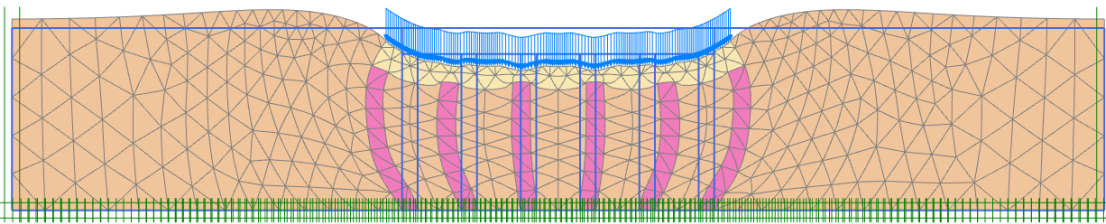


Figure 5.24. Deformed SLS mesh with 6 columns for 30 kg/m^3 (Scale x500).

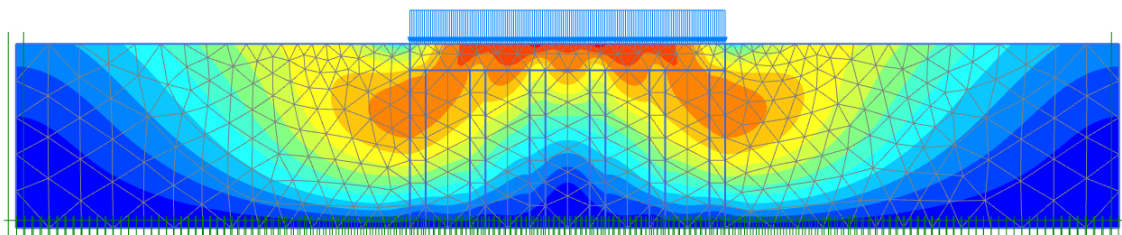


Figure 5.25. Deformation mechanism in Figure 5.24 with shading.

The bearing capacity based on difference C-C distances is seen in Figure 5.26. The bearing capacity is significantly lower than the analytical formulas suggested for the columns with 150 kg/m^3 . For this cement content, the failure stagnates due to the numerical failure mechanism beyond 6 columns. For the mixture with 30 kg/m^3 the analytical and numerical bearing capacity follow each other. However, the analytical bearing capacity is increasing faster than the numerical

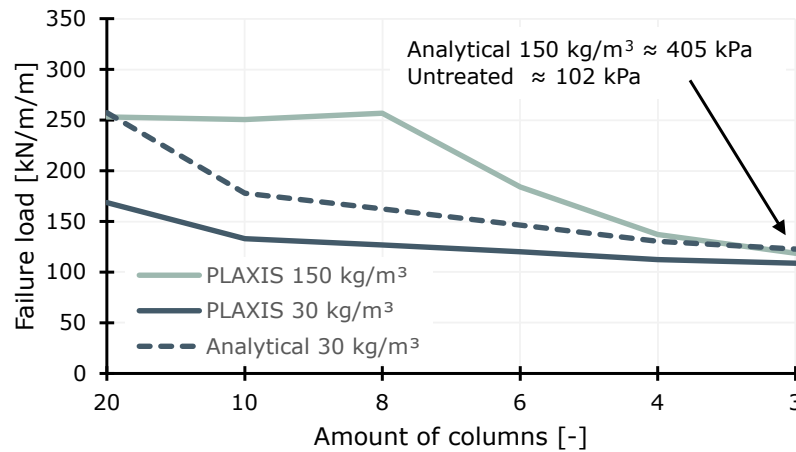


Figure 5.26. C-C effects on the undrained bearing capacity with 150 kg/m^3 and 30 kg/m^3 .

The failure mechanism for the section with 10 columns and 150 kg/m^3 is shown in Figure 5.27. The reason why the bearing capacity stops increasing at this point is that the failure mechanism changes from the expected one to the edges of the pavement structure. This issue does not affect the serviceability limit state.

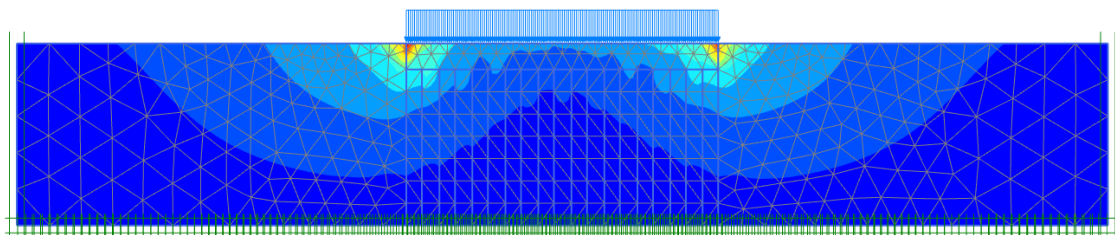


Figure 5.27. Failure mechanism for 10 columns with 150 kg/m^3 with shading.

The failure mechanism for the same section with a cement content of 30 kg/m^3 is seen in Figure 5.28. The failure mechanism for this section corresponds to what is expected, which is why it follows the analytical bearing capacity better.

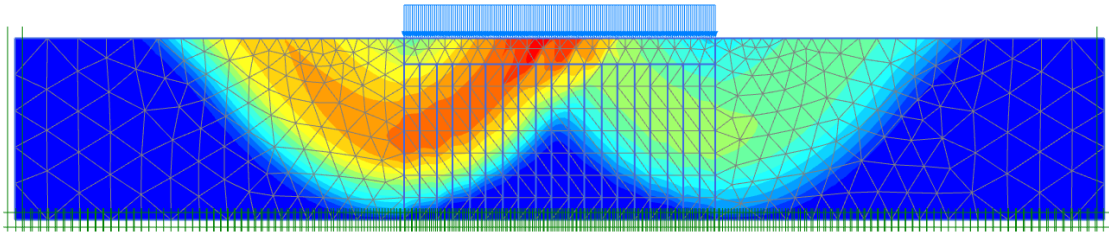


Figure 5.28. Failure mechanism for 10 columns with 30 kg/m^3 with shading.

Drained case

The settlements based on the C-C distance of the columns in the drained case are seen in Figure 5.29. The gyttja and cement stabilized columns are both modeled as HS since this was deemed the best calibration fit at low strains. Compared to the undrained case the settlements are reduced significantly faster for the columns containing 150 kg/m^3 . However, for the columns containing 30 kg/m^3 the reduction is quite similar.

It was found in section 5.3 that the analytical settlement method corresponded well to the drained case. This is why the PLAXIS results are compared to the analytical results in Figure 5.29. For the mixture with 150 kg/m^3 the analytical method is quite accurate. However, for the mixture with 30 kg/m^3 the analytical method significantly underestimates the reduction of the settlements.

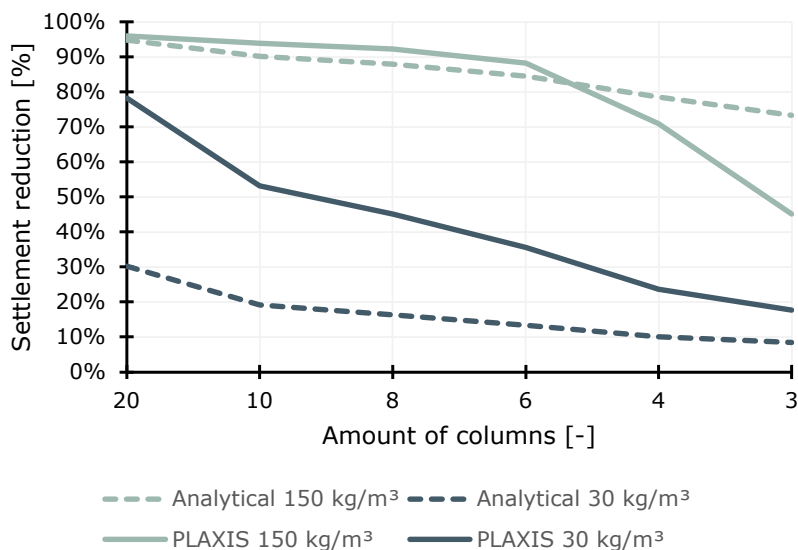


Figure 5.29. Settlement reduction in the drained case for the untreated HS scenario compared to HS cement stabilized columns with 150 kg/m^3 and 30 kg/m^3 .

The deformed mesh for the drained case with 6 columns and 150 kg/m^3 are seen in Figure 5.30 and 5.31. For the drained case the arch effects between the stabilized columns are very clear.

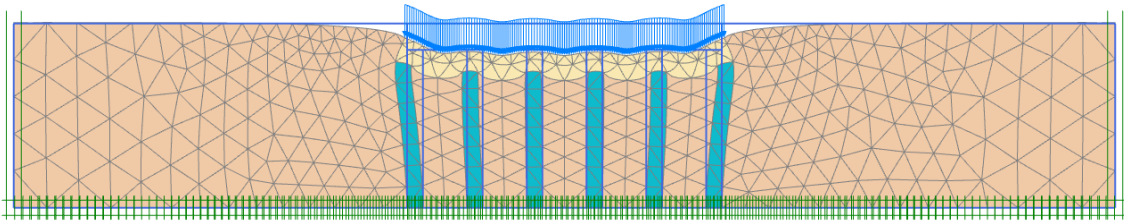


Figure 5.30. Deformed SLS mesh with 6 columns for 150 kg/m^3 (Scale x500).

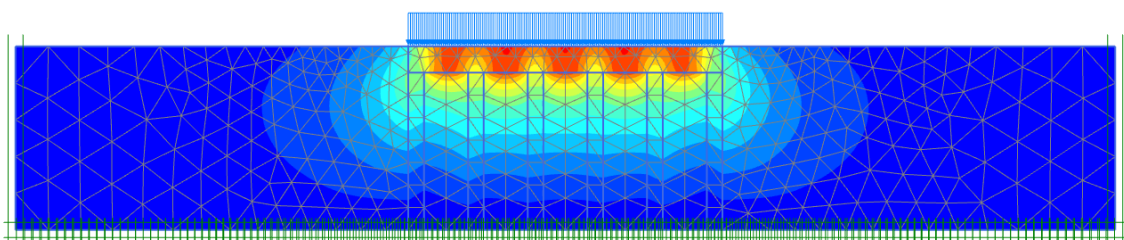


Figure 5.31. Deformation mechanism in Figure 5.30 with shading.

The deformed mesh for the drained case with 6 columns and 30 kg/m^3 are seen in Figure 5.30 and 5.31. This failure mechanism is not characterized by arch effects but is similar to the untreated scenario in section 5.4.

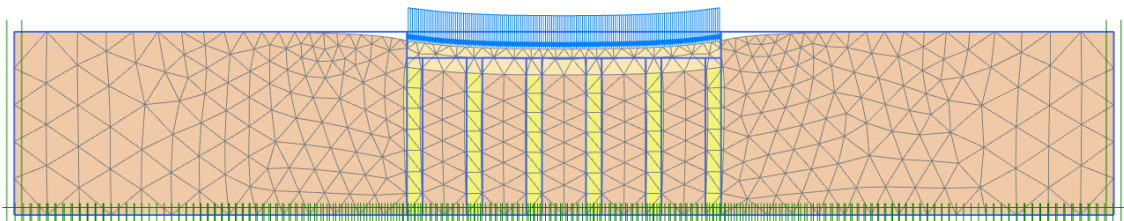


Figure 5.32. Deformed SLS mesh with 6 columns for 30 kg/m^3 (Scale x500).

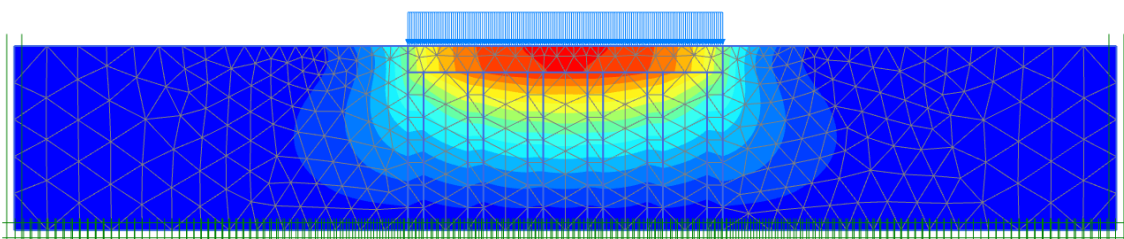


Figure 5.33. Deformation mechanism in Figure 5.32 with shading.

The bearing capacity for the drained case is seen in Figure 5.34. As for the undrained case, the results are subjected to numerical problems for the columns containing

150 kg/m³ and 30 kg/m³. For the columns containing 30 kg/m³ the bearing capacity is slightly underestimated by the analytical expression.

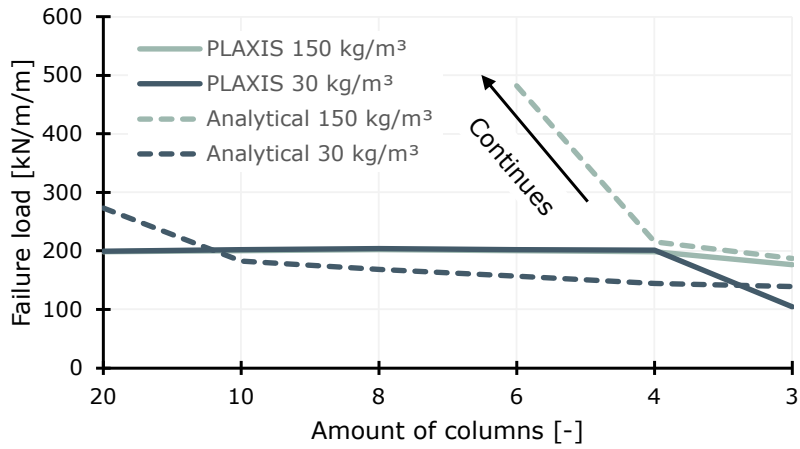


Figure 5.34. C-C effects on the drained bearing capacity with 150 kg/m³ and 30 kg/m³.

The failure mechanism for the model with 6 columns and 150 kg/m³ is seen in Figure 5.35 and 5.36. The failure occurs at the edge of the pavement structure. This failure also occurs for the 30 kg/m³ mixture.

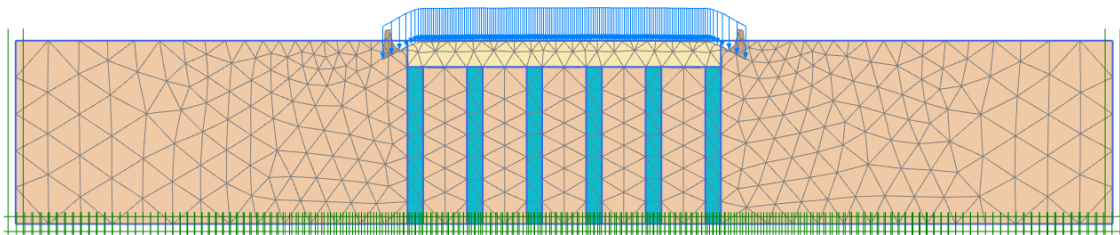


Figure 5.35. Deformed ULS mesh with 6 columns for 150 kg/m³ (Scale x500).

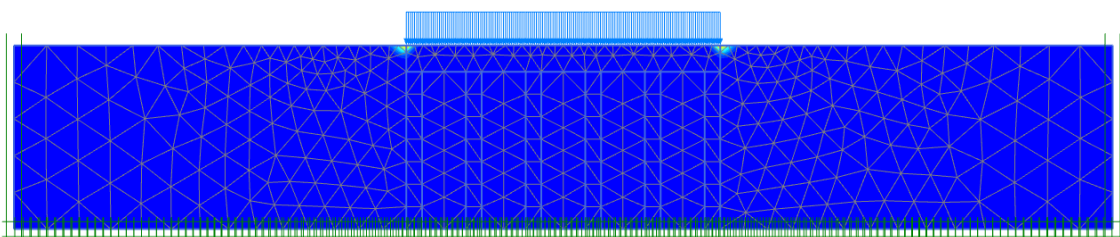


Figure 5.36. Deformation mechanism in Figure 5.35 with shading.

5.5.1 Effects of edge reinforcement

This section investigates the effects of adding extra columns on the outside of the pavement structure, see Figure 5.4. In the undrained case, this could yield lower

settlements in the SLS due to being installed in the failure pattern.

Undrained case

The effect of adding two extra columns on the outside of the pavement structure is shown in Figure 5.37. For both cement contents, there is no benefit in using the extra columns on the outer edges, compared to increasing the number of columns below the pavement structure.

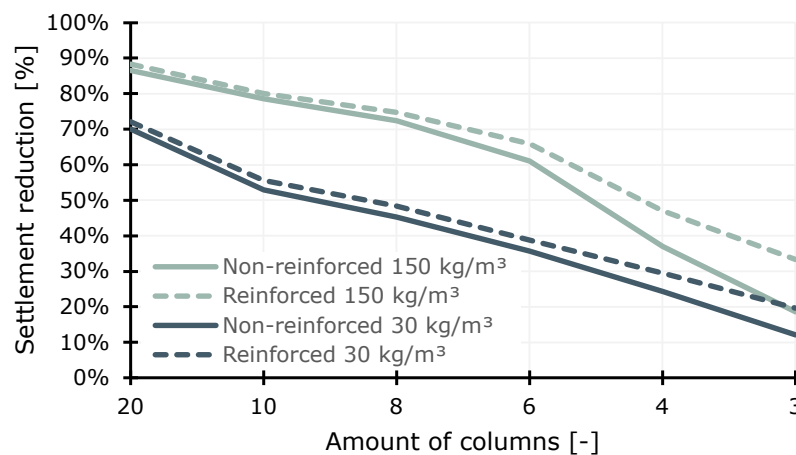


Figure 5.37. Effect of reinforced edges on the settlements. The columns used to reinforce the corners are not included in the number of columns stated.

The deformed mesh for 4 columns with 150 kg/m³ and 30 kg/m³ is shown in Figure 5.38 and 5.39. The corners might be stiffer but the arch effects are still dominating the maximum settlements of the pavement.

Evaluating the ULS with the edge reinforcement shows no significant benefits either. For the mixture with 150 kg/m³ the bearing capacity peaks at fewer columns but the numerical problems at the edges of the pavement structure still occur.

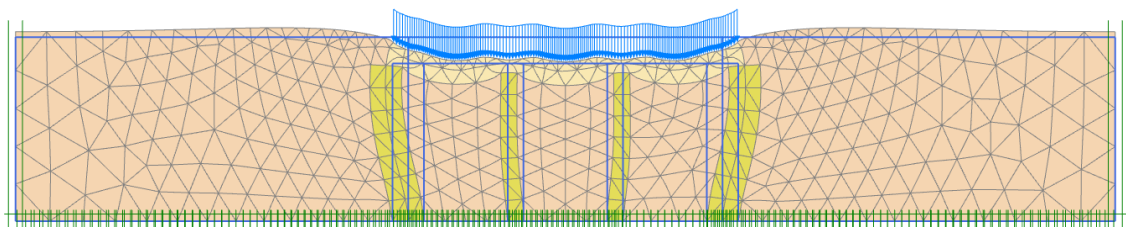


Figure 5.38. Deformed mesh for 4 columns with 150 kg/m³ and corner reinforcement (Scale x500)

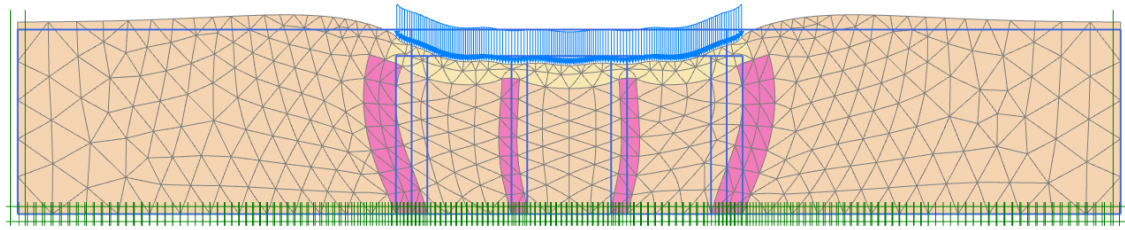


Figure 5.39. Deformed mesh for 4 columns with 30 kg/m^3 and corner reinforcement (Scale x500)

Drained case

The drained case is not evaluated with the edge reinforcement due to the deformation mechanism being changed, see Figure 5.31 and 5.33. The extra columns are therefore expected to yield insignificant changes.

5.5.2 Effects of geonet reinforcement

The effects of using geosynthetics are evaluated by Figure 5.5. This design includes two layers of geonets built into the pavement structure to reduce the settlements. The geonets are installed at the bottom and the middle of the pavement structure. The geonets are modeled as linear elastic geogrids in PLAXIS with the stiffness of 800 kN/m corresponding to maximum 2% tensile strain. The product used for reference is a Miragrid GX 110/30 geonet [TenCate Geosynthetics, 2012].

The geonets are assumed to be anchored in the gyttja beside the pavement structure. However, this might not be the case if the installation were to be performed in reality.

Undrained case

The settlements with and without geonets are shown in Figure 5.40. It is seen that there is no significant difference between having the geonets and not having the geonets. However, this could be due to the geonet not activating for the small surcharge load of 5 kPa . The difference between using and not using geonet is maximum 5%.

The deformation mechanisms with the geonet included are seen in Figure 5.41 and 5.42. Another reason for the geonet not being properly activated could be due to the

geonet being anchored inside the failure zone. The geonet is anchored 4 m outside of the pavement structure.

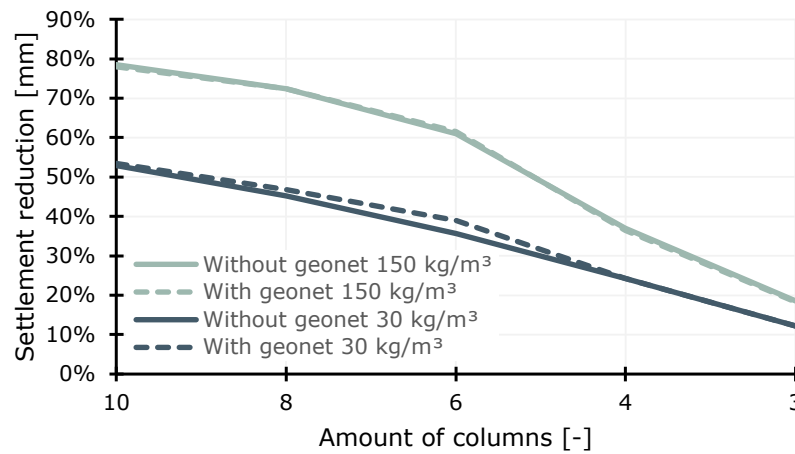


Figure 5.40. C-C effect on the settlements when geonets are used in the undrained case for 150 kg/m³ and 30 kg/m³.

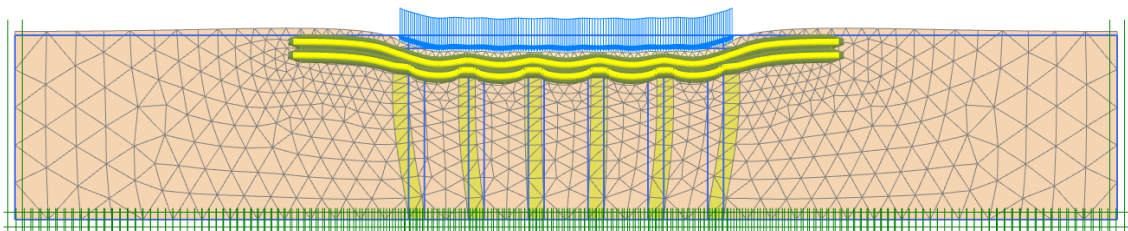


Figure 5.41. Deformed mesh for 150 kg/m³ with two geonets (Scale x500).

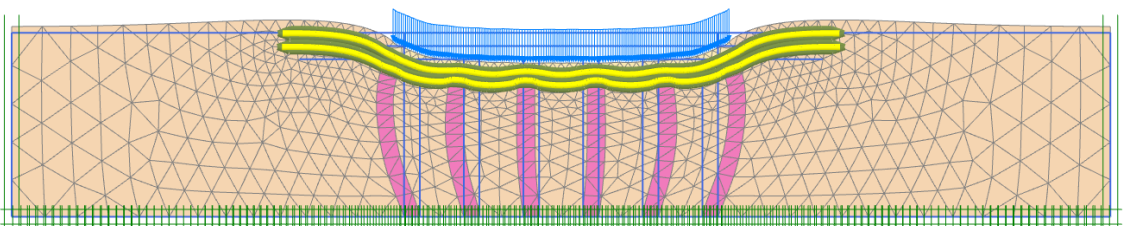


Figure 5.42. Deformed mesh for 30 kg/m³ with two geonets (Scale x500).

Drained case

The effects of using geonets in the drained case are insignificant, as for the undrained case. This strengthens the belief that the load is too small to activate the geonets. The analysis has been carried out with and without the update mesh function since this could be a reason for the geonets not activating [Bentley Systems, 2020].

5.5.3 Sensitivity of column and pavement stiffness

The sensitivity of the calculations presented prior to this section is evaluated by performing a sensitivity analysis on the stiffness of the stabilized columns and the pavement structure. If the columns were to be installed in the field varying strength and stiffness parameters are to be expected. The influence of varying stiffness parameters is investigated by modeling the columns as MC. This reduces the need for changing multiple stiffness parameters at once since the MC model only has one stiffness input parameter. The input parameters for the sensitivity analysis are not included in Appendix D.

Undrained case

The sensitivity analysis is performed on the base scenario in Figure 5.3 with 10 and 6 stabilized columns. These two sections yield a significant settlement reduction and are assumed to be valid options in reality. The results from the sensitivity analysis are shown in Figure 5.43. The black boxes represent the stiffness currently used.

The results in Figure 5.43 both follow a logarithmic trendline, whereas a lower stiffness increases the sensitivity to changes. A stiffness reduction of e.g. 20 MPa for the columns with 150 kg/m³ would not yield any significant changes compared to slight changes in the stiffness for the columns containing 30 kg/m³.

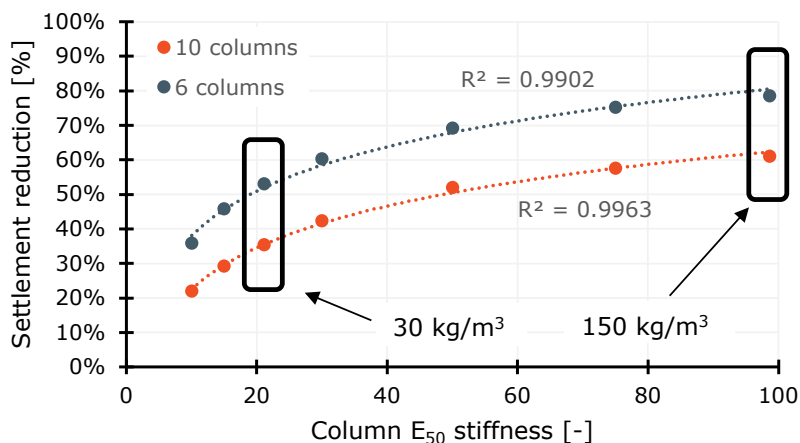


Figure 5.43. Undrained sensitivity analysis on cement stabilized column stiffness.

The sensitivity of the stiffness for the pavement structure is only investigated for the section with 6 stabilized columns, see Figure 5.44. The sensitivity of the pavement

structure also follows a logarithmic trendline. However, the stiffness of the pavement structure is not as sensitive as the columns. The stiffness used is therefore not very influential on the results in the undrained case. The stiffness could potentially be more sensitive for fewer columns since a lower stiffness could increase the arch effects between the columns.

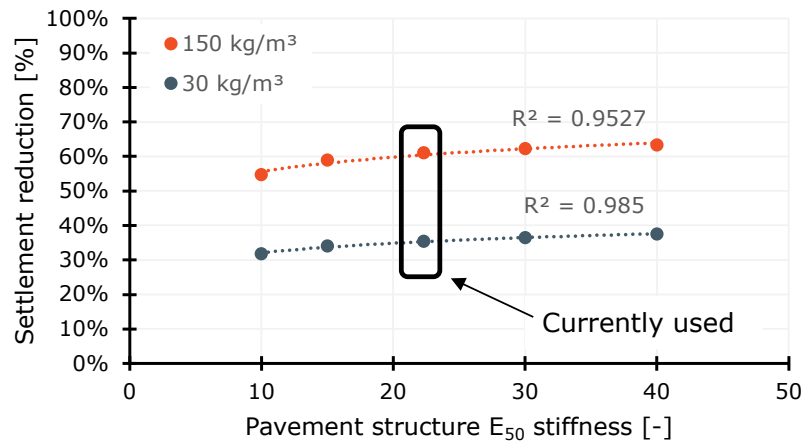


Figure 5.44. Sensitivity analysis on the pavement structure stiffness with 6 stabilized columns in the undrained case.

Drained case

The sensitivity of the columns is investigated for 10 and 6 columns in the drained case as well. As in the undrained case the columns are modeled as MC and the untreated gyttja is modeled as HS. The results from the sensitivity analysis for the drained case are seen in Figure 5.45. As for the undrained case, the columns with 30 kg/m³ are very sensitive to a change in stiffness.

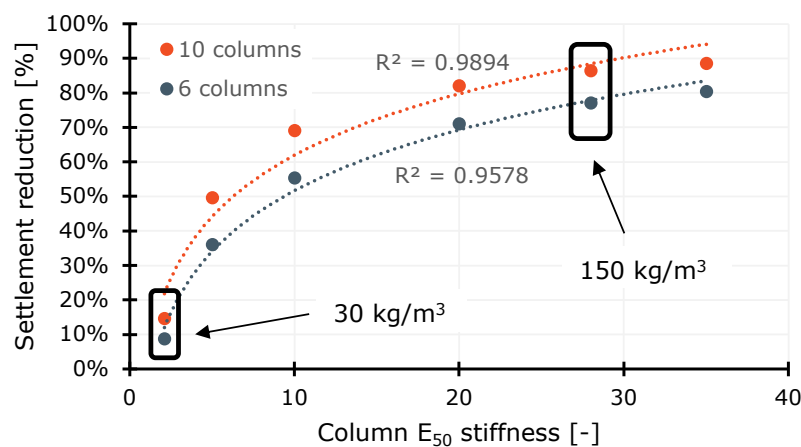


Figure 5.45. Drained sensitivity analysis on cement stabilized column stiffness.

As in the undrained case, the sensitivity of the stiffness of the pavement structure does not influence the results significantly, see Figure 5.46. The low settlement reduction for the 30 kg/m³ mixture is due to the columns being modeled as MC. The calibration showed that MC columns yielded larger settlements than HS columns, see Figure 5.2.

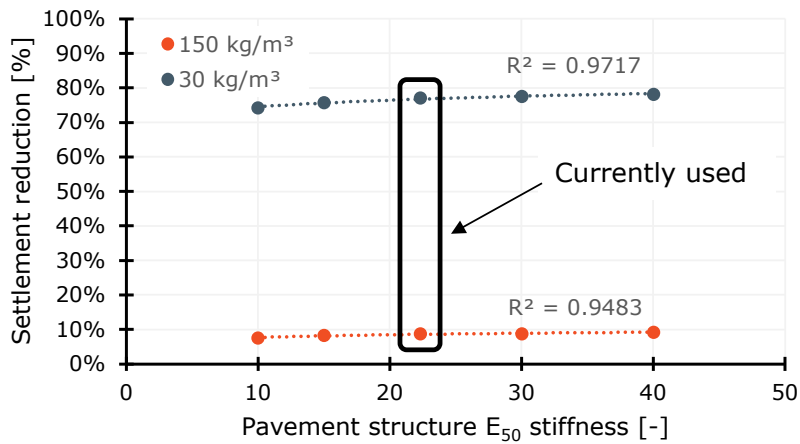


Figure 5.46. Sensitivity analysis on the pavement structure stiffness with 6 stabilized columns in the drained case.

5.5.4 Sensitivity of surcharge load

When cement stabilization is used in other Scandinavian countries it is common for e.g. roads to be built on top of a sand embankment. The embankment yields a higher load which could affect the results presented. To simulate the effects of building an embankment the load is increased with 60 kPa, which can be simplified to a 3 m high sand embankment. By increasing the load instead of modeling the embankment, stability issues and the need for extra columns below the slopes of the embankment are not considered. However, if the embankment were to be built or modeled there would be no need for constructing the pavement structure in the terrain, which presumably would resolve the numerical edge problems.

Increasing the load is also expected to represent the effects of increasing the thickness of the gyttja layer. This is due to the strains increasing in both scenarios, hence showing the general effect.

Undrained case

The results from increasing the load to 65 kPa from 5 kPa for the scenario in Figure 5.3 are shown in Figure 5.47. It is seen that the settlements are reduced even further when the load is increased. This is presumably due to the columns' linear elastic stiffness compared to the untreated soil's hyperbolic stiffness. The untreated scenario yielded 63.4 mm for the 65 kPa load.

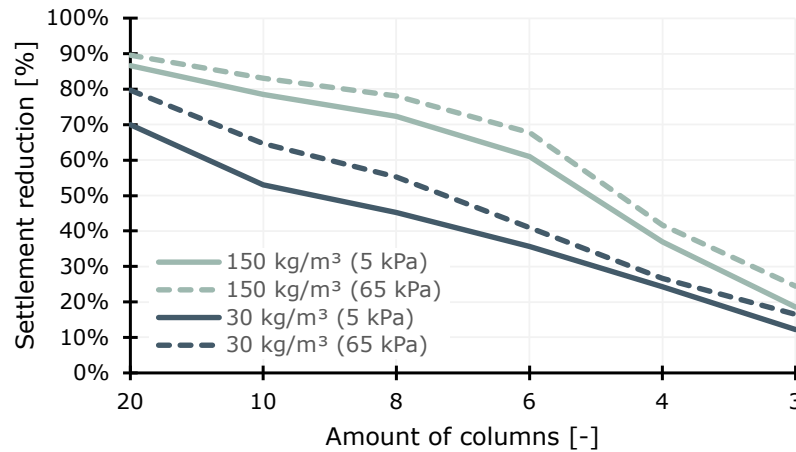


Figure 5.47. C-C effects on settlements for a load of 5 kPa and 65 kPa in the undrained case for both cement contents.

The normalized calibration for the untreated gyttja and the cement stabilized columns with 150 kg/m³ in the undrained case is seen in Figure 5.48. The effect of the stabilized columns' stiffness increases as the strains on the strain-stress curve increase.

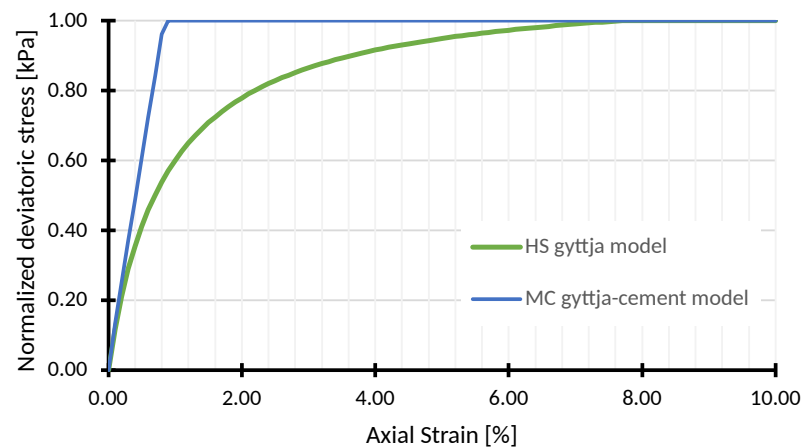


Figure 5.48. Calibrations used during the undrained calculations for the scenario with 150 kg/m³ columns.

The models with geonets included were also subjected to the higher load of 65 kPa. The changes are deemed insignificant.

Drained case

The results from increasing the load to 65 kPa from 5 kPa in the drained case are shown in Figure 5.49. It is seen that the settlement reduction is reduced significantly. The columns are therefore more effective in the drained case when the load is lower.

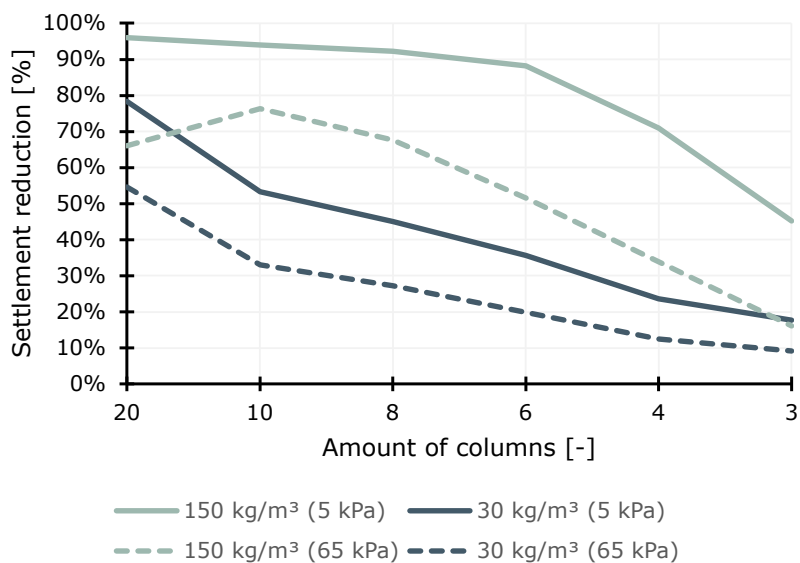


Figure 5.49. C-C effects on settlements for a load of 5 kPa and 65 kPa in the drained case for both cement contents.

The normalized calibration for the untreated gyttja and the cement stabilized columns with 150 kg/m³ in the drained case is seen in Figure 5.50. One factor influencing the magnitude of the reduced settlements for the increased load is that the stiffness of the columns decreases significantly when the strains increase.

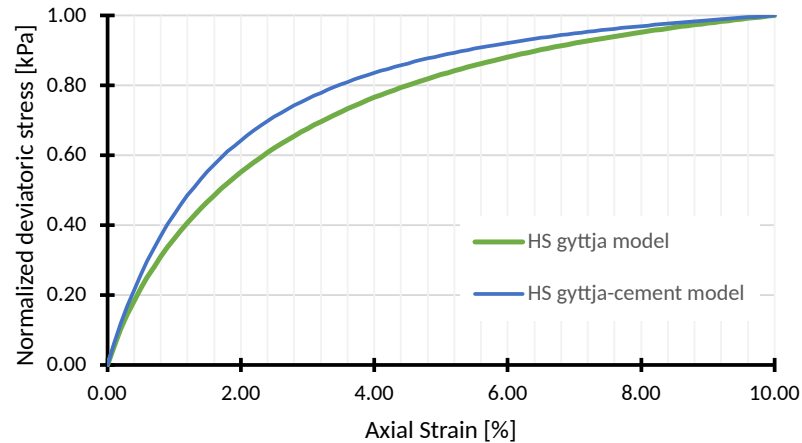


Figure 5.50. Calibrations used during the drained calculations for the scenario with 150 kg/m^3 columns.

The increase in surcharge load ensures a slightly better activation of the geonets used in section 5.5.2. The load increase to 65 kPa from 5 kPa yields up to 10 % lower settlements compared to the scenario without geonets, see Figure 5.51. However, the columns containing 30 kg/m^3 are still not affected by the use of geonets.

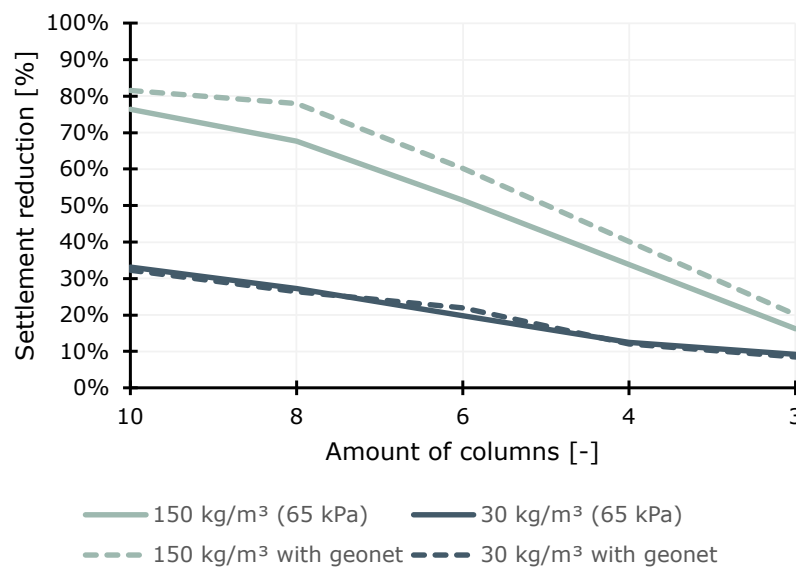
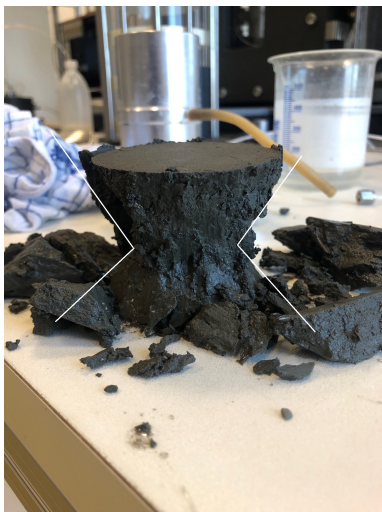


Figure 5.51. Effects of using geonets for the increased of 65 kPa in the drained case.

This chapter seeks to discuss some of the main topics throughout the thesis. Furthermore, ideas for further research are presented.

6.1 Triaxial test dimensions

Based on Ibsen et al. [2012] single-height triaxial tests were used to evaluate the effects of adding FutureCem cement to Aalborg gyttja. Using single-height triaxial specimens should yield a more homogeneous stress and strain field and avoid the development of shear bands. However, it was not possible to obtain a homogeneous stress and strain field, partly due to the porous discs used as end plates. The failure mechanisms observed are seen in Figure 6.1. The shear band failure was only observed for one test.



(a) Rough end plates failure mechanism.



(b) Shear band failure mechanism.

Figure 6.1. Failure mechanism of specimens with 150 kg/m^3 after CU test.

In the geotechnical industry, double-height triaxial tests are usually the standard. To investigate the difference between single-height and double-height triaxial tests a double-height CU triaxial test with 150 kg/m^3 and 7 days of curing was performed.

The comparison of the stress-strain curve for the single-height and double-height tests is seen in Figure 6.2. The observations correspond to what was observed in Ibsen et al. [2012], where the stress-strain curve is shortened and the peak strength is larger. The shortening in the stress-strain curve is due to the shear band failure for the $H/D = 2$ specimen, whereas the strains in the failure zone are unknown. The pore pressure for each test is seen in Figure 6.3. No significant difference between the two specimens is observed. The $H/D = 2$ CU test is not included in the Appendix.

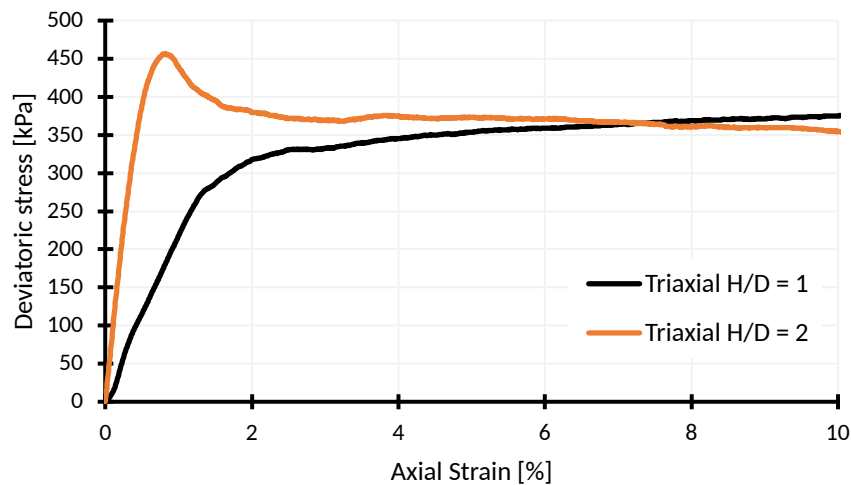


Figure 6.2. Comparison of stress-strain curve for different H/D ratios with 150 kg/m^3 .

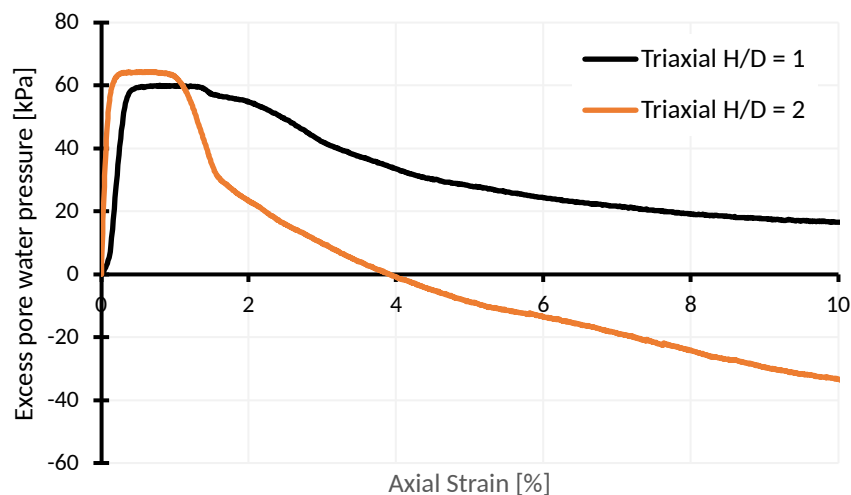


Figure 6.3. Comparison of excess pore water pressure for different H/D ratios with 150 kg/m^3 .

When feasibility studies on soil stabilization are carried out in Sweden and Norway uniaxial compression tests are usually used to evaluate the strength and stiffness

gain. The uniaxial tests are accompanied by prior experience and knowledge. The triaxial tests with different H/D ratios are compared to a uniaxial compression test from Tanderup [2022] with 150 kg/m^3 FutureCem cement and 7 days of curing without a pre-load in Figure 6.4. It is seen that the uniaxial test overestimates the strength significantly compared to the triaxial tests. Due to the low failure strain for the uniaxial test, the stiffness is also quite high. It can therefore be concluded that the strength and stiffness gain are highly affected by the test methodology used. Caution should therefore be taken when using e.g. uniaxial compression tests since these can deviate significantly from triaxial tests.

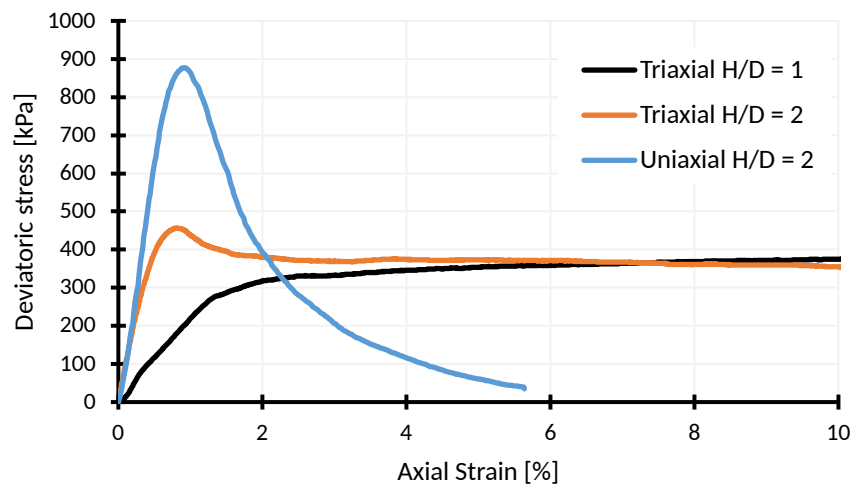


Figure 6.4. Comparison of stress-strain curve for different compression tests with 150 kg/m^3 and a curing period of 7 days.

6.2 Small versus large amounts of binder

To investigate the effect of using small and large amounts of binder several advanced laboratory tests were carried out using a cement content of 150 kg/m^3 and 30 kg/m^3 . The primary tests performed to assess the strength and stiffness gain were CU and CD triaxial tests. The undrained shear strength development was described best with the Modified Mitchell formula where $K = 70$ was reduced to $K = 18$, see Equation (6.1).

The undrained shear strength was $\approx 50 \text{ kPa}$ for the 30 kg/m^3 mixture and $\approx 420 \text{ kPa}$ for the 150 kg/m^3 mixture after 28 days. Increasing the binder amount by a factor of 5, therefore, increases the undrained shear strength by a factor of 8.4.

$$C_u = C_{u(d_0)} + (15 \cdot C) \cdot \log\left(\frac{d}{d_0}\right) \quad (\text{Modified Mitchell}) \quad (6.1)$$

The undrained secant stiffness correlated to the undrained shear strength according to Equation (6.2) and (6.3). It is seen that the low cement content has a significantly larger undrained stiffness development.

$$E_{u50} \approx 300 \cdot C_u \quad (30 \text{ kg/m}^3) \quad (6.2)$$

$$E_{u50} \approx 210 \cdot C_u \quad (150 \text{ kg/m}^3) \quad (6.3)$$

For the drained case the high cement content yielded the largest stiffness increase, see Equation (6.4) and (6.5). The low cement content only yielded a drained secant stiffness a factor 1.4 larger than for the SoilTest calibration of the untreated gyttja.

$$E_{50} \approx 55 \cdot C_u \quad (30 \text{ kg/m}^3) \quad (6.4)$$

$$E_{50} \approx 110 \cdot C_u \quad (150 \text{ kg/m}^3) \quad (6.5)$$

The settlement reduction for the untreated scenario based on the cement content and center-to-center distance for the columns is seen in Figure 6.5. The serviceability load of 5 kPa is used. It is seen that high cement content results in the largest reduction in settlements. However, the low cement content of 30 kg/m³ still reduces the settlements significantly.

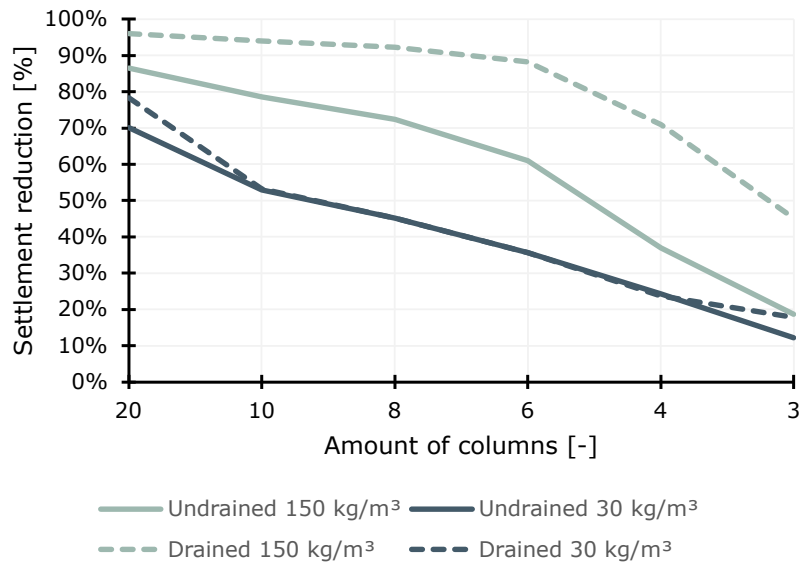


Figure 6.5. Settlement reduction for the drained and undrained case.

If the cement content for the designs in Figure 6.5 is considered there is a significant difference between the two binder amounts, see Figure 6.6. The low cement content

yields a settlement reduction of 70 % compared to 35 % for the high cement content for the same material use.

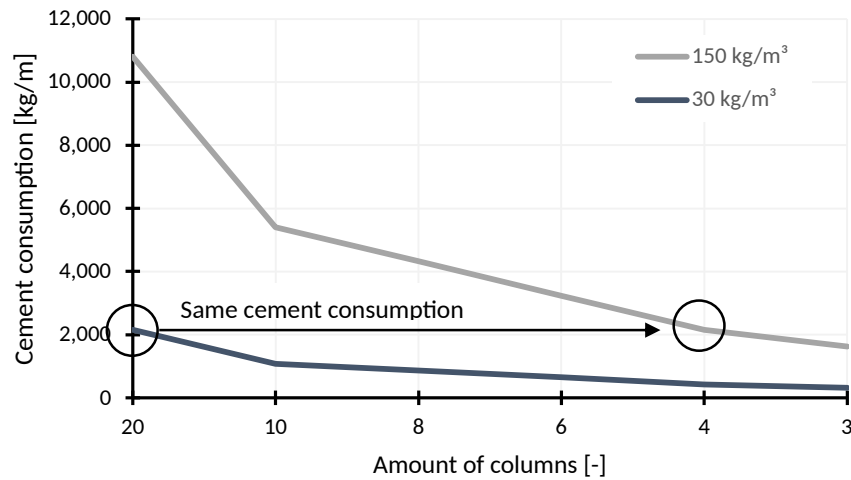


Figure 6.6. Cement usage versus the amount of stabilized columns.

Further effects of adding the FutureCem cement to the untreated gyttja, besides a significant strength and stiffness development, are changes in pH value and Atterberg Limits. For the high cement content, the pH increased beyond 12, which should ensure long-term strength and stiffness development [Al-Jabban, 2019]. The consistency became close to non-plastic after 28 days of curing. The pH value for the low cement content decreased below 10, whereas the long-term properties are expected to be less significant [Al-Jabban, 2019]. The Atterberg Limits for the low cement content did not show significant changes compared to the untreated gyttja.

As described above using a low cement content can yield a significant reduction in cement consumption and can therefore be highly beneficial. However, the uncertainties also increase since the long-term strength development is expected to be insignificant. It was found in chapter 5 that the sensitivity of the stiffness for the columns with 30 kg/m³ were much more sensitive than the ones with 150 kg/m³. Performing the stabilization with 30 kg/m³ are therefore also more risky.

6.3 The use of numerical models versus analytical

Cement stabilization is commonly evaluated by the use of analytical methods. Analytical methods often rely on simplified assumptions dictating the failure/deformation mechanism. When using cement stabilization the serviceability limit state

is evaluated by a simple linear elastic approach where the stabilized columns and the untreated soil is set to move as one continuum, hence yielding equal settlements. If these assumptions were complied with in PLAXIS, the analytical and numerical results were in agreement for the columns containing 150 kg/m^3 , see Figure 6.7. However, when using other material models than Linear Elastic (LE with $\gamma_{sat} = \gamma_{unsat} = 0$ and $\nu' = 0$) the settlements started to deviate from the analytical.

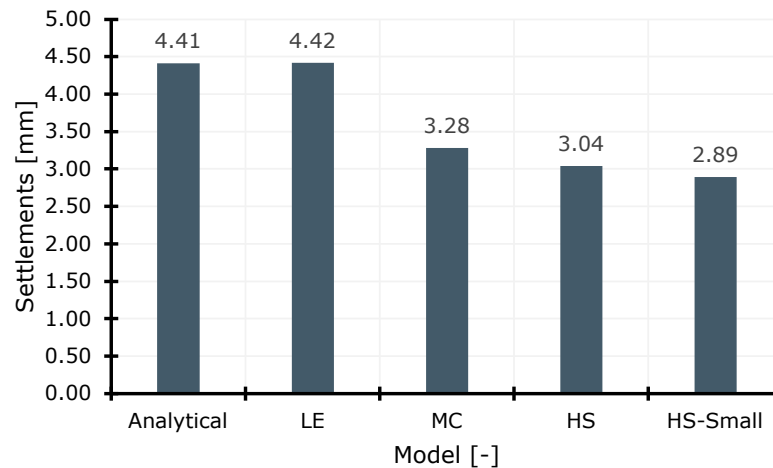


Figure 6.7. Comparison between PLAXIS and analytical SLS for the drained case.

The analytical method is compared to a more realistic scenario with a pavement structure on top of the stabilized area instead of a stiff plate in Figure 6.8. When the foundation is stiffer the analytical results yield a good fit with the numerical. However, when the stiffness of the columns decreases, as for the 30 kg/m^3 mixture, the analytical method yielded significantly larger settlements than the numerical.

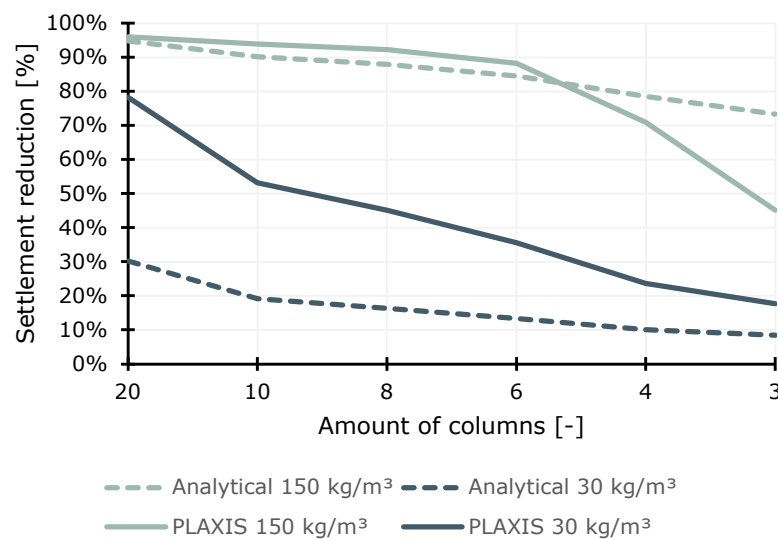


Figure 6.8. Settlement reduction in the drained case for PLAXIS and analytical.

The analytical method used to estimate the bearing capacity in the ultimate limit state is based on the general bearing capacity formula with an increased strength based on the stabilization ratio. The correlation between the analytical and numerical methods is seen in Figure 6.9 for the undrained case. For both cement contents, the bearing capacity is overestimated, especially for the high cement content. The bearing capacity for the high cement content stops increasing at 8 columns due to numerical problems.

The observation for the drained case was similar, even though the bearing capacity was slightly underestimated for the columns containing 30 kg/m^3 .

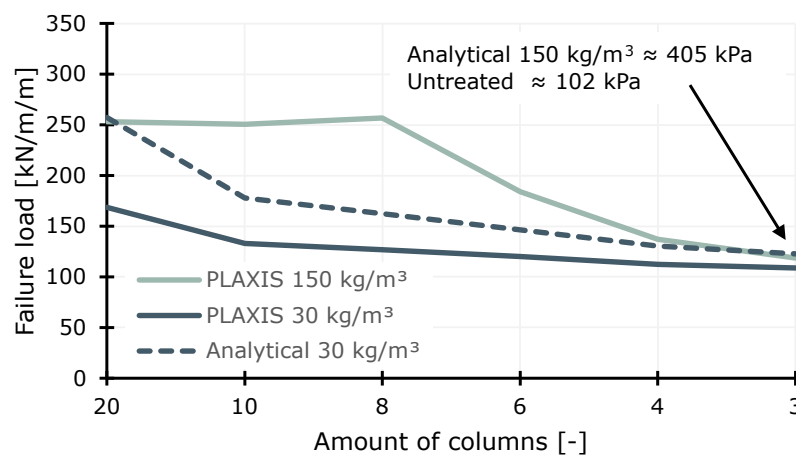


Figure 6.9. Bearing capacity with 150 kg/m^3 and 30 kg/m^3 for the undrained case.

Based on the numerical and analytical comparisons above, it is seen that numerical software can optimize a project's design. By using PLAXIS the 30 kg/m^3 mixture becomes a more viable option, since the settlements are significantly lower for the numerical models compared to the analytical. However, it is important to consider the effect of different input parameters in PLAXIS, to ensure that the model corresponds to reality.

For this thesis, the effects of the input parameters were studied using the SoilTest module in PLAXIS. The effect of using the raw small strain stiffness of 163.6 MPa compared to the calibrated input of 40 MPa is seen in Figure 6.10. If the raw data were used without the SoilTest check the settlements would be significantly reduced in the drained case. Furthermore, it is seen that the constitutive model with the best-fit changes depends on the magnitude of the deviatoric stresses. This emphasized the importance of using correct constitutive models to simulate soil behavior.

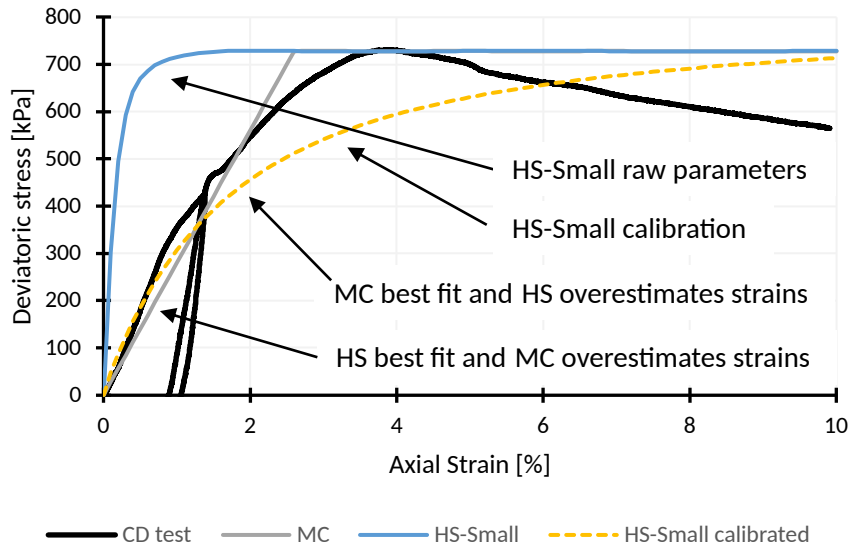


Figure 6.10. PLAXIS SoilTest calibration of drained 150 kg/m³ mixture. The HS-Small calibration is visually identical to not included HS raw.

It was found in chapter 5 that the columns were very sensitive to their stiffness. Regardless of using numerical or analytical models, it is therefore important to consider how the stiffness parameters are obtained. Since the analytical method corresponds to the drained case, the stiffness should be obtained from CD triaxial tests. However, the Scandinavian standard is using uniaxial compression tests. But as described in section 6.1 the uniaxial stiffness is much larger than the triaxial. Furthermore, the uniaxial tests are undrained, whereas the stiffness is expected to be significantly larger than for a drained test, see section 6.2. The normalized settlements based on different stiffness' from different tests are seen in Figure 6.11 based on the analytical method from Larsson [2006]. The gyttja stiffness is set to 1.5 MPa and the other stiffness are 113.0 MPa, 90.9 MPa, 22.3 MPa and 24.7 MPa. The settlements increase 417% when using the CD stiffness instead of uniaxial.

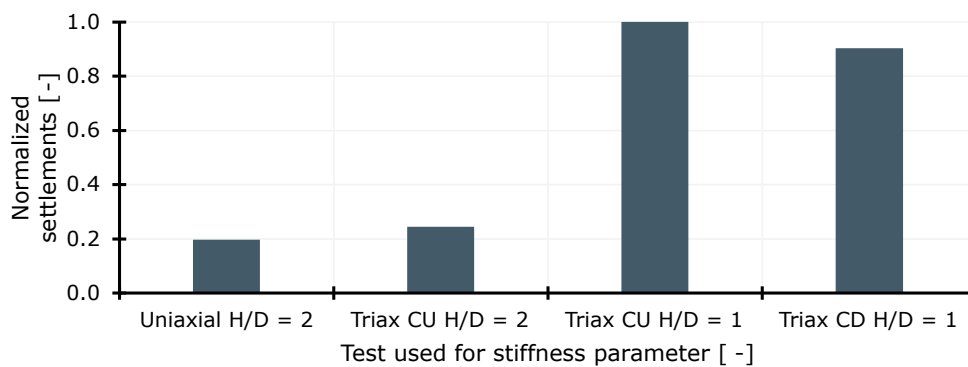


Figure 6.11. Cement stabilized settlements based on test stiffness used.

The large increase in settlements when using the correct stiffness from the CD triaxial test, emphasizes the importance of how the stiffness is obtained. The stiffness is generally much larger for the uniaxial test or the double-height triaxial test. All specimens used for the comparison in Figure 6.11 contain 150 kg/m^3 and have cured for 7 days. The uniaxial test is from Tanderup [2022].

6.4 Sustainability evaluation

In the introduction, cement stabilization was compared to mass exchange and a piled foundation in terms of CO_2 emission. If the target settlement reduction is set to 50% for the cement stabilized solutions the CO_2 emission for cement stabilization, compared to mass exchange, is seen in Figure 6.12. It is seen that the low cement content is less emissive after a transportation distance of approximately 15 km. However, as emphasized earlier the columns containing 30 kg/m^3 are especially sensitive to deviations in stiffness, hence the solution is associated with a higher risk. If the columns containing 150 kg/m^3 are used, the transportation distance needs to be beyond 50 km.

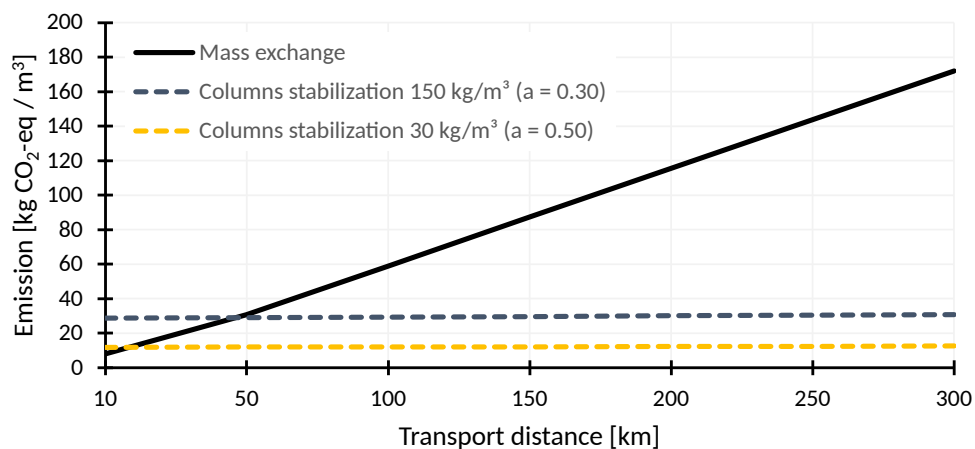


Figure 6.12. Comparison of CO_2 emission from mass exchange for cement stabilization with a target settlement reduction of 50%.

The CO_2 emission for a transport distance of 50 km is evaluated in terms of staged emission in Figure 6.13. For the mass exchange solution, the emission is nearly solely based on transportation. For the stabilization solution with 30 kg/m^3 , the installation covers a significant amount of the total emission, compared to the solution with 150 kg/m^3 . A less emissive installation procedure would therefore decrease the CO_2 emission substantially when using small amounts of cement.

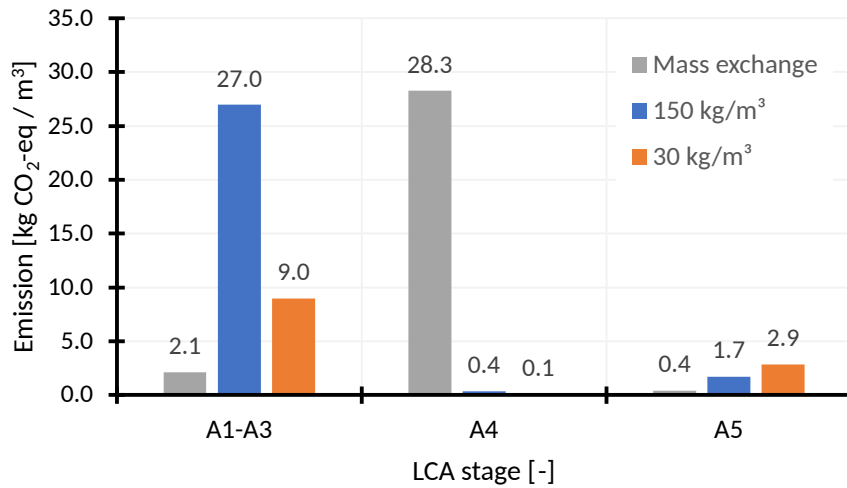


Figure 6.13. Break down of LCA stages from Figure 6.12 for a transport distance of 50 km.

The CO₂ emission from stage A1-A5 is compared to the amount of columns and the cement consumption in Figure 6.14. Even though the installation procedure is highly emissive, the use of small amounts of binder can still be very beneficial for lowering the CO₂ emission.

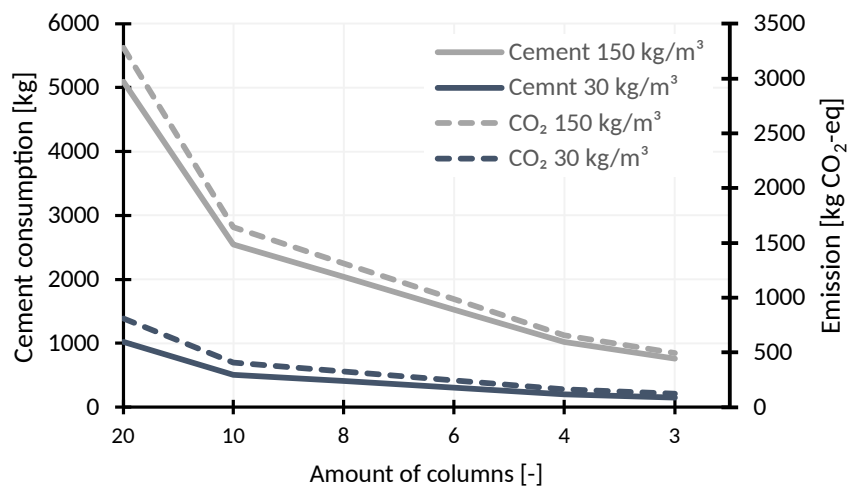


Figure 6.14. Comparison of CO₂ emission based on amount of columns installed.

Since the numerical models are based on plane strain, it is not possible to compare cement stabilization directly to a piled foundation. Based on the findings in chapter 5 it is expected that the columns containing 150 kg/m³ can be directly substituted with concrete piles due to the high stiffness increase. The concrete piles are expected to be longer than the stabilized columns, due to drag-down effects for the piles, whereas the substitution presumably can yield a lower CO₂ emission. To conclude

whether cement stabilization is a less emission solution compared to reinforced concrete piles 3D calculations have to be carried out. This will also reveal whether the low cement content is a potential substitution.

6.5 Further research

This section presents possible ideas for further research in the field of cement stabilization field.

6.5.1 Laboratory correlations to the field

Cement stabilized laboratory cast specimens were evaluated in chapter 4 to quantify the strength and stiffness gain. However, the correlations between the field installations and laboratory specimens are unknown. To investigate this correlation full-scale models could be installed in the field where intact specimens and CPTs could be utilized to establish the correlation. The intact specimens could be subjected to triaxial tests for calibration purposes.

Field tests could also involve the correlation between the shear wave velocity and the undrained shear strength. In chapter 4 CU triaxial tests and bender element test revealed the correlations in Equation (6.6) and (6.7).

$$C_u \approx 3.03 \cdot V_s - 311 \quad (30 \text{ kg/m}^3) \quad (6.6)$$

$$C_u \approx 2.84 \cdot V_s - 519 \quad (150 \text{ kg/m}^3) \quad (6.7)$$

Before performing field tests a sensitivity study of the undrained shear strength and shear wave velocity could be performed. It is expected that there will be some deviations in the parameters based on e.g. the casting procedure. Especially because the cyclic triaxial test for the 30 kg/m³ mixture yielded a larger shear modulus than found by the bender element tests.

6.5.2 Curing periods beyond 28 days

Curing periods of 7, 14, 21, and 28 days were investigated in this thesis. Further research could be investigating the influence of curing periods beyond these. The

pH value for the 150 kg/m^3 mixture suggested a good long-term development in strength, while the pH value for the mixture with 30 kg/m^3 suggested low long-term chemical reactions based on studies in Al-Jabban [2019].

6.5.3 Numerical modeling in 3D

The numerical modeling in PLAXIS 2D revealed some significant improvements, compared to the analytical method commonly used. This was especially the case for the mixture containing 30 kg/m^3 where the analytical model yielded significantly larger settlements, see Figure 6.8.

For the majority of the analysis arch effects were deemed critical for the settlements, especially for the drained case. If PLAXIS 3D were used instead of PLAXIS 2D the coverage ratio could probably be reduced even further. Due to the plane strain effects in PLAXIS 2D the grid pattern and mass stabilization could only be investigated. If PLAXIS 3D were to be used the grid pattern could be investigated. This could reveal a design with a lower CO_2 emission. This could also reveal whether cement stabilization could be a sustainable substitution for reinforced concrete piles.

Another subject to investigate with numerical modeling is the effect of different consolidation stresses for the CU and CD tests. An effective consolidation stress of 30 kPa was investigated in this thesis. This could e.g. be an effective consolidation stress of 100 kPa , which corresponds better to greater depths. Performing multiple CD triaxial tests at different effective stresses could also be used to derive the correct $\text{power}(m)$ value for the HS soil model in PLAXIS.

6.5.4 Other types of soil

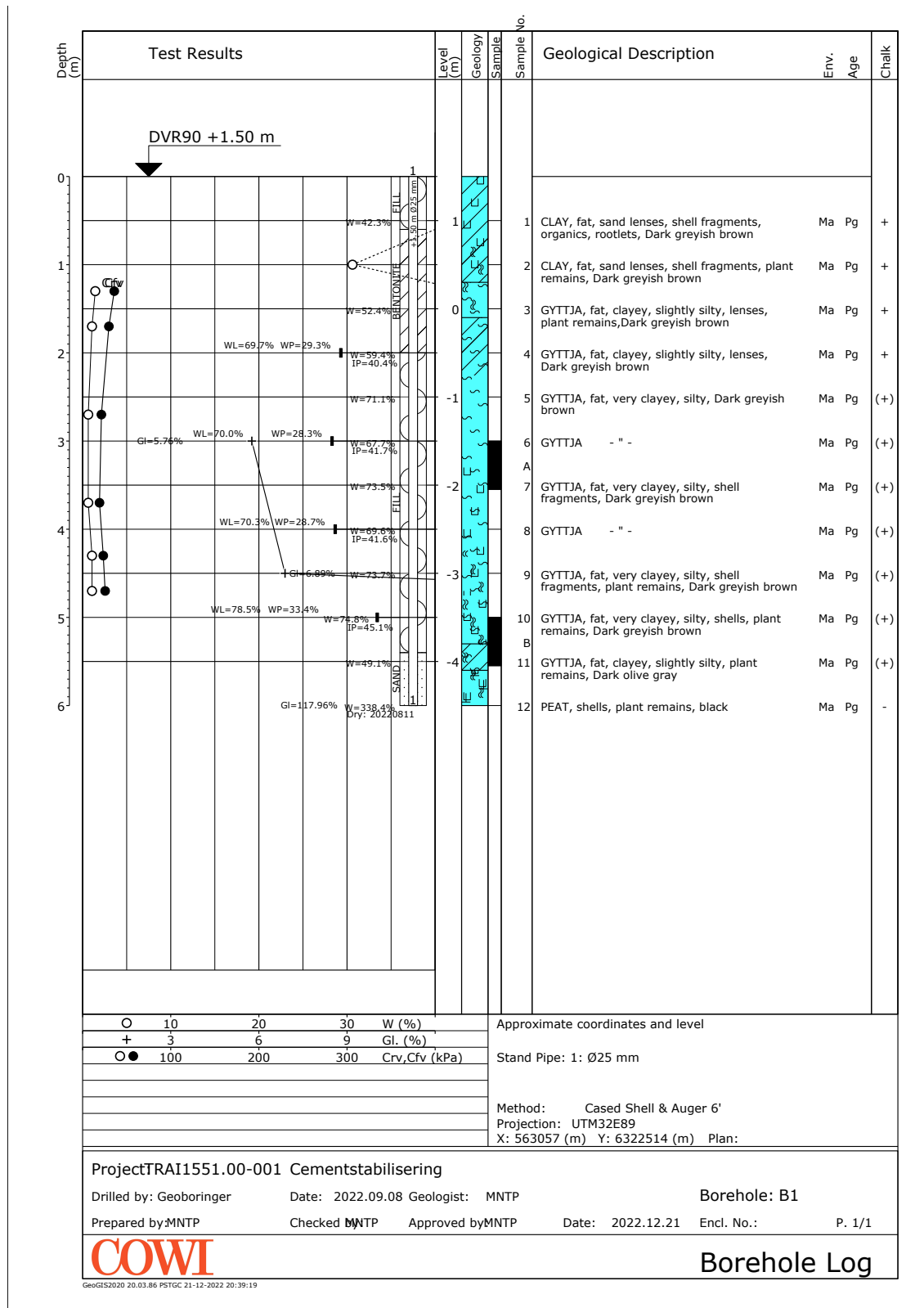
A Holocene Aalborg gyttja was investigated in this thesis. Further research could investigate other Danish gyttja types, to evaluate if the observations correlate to other gyttja types. The research could also investigate other types of Danish soils, to form a broader knowledge about cement stabilization of Danish soil types.

This thesis investigated the effects of cement stabilizing Aalborg gyttja with the CO₂ reduced FutureCem cement from Aalborg Portland. A high and low cement content of 150 kg/m³ and 30 kg/m³ was used to quantify how they managed in relation to one another. The specimens were cast in the laboratory by mixing remolded gyttja with the cement and storing the mix in metal cylinders reflecting the test dimensions.

The laboratory study consisted of CU triaxial, CD triaxial, cyclic triaxial, bender element, and oedometer tests. The tests were performed with 7, 14, 21, or 28 days of curing to monitor the strength and stiffness development. It was found that specimens with both cement contents had significant mechanical and physical changes. Generally, the specimens containing 150 kg/m³ showed a much larger strength and stiffness increase, compared to the specimens containing 30 kg/m³.

The numerical study sought to investigate the influence of cement stabilizing below a road section with different column spacing. The laboratory tests were used to calibrate simple and advanced constitutive soil models in PLAXIS 2D using the SoilTest module. It was found that the analytical method used to estimate the settlements were quite accurate in the drained case for the stiff columns containing 150 kg/m³. However, for the less stiff columns containing 30 kg/m³ the analytical method significantly overestimates the settlements. Furthermore, the numerical study revealed that the columns with 30 kg/m³ still showed a reasonable settlement reduction compared to the 150 kg/m³ columns. The use of advanced constitutive models was deemed redundant due to the uncertainty associated with the tests.

Finally, it was found that using low cement contents can be very beneficial for lowering the CO₂ emission from cement stabilization compared to high cement contents. Using a low cement content is however associated with an increased risk since the sensitivity of the stiffness increases drastically. Based on the stiffness sensitivity, the current Scandinavian method for obtaining the stiffness by undrained uniaxial compression tests was questioned, since CD triaxial tests yield a more accurate stiffness. Using the CD stiffness yielded 457 % larger settlements.



This appendix describes how the Life Cycle Assessments (LCAs) are performed. This involves listing the Environmental Product Declarations (EPDs) used and a conceptual description of how the different construction stages are evaluated. The stages considered when assessing the different foundations CO₂ emission are:

- A1-A3: Raw material extraction, transportation, and production
- A4: Transportation from the manufacturer to the construction site
- A5: Installation on-site

Generally, a program developed by Vejdirektoratet (The Danish Road Directorate) called InfraLCA has been used to calculate the CO₂ emissions [The Danish Road Directorate, 2023]. InfraLCA is designed to reflect Danish practice and to unify the way CO₂ emissions are assessed in Denmark. However, some EPDs are obtained from the manufacturers due to being more project specific or missing in InfraLCA. The total CO₂ emission in this thesis is calculated according to Equation (B.1).

$$\text{CO}_2 \text{ emission [kg CO}_2\text{-eq]} = \text{A1-A3} + \text{A4} + \text{A5} \quad (\text{B.1})$$

The three foundation options considered are mass exchange, piled foundation, and cement stabilization. These options are considered since mass exchange and piled foundation reflect current Danish options used when soft soils are encountered at shallow and great depths when constructing e.g. roads.

B.1 Mass exchange

The EPDs used to assess the CO₂ emission from mass exchange are shown in Table B.1. It is seen that each EPD used is associated with the stage number being utilized, as well as the reference name used in the calculations. The excavation EPD describes the average emission from the excavation of sand and gravel materials supplied [The Danish Road Directorate, 2023]. The truck describes the standard 26-ton truck used

for transportation in InfraLCA [The Danish Road Directorate, 2023]. Removal and built-in describe the diesel fuel usage of the machinery used for excavation on-site and built-in on-site [The Danish Road Directorate, 2023]. The diesel EPD is used to calculate CO₂ emissions from the machinery [The Danish Road Directorate, 2023].

Table B.1. EPDs used for mass exchange CO₂ emission calculations.

Stage	Name	Value	Unit
A1-A3	Excavation	1.05	kg CO ₂ -eq/t
A4	Truck	$8.97 \cdot 10^{-2}$	kg CO ₂ -eq/(t · km)
A5	Removal	$7.90 \cdot 10^{-2}$	l/m ³
A5	Built-in	$4.89 \cdot 10^{-2}$	l/m ³
A5	Diesel	3.33	kg CO ₂ -eq/l

The CO₂ emission from extracting the sand and gravel materials used as engineered fill is calculated according to Equation (B.2). The density of the gyttja is set to 1.6 t/m³ and the sand/gravel is set to 2.0 t/m³.

$$A1-A3 = \text{Soil volume [m}^3] \cdot \text{Density [t/m}^3] \cdot \underbrace{\text{Excavation}}_{\text{Table B.1}} [\text{kg CO}_2\text{-eq/t}] \quad (\text{B.2})$$

The emissions from transporting the engineered fill to the construction site are calculated according to Equation (B.3). The transportation distance is multiplied by 1.75 to take the trip back into account [The Danish Road Directorate, 2023].

$$A4 = \text{Soil mass [t]} \cdot \text{Distance [km]} \cdot 1.75 \cdot \underbrace{\text{Truck}}_{\text{Table B.1}} [\text{kg CO}_2\text{-eq/(t · km)}] \quad (\text{B.3})$$

The emissions from removing the in-situ soil and constructing the sand cushion are determined according to Equation (B.4) and (B.5). The removal of the in-situ soil is assumed to be above the groundwater table based on the EPD used [The Danish Road Directorate, 2023].

$$A5 = \text{Soil volume [m}^3] \cdot \underbrace{\text{Built-in}}_{\text{Table B.1}} [\text{l/m}^3] \cdot \underbrace{\text{Diesel}}_{\text{Table B.1}} [\text{kg CO}_2\text{-eq/l}] \quad (\text{B.4})$$

$$A5 = \text{Soil volume [m}^3] \cdot \underbrace{\text{Removal}}_{\text{Table B.1}} [\text{l/m}^3] \cdot \underbrace{\text{Diesel}}_{\text{Table B.1}} [\text{kg CO}_2\text{-eq/l}] \quad (\text{B.5})$$

B.2 Piled foundation

The EPDs used to assess the CO₂ emission from the deep-embedded concrete piled foundation are shown in Table B.2. The pile emission is based on type 6 piles

with a cross-sectional area of 0.25 x 0.25 m [Centrumpæle, 2021]. The lorry used to transport the piles is specified by the manufacturer and is based on transporting 1 kg for 100 km [Centrumpæle, 2021]. The installation emission is based on an installation time of 17.5 min and hourly diesel use of 16 l. These estimates are provided by Arkil A/S and are specified for a 16 m pile during normal installation conditions. The factor is solely based on the installation time and fuel use.

Table B.2. EPDs used for piled foundation CO₂ emission calculations.

Stage	Name	Value	Unit
A1-A3	Pile	$2.59 \cdot 10^1$	kg CO ₂ -eq/m
A4	Lorry	$6.63 \cdot 10^{-3}$	kg CO ₂ -eq/kg
A5	Installation	0.21	1/l

The CO₂ emission from manufacturing the piles is calculated according to Equation (B.6). It is seen that this emission is solely based on the length of the piles.

$$A1-A3 = \text{Length [m]} \cdot \underbrace{\text{Pile}}_{\text{Table B.2}} [\text{kg CO}_2\text{-eq/m}] \quad (\text{B.6})$$

The emission transportation emission from the manufacturer to the site is calculated according to Equation (B.7). The transportation distance is divided by 100 km to normalize the transportation distance according to the EPD [Centrumpæle, 2021].

$$A4 = \text{Pile mass [kg]} \cdot \left(\frac{\text{Distance [km]}}{100 [\text{km}]} \right) \cdot 1.75 \cdot \underbrace{\text{Lorry}}_{\text{Table B.2}} [\text{kg CO}_2\text{-eq/kg}] \quad (\text{B.7})$$

The emission from installing the piles on-site are calculated according to Equation (B.8). The total length of the piles is divided by 16 m to normalize the installation emission according to the 16 m pile the data are based on.

$$A5 = \left(\frac{\text{Pile length [m]}}{16 [\text{m}]} \right) / \underbrace{\text{Installation}}_{\text{Table B.2}} [1/l] \cdot \underbrace{\text{Diesel}}_{\text{Table B.1}} [\text{kg CO}_2\text{-eq/l}] \quad (\text{B.8})$$

B.3 Cement stabilization

The EPDs used to assess the CO₂ emission from using cement stabilization are shown in Table B.3. The FutureCem EPD is based on manufacturing 1.000 kg cement [Aalborg Portland, 2019]. The fuel use is based on installing 82.5 m stabilized columns an hour using 40 l of diesel. This information is provided by Soil Mixing Group AB.

Table B.3. EPDs used for cement stabilized CO₂ emission calculations.

Stage	Name	Value	Unit
A1-A3	FutureCem	$5.99 \cdot 10^2$	kg CO ₂ -eq/t
A5	Fuel-use	$4.00 \cdot 10^1$	l

The CO₂ emission from manufacturing the cement is calculated according to Equation (B.9). It is seen that the emission is solely based on the total cement amount used in the columns.

$$A1-A3 = \text{Cement mass [t]} \cdot \underbrace{\text{FutureCem}}_{\text{Table B.3}} [\text{kg CO}_2\text{-eq/t}] \quad (\text{B.9})$$

The emission from transporting the cement to the construction site is calculated according to Equation (B.10). The general 26-ton truck from InfraLCA is assumed to be used [The Danish Road Directorate, 2023].

$$A4 = \text{Cement mass [t]} \cdot \text{Distance [km]} \cdot 1.75 \cdot \underbrace{\text{Truck}}_{\text{Table B.1}} [\text{kg CO}_2\text{-eq/t}] \quad (\text{B.10})$$

The emission from installing the columns is calculated according to Equation (B.11). The total length of the columns is divided by 82.5 m to normalize the data to fit the EPD provided by Soil Mixing Group AB.

$$A5 = \left(\frac{\text{Column length [m]}}{82.5 [\text{m}]} \right) \cdot \underbrace{\text{Fuel-use}}_{\text{Table B.3}} [\text{l}] \cdot \underbrace{\text{Diesel}}_{\text{Table B.1}} [\text{kg CO}_2\text{-eq/l}] \quad (\text{B.11})$$

When cement stabilization is compared to mass exchange in the main report the coverage ratio is utilized to calculate the emission. The expressions above are therefore slightly modified. However, the expressions above still explain the method.

This appendix describes the primary theory used to interpret and analyze the laboratory test performed. The appendix will not act as a detailed step-by-step procedure to perform the respective laboratory tests, since these are performed according to standards and GDS manuals.

C.1 Standard triaxial tests

The apparatus used to perform the Consolidated Undrained (CU) and Consolidated Drained (CD) triaxial tests are seen in Figure C.1. The CU and CD tests are performed according to The Danish Standard Association [2018] and GDS Instruments [2016].



Figure C.1. GDS Triaxial Automated System (GDSTAS) setup.

The standard triaxial test conducted in this thesis was CU and CD tests. The

test specimens were placed in the triaxial apparatus, where they were connected to the pedestal and top cap by a latex membrane and secured by two o-rings. This ensured a closed system without water exchange between the inside and outside of the elastic membrane. The triaxial cell was then connected to the load frame and filled with demineralized water. The specimens were then flushed with CO₂ and afterward saturated with demineralized water.

After the saturation of the specimen the cell pressure and back pressure were ramped up to respectively 530 kPa and 500 kPa. The ramp of procedure for all specimens is shown in Figure C.2. The stress ramp-up ensured an effective consolidation stress of 30 kPa for full consolidation. The transducers used to control the stresses were calibrated according to GDS Instruments [2017] beforehand.

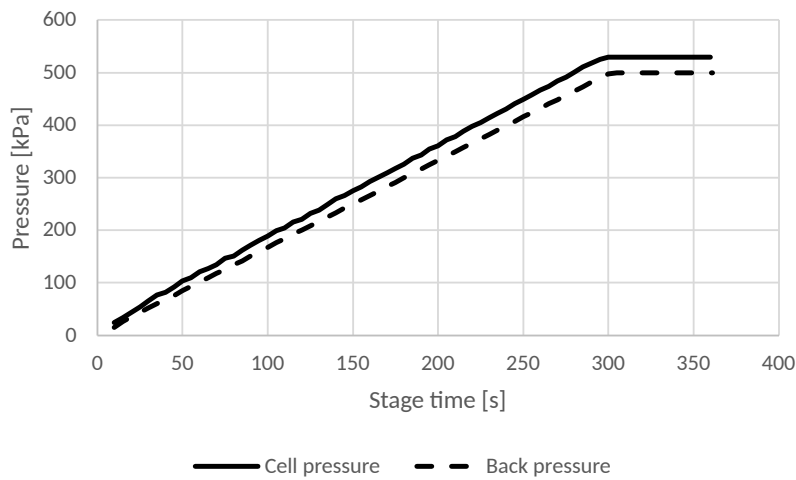


Figure C.2. Stress ramp-up stage.

At the end of consolidation, the specimens were subjected to three consecutive B-checks. The Skempton B-checks were performed to evaluate the saturation of the specimens. Three B-checks were performed, since performing only one B-check could yield a B-value above one, which should not be possible. The B-value was calculated according to Equation (C.1) [The Danish Standard Association, 2018].

$$B = \frac{\Delta\sigma_{back}}{\Delta\sigma_{cell}} \quad (C.1)$$

B	Skempton B value [-]
$\Delta\sigma_{back}$	Change in back pressure [kPa]
$\Delta\sigma_{cell}$	Change in cell pressure [kPa]

A saturation level beyond 0.95 was difficult to achieve. Usually, the saturation level ended up being between 0.8-0.9. This is expected to be due to the cementitious

bonds trapping air inside the specimen. Because of the impermeability of the specimens some specimens took 30 minutes to saturate with water before the stresses were ramped up. Low saturation levels around 0.8 were also observed in Gebretsadik [2014] on cemented clay. After the B-checks, the CU and CD tests were executed.

Consolidation Undrained triaxial tests

The CU tests were performed to acquire the undrained shear strength and the undrained secant stiffness. The undrained shear strength is calculated according to Equation (C.2).

$$S_u = \frac{q_f}{2} \quad (\text{C.2})$$

S_u	Undrained shear strength [kPa]
q_f	Deviatoric stress at failure [kPa]

The deviatoric stress at failure is determined according to the peak on the stress-strain curve for the CU tests. If no peak was observed the value at 10% strain was used. The deviatoric stress is calculated according to Equation (C.3). The results are not corrected according to The Danish Standard Association [2018] due to this having a minor influence.

$$q = \frac{F}{A_{corr}} \quad (\text{C.3})$$

q	Deviatoric stress [kPa]
F	Force measurement from the load cell [kN]
A_{corr}	Corrected cross-sectional area [m ²]

The corrected cross-sectional area during the triaxial test stages is calculated according to Equation (C.4). Other parameters like the height after consolidation etc. are calculated according to The Danish Standard Association [2018].

$$A_{corr} = \frac{V_i - \Delta V}{H_i - \Delta H} \quad (\text{C.4})$$

V_i	Initial volume of specimen [kPa]
ΔV	Change in volume [kN]
H_i	Initial height of specimen [kPa]
ΔH	Change in height [kN]

The undrained secant stiffness corresponding to 50% strength is determined according to Equation (C.5).

$$E_{u50} = \frac{q_f/2}{\varepsilon_v(q_f)} \quad (\text{C.5})$$

E_{u50}	Undrained secant stiffness [kPa]
$\varepsilon_v(q_f)$	Vertical strain corresponding to 50% strength [-]

Consolidation Drained triaxial tests

The CD tests were performed to acquire the triaxial friction angle and the drained secant stiffness. The friction angle is calculated according to Equation (C.6) [Budhu, 2021]. The effective vertical stress is determined as the stress induced by the load cell summed with the effective vertical consolidation stress.

$$\varphi = \sin^{-1} \left(\frac{\sigma'_1 - \sigma'_3}{\sigma'_1 + \sigma'_3} \right) \quad (\text{C.6})$$

φ	Friction angle [°]
$(\sigma'_1 - \sigma'_3)$	Effective deviatoric stress [kPa]
σ'_1	Effective vertical stress [kPa]
σ'_3	Effective radial stress [kPa]

The deviatoric stress is determined according to Equation (C.7) where the corrected area is determined according to Equation (C.4).

$$(\sigma'_1 - \sigma'_3) = q = \frac{F}{A_{corr}} \quad (\text{C.7})$$

The drained secant stiffness corresponding to 50% strength is determined according to Equation (C.8). Again the peak deviatoric stress or the deviatoric stress at 10% strain was used.

$$E_{50} = \frac{q_f/2}{\varepsilon_v(q_f)} \quad (\text{C.8})$$

E_{50}	Drained secant stiffness [kPa]
----------	--------------------------------

C.2 Cyclic triaxial tests

The apparatus used to perform the cyclic triaxial tests are seen in Figure C.3. The cyclic tests are performed according to GDS Instruments [2016].

The cyclic triaxial tests are subjected to the same stress ramp-up and consolidation procedure used for the standard triaxial tests, see section C.1. The purpose of the cyclic triaxial tests is to investigate the cyclic degradation of the material for the serviceability traffic load of 5 kPa. The cyclic triaxial tests were therefore conducted as stress-controlled with a frequency of 0.1 Hz.

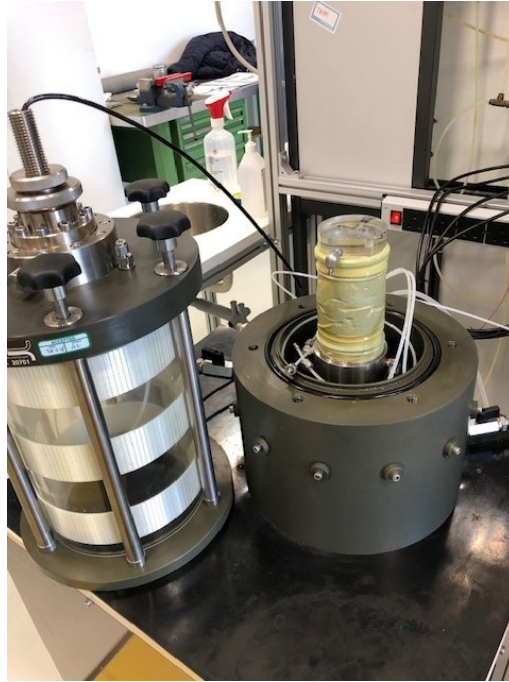


Figure C.3. GDS Advanced Dynamic Triaxial Testing System (DYNTTS) setup.

The shear modulus is calculated according to Equation (C.9).

$$G = \frac{\sigma_d}{\gamma_v} \quad (\text{C.9})$$

G	Shear modulus [kPa]
σ_d	Deviatoric stress [kPa]
γ_v	Vertical shear strain [-]

The shear strains are calculated according to Equation (C.10) [Mirshekari, 2017]. Poisson's ratio is assumed to be equal to 0.3 for all cyclic tests.

$$\gamma_v = \varepsilon_v \cdot (1 + \nu) \quad (\text{C.10})$$

ε_v	Vertical strain [-]
ν	Poisson's ratio [-]

C.3 Bender element tests

The bender element tests were performed in the GDS Triaxial Automated System, see Figure C.1. However, the pedestal and top cap were exchanged with bender element compatible devices, see Figure C.4. The tests are performed according to GDS Instruments [2014] and GDS Instruments [2023].



Figure C.4. GDS Bender Element System (GDSBES) setup in GDSTAS.

A soil sample is placed in between the GDSBES source/receivers shown in Figure C.4. The cement stabilized specimens was equipped with a latex membrane and consolidated to an effective stress level of 30 kPa, as for the other specimens tested.

The test is conducted by sending an excitation voltage through the soil. The velocity and amplitude of the wave are then recorded by the receiver. Based on the time delay between the send and received wave, as well as the travel distance of the wave, the shear wave velocity can be estimated, see Equation C.11. The travel distance for the wave is equal to the height subtracted for the length of the bender element tips (7 mm).

$$V_s = \frac{L_{wave}}{t_{wave}} \quad (C.11)$$

V_s		Shear wave velocity [m/s]
L_{wave}		Travel distance for the shear wave [mm]
t_{wave}		Travel time for the shear wave [ms]

Prior to the bender element tests, the bender element signal was calibrated to ensure the correct phase orientation, see Figure C.5.

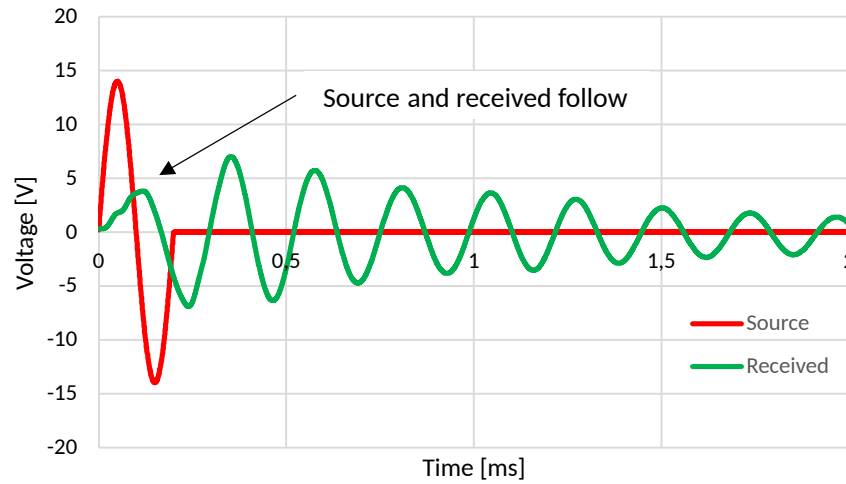


Figure C.5. Peak-to-peak interception of bender element signals.

The method used to intercept the bender element signals is the peak-to-peak method. When the peak-to-peak method is used the travel time for the shear wave, is determined as the first received peak from the source signal, see Figure C.6.

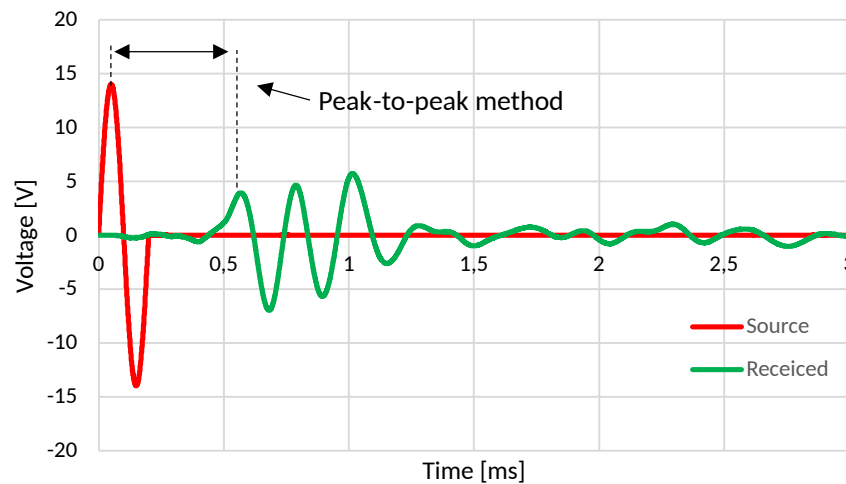


Figure C.6. Peak-to-peak interception of bender element signals.

The small strain stiffness can be derived based on Equation (C.12) [Zhu et al., 2008].

$$G_{max} = \rho \cdot V_s^2 \quad (\text{C.12})$$

G_{max}	Small strain stiffness [Pa]
ρ	Soil density [kg/m^3]
V_s	Shear wave velocity [m/s]

The stiffness of the soil can be classified according to the National Earthquake Hazards Reduction Program (NEHRP), see Table C.1.

Table C.1. Correlation between shear wave velocity and soil type [Building Seismic Safety Council, 1994].

Hard rock	$v_s > 1.500 \text{ m/s}$
Rock	$760 \text{ m/s} < v_s \leq 1.500 \text{ m/s}$
Very dense soil and soft rock	$360 \text{ m/s} < v_s \leq 760 \text{ m/s}$
Stiff soil	$180 \text{ m/s} \leq v_s \leq 360 \text{ m/s}$
Other*	$v_s < 180 \text{ m/s}$

* Defined as e.g. clay with $S_u < 25 \text{ kPa}$

C.4 Oedometer tests

The apparatus used to perform the oedometer tests are seen in Figure C.7. The oedometer tests are performed according to GDS Instruments [2016] and The European Committee For Standardization [2017].

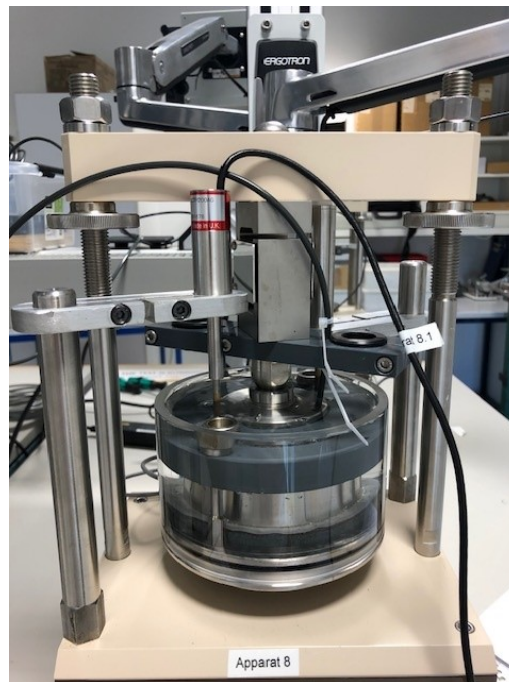


Figure C.7. GDS Automatic Oedometer System (GDSAOS) setup

The oedometer tests are intercepted according to the log-time method. An example of the interception of the end of consolidation is seen in Figure C.8. For this load step the primary consolidation is determined to end at about 1,500 seconds.

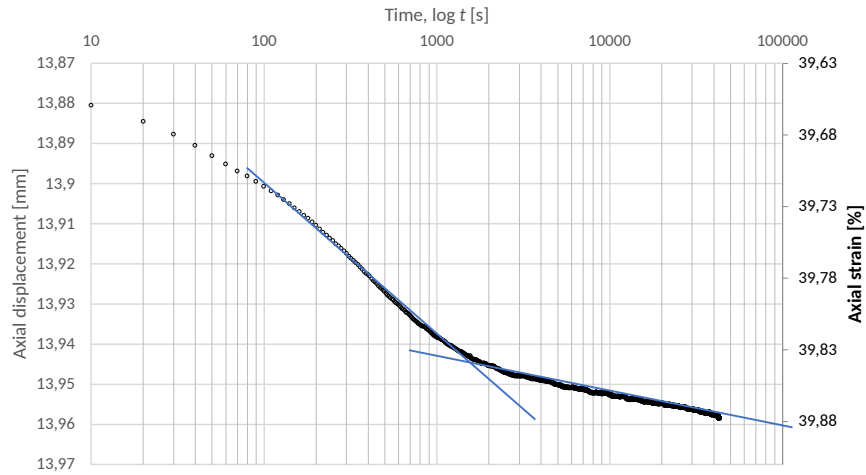


Figure C.8. In-situ consolidation curve for load step 15.

The modified compression index is determined according to equation (C.13) [Karl Terzaghi and others, 1996].

$$C_{\varepsilon C} = \frac{\varepsilon_2 - \varepsilon_1}{\log(\sigma'_2/\sigma'_1)} \quad (\text{C.13})$$

$C_{\varepsilon C}$ | Modified compression index [-]

The oedometer modulus is determined according to equation (C.14) [Budhu, 2021].

$$E_{oed} = \frac{\sigma'_2 - \sigma'_1}{\varepsilon_2 - \varepsilon_1} \quad (\text{C.14})$$

E_{oed} | Oedometer modulus [MPa]

This appendix describes the calibration and build-up of the numerical PLAXIS 2D models used to evaluate the effect of cement stabilization. Firstly the input parameters for the different soil models used are put forward. The staged construction of the PLAXIS models is then presented with a convergence analysis to justify the mesh type used. Lastly, the soil and structural parameters used in the calculations are showcased.

D.1 Material models investigated

The material models used to simulate the soil behavior and evaluate the effects of cement stabilization are presented below. The input parameters are based on Bentley Systems [2023].

D.1.1 Linear-Elastic (LE)

The linear elastic material model is used to compare the numerical and analytical models. Furthermore, this model is used for the structural plate and geogrid elements. The input parameters for this material model are listed below.

E	[kPa]	Secant stiffness
ν	[-]	Poisson's ratio

D.1.2 Mohr-Coulomb (MC)

The Mohr-Coulomb material model is used for a large proportion of the analysis performed. The Mohr-Coulomb model is a linear elastic perfectly plastic model. The input parameters for the undrained case are listed below. The soil is modeled as Undrained B.

E'	[kPa]	Secant stiffness
ν'	[-]	Poisson's ratio
S_u	[kPa]	Undrained shear strength

The input parameters for the drained case are listed below.

E'	[kPa]	Secant stiffness
ν'	[-]	Poisson's ratio
c'	[kPa]	Effective cohesion
φ'	[°]	Friction angle

D.1.3 Hardening Soil (HS)

The Hardening Soil material model is a non-linear soil model, which is also used for a large amount of the analysis. The HS model is based on a hyperbolic stress-strain curve, compared to the traditional linear-elastic stress-strain curve by MC.

The input parameters for the undrained case are listed below. Undrained B is used.

$E_{50,ref}$	[kPa]	Reference secant stiffness
$E_{oed,ref}$	[kPa]	Reference oedometer modulus
$E_{ur,ref}$	[kPa]	Reference unloading-reloading modulus
power(m)	[-]	Hardening parameter
$S_{u,ref}$	[kPa]	Reference undrained shear strength

The drained parameters are listed below.

$E_{50,ref}$	[kPa]	Reference secant stiffness
$E_{oed,ref}$	[kPa]	Reference oedometer modulus
$E_{ur,ref}$	[kPa]	Reference unloading-reloading modulus
power(m)	[-]	Hardening parameter
c'_{ref}	[kPa]	Reference effective cohesion
φ	[°]	Friction angle
$K0_{NC}$	[-]	Coefficient of earth pressure for the normally consolidated state

When choosing the oedometer modulus and unloading-reloading modulus PLAXIS has some recommendations and criteria for minimum and maximum values. The recommended relationship for the oedometer modulus and unloading-reloading modulus are listed below.

$$E_{oed} \approx E_{50} \quad (D.1)$$

$$E_{ur} \approx 3 \cdot E_{50} \quad (\text{D.2})$$

D.1.4 Hardening Soil with Small Strain (HS-Small)

The HS-Small material model is considered the same as the HS model with an increased stiffness at the beginning of the stress-strain curve. The additional parameters are obtained by bender element and cyclic triaxial tests. The extra parameters which are necessary for the HS-Small model for the undrained and drained case are stated below. The undrained modeling is performed as Undrained B as well.

$G_{0,ref}$	[kPa]	Reference value for the initial small-strain shear modulus
$\gamma_{0.7}$	[-]	Strain level for shear modulus reduction of 70 %

D.2 Staged construction of PLAXIS models

This section describes the staged construction of the base PLAXIS model used during the analysis. This reflects the general phase construction for all models with small deviations. The first phase is the initial phase reflecting the current conditions, see Figure D.1. The initial phase consists solely of untreated gyttja.

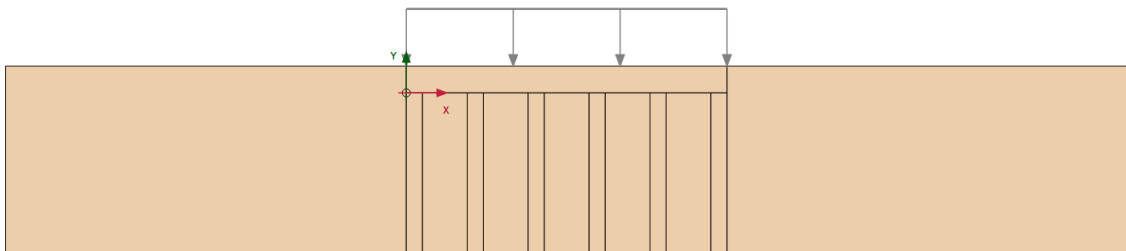


Figure D.1. Initial phase.

After the initial phase, a nil-step is created to ensure the equilibrium of the stresses. The nil-step phase is identical to the initial phase, see Figure D.2.

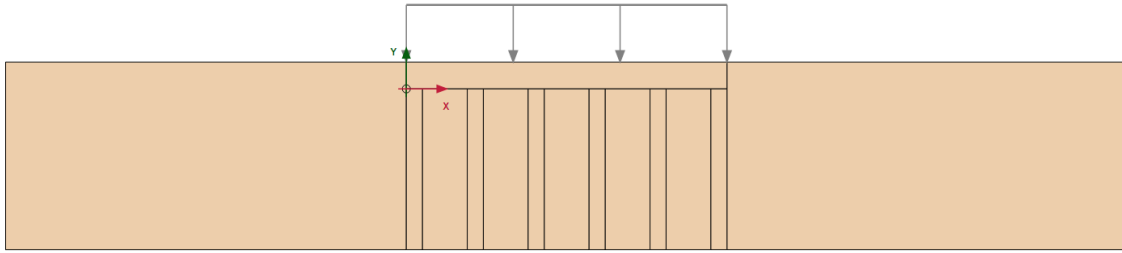


Figure D.2. Nil-step phase.

In the next phase the cement stabilized columns are installed, see Figure D.3. The columns are assumed installed from 1 m below the surface until the end of the gyttja layer. The length of the columns are 6 m.

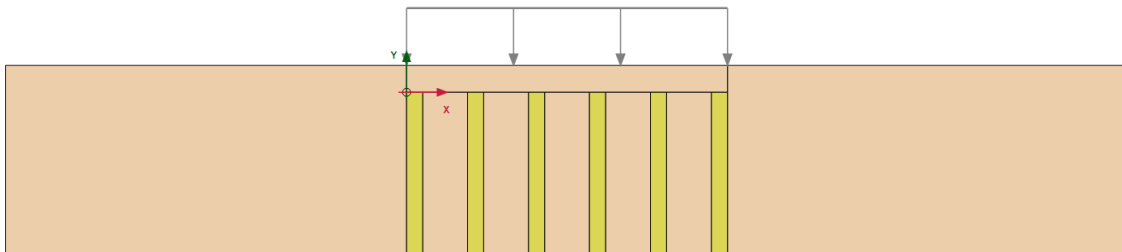


Figure D.3. Column installation phase.

In the next phase the pavement structure is constructed, see Figure D.4. The pavement structure is assumed to have a thickness of 1 m.

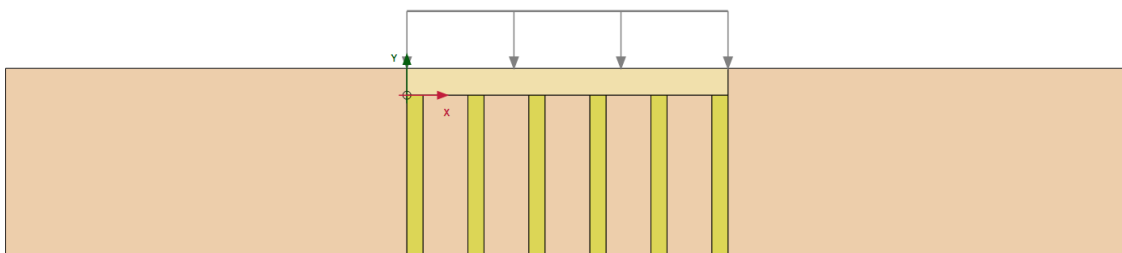


Figure D.4. Pavement structure construction phase.

In the final phase the serviceability load of 5 kPa is activated, see Figure D.5. When the bearing capacity is evaluated the load is increased until failure. Since the load is applied in steps, the multiplication of reached phase proportion, M_{stage} , and the load, q_{ref} , is assumed to represent the bearing capacity.

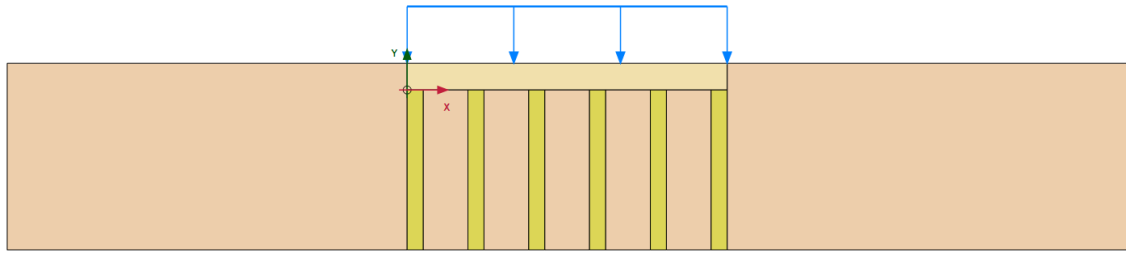


Figure D.5. Loading phase.

D.3 Convergence analysis

To ensure reliable results a convergence analysis was performed. The convergence analysis was performed on the base model with 6 stabilized columns, see Figure D.5. The results from the convergence analysis are seen in Figure D.6. When the 'Very fine' mesh is applied the relative error is only 0.6% which is found acceptable.

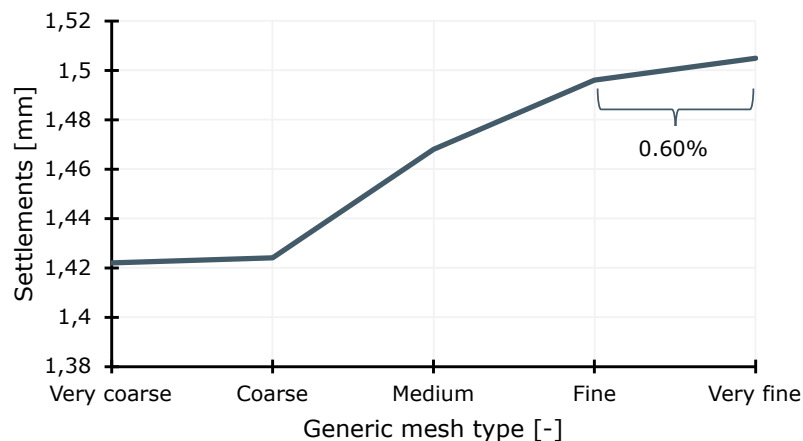


Figure D.6. Convergence analysis for the base scenario with 6 columns.

The meshes generated and used for the convergence analysis are shown below.

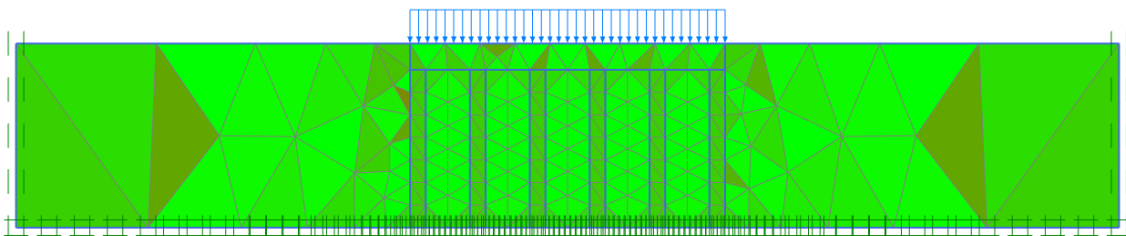


Figure D.7. Very coarse mesh.

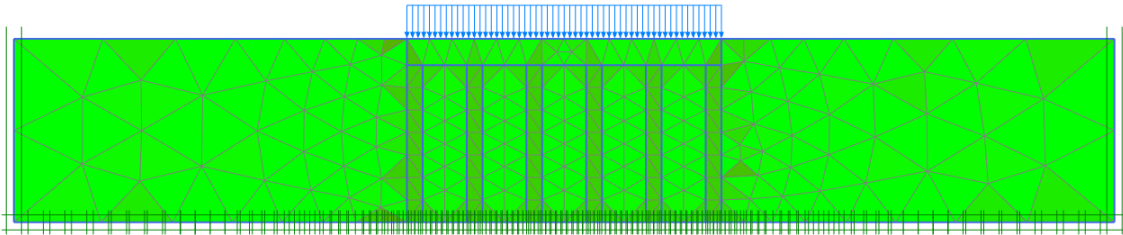


Figure D.8. Coarse mesh.

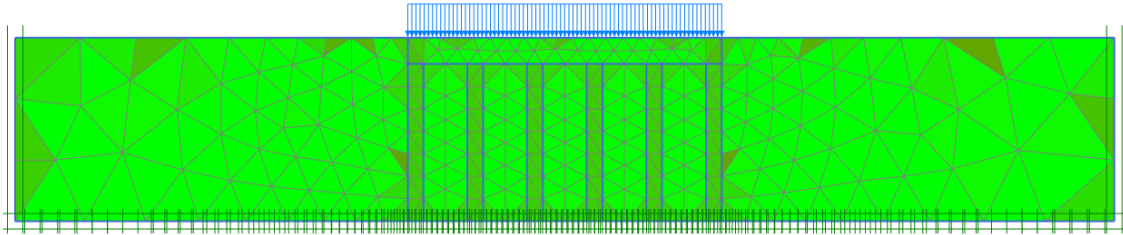


Figure D.9. Medium mesh.

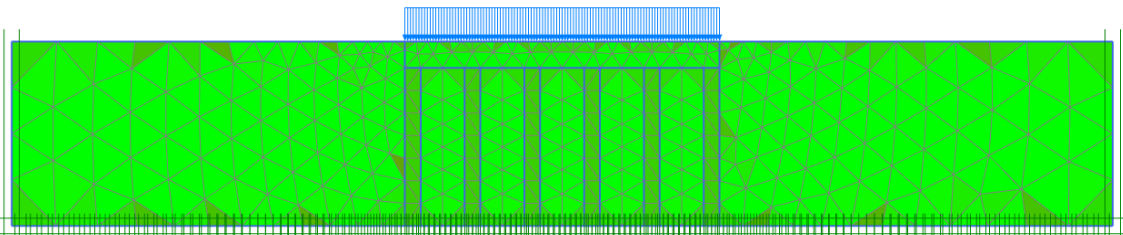


Figure D.10. Fine mesh.

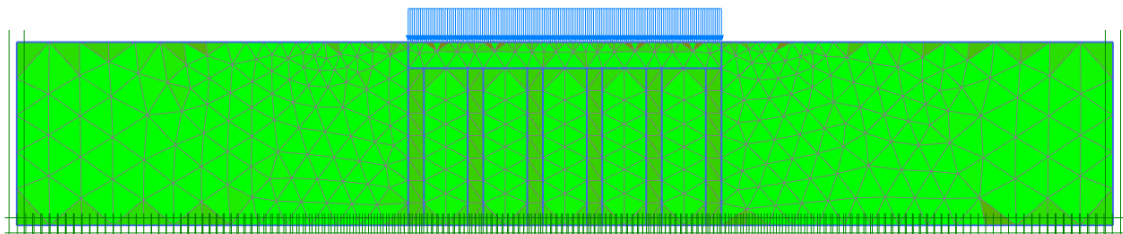


Figure D.11. Very fine mesh.

D.4 Soil parameters used

This section presents the soil parameters used during the calculations. The parameters in Equation (D.3), (D.4) and (D.5) are fixed for all models except the LE models used for the analytical comparison.

$$\nu = \nu' = 0.3 \tag{D.3}$$

$$\gamma_{sat} = \gamma_{unsat} = 16 \text{ kN/m}^3 \quad (\text{Gyttja and columns}) \quad (\text{D.4})$$

$$\gamma_{sat} = 20 \text{ kN/m}^3 \quad \text{and} \quad \gamma_{unsat} = 18 \text{ kN/m}^3 \quad (\text{Pavement structure}) \quad (\text{D.5})$$

When calibrating the drained HS models the normally consolidated $K0$ value should be specified. This is calculated according to Equation (D.6) [Bentley Systems, 2023].

$$K0_{NC} = 1 - \sin(\varphi) \quad (\text{D.6})$$

The hardening parameter for HS and HS-Small is set according to Equation (D.7).

$$\text{power(m)} = 0.5 \quad (\text{D.7})$$

The degradation parameter for HS-Small is set according to Equation (D.8).

$$\gamma_{0.7} = 0.01 \quad (\text{D.8})$$

The dilation angle is estimated from Equation (D.9).

$$\psi = \varphi - 30 \quad (\text{D.9})$$

The reference pressure for the HS models is set according to Equation (D.10).

$$p_{ref} = 30 \text{ kPa} \quad (\text{D.10})$$

The oedometer modulus and unloading-reloading modulus are as a rule of thumb estimated from Equation (D.11) and (D.12). For a few of the calibrations, E_{oed} has to be reduced significantly due to PLAXIS criterions.

$$E_{oed} = E_{50} \quad (\text{D.11})$$

$$E_{ur} = 2 \cdot E_{50} \quad (\text{D.12})$$

In the upcoming tables, the soil parameters are specified for undrained and drained conditions for the different soil models used. The cement stabilized columns are referred to according to Equation (D.13).

$$\underbrace{28/21/14/7}_{\text{Curing period}} + \underbrace{CEM150/CEM30}_{\text{Cement content}} \quad (\text{D.13})$$

The soils used to use for LE modeling are specified in Table D.1 and D.2. For the drained models $\nu' = 0$ and $\gamma_{sat} = \gamma_{unsat} = 0 \text{ kN/m}^3$ apply. For the undrained

models $\nu_u = 0.495$ and $\gamma_{sat} = \gamma_{unsat} = 0 \text{ kN/m}^3$ apply. The LE models are only used to investigate the correlation to the analytical formulas.

Table D.1. LE model parameters (Undrained C).

Soil type	E_u [kPa]
Gyttja:	2,500
28CEM150:	98,650

Table D.2. LE model parameters (Drained).

Soil type	E' [kPa]
Gyttja:	1,500
28CEM150:	28,000

The parameters used for the MC models in undrained and drained conditions are shown in Table D.3 and D.4. For the cement stabilized columns the effective cohesion is assumed equal to zero, due to a lack of CD test to determine the exact friction angle and effective cohesion.

Table D.3. MC model parameters (Undrained B).

Soil type	E' [kPa]	S_u [kPa]
Gyttja:	2,500	19.2
28CEM150:	98,650	417.1
28CEM30:	21,110	50.0

Table D.4. MC model parameters (Drained).

Soil type	E' [kPa]	φ [°]	c' [kPa]
Gyttja:	1,250	24.7	0
28CEM150:	28,000	67.5	0
28CEM30:	2,100	40.6	0

The HS model parameters for undrained and drained conditions are seen in Table D.5 and D.6. The drained HS gyttja model was the only HS model where it was necessary to calibrate the secant stiffness due to a bad initial fit.

Table D.5. HS model parameters (Undrained B).

Soil type	E_{50} [kPa]	E_{oed} [kPa]	E_{ur} [kPa]	S_u [kPa]
Gyttja:	2,500	2,500	5,000	19.2
28CEM150:	98,650	98,650	197,300	417.1
28CEM30:	21,110	21,110	42,200	50.0

Table D.6. HS model parameters (Drained).

Soil type	E_{50} [kPa]	E_{oed} [kPa]	E_{ur} [kPa]	φ [°]	c' [kPa]
Gyttja:	1,500	1,500	3,000	30	0
28CEM150:	28,000	10,000	88,000	67.5	0
28CEM30:	2,100	2,100	11,200	40.6	0

The HS-Small parameters used for the undrained and drained case are seen in Table D.7 and D.8. For the drained case PLAXIS criteria and errors yielded changes in the estimated parameters.

Table D.7. HS-Small parameters (Undrained B).

Soil type	E_{50} [kPa]	E_{oed} [kPa]	E_{ur} [kPa]	G_0 [kPa]	S_u [°]
Gyttja:	2,500	2,500	5,000	2,100	19.2
28CEM150:	98,650	98,650	197,300	163,600	417.0
28CEM30:	12,110	21,110	42,200	25,000	50.0

Table D.8. HS-Small parameters (Drained).

Soil type	E_{50} [kPa]	E_{oed} [kPa]	E_{ur} [kPa]	G_0 [kPa]	φ [°]	c' [kPa]
Gyttja:	1,500	1,500	3,000	1,300	30.0	0
28CEM150:	28,000	10,000	88,000	40,000	67.5	0
28CEM30:	2,100	2,100	11,200	5,000	40.6	0

D.5 Structure parameters used

The plate input parameters used for the comparison between the analytical and numerical results are seen in Table D.9. The plate is assumed isotropic.

Table D.9. Plate input parameters.

EA [kN/m]	EI [kN m ² / m]	w [kN/m/m]	ν [-]
$10.0 \cdot 10^9$	$10.0 \cdot 10^6$	1.0	0.3

The geogrid input parameters are seen in Table D.10. The geogrid is assumed isotropic. The geonet is assumed linear elastic.

Table D.10. Geogrid input parameters.

EA [kN/m]
800

E.1 Triaxial01: CU test depth 5.5-5.5 m

This test was performed on in-situ material from depth 5.0-5.5 m.

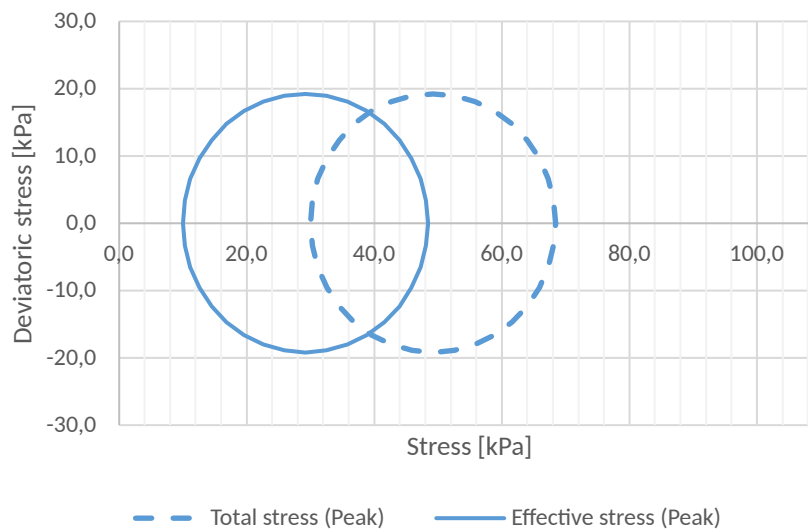


Figure E.1. Mohr's circles associated with the test.

Test description:

The test was performed using a GDS triaxial cell using GDSLab v2.5.4.28 software. Further information about this test can be found in Tanderup [2022].

Cement amount:	0 kg/m ³		Before	After
Temp. lab:	19 to 20.5 °C	Water content, w:	54.8 %	56.2 %
Diameter, d:	70 mm	Saturation, S:	87.6 %	-
Pore water:	Demineralised	Void ratio, e:	1.66	-
Test type:	CU	Height, h:	140 mm	-
Shear rate, v:	0.02 mm/min	Unit weight, γ	15.2 kN/m ³	-
Test date:	30/09 to 04/10/2022			

Results:

$(C_u)_p$:	19.2 kPa
$(E)_{u50}$	2.51 kPa

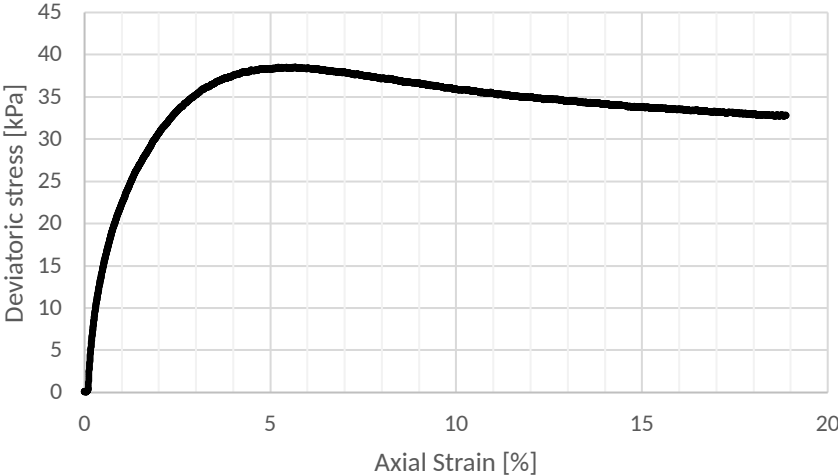


Figure E.2. Deviatoric stress during CU test.

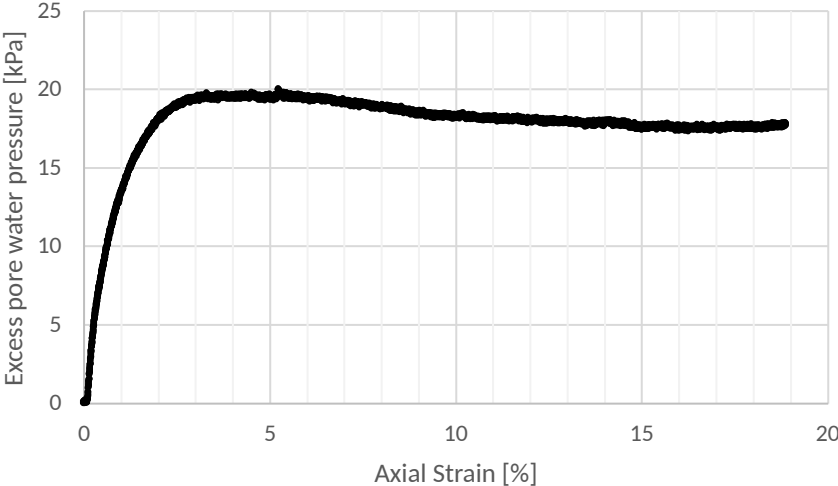


Figure E.3. Excess pore pressure during CU test.

E.2 Triaxial02: CD test depth 1.5-2.0 m

This test was performed on in situ material from boring B2 depth 1.5-2.0 m.

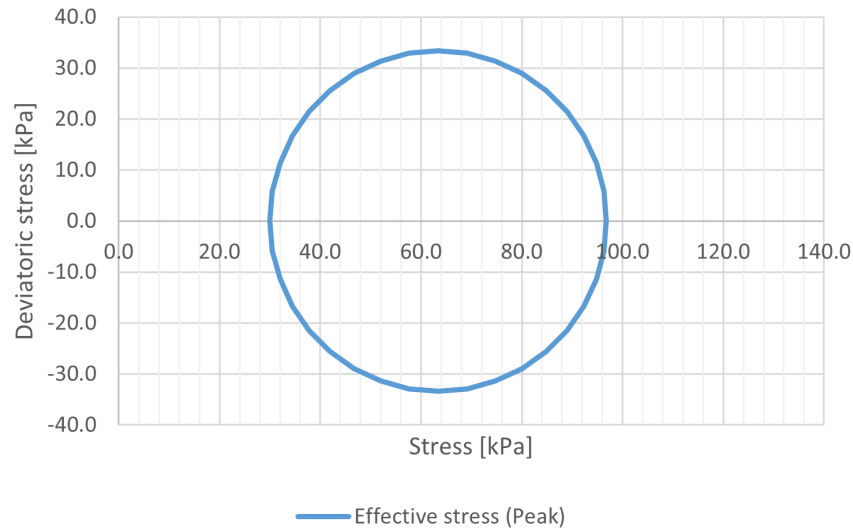


Figure E.4. Mohr's circles associated with the test..

Test description:

The test was performed using a GDS triaxial cell using GDSLab v2.5.4.28 software. Further information about this test can be found in Tanderup [2022].

Cement amount:	0 kg/m ³		Before	After
Temp. lab:	19 to 20.5 °C	Water content, w:	59.9 %	52.7 %
Diameter, d:	70 mm	Saturation, S:	97.4 %	
Pore water:	Demineralised	Void ratio, e:	1.64	
Test type:	CD ($\sigma' = 30$ kPa)	Height, h:	140 mm	
Shear rate, v:	0.006 mm/min	Unit weight, γ	16.2 kN/m ³	
Test date:	25/11 to 29/11/2022			

Results:

$(E)_{50}$:	1.3 MPa
$(\varphi')_{10\%}$:	31.8 °

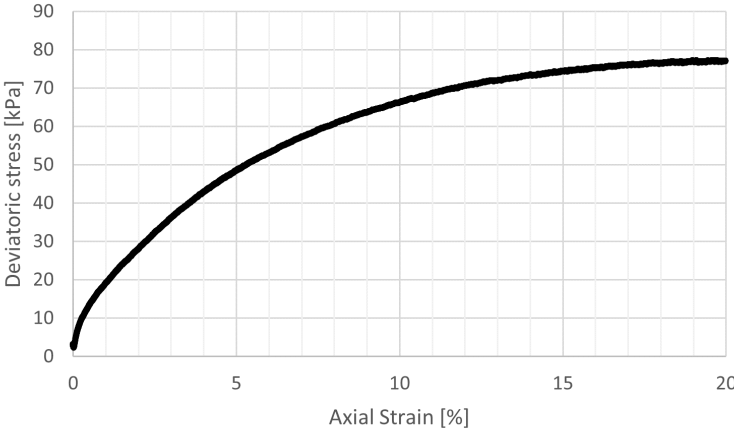


Figure E.5. Deviatoric stress during CD test.

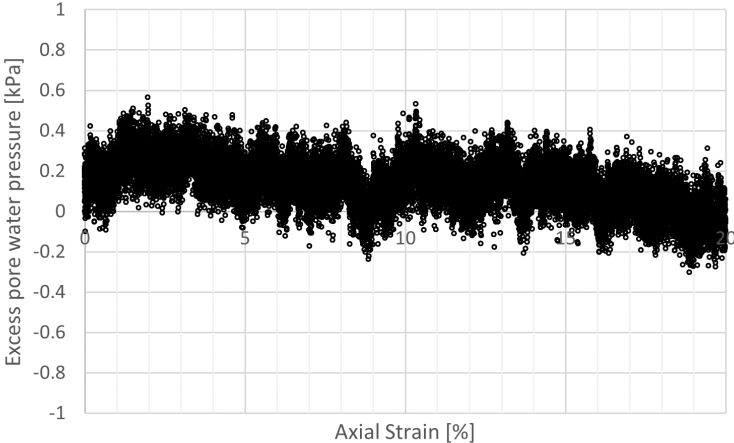


Figure E.6. Excess pore pressure during CD test.

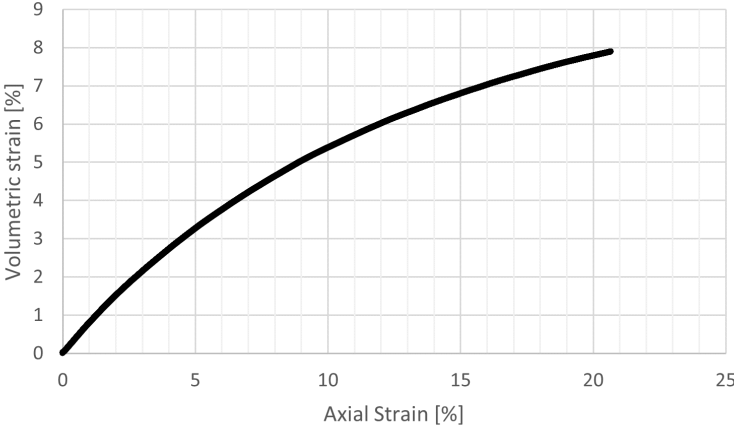


Figure E.7. Volumetric strain during CD test.

E.3 Oedometer01: Depth 3.0-3.5 m

This test was performed on in-situ material from depth 3.0-3.5 m.

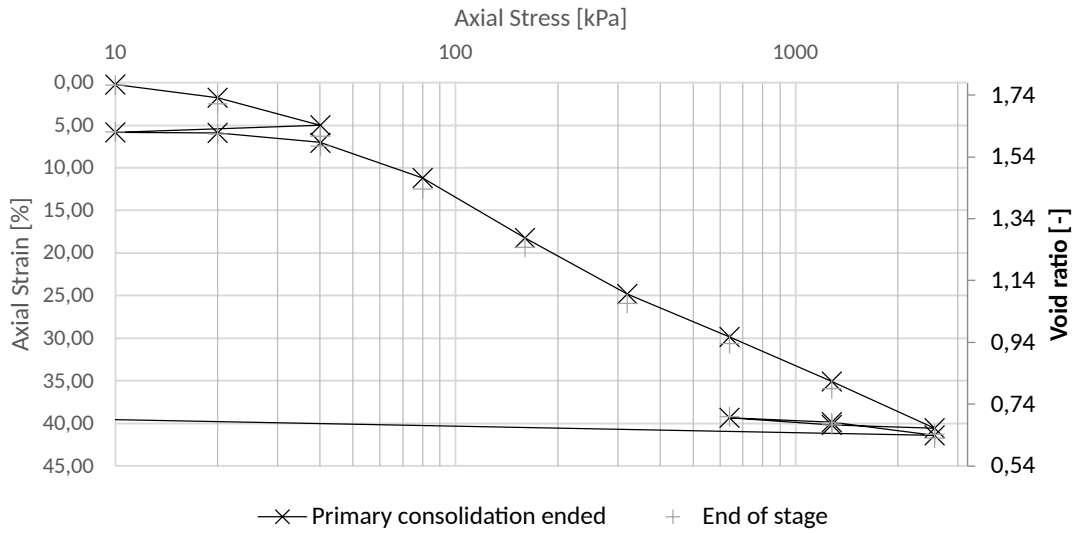


Figure E.8. Stress strain curve.

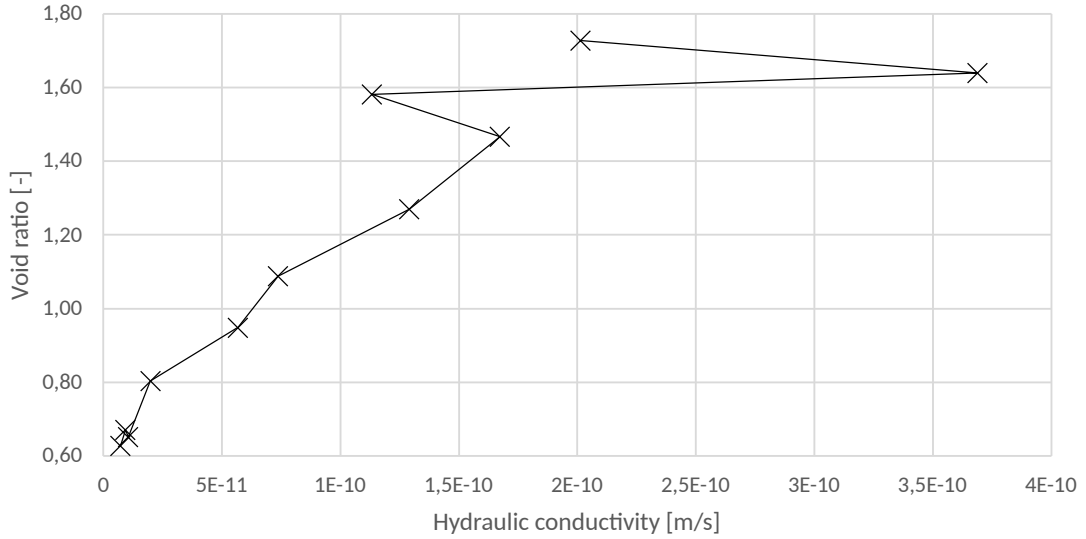


Figure E.9. Hydraulic conductivity.

Test description:

The test was performed using a GDSAOS with GDSLlab v2.5.4.28 software. The remaining test data can be found in Tanderup [2022].

Cement amount:	0 kg/m ³		Before	After
Saturated after:	60 s	Water content, w:	67.8 %	36.0 %
Temp. lab:	19 to 20.5 °C	Saturation, S:	101.4 %	112.5 %
Diameter, d:	70 mm	Void ratio, e:	1.78	0.85
Pore water:	Demineralised	Height, h:	35 mm	23 mm
Test date:	13/09 to 10/10/2022	Unit weight, γ	15.8 kN/m ³	19.2 kN/m ³
Results:				
$C_{\varepsilon C}$ (80-2560):	19.5 %			
E_{oed} (10-40):	2.5 MPa			
E_{oed} (640-2560):	92.4 MPa			
σ'_{pc} :	50 kPa			

Table E.1. Results from oedometer test.

σ_v [kPa]	t_{end} [min]	ε_{int} [%]	ε_{100} [%]	ε_{end} [%]	e_{100} [-]	k [m/s]	C_v [m ² /s]	$C_{\varepsilon C}$ [%]	E_{oed} [MPa]
10	2880	0	0.21	0.27	1.80	-	-	-	-
20	2880	0.27	1.76	2.50	1.75	2.01E-10	1.30E-08	5.15	0.65
40	2880	2.50	4.97	6.30	1.66	3.69E-10	2.30E-08	10.66	0.62
10	2880	6.30	5.85	5.75	1.64	-	-	-1.46	-3.41
20	4320	5.75	5.93	6.01	1.64	-	-	0.27	12.50
40	6000	6.01	7.03	7.45	1.61	1.13E-10	2.06E-08	3.65	1.82
80	2820	7.45	11.18	12.46	1.49	1.67E-10	1.61E-08	13.79	0.96
160	1680	12.46	18.25	19.31	1.29	1.29E-10	1.46E-08	23.49	1.13
320	1260	19.31	24.82	25.91	1.11	7.37E-11	1.80E-08	21.83	2.44
640	1440	25.91	29.84	30.61	0.97	5.68E-11	3.62E-08	16.68	6.37
1280	1260	30.61	35.09	35.89	0.82	1.99E-11	2.42E-08	17.43	12.19
2560	840	35.89	40.55	41.27	0.67	1.05E-11	2.45E-08	18.15	23.43
1280	600	41.27	40.19	40.15	0.68	-	-	1.21	352.20
640	720	40.15	39.30	39.21	0.70	-	-	2.95	72.10
1280	720	39.21	39.84	39.88	0.69	9.25E-12	1.10E-07	1.80	118.02
2560	720	39.88	41.38	41.68	0.64	7.11E-12	5.92E-08	5.10	83.35
0	2880	41.68	31.13	30.15	0.93	-	-	0.76	24.97

The oedometer data for the selected load step are presented on the following pages. The lines used for interpreting the end of primary consolidation are kept. The load steps are marked with either "Loading", "Unloading" or "Reloading" according to the load program in the table above.

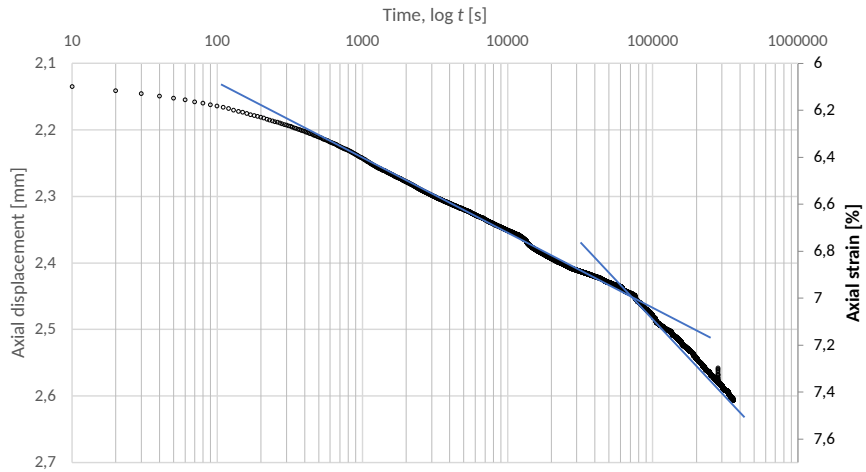


Figure E.10. Load step 6 (Reloading). 40 kPa.

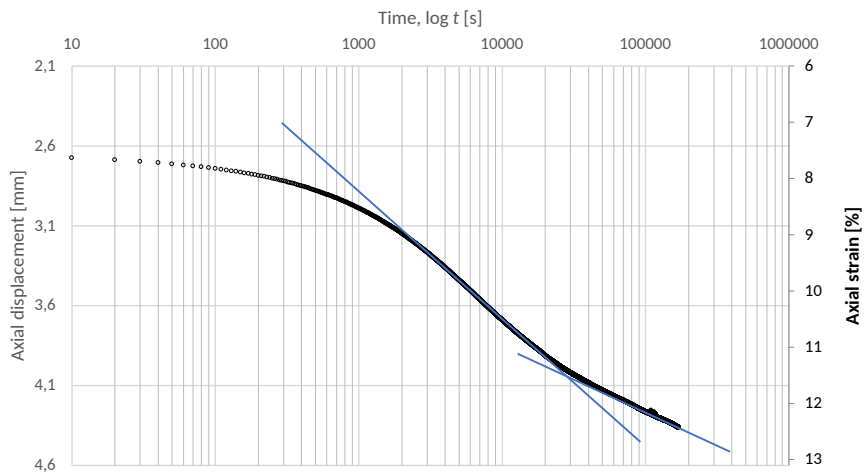


Figure E.11. Load step 7 (Loading). 80 kPa.

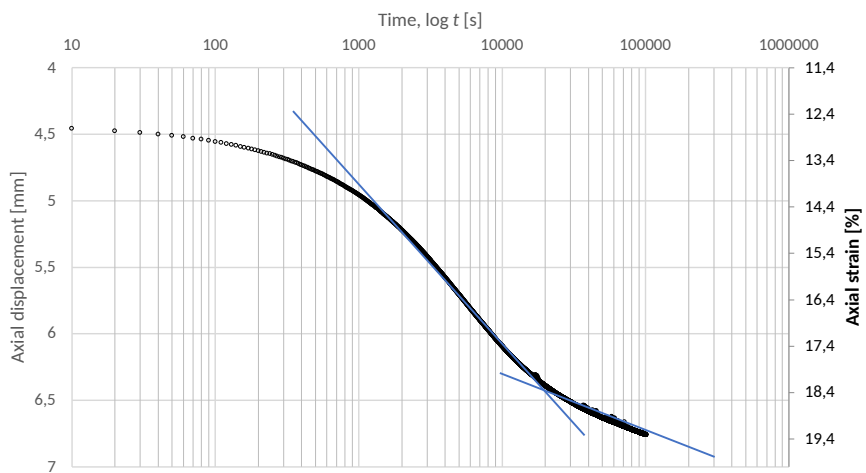


Figure E.12. Load step 8 (Loading). 160 kPa.

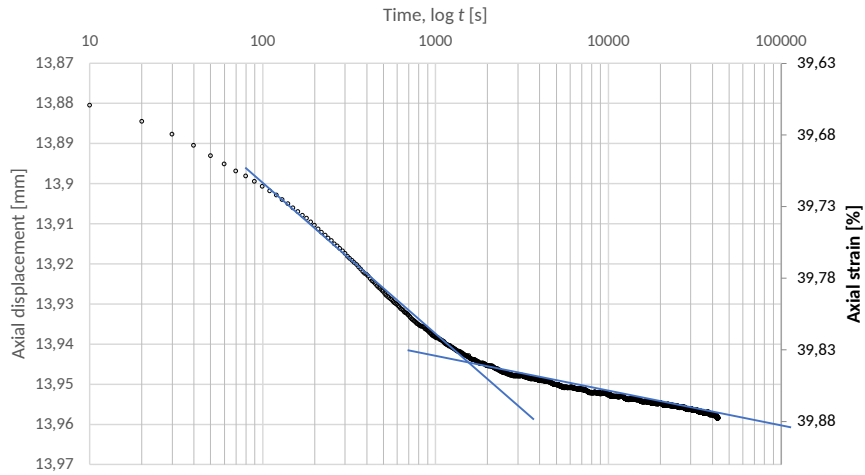


Figure E.13. Load step 15 (Reloading). 1280 kPa.

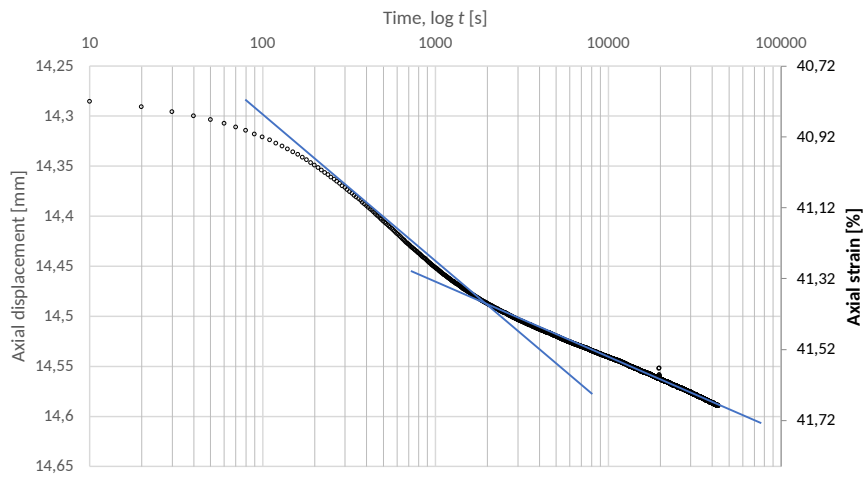


Figure E.14. Load step 16 (Reloading). 2560 kPa.

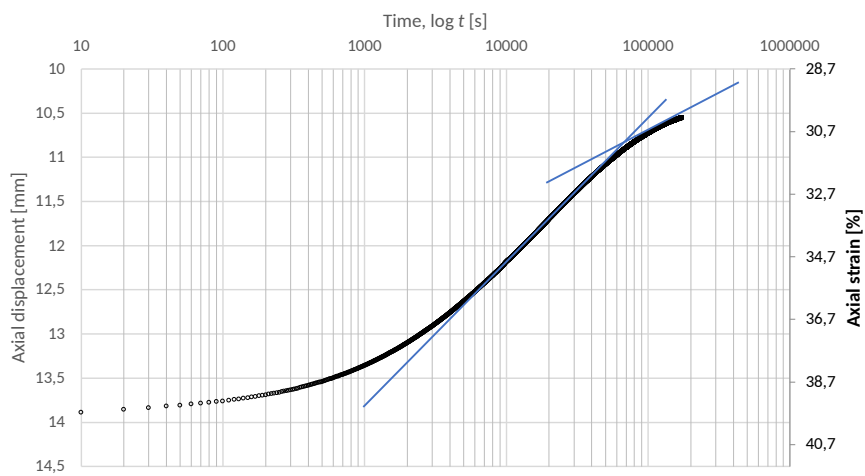


Figure E.15. Load step 17 (Unloading). 0 kPa.

E.4 BenderElement01: Depth 3.0-3.5 m

This test was performed on in-situ material from depth 3.0-3.5 m.

Test description:

The test was performed using the GDS bender element system using GDS BES v2.2.13 software. The test was performed using a single excitation voltage shot, hence the abnormal receiver wave.

Cement amount:	0 kg/m ³		Before	After
Temp. lab:	19 to 20.5 °C	Water content, w:	68.6 %	-
Diameter, d:	-	Saturation, S:	-	-
Wavetype:	Sine	Void ratio, e:	-	-
Wave period:	0.2 ms	Height, h:	53 mm	-
Test date:	23/03/2022	Unit weight, γ	-	-

Results:

V_s : 27.7 m/s

1) Subtracted the transmitter height of 7 mm

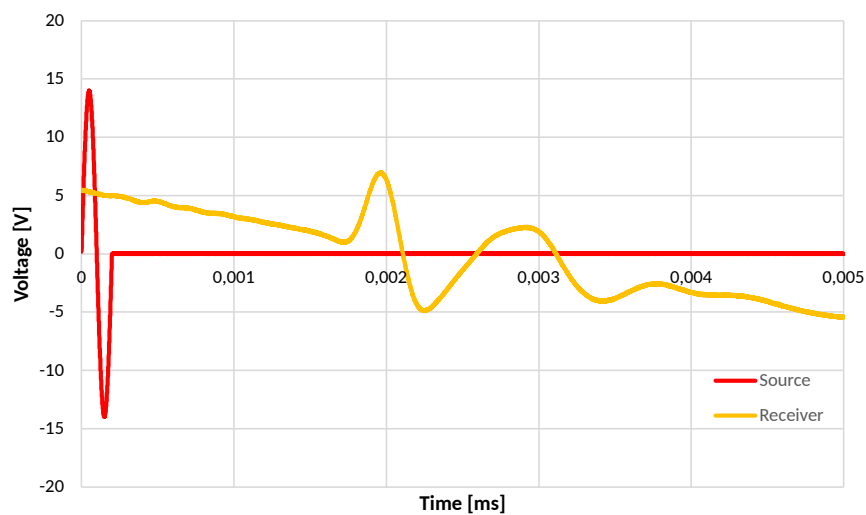


Figure E.16. Shear wave velocity for in-situ specimen with $\sigma_3 = 0$.

Cement specimens 30 kg/m³



F.1 Triaxial03: CU test curing for 7 days at 20 °C

This CU test was performed on a gyttja-cement specimen that cured for 7 days.

Test description:				
The test was performed using a GDS triaxial cell using GDSLab v2.5.4.28 software.				
Cement amount:	30 kg/m ³		Before	After
Curing period:	7 days ¹⁾	Water content, w:	61.8 %	69.9 %
Curing temp.:	19 to 20.5 °C	Saturation, S:	91.0 %	-
Diameter, d:	70 mm	Height, h:	70 mm	-
Pore water:	Demineralised	Void ratio, e:	1.46	-
Test type:	CU ($\sigma' = 30$ kPa)	Unit weight, γ	15.9 kN/m ³	-
Shear rate, v:	0.1 mm/min		Remoulded²⁾	Cement added²⁾
Test data:	27/03 to 28/03/2023	Water content, w:	97.2 %	64.1 %
Primary results:			Secondary results:	
S_u	18.5 kPa		pH ³⁾	11.1
$(E)_{u50}$	8.4 MPa		LL ³⁾	94.9 %
			PL ³⁾	43.5 %

1) The last ≈ 24 hours of curing were performed in the triaxial cell during consolidation

2) Water contents when mixing the specimen before curing

3) Determined on the same day as the triaxial test was finished

Stage	Description of triaxial test stages
1	Ramp up to a cell pressure of 530 kPa and back pressure of 500 kPa.
2	Consolidation.
3	B-check to verify saturation level.
4	Execution of CU test.

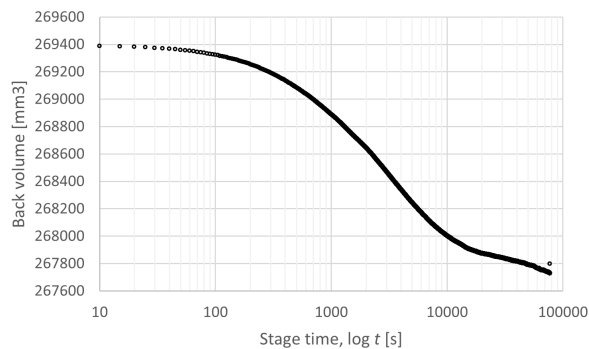


Figure F.1. Stage 2.

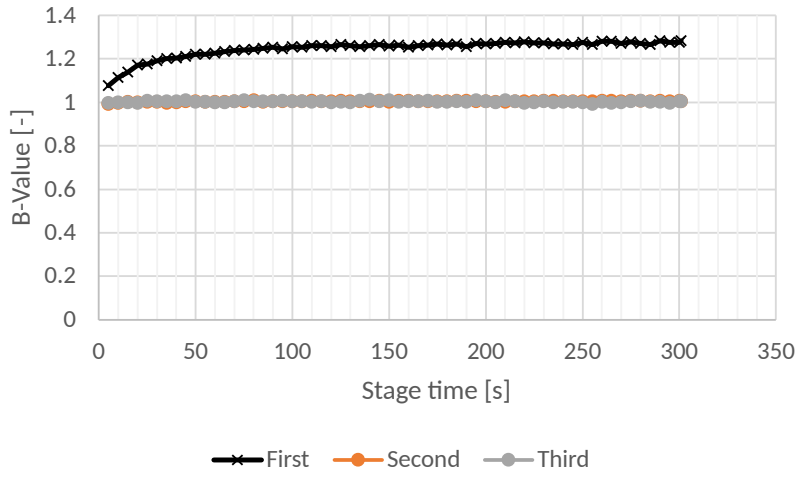


Figure F.2. Stage 3.

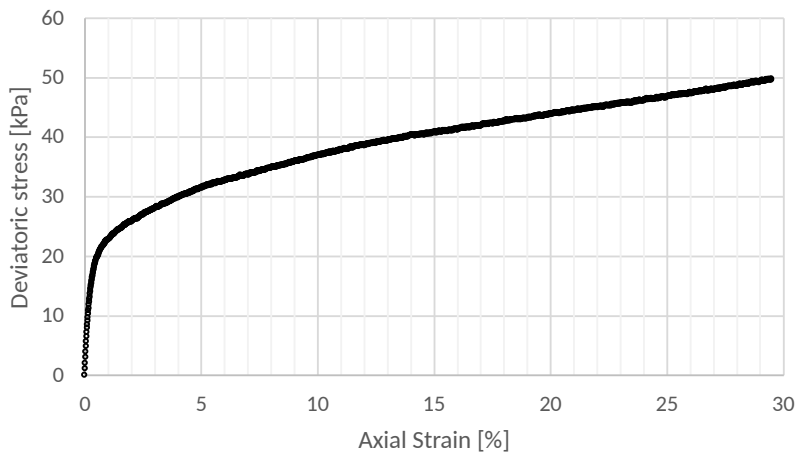


Figure F.3. Stage 4.

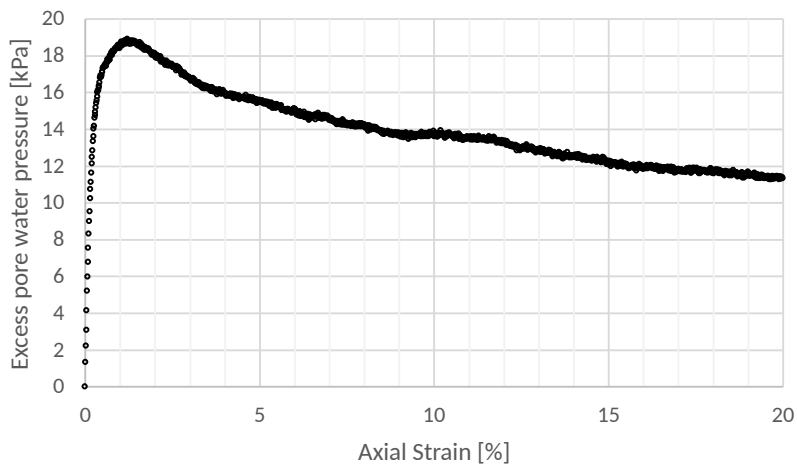


Figure F.4. Stage 4.

F.2 Triaxial04: CU test curing for 14 days at 20 °C

This CU test was performed on a gyttja-cement specimen that cured for 14 days.

Test description:

The test was performed using a GDS triaxial cell using GDSLab v2.5.4.28 software.

Cement amount:	30 kg/m ³		Before	After
Curing period:	14 days ¹⁾	Water content, w:	51.3 %	60.6 %
Curing temp.:	19 to 20.5 °C	Saturation, S:	91.9 %	-
Diameter, d:	70 mm	Height, h:	70 mm	-
Pore water:	Demineralised	Void ratio, e:	1.49	-
Test type:	CU ($\sigma' = 30$ kPa)	Unit weight, γ	15.9 kN/m ³	-
Shear rate, v:	0.1 mm/min		Remoulded²⁾	Cement added²⁾
Test data:	20/03 to 21/03/2023	Water content, w:	58.1 %	55.8 %
Primary results:			Secondary results:	
S_u	39.3 kPa		pH ³⁾	11.1
$(E)_{u50}$	3.6 MPa		LL ³⁾	89.1 %
			PL ³⁾	43.3 %

1) The last ≈ 24 hours of curing were performed in the triaxial cell during consolidation

2) Water contents when mixing the specimen before curing

3) Determined on the same day as the triaxial test was finished

Stage	Description of triaxial test stages
1	Ramp up to a cell pressure of 530 kPa and back pressure of 500 kPa.
2	Consolidation.
3	B-check to verify saturation level.
4	Execution of CU test.

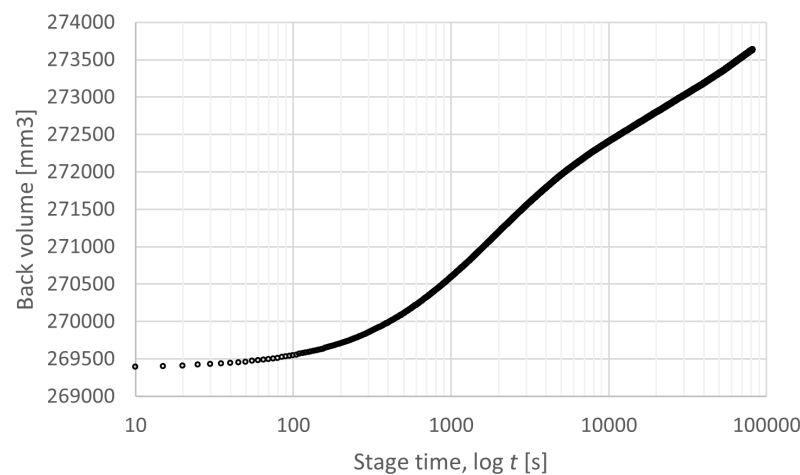


Figure F.5. Stage 2.

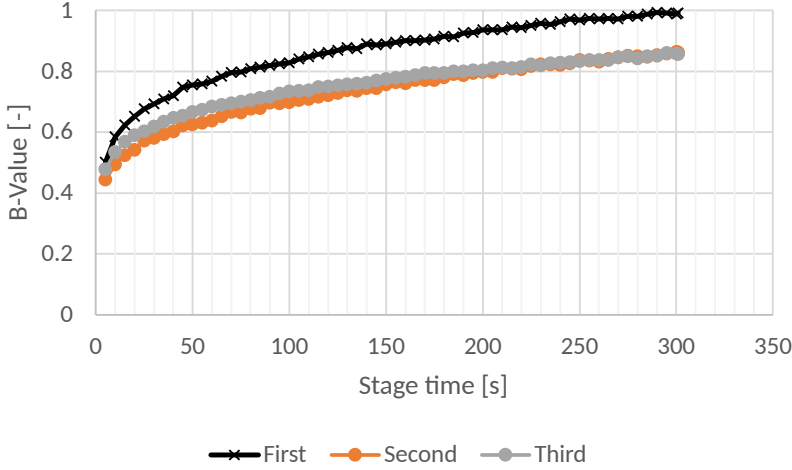


Figure F.6. Stage 3.

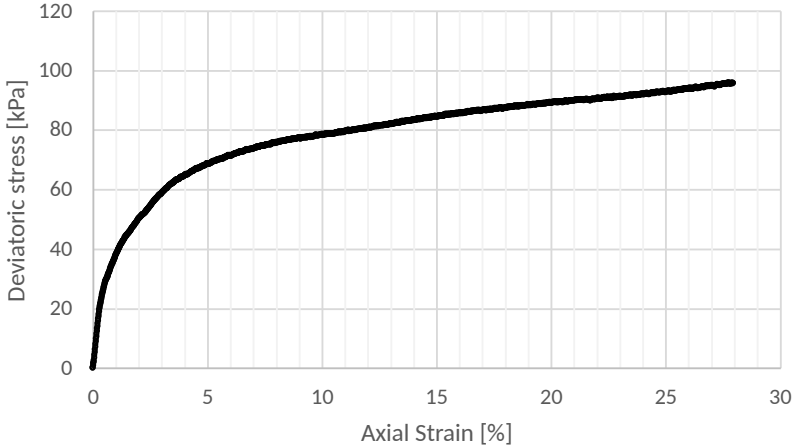


Figure F.7. Stage 4.

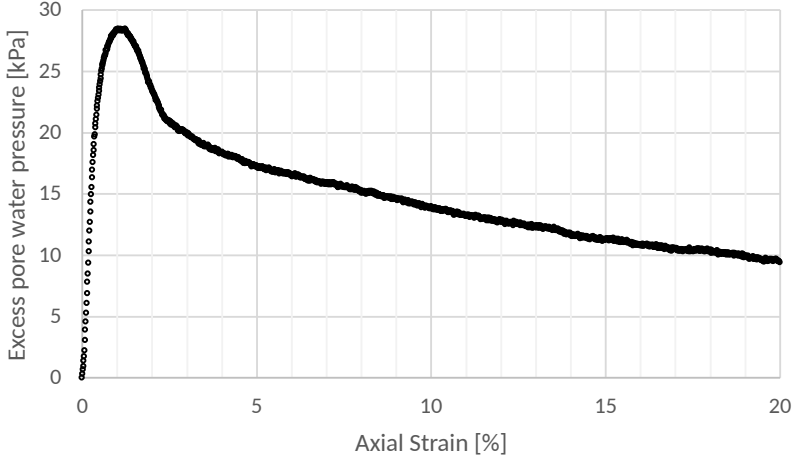


Figure F.8. Stage 4.

F.3 Triaxial05: CU test curing for 21 days at 20 °C

This CU test was performed on a gyttja-cement specimen that cured for 21 days.

Test description:

The test was performed using a GDS triaxial cell using GDSLab v2.5.4.28 software.

Cement amount:	30 kg/m ³		Before	After
Curing period:	21 days ¹⁾	Water content, w:	51.3 %	60.3 %
Curing temp.:	19 to 20.5 °C	Saturation, S:	91.9 %	-
Diameter, d:	70 mm	Height, h:	70 mm	-
Pore water:	Demineralised	Void ratio, e:	1.48	-
Test type:	CU ($\sigma' = 30$ kPa)	Unit weight, γ	15.9 kN/m ³	-
Shear rate, v:	0.1 mm/min		Remoulded²⁾	Cement added²⁾
Test data:	27/03 to 28/03/2023	Water content, w:	58.1 %	55.8 %
Primary results:			Secondary results:	
S_u	26.5 kPa		pH ³⁾	10.3
$(E)_{u50}$	9.6 MPa		LL ³⁾	88.8 %
			PL ³⁾	45.1 %

1) The last ≈ 24 hours of curing were performed in the triaxial cell during consolidation

2) Water contents when mixing the specimen before curing

3) Determined on the same day as the triaxial test was finished

Stage	Description of triaxial test stages
1	Ramp up to a cell pressure of 530 kPa and back pressure of 500 kPa.
2	Consolidation.
3	B-check to verify saturation level.
4	Execution of CU test.

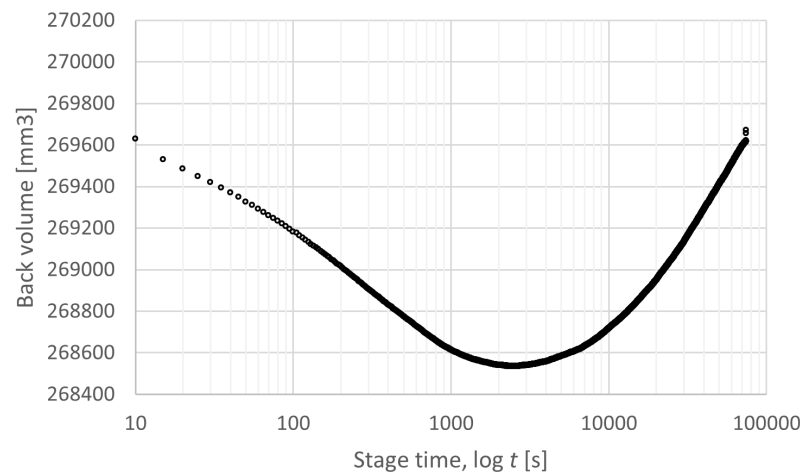


Figure F.9. Stage 2.

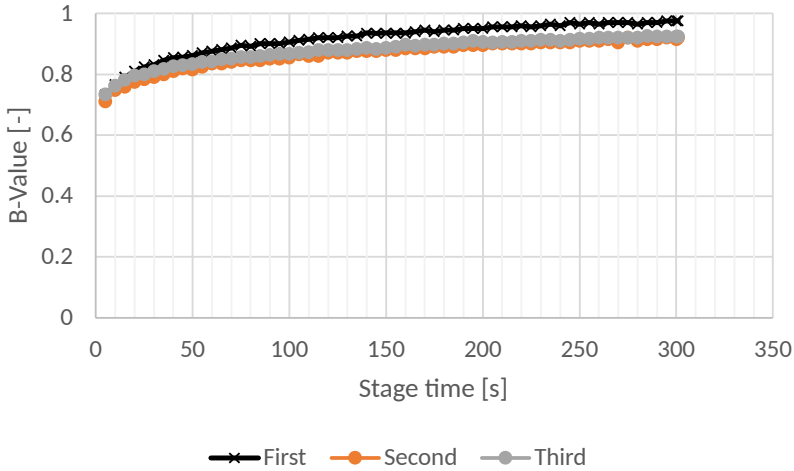


Figure F.10. Stage 3.

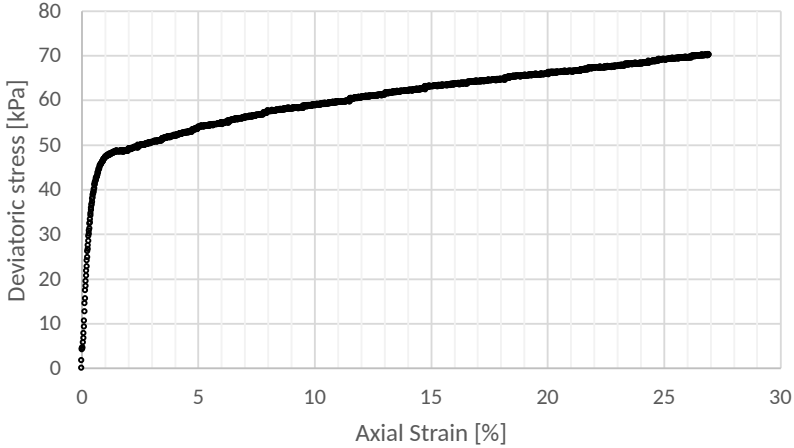


Figure F.11. Stage 4.

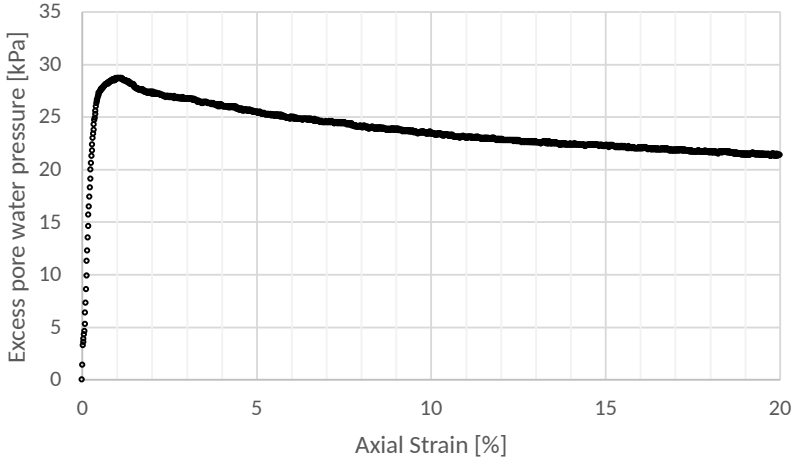


Figure F.12. Stage 4.

F.4 Triaxial06: CU test curing for 28 days at 20 °C

This CU test was performed on a gyttja-cement specimen that cured for 28 days.

Test description:				
The test was performed using a GDS triaxial cell using GDSLab v2.5.4.28 software.				
Cement amount:	30 kg/m ³		Before	After
Curing period:	28 days ¹⁾	Water content, w:	49.2 %	60.1 %
Curing temp.:	19 to 20.5 °C	Saturation, S:	90.1 %	-
Diameter, d:	70 mm	Height, h:	70 mm	-
Pore water:	Demineralised	Void ratio, e:	1.45	-
Test type:	CU ($\sigma' = 30$ kPa)	Unit weight, γ	15.9 kN/m ³	-
Shear rate, v:	0.1 mm/min		Remoulded²⁾	Cement added²⁾
Test data:	03/04 to 04/03/2023	Water content, w:	58.1 %	55.8 %
Primary results:		Secondary results:		
S_u	50.8 kPa	pH ³⁾	10.7	
$(E)_{u50}$	21.1 MPa	LL ³⁾	85.3 %	
		PL ³⁾	50.4 %	

1) The last ≈ 24 hours of curing were performed in the triaxial cell during consolidation

2) Water contents when mixing the specimen before curing

3) Determined on the same day as the triaxial test was finished

Stage	Description of triaxial test stages
1	Ramp up to a cell pressure of 530 kPa and back pressure of 500 kPa.
2	Consolidation.
3	B-check to verify saturation level.
4	Execution of CU test.

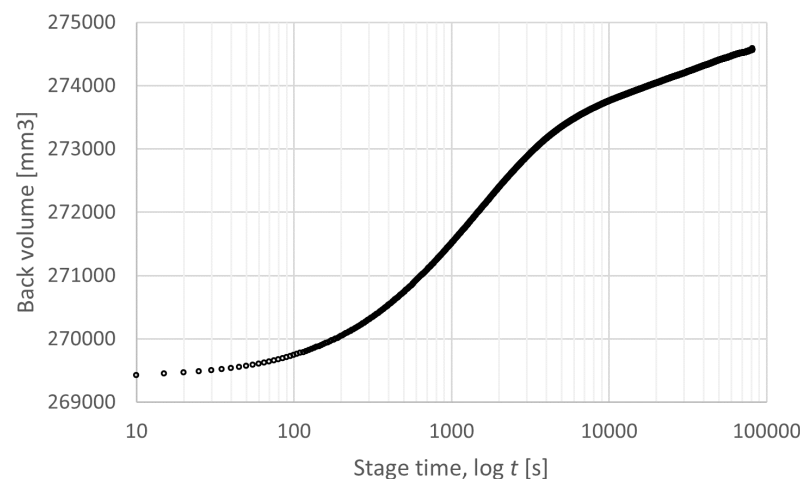


Figure F.13. Stage 2.

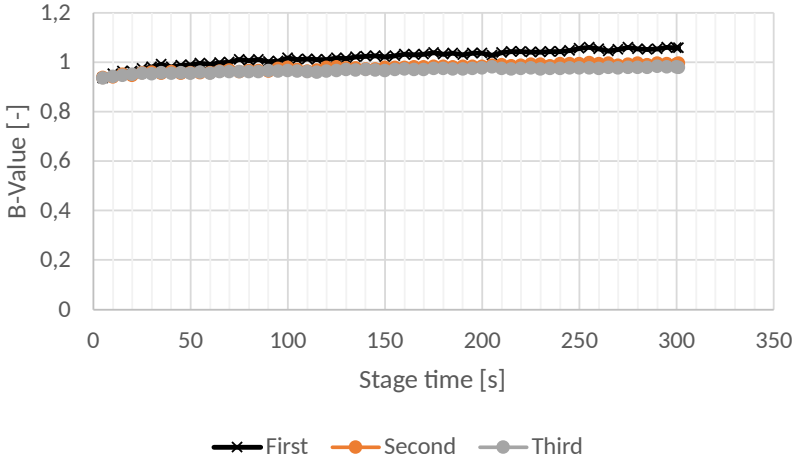


Figure F.14. Stage 3.

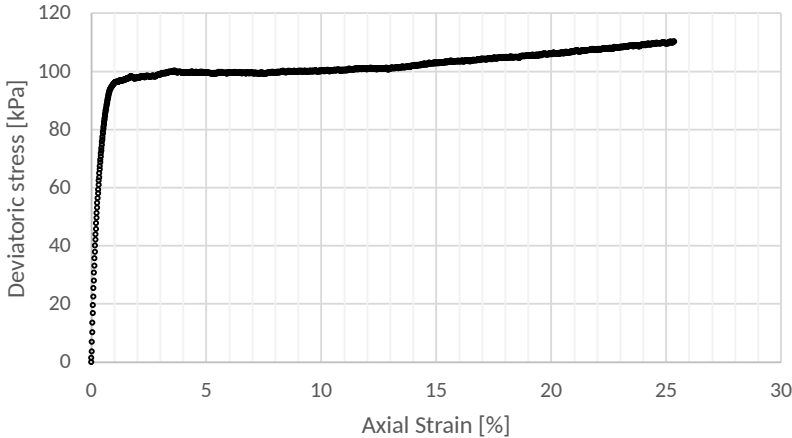


Figure F.15. Stage 4.

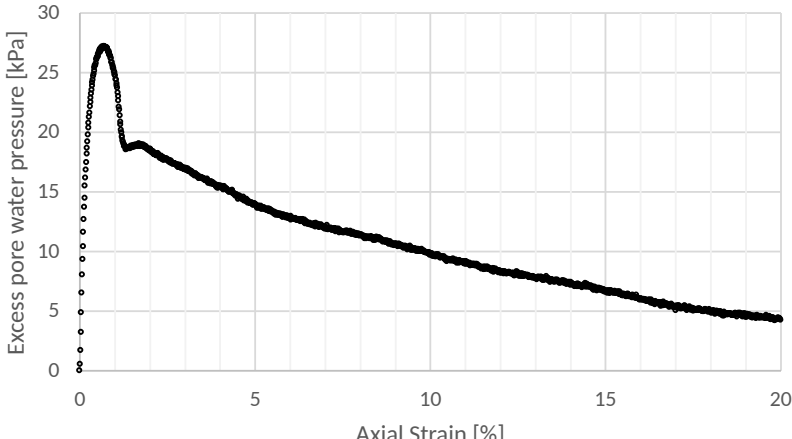


Figure F.16. Stage 4.

F.5 Triaxial07: CU test curing for 25 days at 8 °C

This CU test was performed on a gyttja-cement specimen that cured for 26 days.

Test description:

The test was performed using a GDS triaxial cell using GDSLab v2.5.4.28 software.

Cement amount:	30 kg/m ³		Before	After
Curing period:	26 days ¹⁾	Water content, w:	55.4 %	70.4 %
Curing temp.:	8 °C	Saturation, S:	95.6 %	-
Diameter, d:	70 mm	Height, h:	70 mm	-
Pore water:	Demineralised	Void ratio, e:	1.54	-
Test type:	CU ($\sigma' = 30$ kPa)	Unit weight, γ	15.9 kN/m ³	-
Shear rate, v:	0.1 mm/min		Remoulded²⁾	Cement added²⁾
Test data:	02/04 to 03/03/2023	Water content, w:	62.2 %	56.7 %
Primary results:			Secondary results:	
S_u	26.0 kPa		pH ³⁾	10.8
$(E)_{u50}$	7.0 MPa			

1) The last ≈ 24 hours of curing were performed in the triaxial cell during consolidation

2) Water contents when mixing the specimen before curing

3) Determined on the same day as the triaxial test was finished

Stage	Description of triaxial test stages
1	Ramp up to a cell pressure of 530 kPa and back pressure of 500 kPa.
2	Consolidation.
3	B-check to verify saturation level.
4	Execution of CU test.

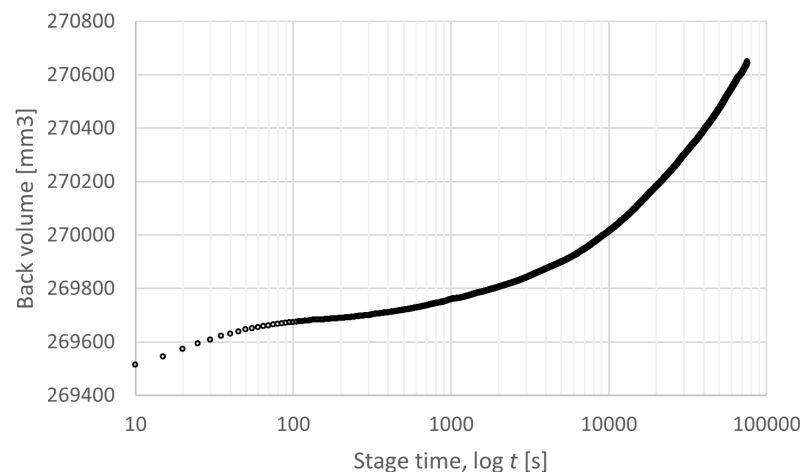


Figure F.17. Stage 2.

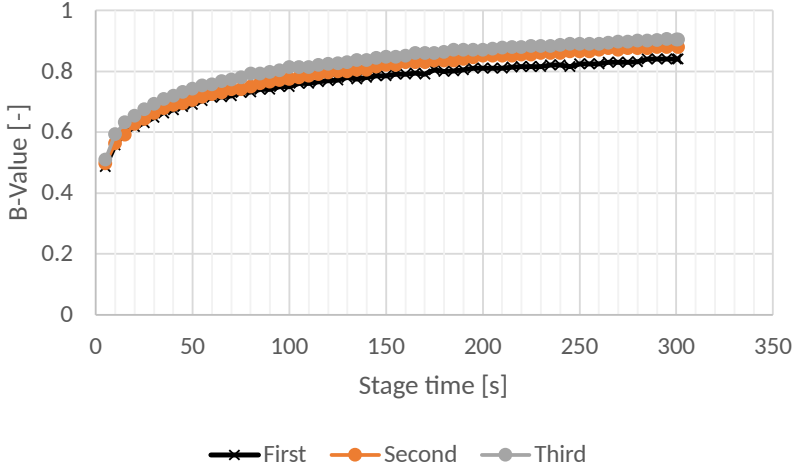


Figure F.18. Stage 3.

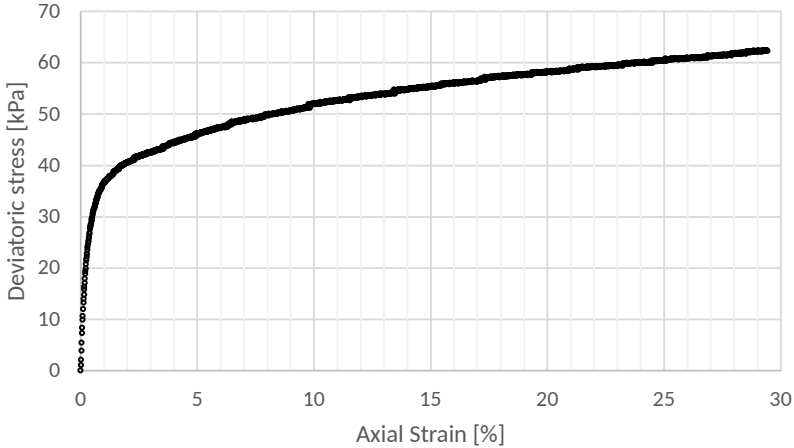


Figure F.19. Stage 4.

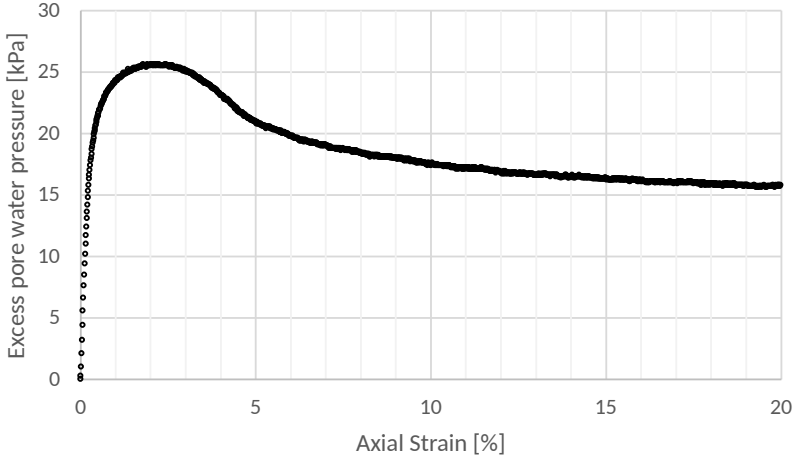


Figure F.20. Stage 4.

F.6 Triaxial08: CU test curing for 54 days at 8 °C

This CU test was performed on a gyttja-cement specimen that cured for 55 days.

Test description:

The test was performed using a GDS triaxial cell using GDSLab v2.5.4.28 software.

The load cell measurements were unclear, hence the correct curve was estimated.

Cement amount:	30 kg/m ³		Before	After
Curing period:	55 days ¹⁾	Water content, w:	-	66.1 %
Curing temp.:	8 °C	Saturation, S:	-	-
Diameter, d:	70 mm	Height, h:	70 mm	-
Pore water:	Demineralised	Void ratio, e:	-	-
Test type:	CU ($\sigma' = 30$ kPa)	Unit weight, γ	15.8 kN/m ³	-
Shear rate, v:	0.1 mm/min		Remoulded²⁾	Cement added²⁾
Test data:	01/05 to 02/05/2023	Water content, w:	62.2 %	56.7 %
Primary results:			Secondary results:	
S_u	33.2 kPa		pH ³⁾	11.0
$(E)_{u50}$	10.1 MPa			

1) The last ≈ 24 hours of curing were performed in the triaxial cell during consolidation

2) Water contents when mixing the specimen before curing

3) Determined on the same day as the triaxial test was finished

Stage	Description of triaxial test stages
1	Ramp up to a cell pressure of 530 kPa and back pressure of 500 kPa.
2	Consolidation.
3	B-check to verify saturation level.
4	Execution of CU test.

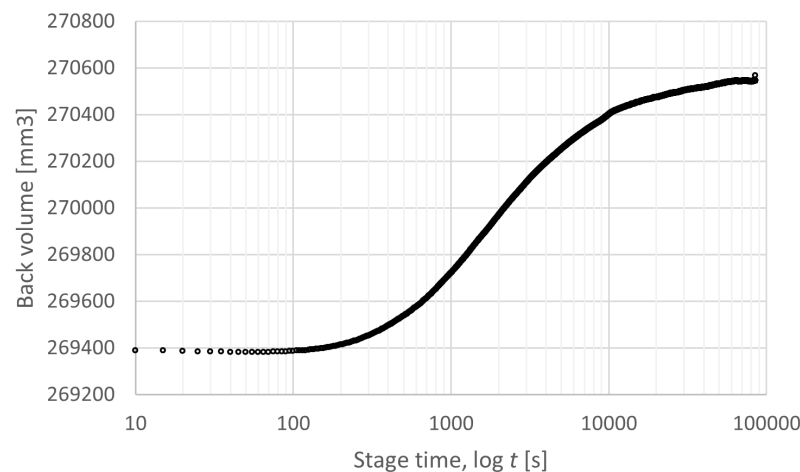


Figure F.21. Stage 2.

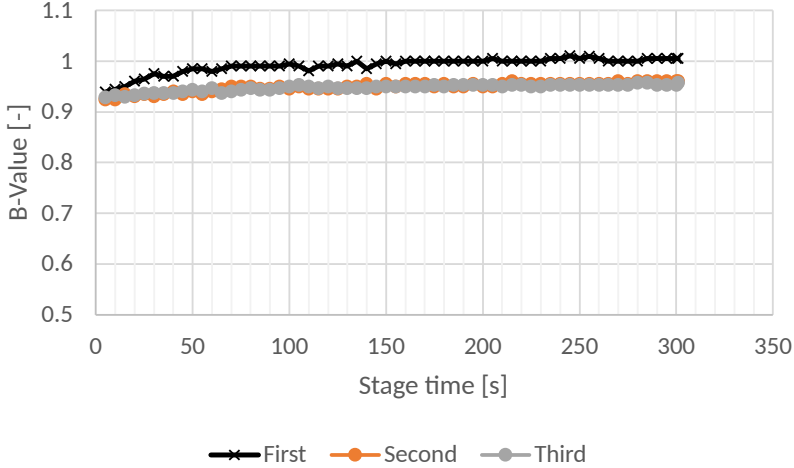


Figure F.22. Stage 3.

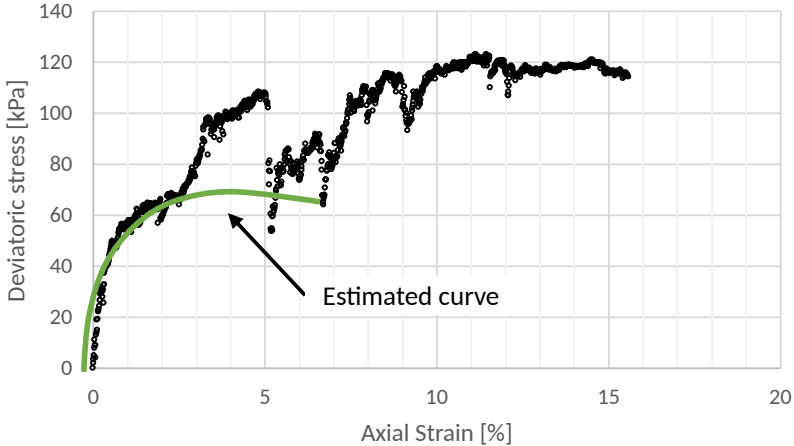


Figure F.23. Stage 4.

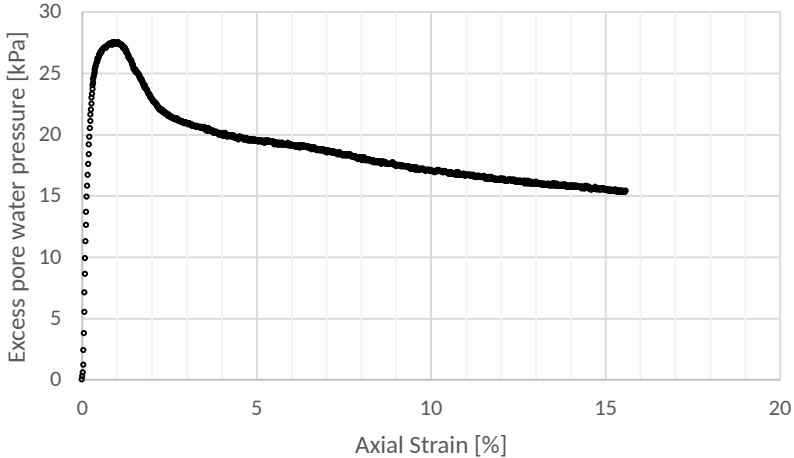


Figure F.24. Stage 4.

F.7 Triaxial09: CU test curing for 83 days at 8 °C

This CU test was performed on a gyttja-cement specimen that cured for 84 days.

Test description:

The test was performed using a GDS triaxial cell using GDSLab v2.5.4.28 software.

Cement amount:	30 kg/m ³		Before	After
Curing period:	84 days ¹⁾	Water content, w:	55.4 %	70.4 %
Curing temp.:	8 °C	Saturation, S:	95.6 %	-
Diameter, d:	70 mm	Height, h:	70 mm	-
Pore water:	Demineralised	Void ratio, e:	1.54	-
Test type:	CU ($\sigma' = 30$ kPa)	Unit weight, γ	15.9 kN/m ³	-
Shear rate, v:	0.1 mm/min		Remoulded²⁾	Cement added²⁾
Test data:	30/05 to 31/05/2023	Water content, w:	62.2 %	56.7 %

Primary results:

S_u	30.0 kPa
$(E)_{u50}$	7.9 MPa

1) The last ≈ 24 hours of curing were performed in the triaxial cell during consolidation

2) Water contents when mixing the specimen before curing

Stage	Description of triaxial test stages
1	Ramp up to a cell pressure of 530 kPa and back pressure of 500 kPa.
2	Consolidation.
3	B-check to verify saturation level.
4	Execution of CU test.

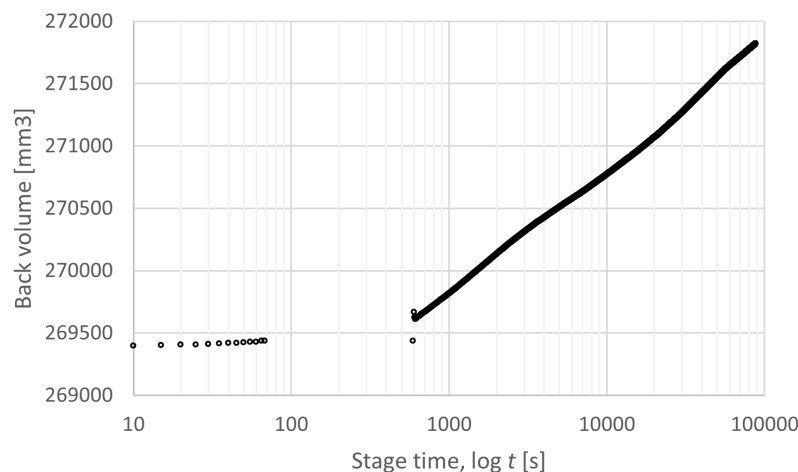


Figure F.25. Stage 2.

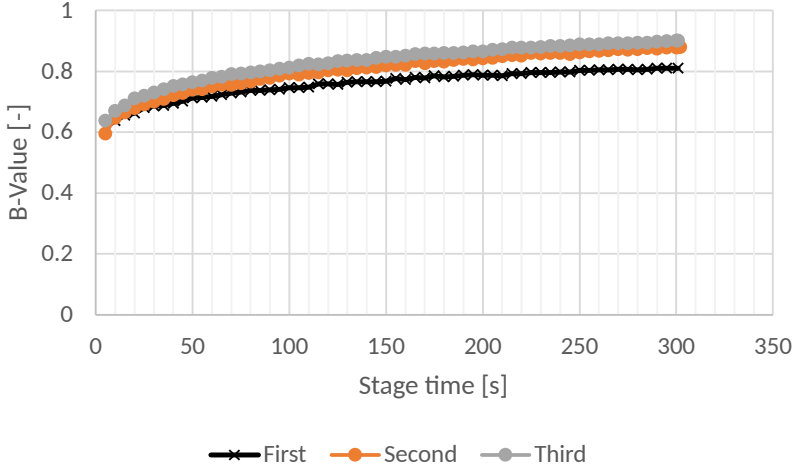


Figure F.26. Stage 3.

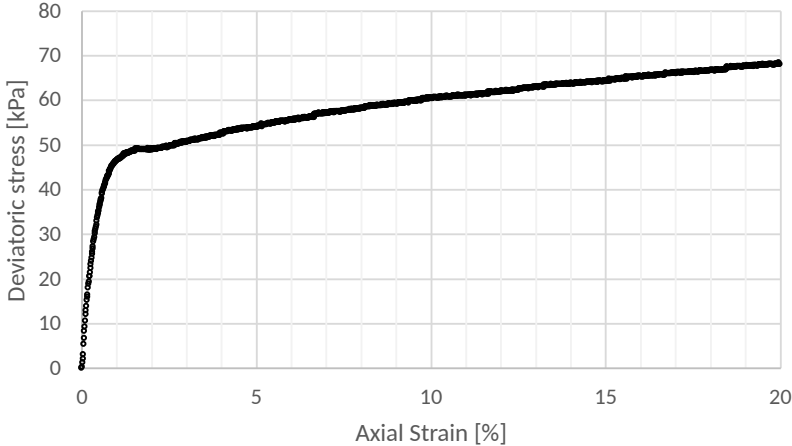


Figure F.27. Stage 4.

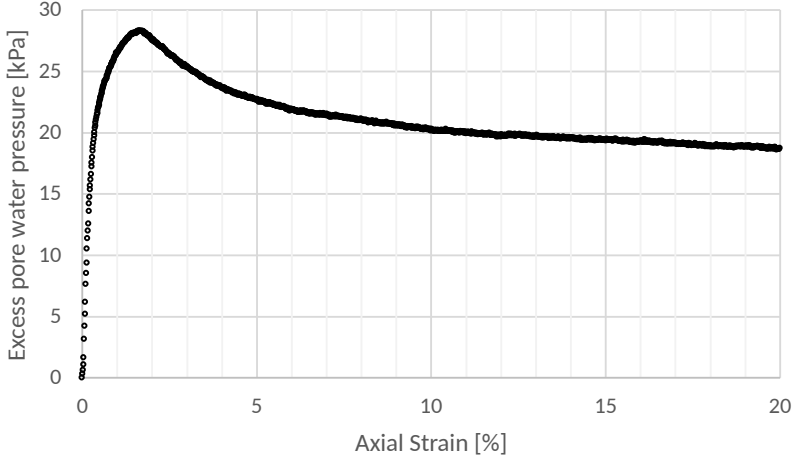


Figure F.28. Stage 4.

F.8 Triaxial10: CD test curing for 7 days at 20 °C

This CU test was performed on a gyttja-cement specimen that cured for 7 days.

Test description:

The test was performed using a GDS triaxial cell using GDSLab v2.5.4.28 software.

Cement amount:	30 kg/m ³		Before	After
Curing period:	7 days ¹⁾	Water content, w:	78.9 %	68.0 %
Curing temp.:	19 to 20.5 °C	Saturation, S:	108.7 %	-
Diameter, d:	70 mm	Height, h:	70 mm	-
Pore water:	Demineralised	Void ratio, e:	1.93	-
Test type:	CD ($\sigma' = 30$ kPa)	Unit weight, γ	15.9 kN/m ³	-
Shear rate, v:	0.003 mm/min		Remoulded²⁾	Cement added²⁾
Test data:	15/05 to 19/05/2023	Water content, w:	82.5 %	81.0 %

Primary results:

φ'	44.6°
$(E')_{50}$	0.9 MPa
$(E')_{ur}$	12.8 MPa

1) The last ≈ 24 hours of curing were performed in the triaxial cell during consolidation

2) Water contents when mixing the specimen before curing

Stage	Description of triaxial test stages
1	Ramp up to a cell pressure of 530 kPa and back pressure of 500 kPa.
2	Consolidation.
3	B-check to verify saturation level.
4	Execution of CU test.

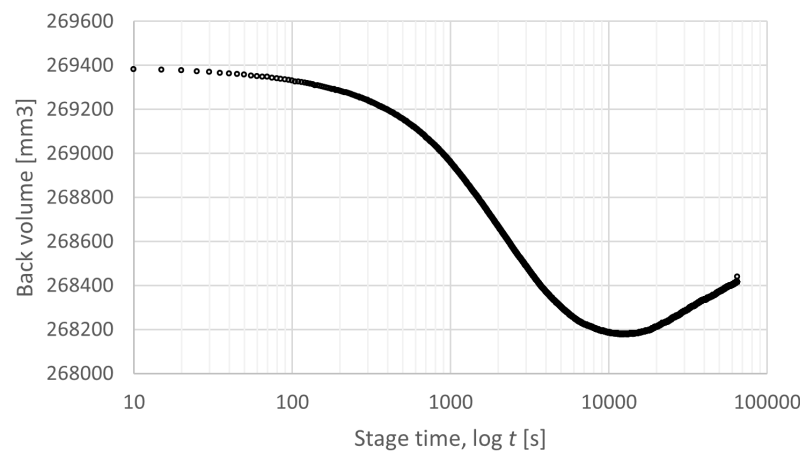


Figure F.29. Stage 2.

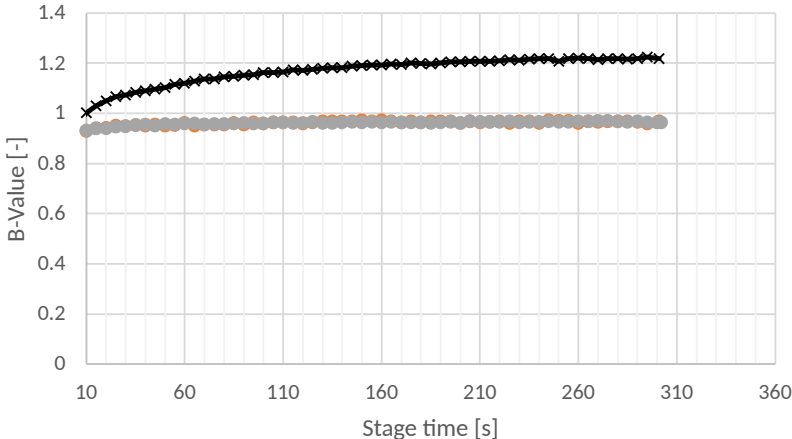


Figure F.30. Stage 3.

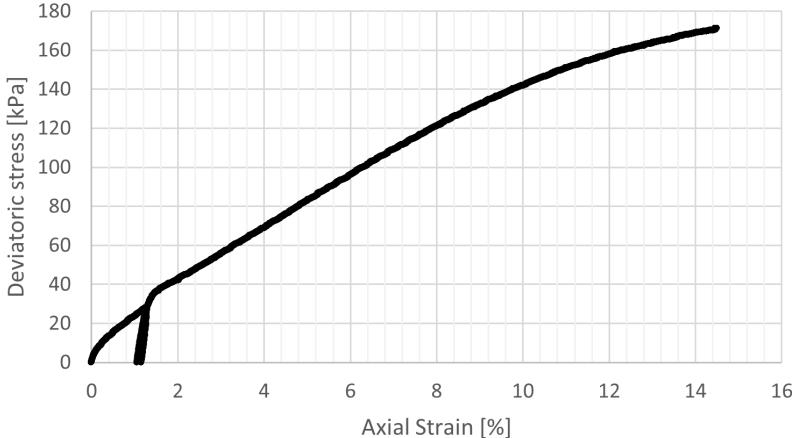


Figure F.31. Stage 4.

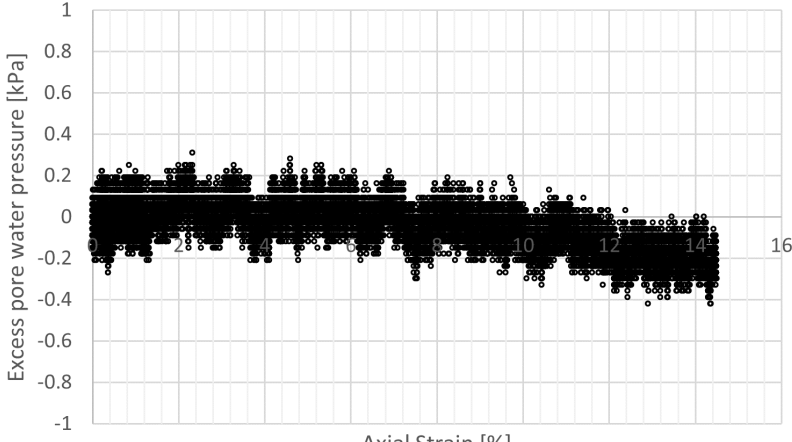


Figure F.32. Stage 4.

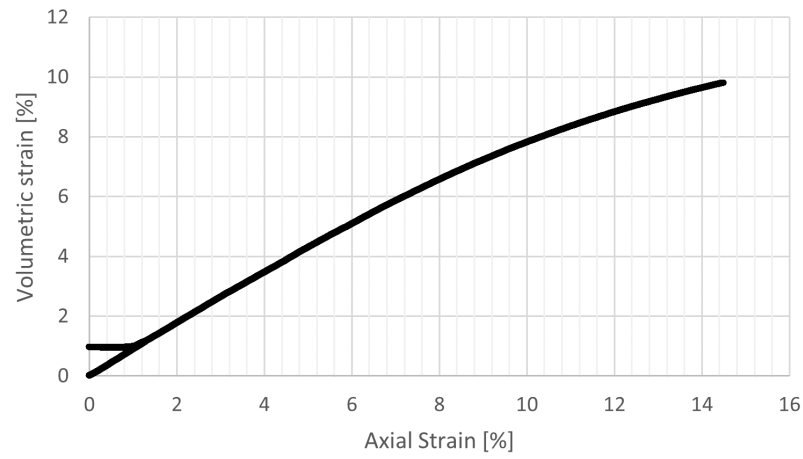


Figure F.33. Stage 4.

F.9 Triaxial11: CD test curing for 14 days at 20 °C

This CU test was performed on a gyttja-cement specimen that cured for 14 days.

Test description:

The test was performed using a GDS triaxial cell using GDSLab v2.5.4.28 software.

		Before	After
Cement amount:	30 kg/m ³		
Curing period:	14 days ¹⁾	Water content, w:	80.6 %
Curing temp.:	19 to 20.5 °C	Saturation, S:	101.5 %
Diameter, d:	70 mm	Height, h:	70 mm
Pore water:	Demineralised	Void ratio, e:	2.11
Test type:	CD ($\sigma' = 30$ kPa)	Unit weight, γ	15.1 kN/m ³
Shear rate, v:	0.003 mm/min	Remoulded²⁾	Cement added²⁾
Test data:	22/05 to 26/05/2023	Water content, w:	82.5 %
			81.0 %

Primary results:

φ'	41.5°
$(E')_{50}$	1.6 MPa
$(E')_{ur}$	10.3 MPa

1) The last ≈ 24 hours of curing were performed in the triaxial cell during consolidation

2) Water contents when mixing the specimen before curing

Stage	Description of triaxial test stages
1	Ramp up to a cell pressure of 530 kPa and back pressure of 500 kPa.
2	Consolidation.
3	B-check to verify saturation level.
4	Execution of CU test.

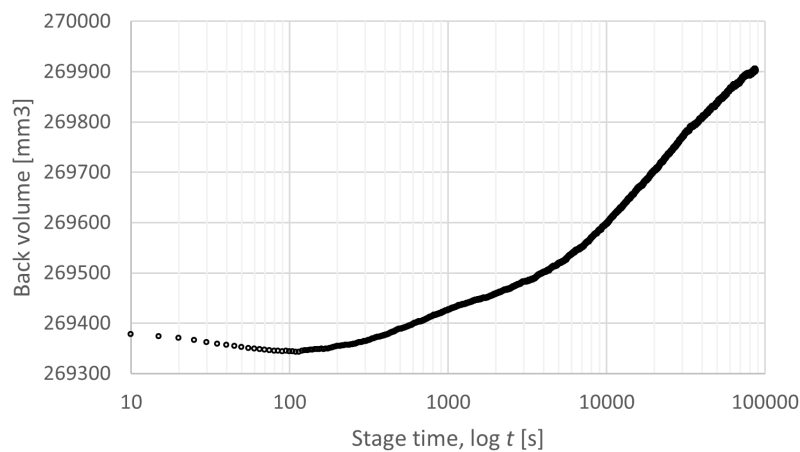


Figure F.34. Stage 2.

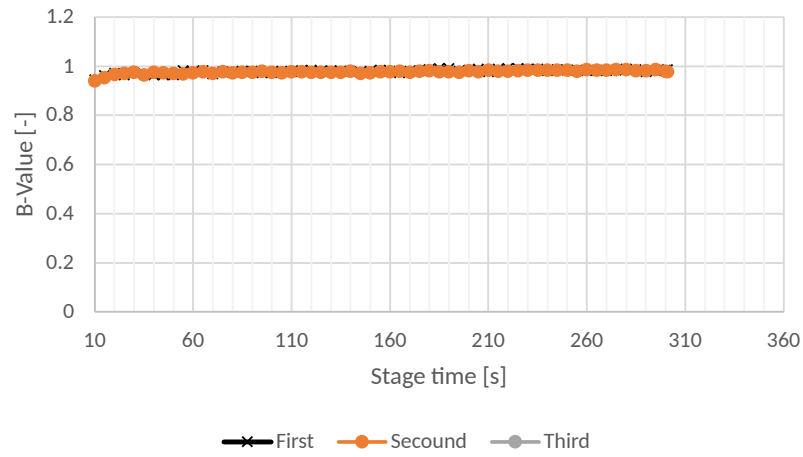


Figure F.35. Stage 3.

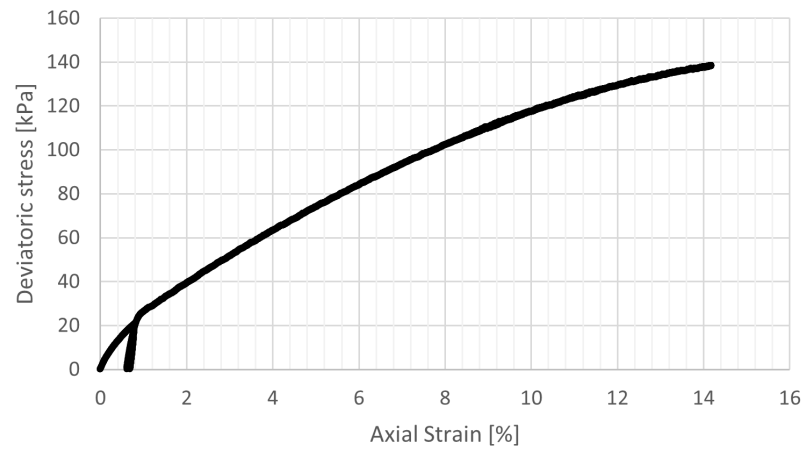


Figure F.36. Stage 4.

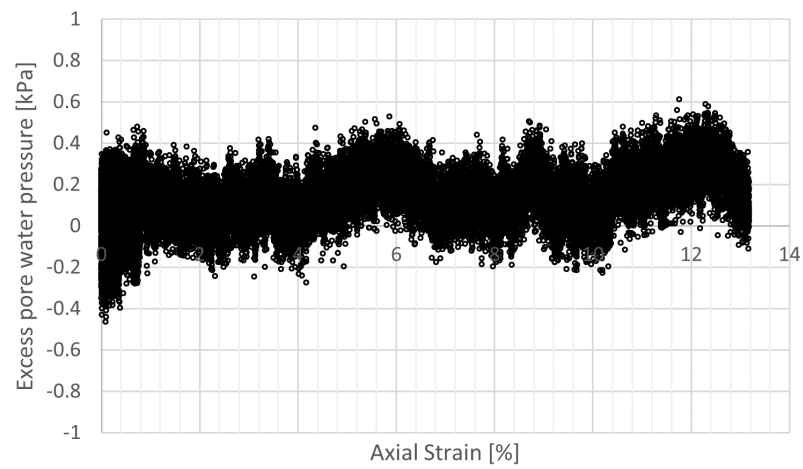


Figure F.37. Stage 4.

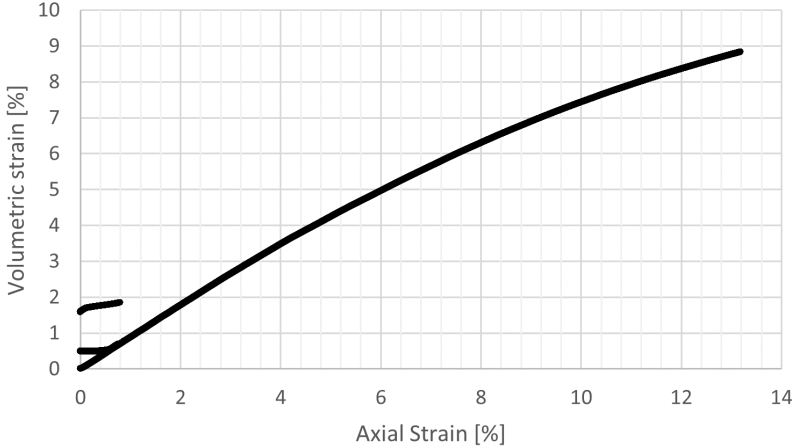


Figure F.38. Stage 4.

F.10 Triaxial12: CD test curing for 28 days at 20 °C

This CU test was performed on a gyttja-cement specimen that cured for 28 days.

Test description:				
The test was performed using a GDS triaxial cell using GDSLab v2.5.4.28 software.				
Cement amount:	30 kg/m ³		Before	After
Curing period:	28 days ¹⁾	Water content, w:	50.8 %	54.3 %
Curing temp.:	19 to 20.5 °C	Saturation, S:	89.5 %	-
Diameter, d:	70 mm	Height, h:	70 mm	-
Pore water:	Demineralised	Void ratio, e:	1.51	-
Test type:	CD ($\sigma' = 30$ kPa)	Unit weight, γ	15.7 kN/m ³	-
Shear rate, v:	0.003 mm/min		Remoulded²⁾	Cement added²⁾
Test data:	15/05 to 19/05/2023	Water content, w:	60.0 %	58.2 %
Primary results:				
φ'	40.6°			
$(E')_{50}$	2.1 MPa			
$(E')_{ur}$	11.2 MPa			

1) The last ≈ 24 hours of curing were performed in the triaxial cell during consolidation

2) Water contents when mixing the specimen before curing

Stage	Description of triaxial test stages
1	Ramp up to a cell pressure of 530 kPa and back pressure of 500 kPa.
2	Consolidation.
3	B-check to verify saturation level.
4	Execution of CU test.

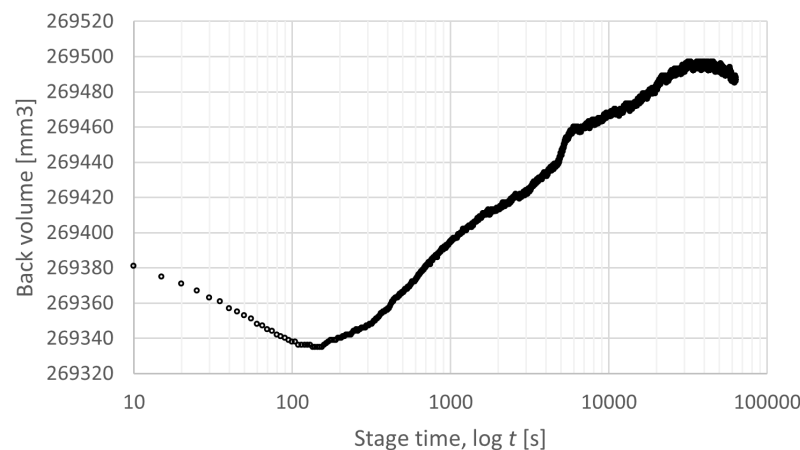


Figure F.39. Stage 2.

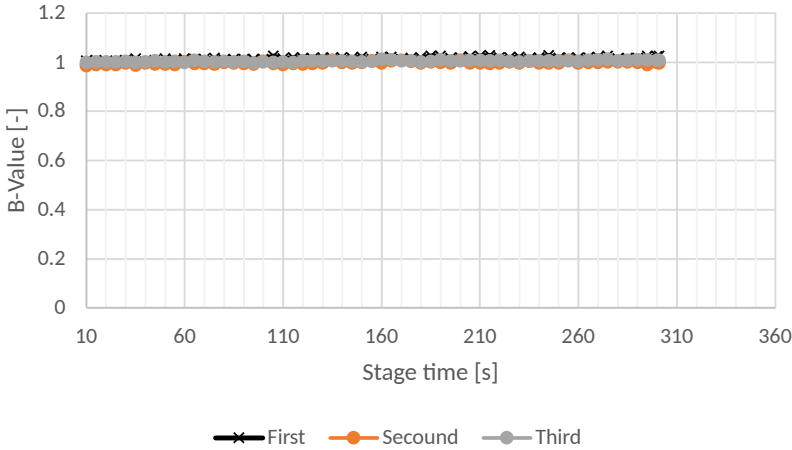


Figure F.40. Stage 3.

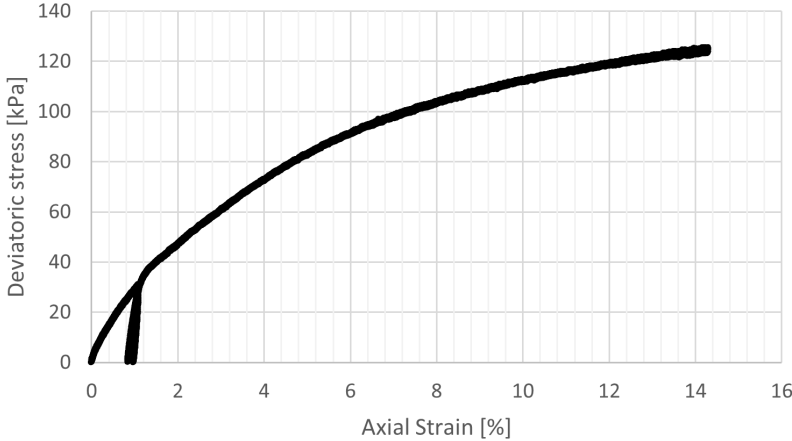


Figure F.41. Stage 4.

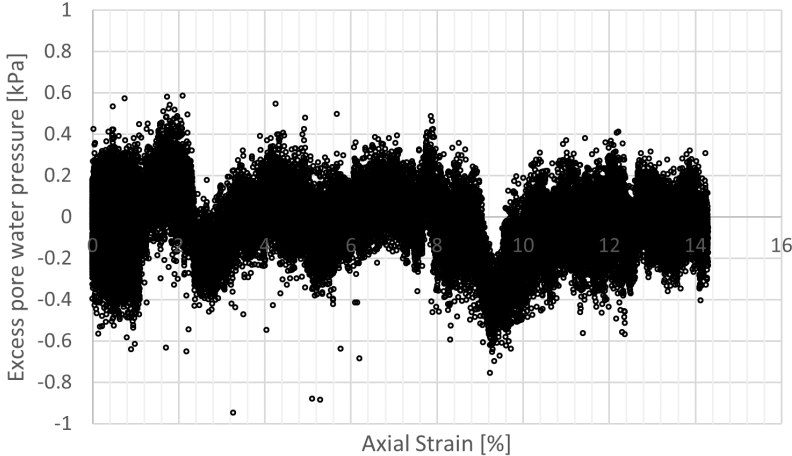


Figure F.42. Stage 4.

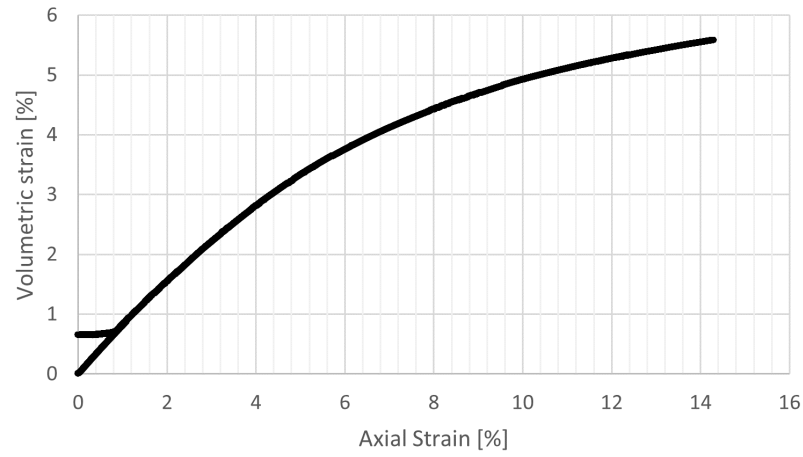


Figure F.43. Stage 4.

F.11 Triaxial13: Cyclic test curing for 28 days at 20 °C

This cyclic test was performed on a gyttja-cement specimen that cured for 28 days.

Test description:

The test was performed using a GDS advanced dynamic triaxial cell using GDSLab v2.5.4.28 software.

Cement amount:	30 kg/m ³		Before	After
Curing period:	28 days ¹⁾	Water content, w:	48.8 %	-
Curing temp.:	19 to 20.5 °C	Saturation, S:	90.5 %	-
Diameter, d:	70 mm	Height, h:	70 mm	-
Pore water:	Demineralised	Void ratio, e:	1.43	-
Test type:	Cyclic ($\sigma' = 30$ kPa)	Unit weight, γ	15.9 kN/m ³	-
Frequency:	0.1 Hz		Remoulded²⁾	Cement added²⁾
Test data:	03/04 to 06/04/2023	Water content, w:	58.1 %	55.8 %

Primary results:

See Figure 4.27

1) The last ≈ 24 hours of curing were performed in the triaxial cell during consolidation

2) Water contents when mixing the specimen before curing

Stage	Description of triaxial test stages
1	Ramp up to a cell pressure of 530 kPa and back pressure of 500 kPa.
2	Consolidation.
3	B-check to verify saturation level.
4	Execution of cyclic test.

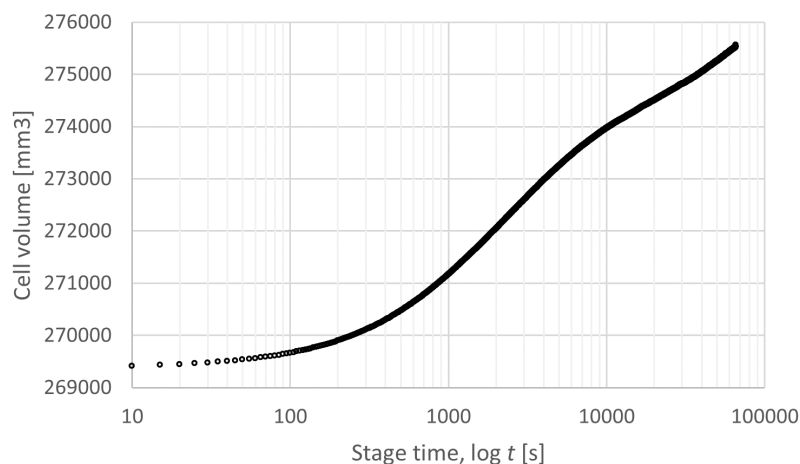


Figure F.44. Stage 2.

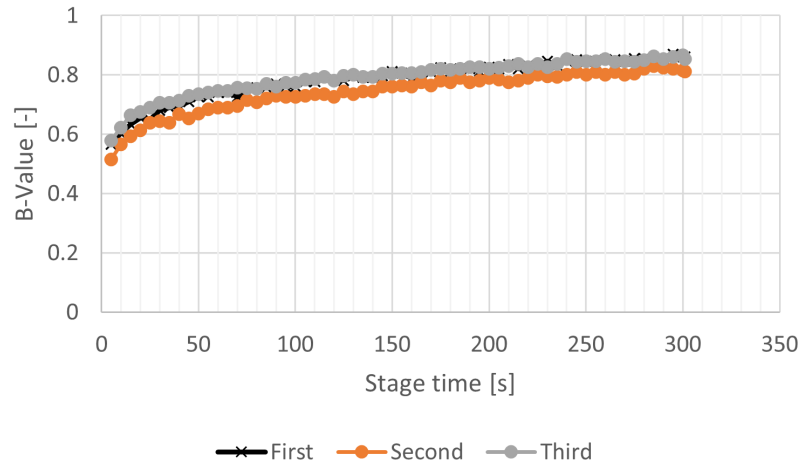


Figure F.45. Stage 3.

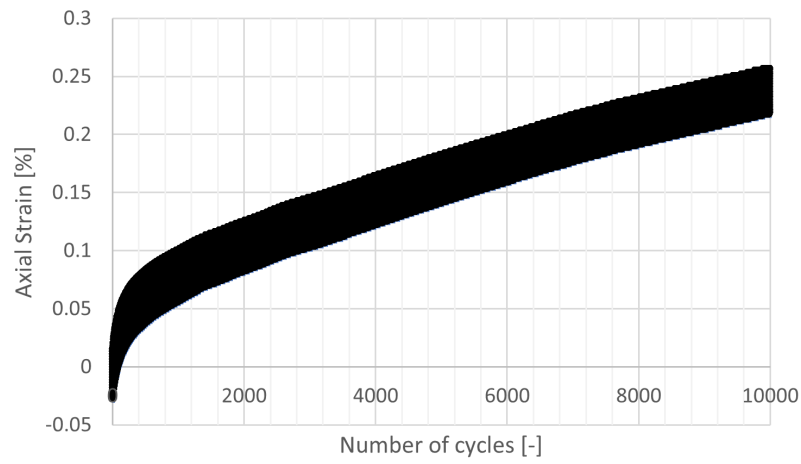


Figure F.46. Stage 4.

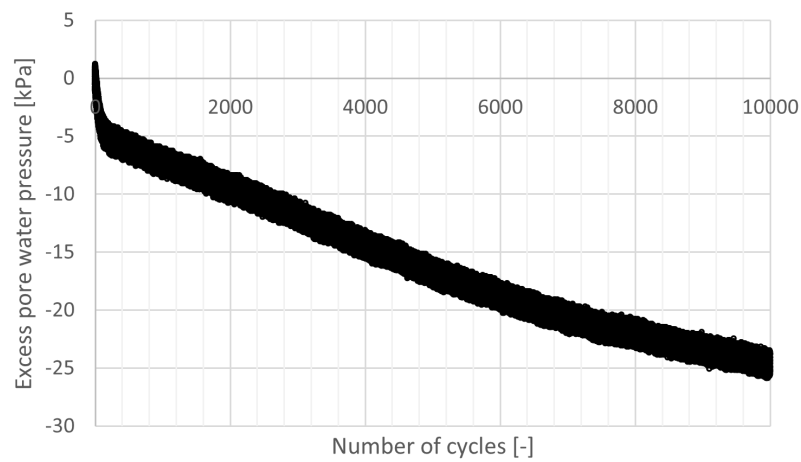


Figure F.47. Stage 4.

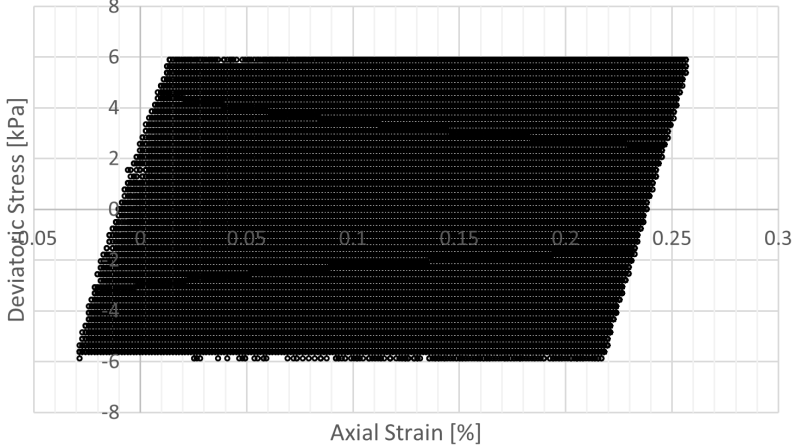


Figure F.48. Stage 4.

F.12 Oedometer02: Curing for 28 days at 20 °C (Swell log)

This test was performed on a gyttja-cement specimen that cured inside the oedometer ring for 28 days.

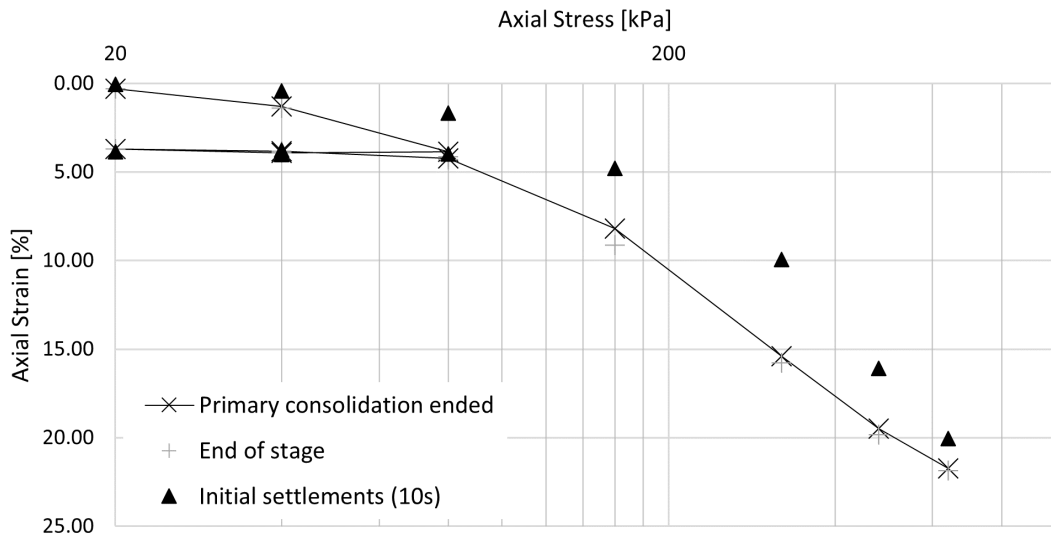


Figure F.49. Stress strain curve.

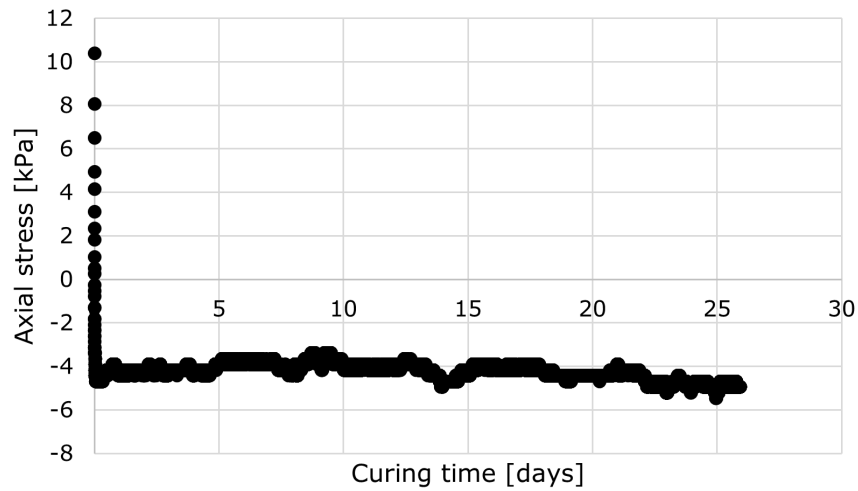


Figure F.50. Swelling log while curing.

Test description:

The test was performed using a GDSAOS with GDSLlab v2.5.4.28 software.

Cement amount:		30 kg/m ³		Before	After
Cement type:	FutureCem	Water content, w:	61.6 %	61.6 %	35.7 %
Temp. lab:	19 to 20.5 °C	Saturation, S:	99.8 %	99.8 %	106.0
Diameter, d:	70 mm	Void ratio, e:	1.64	1.64	0.90
Pore water:	Demineralised	Height, h:	35 mm	35 mm	27 mm
Test data:	27/02 to 27/04/2023	Unit weight, γ	15.9 kN/m ³	15.9 kN/m ³	18.7 kN/m ³
			Remoulded¹⁾	Cement added¹⁾	
		Water content, w:	64.1 %	64.1 %	61.6 %

Results:

See Table F.1

1) Water contents when mixing the specimen prior to curing

Table F.1. Results from oedometer test.

σ_v [kPa]	t_{end} [min]	ε_{100} [%]	ε_{end} [%]	ε_{int} [%]	$C_{\varepsilon C}$ [%]	E_{oed} [MPa]
20	720	0.29	0.29	0	-	-
40	720	1.31	1.38	0.29	3.40	1.96
80	720	3.86	4.13	1.38	8.45	1.57
40	720	3.93	3.91	4.13	-0.25	-52.63
20	720	3.72	3.72	3.91	0.71	9.30
40	720	3.83	3.83	3.72	0.37	18.16
80	720	4.23	4.29	3.83	1.35	9.86
160	720	8.19	9.12	4.29	13.15	2.02
320	720	15.40	15.76	9.12	23.94	2.22
480	720	19.49	19.83	15.76	23.26	3.91
640	720	21.73	21.86	19.83	17.88	7.16

On the following pages, the oedometer data for each load step are presented. The lines used for interpreting the end of primary consolidation are kept.

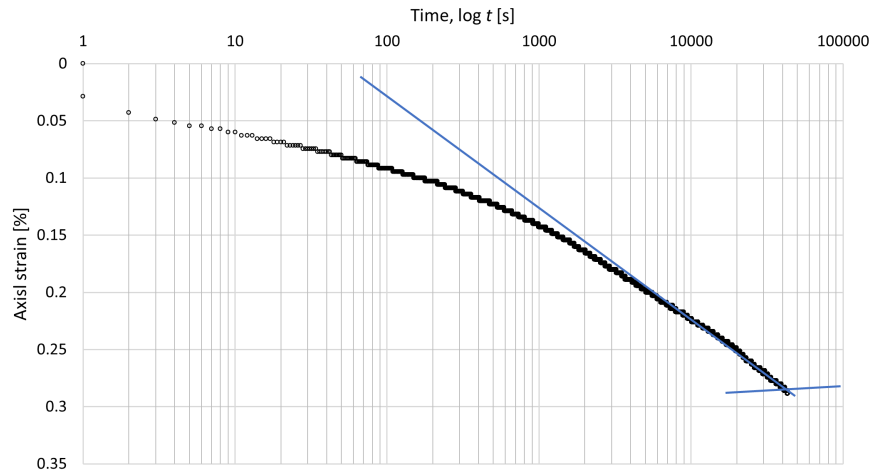


Figure F.51. Load step 1.

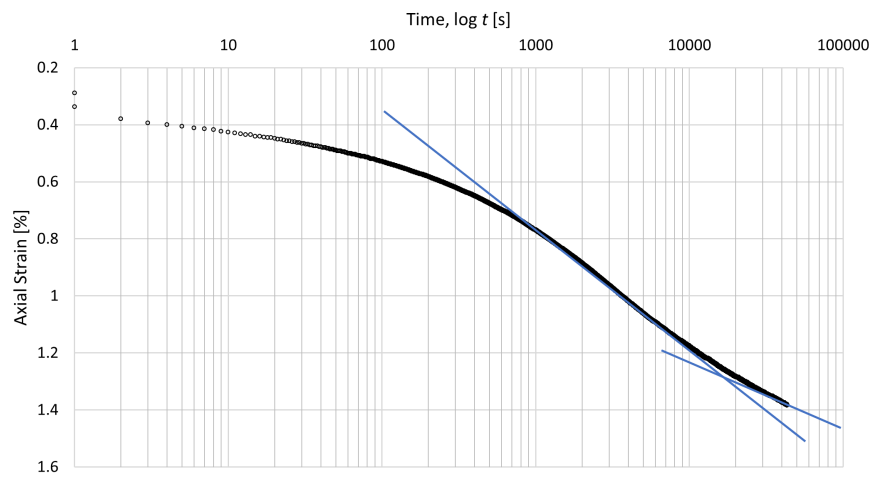


Figure F.52. Load step 2.

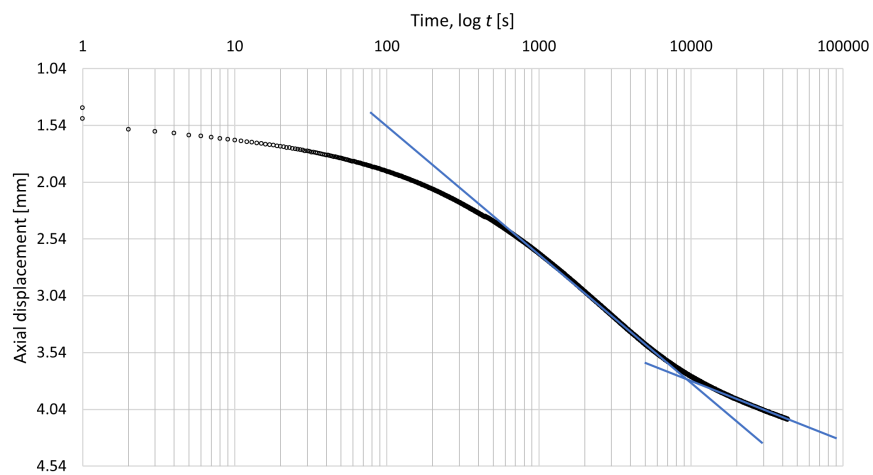


Figure F.53. Load step 3.

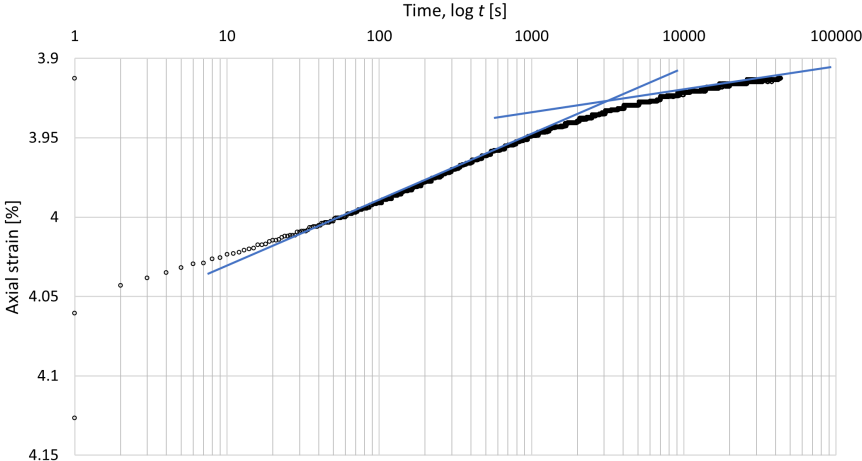


Figure F.54. Load step 4.

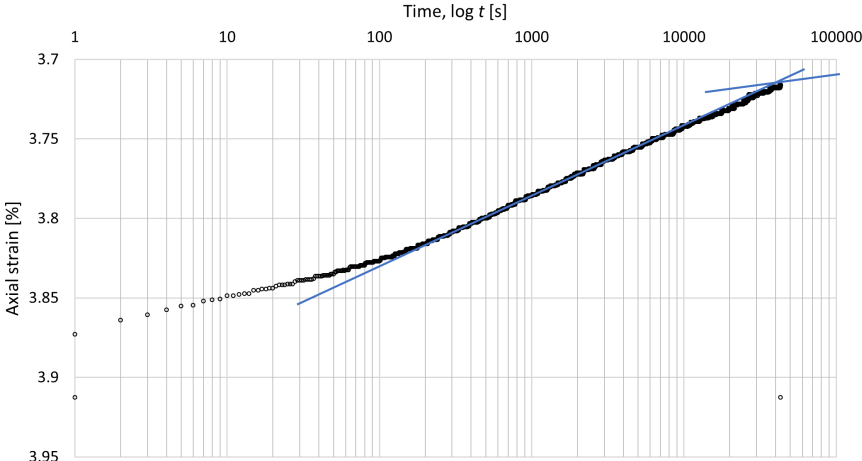


Figure F.55. Load step 5.

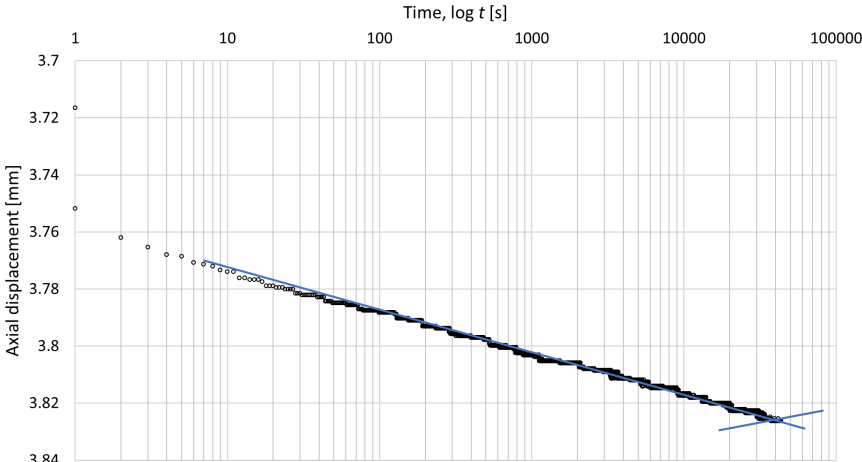


Figure F.56. Load step 6.

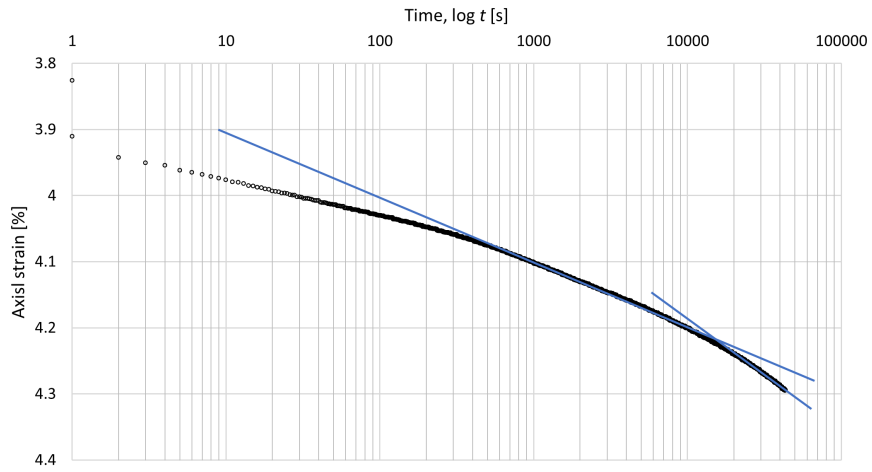


Figure F.57. Load step 7.

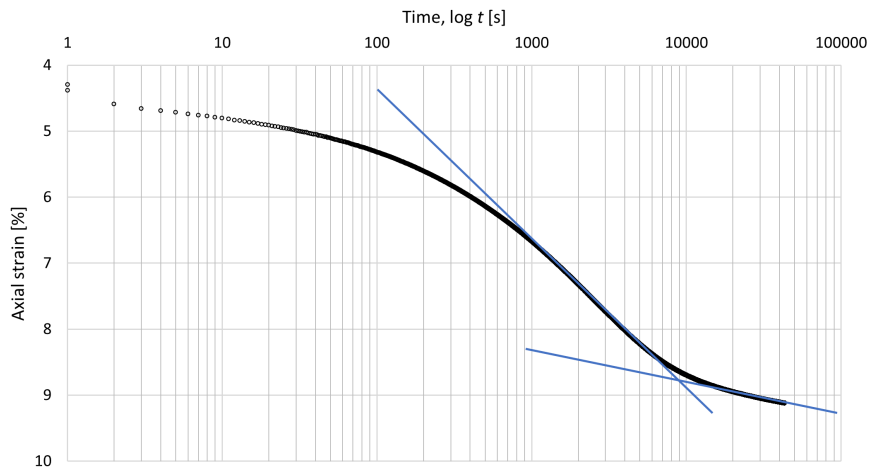


Figure F.58. Load step 8.

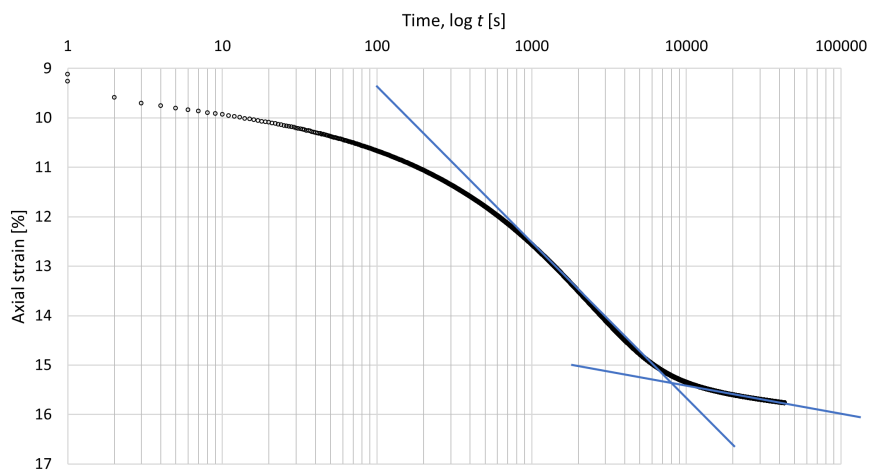


Figure F.59. Load step 9.

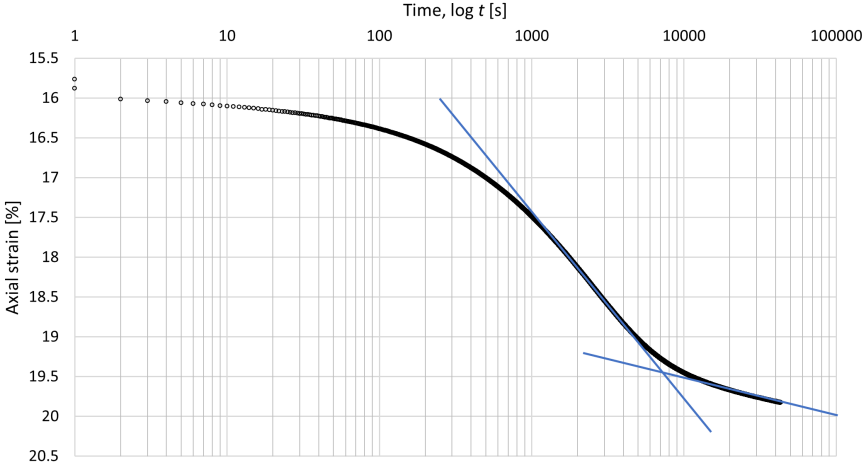


Figure F.60. Load step 10.

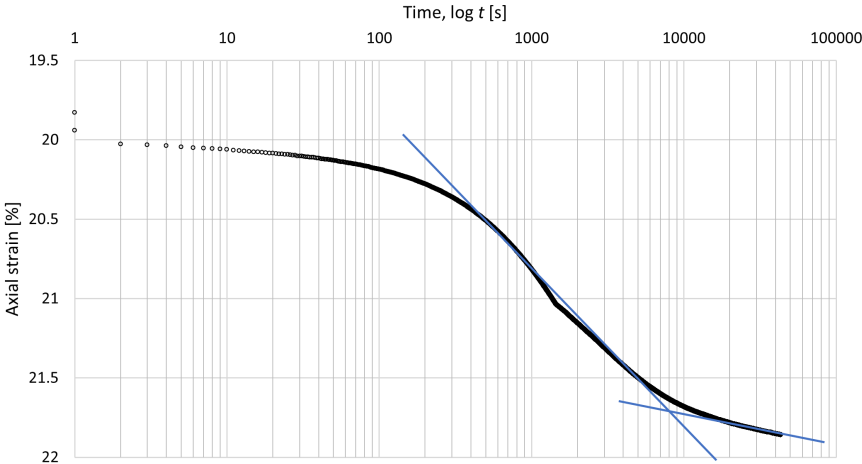


Figure F.61. Load step 11.

F.13 BenderElement02: Curing for 28 days at 20 °C (V_s log)

This test was performed on a gyttja-cement specimen that cured inside the triaxial cell until 28 days.

Test description:

The test was performed using the GDS bender element system using GDS BES v2.2.13 software.

Cement amount:	30 kg/m ³		Before	After
Temp. lab:	19 to 20.5 °C	Water content, w:	63.4 %	-
Diameter, d:	70 mm	Saturation, S:	-	-
Wavetype:	Sine	Void ratio, e:	-	-
Wave period:	0.2 ms	Height, h ¹⁾ :	63 mm	-
Test date:	24/03 to 17/04/2023	Unit weight, γ	16.0 kN/m ³	-
			Remoulded²⁾	Cement added²⁾
		Water content, w:	64.1 %	61.6 %

Results:

V_s (7 days):	109.3 m/s
V_s (14 days):	114.8 m/s
V_s (21 days):	116.1 m/s
V_s (28 days):	118.9 m/s

- 1) Subtracted the transmitter height of 7 mm
- 2) Water contents when mixing the specimen prior to curing

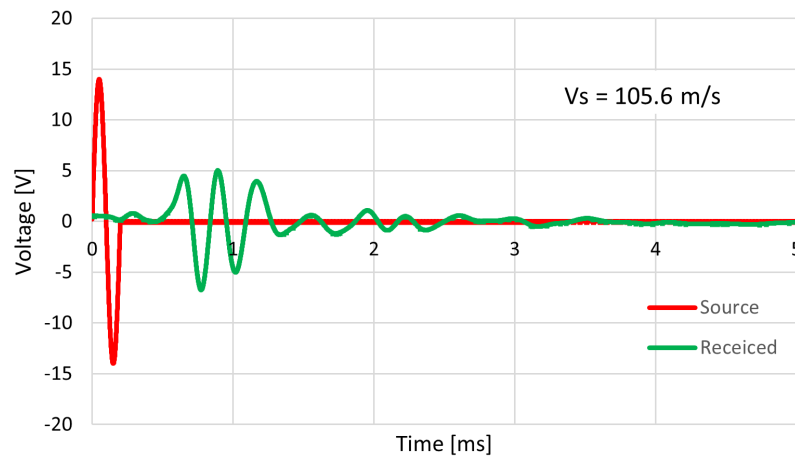


Figure F.62. Day 5.

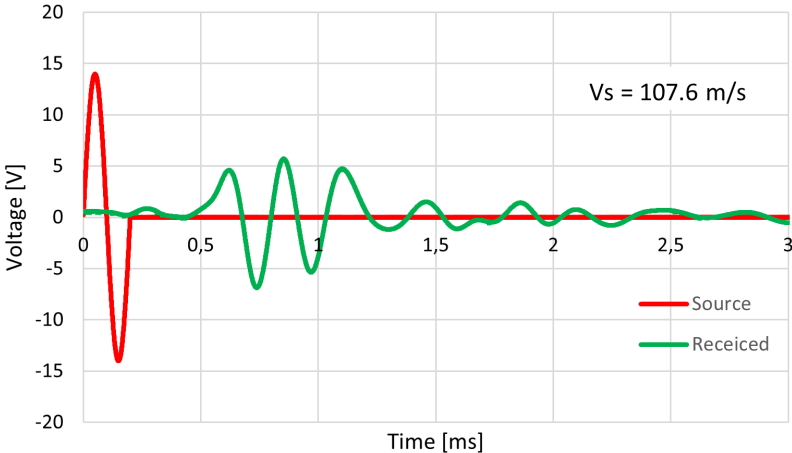


Figure F.63. Day 6.

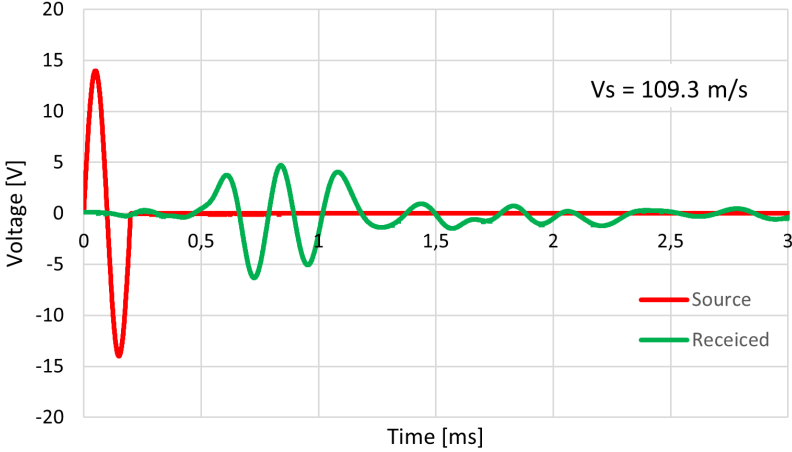


Figure F.64. Day 7.

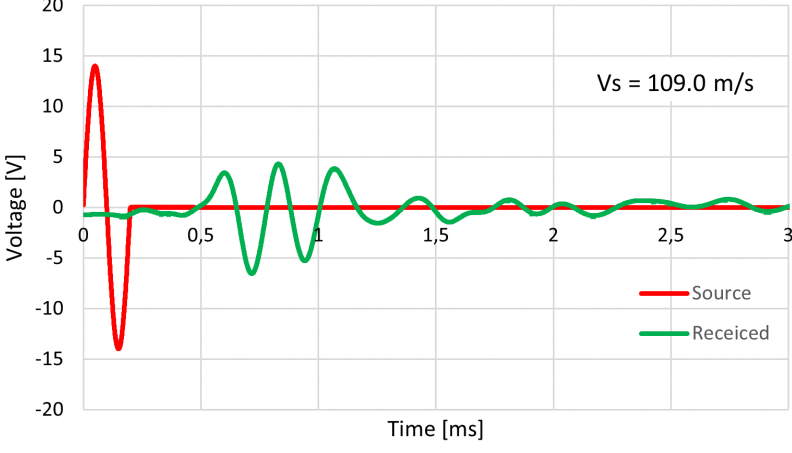


Figure F.65. Day 8.

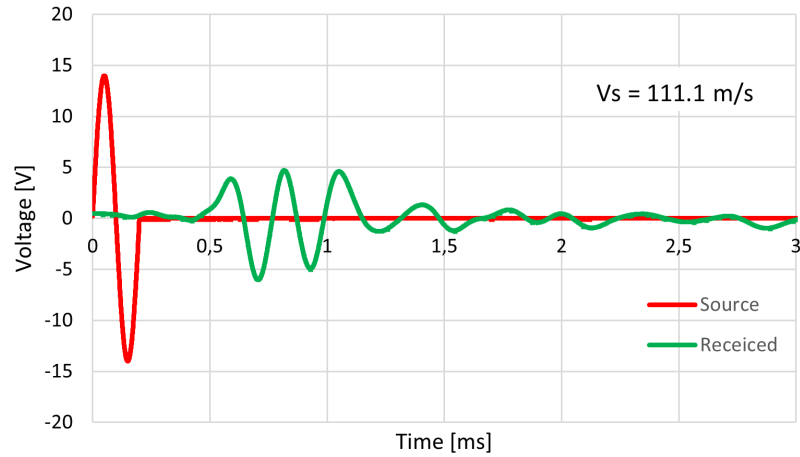


Figure F.66. Day 10.

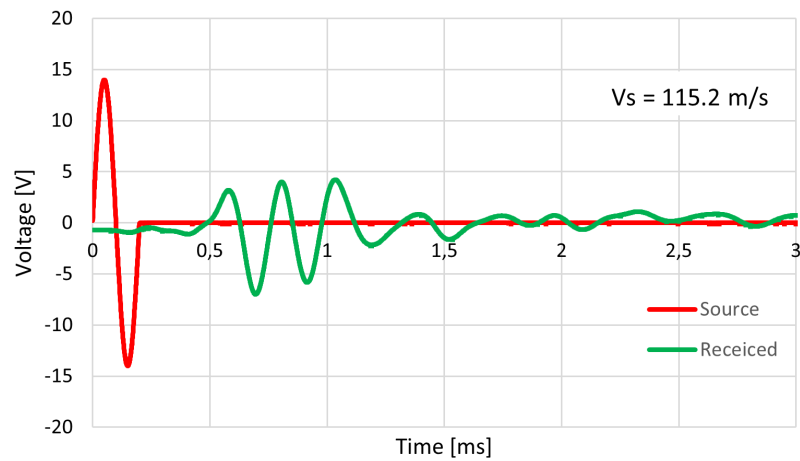


Figure F.67. Day 13.

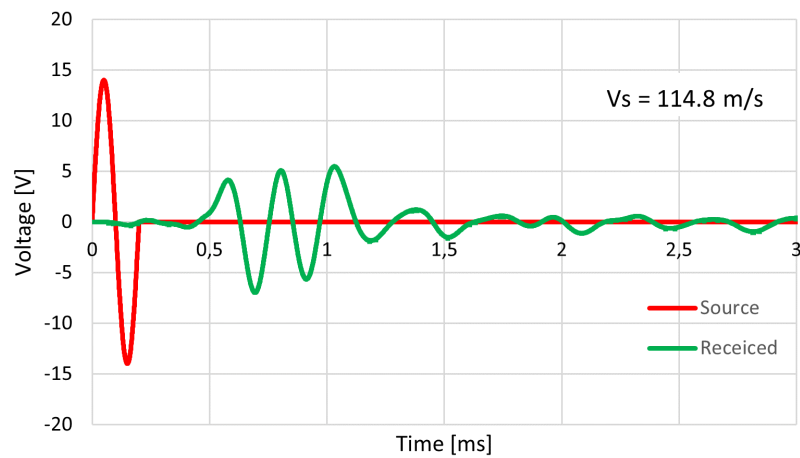


Figure F.68. Day 14.

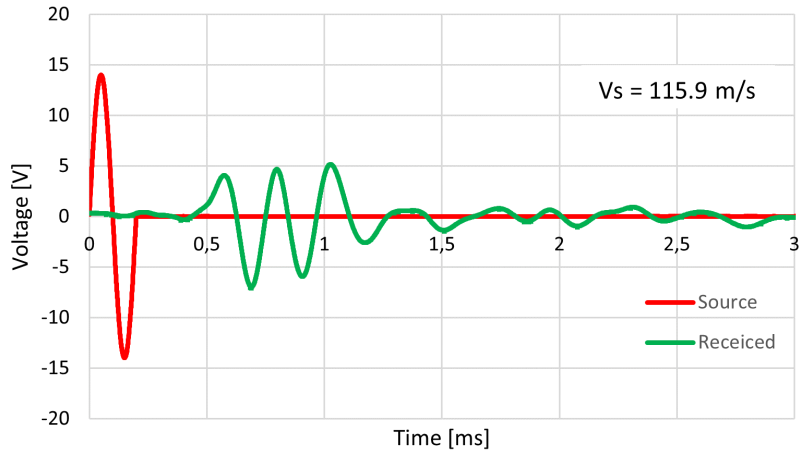


Figure F.69. Day 17.

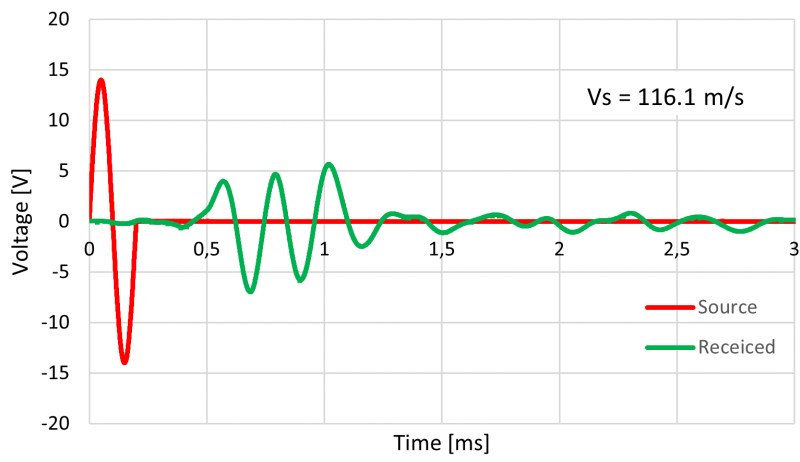


Figure F.70. Day 21.

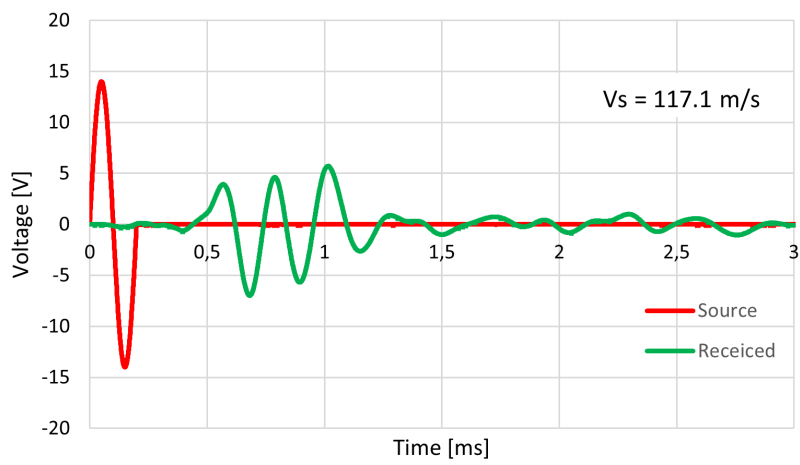


Figure F.71. Day 24.

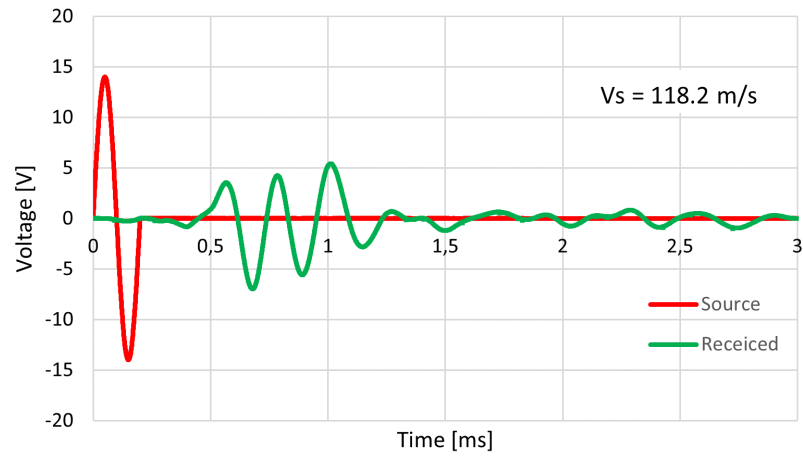


Figure F.72. Day 27.

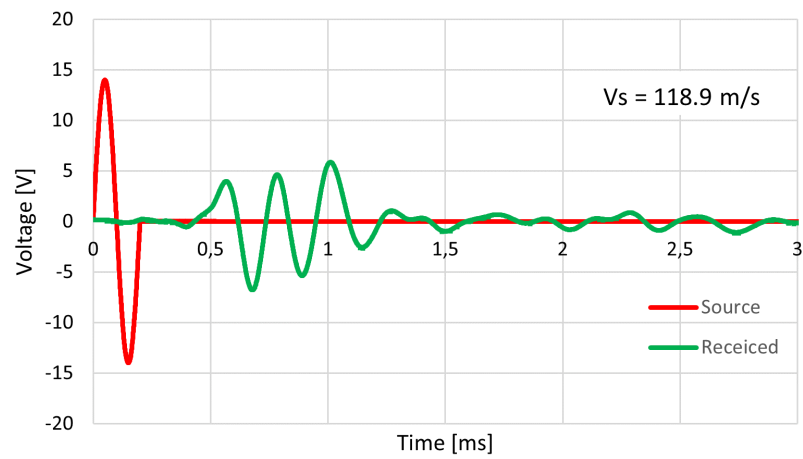


Figure F.73. Day 28.

Cement specimens 150 kg/m³



G.1 Triaxial14: CU test curing for 7 days at 20 °C

This CU test was performed on a gyttja-cement specimen that cured for 7 days.

Test description:				
The test was performed using a GDS triaxial cell using GDSLab v2.5.4.28 software.				
Cement amount:	150 kg/m ³		Before	After
Curing period:	7 days ¹⁾	Water content, w:	74.4 %	77.8 %
Curing temp.:	19 to 20.5 °C	Saturation, S:	101.8 %	-
Diameter, d:	70 mm	Height, h:	70 mm	-
Pore water:	Demineralised	Void ratio, e:	1.94	-
Test type:	CU ($\sigma = 30$ kPa)	Unit weight, γ	15.5 kN/m ³	-
Shear rate, v:	0.1 mm/min		Remoulded²⁾	Cement added²⁾
Test data:	10/04 to 11/04/2023	Water content, w:	97.4 %	80.0 %
Primary results:			Secondary results:	
S_u	187.5 kPa		pH ³⁾	12.4
$(E)_{u50}$	22.3 MPa		LL ³⁾	100.0 %
			PL ³⁾	80.1 %

1) The last ≈ 24 hours of curing were performed in the triaxial cell during consolidation

2) Water contents when mixing the specimen before curing

3) Determined on the same day as the triaxial test was finished

Stage	Description of triaxial test stages
1	Ramp up to a cell pressure of 530 kPa and back pressure of 500 kPa.
2	Consolidation.
3	B-check to verify saturation level.
4	Execution of CU test.

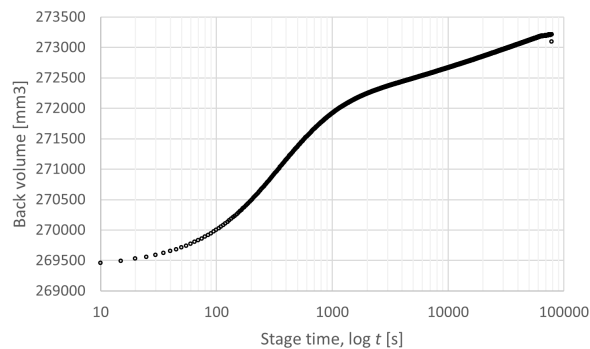


Figure G.1. Stage 2.

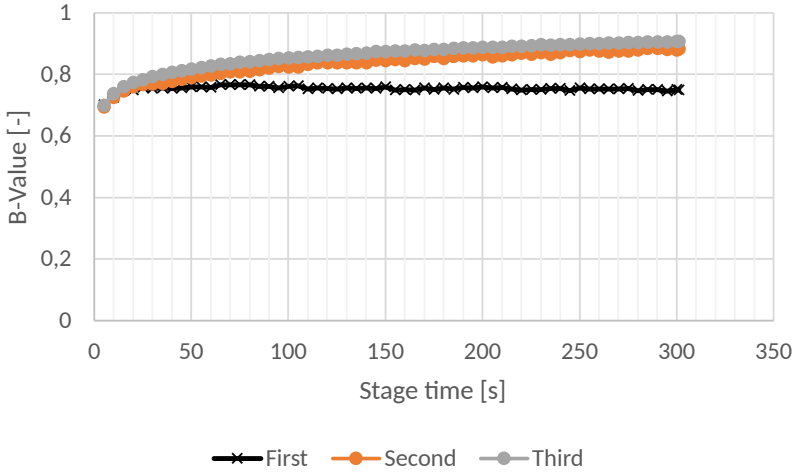


Figure G.2. Stage 3.

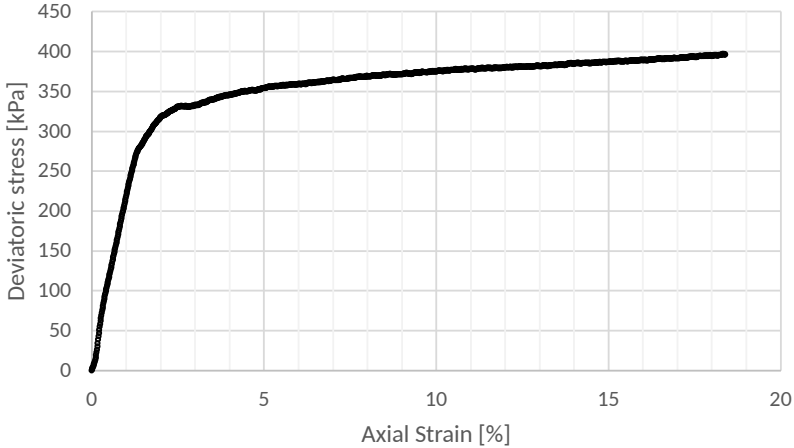


Figure G.3. Stage 4.

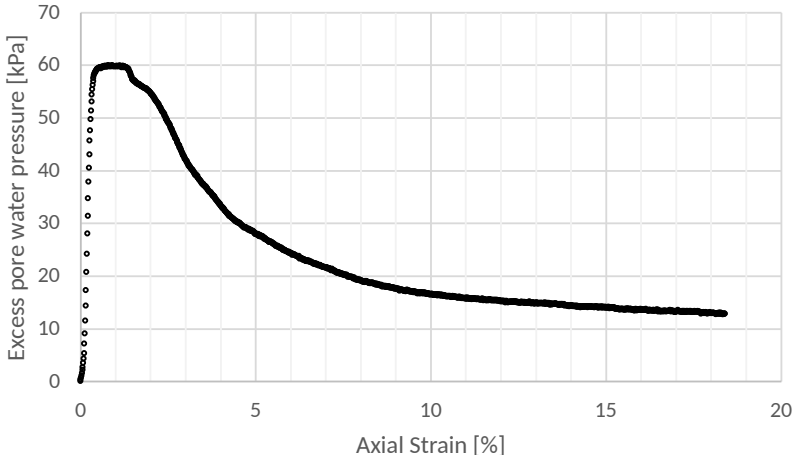


Figure G.4. Stage 4.

G.2 Triaxial15: CU test curing for 14 days at 20 °C

This CU test was performed on a gyttja-cement specimen that cured for 14 days.

Test description:				
The test was performed using a GDS triaxial cell using GDSLab v2.5.4.28 software.				
Cement amount:	150 kg/m ³		Before	After
Curing period:	14 days ¹⁾	Water content, w:	80.9 %	77.9 %
Curing temp.:	19 to 20.5 °C	Saturation, S:	106.8 %	-
Diameter, d:	70 mm	Height, h:	70 mm	-
Pore water:	Demineralised	Void ratio, e:	2.02	-
Test type:	CU ($\sigma = 30$ kPa)	Unit weight, γ	15.6 kN/m ³	-
Shear rate, v:	0.1 mm/min		Remoulded²⁾	Cement added²⁾
Test data:	17/04 to 18/04/2023	Water content, w:	97.4 %	80.0 %
Primary results:			Secondary results:	
S_u	273.3 kPa		pH ³⁾	12.9
$(E)_{u50}$	35.2 MPa		LL ³⁾	100.4 %
			PL ³⁾	80.2 %

1) The last ≈ 24 hours of curing were performed in the triaxial cell during consolidation

2) Water contents when mixing the specimen before curing

3) Determined on the same day as the triaxial test was finished

Stage	Description of triaxial test stages
1	Ramp up to a cell pressure of 530 kPa and back pressure of 500 kPa.
2	Consolidation.
3	B-check to verify saturation level.
4	Execution of CU test.

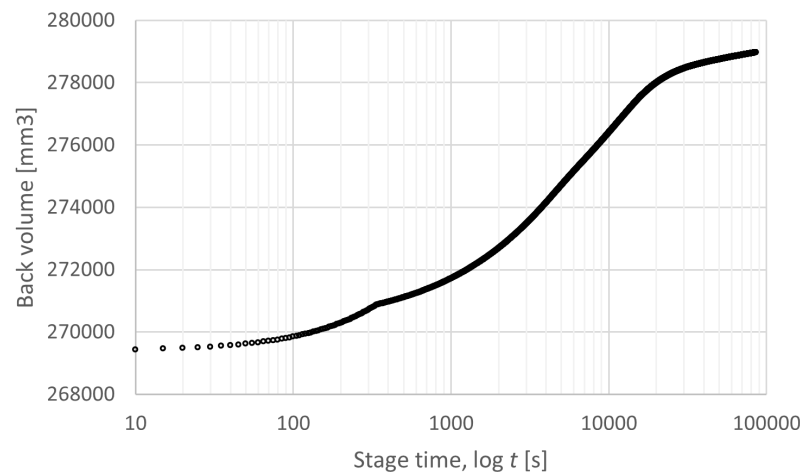


Figure G.5. Stage 2.

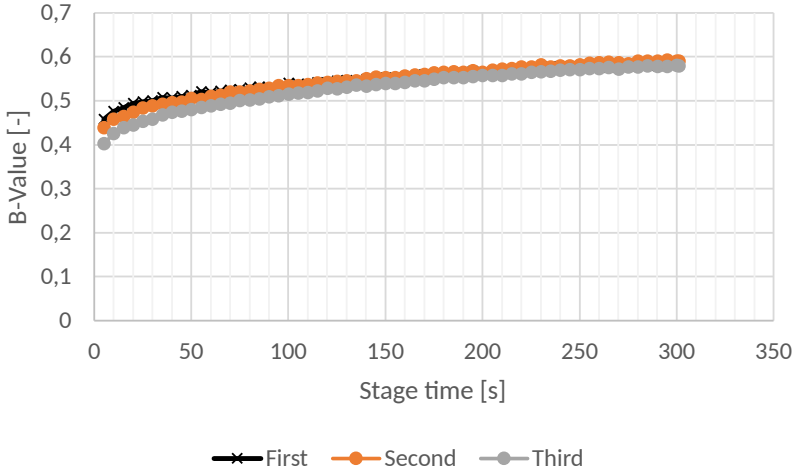


Figure G.6. Stage 3.

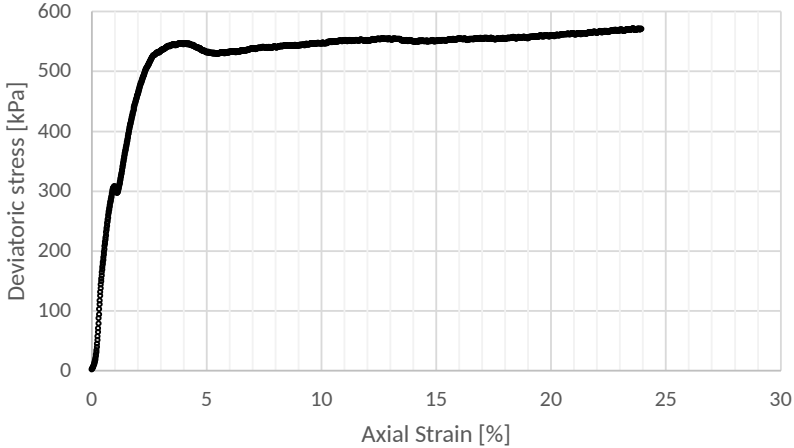


Figure G.7. Stage 4.

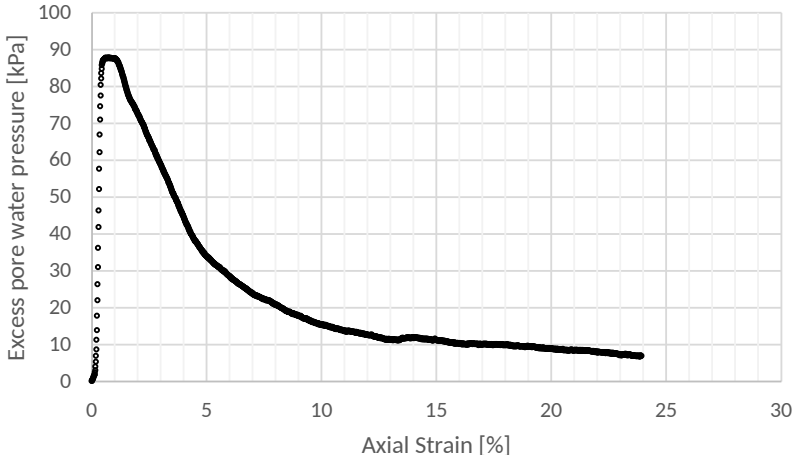


Figure G.8. Stage 4.

G.3 Triaxial16: CU test curing for 21 days at 20 °C

This CU test was performed on a gyttja-cement specimen that cured for 21 days.

Test description:				
The test was performed using a GDS triaxial cell using GDSLab v2.5.4.28 software.				
Cement amount:	150 kg/m ³		Before	After
Curing period:	21 days ¹⁾	Water content, w:	68.9 %	80.3 %
Curing temp.:	19 to 20.5 °C	Saturation, S:	101.2 %	-
Diameter, d:	70 mm	Height, h:	70 mm	-
Pore water:	Demineralised	Void ratio, e:	1.81	-
Test type:	CU ($\sigma = 30$ kPa)	Unit weight, γ	15.7 kN/m ³	-
Shear rate, v:	0.1 mm/min		Remoulded²⁾	Cement added²⁾
Test data:	24/04 to 25/04/2023	Water content, w:	97.4 %	80.0 %
Primary results:			Secondary results:	
S_u	280.1 kPa		pH ³⁾	12.3
$(E)_{u50}$	72.2 MPa		LL ³⁾	105.4 %
			PL ³⁾	92.7 %

1) The last ≈ 24 hours of curing were performed in the triaxial cell during consolidation

2) Water contents when mixing the specimen before curing

3) Determined on the same day as the triaxial test was finished

Stage	Description of triaxial test stages
1	Ramp up to a cell pressure of 530 kPa and back pressure of 500 kPa.
2	Consolidation.
3	B-check to verify saturation level.
4	Execution of CU test.

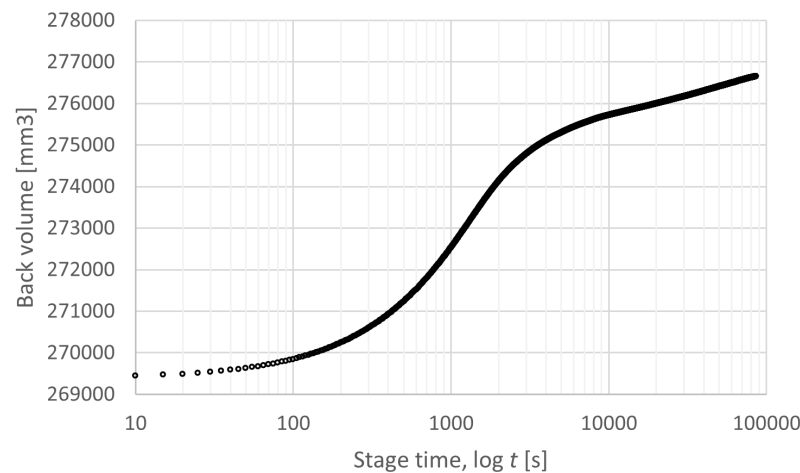


Figure G.9. Stage 2.

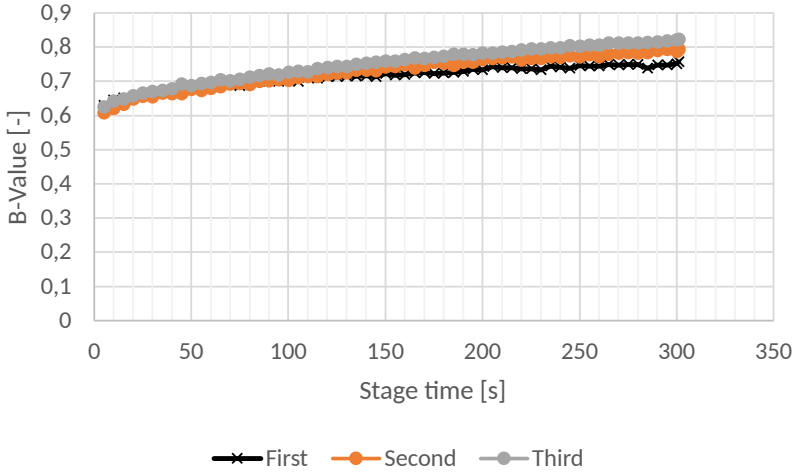


Figure G.10. Stage 3.

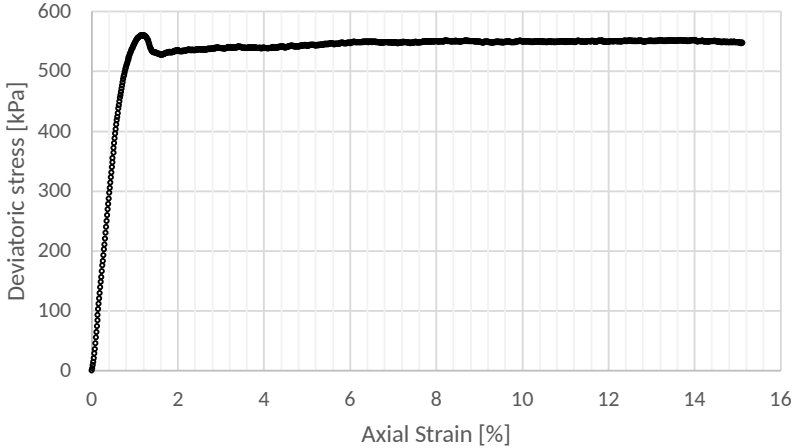


Figure G.11. Stage 4.

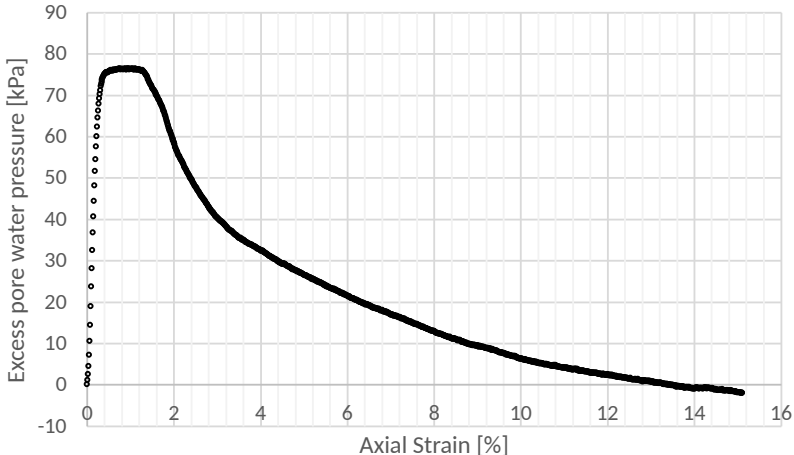


Figure G.12. Stage 4.

G.4 Triaxial17: CU test curing for 28 days at 20 °C

This CU test was performed on a gyttja-cement specimen that cured for 28 days.

Test description:				
The test was performed using a GDS triaxial cell using GDSLab v2.5.4.28 software.				
Cement amount:	150 kg/m ³		Before	After
Curing period:	28 days ¹⁾	Water content, w:	94.5 %	75.0 %
Curing temp.:	19 to 20.5 °C	Saturation, S:	111.4 %	-
Diameter, d:	70 mm	Height, h:	70 mm	-
Pore water:	Demineralised	Void ratio, e:	2.26	-
Test type:	CU ($\sigma = 30$ kPa)	Unit weight, γ	15.6 kN/m ³	-
Shear rate, v:	0.1 mm/min		Remoulded²⁾	Cement added²⁾
Test data:	01/05 to 02/05/2023	Water content, w:	97.4 %	80.0 %
Primary results:			Secondary results:	
S_u	417.1 kPa		pH ³⁾	12.4
$(E)_{u50}$	98.7 MPa		LL ³⁾	103.5 %
			PL ³⁾	95.9 %

1) The last ≈ 24 hours of curing were performed in the triaxial cell during consolidation

2) Water contents when mixing the specimen before curing

3) Determined on the same day as the triaxial test was finished

Stage	Description of triaxial test stages
1	Ramp up to a cell pressure of 530 kPa and back pressure of 500 kPa.
2	Consolidation.
3	B-check to verify saturation level.
4	Execution of CU test.

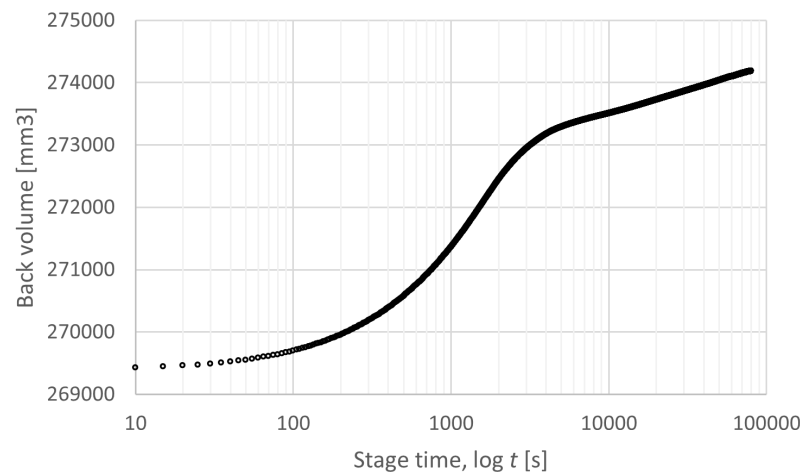


Figure G.13. Stage 2.

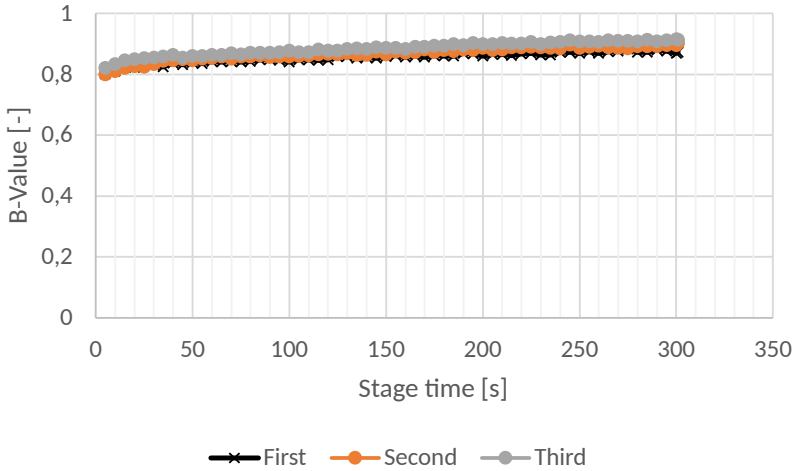


Figure G.14. Stage 3.

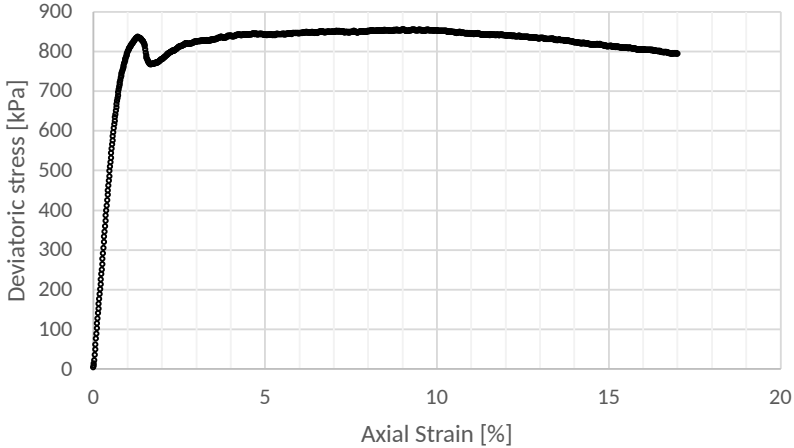


Figure G.15. Stage 4.

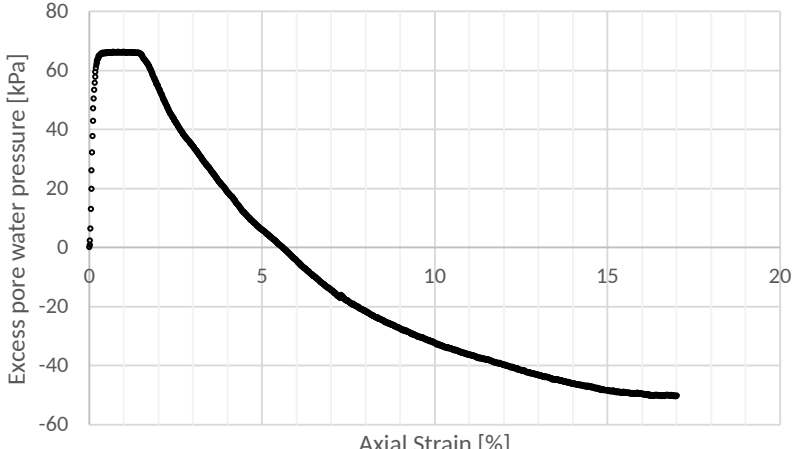


Figure G.16. Stage 4.

G.5 Triaxial18: CD test curing for 7 days at 20 °C

This CD test was performed on a gyttja-cement specimen that cured for 7 days.

Test description:

The test was performed using a GDS triaxial cell using GDSLab v2.5.4.28 software.

Cement amount:	150 kg/m ³		Before	After
Curing period:	7 days ¹⁾	Water content, w:	69.5 %	73.6 %
Curing temp.:	19 to 20.5 °C	Saturation, S:	97.4 %	-
Diameter, d:	70 mm	Height, h:	70 mm	-
Pore water:	Demineralised	Void ratio, e:	1.90	-
Test type:	CD ($\sigma' = 30$ kPa)	Unit weight, γ	15.3 kN/m ³	-
Shear rate, v:	0.003 mm/min		Remoulded²⁾	Cement added²⁾
Test data:	24/04 to 28/04/2023	Water content, w:	82.5 %	81.0 %

Primary results:

φ'	62.8°
$(E')_{50}$	24.7 MPa
$(E')_{ur}$	127.1 MPa

1) The last ≈ 24 hours of curing were performed in the triaxial cell during consolidation

2) Water contents when mixing the specimen before curing

Stage	Description of triaxial test stages
1	Ramp up to a cell pressure of 530 kPa and back pressure of 500 kPa.
2	Consolidation.
3	B-check to verify saturation level.
4	Execution of CD test.

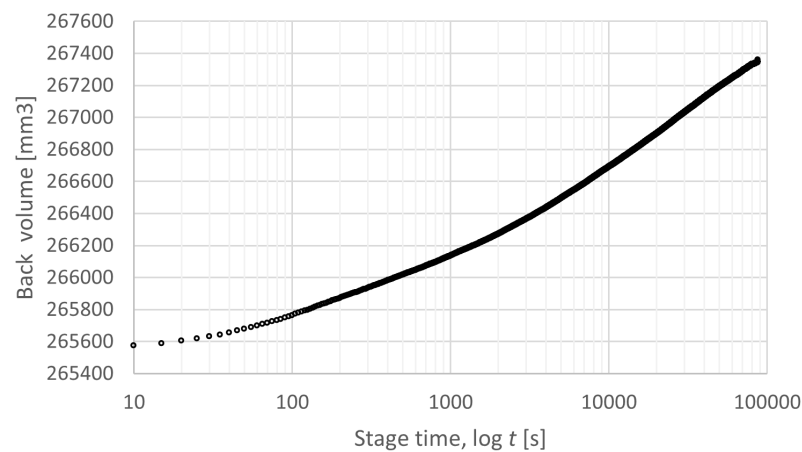


Figure G.17. Stage 2.

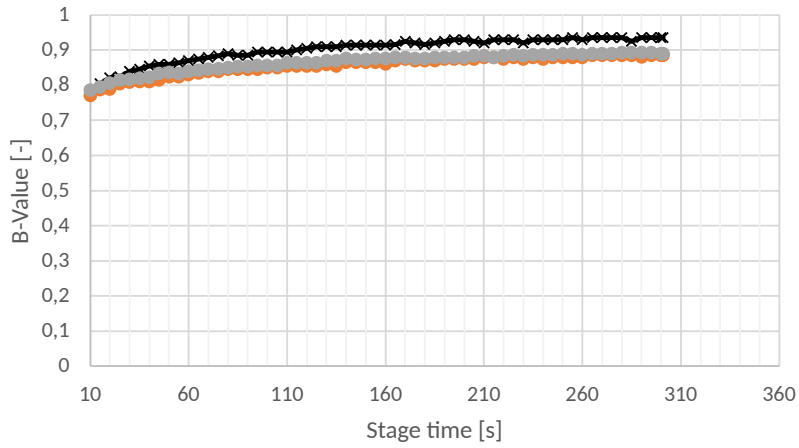


Figure G.18. Stage 3.

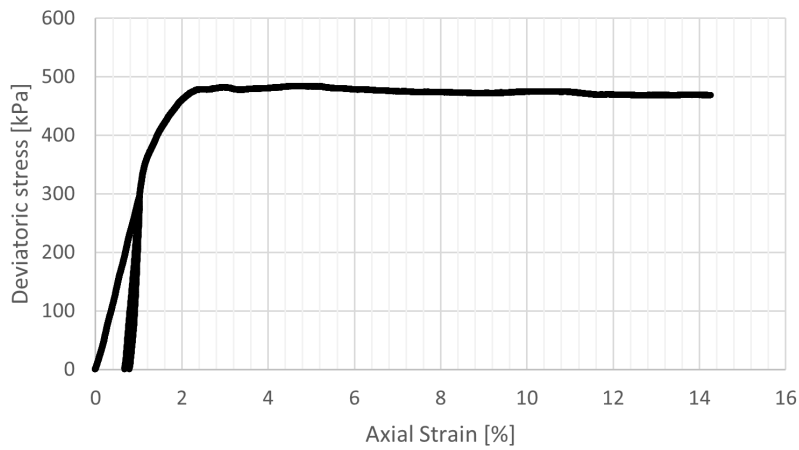


Figure G.19. Stage 4.

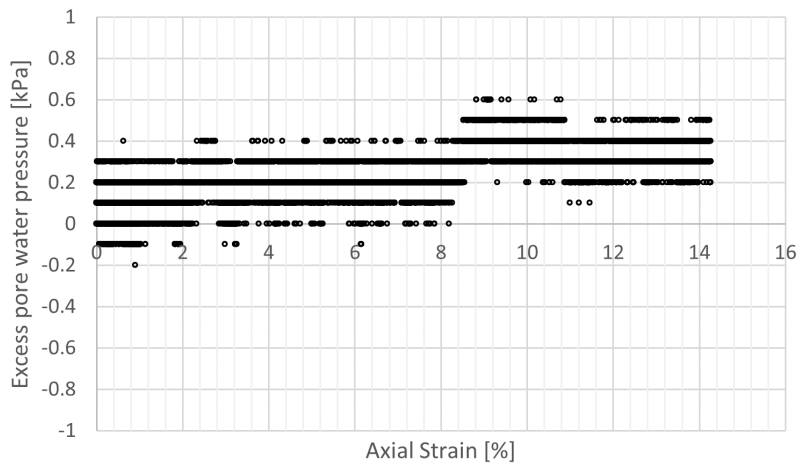


Figure G.20. Stage 4.

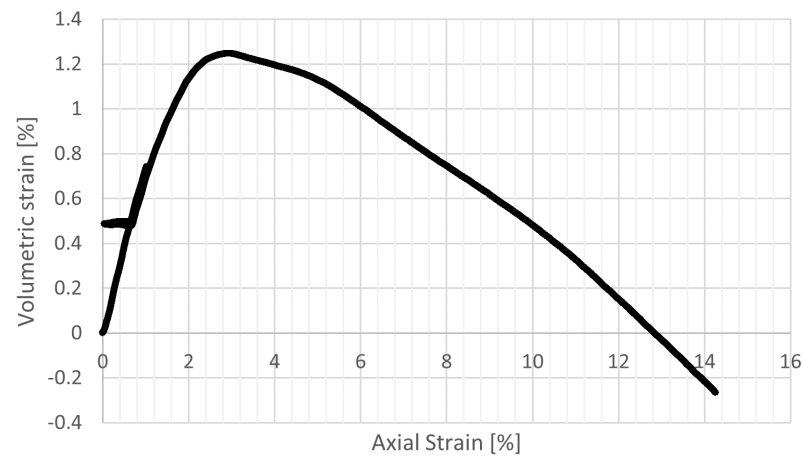


Figure G.21. Stage 4.

G.6 Triaxial19: CD test curing for 14 days at 20 °C

This CD test was performed on a gyttja-cement specimen that cured for 14 days.

Test description:				
The test was performed using a GDS triaxial cell using GDSLab v2.5.4.28 software.				
Cement amount:	150 kg/m ³		Before	After
Curing period:	14 days ¹⁾	Water content, w:	62.2 %	70.8 %
Curing temp.:	19 to 20.5 °C	Saturation, S:	93.0 %	-
Diameter, d:	70 mm	Height, h:	70 mm	-
Pore water:	Demineralised	Void ratio, e:	1.78	-
Test type:	CD ($\sigma' = 30$ kPa)	Unit weight, γ	15.9 kN/m ³	-
Shear rate, v:	0.003 mm/min		Remoulded²⁾	Cement added²⁾
Test data:	08/05 to 12/05/2023	Water content, w:	82.5 %	81.0 %
Primary results:				
ϕ'	64.8°			
$(E')_{50}$	30.4 MPa			
$(E')_{ur}$	76.1 MPa			

1) The last ≈ 24 hours of curing were performed in the triaxial cell during consolidation

2) Water contents when mixing the specimen before curing

Stage	Description of triaxial test stages
1	Ramp up to a cell pressure of 530 kPa and back pressure of 500 kPa.
2	Consolidation.
3	B-check to verify saturation level.
4	Execution of CD test.

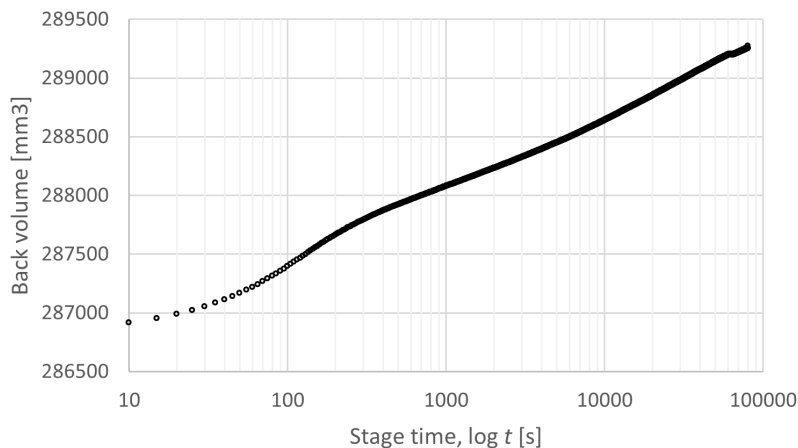


Figure G.22. Stage 2.

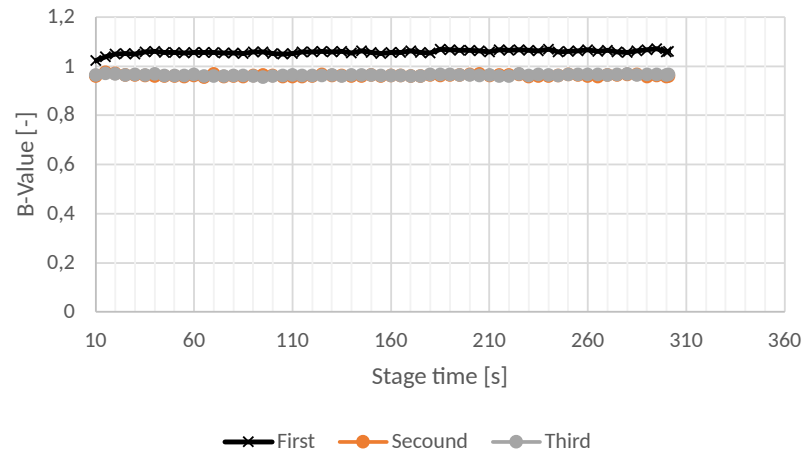


Figure G.23. Stage 3.

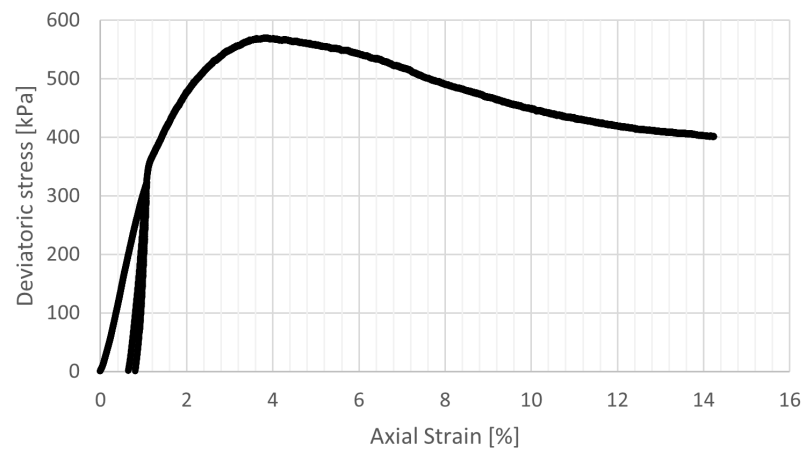


Figure G.24. Stage 4.

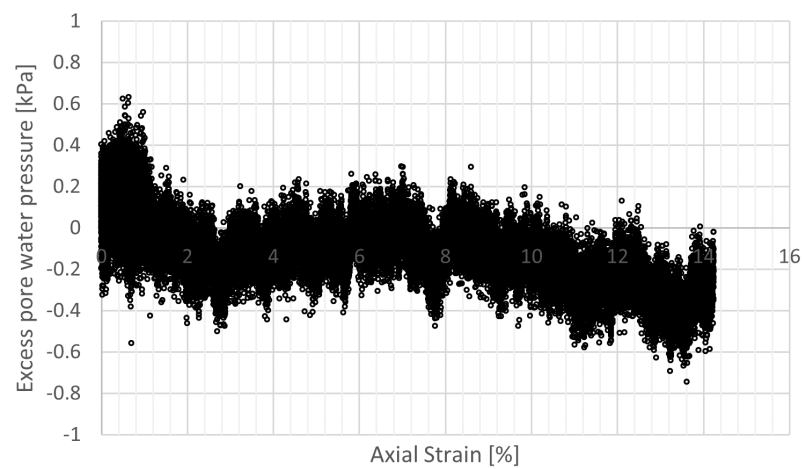


Figure G.25. Stage 4.

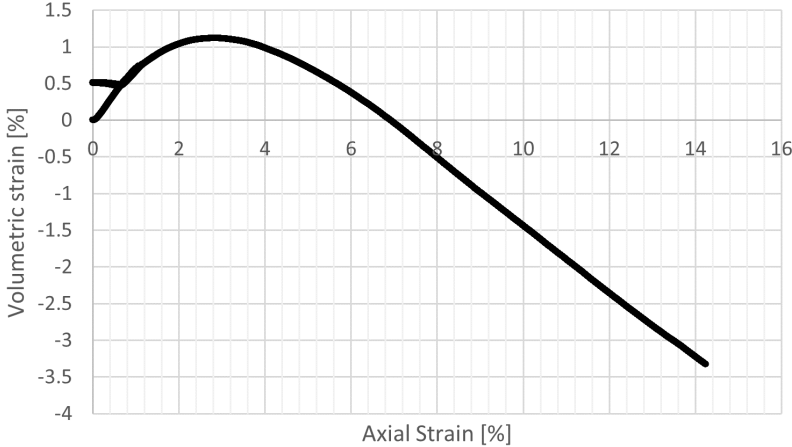


Figure G.26. Stage 4.

G.7 Triaxial20: CD test curing for 28 days at 20 °C

This CD test was performed on a gyttja-cement specimen that cured for 28 days.

Test description:

The test was performed using a GDS triaxial cell using GDSLab v2.5.4.28 software.

Cement amount:	150 kg/m ³		Before	After
Curing period:	28 days ¹⁾	Water content, w:	61.9 %	-
Curing temp.:	19 to 20.5 °C	Saturation, S:	98.4 %	-
Diameter, d:	70 mm	Height, h:	70 mm	-
Pore water:	Demineralised	Void ratio, e:	1.67	-
Test type:	CD ($\sigma' = 30$ kPa)	Unit weight, γ	15.8 kN/m ³	-
Shear rate, v:	0.003 mm/min		Remoulded²⁾	Cement added²⁾
Test data:	22/05 to 26/05/2023	Water content, w:	88.8 %	74.1 %

Primary results:

φ'	67.5°
$(E')_{50}$	28.1 MPa
$(E')_{ur}$	88.1 MPa

1) The last ≈ 24 hours of curing were performed in the triaxial cell during consolidation

2) Water contents when mixing the specimen before curing

Stage	Description of triaxial test stages
1	Ramp up to a cell pressure of 530 kPa and back pressure of 500 kPa.
2	Consolidation.
3	B-check to verify saturation level.
4	Execution of CD test.

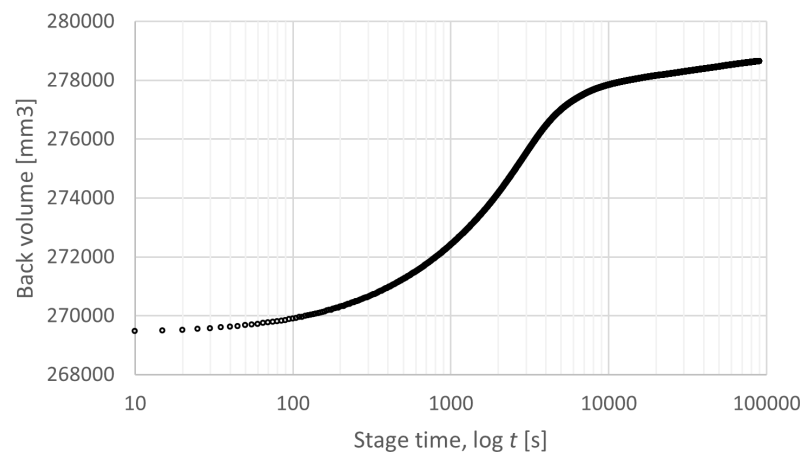


Figure G.27. Stage 2.

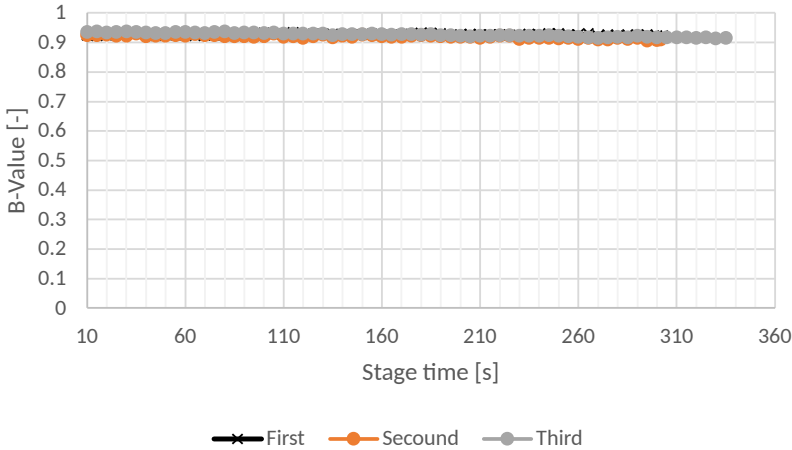


Figure G.28. Stage 3.

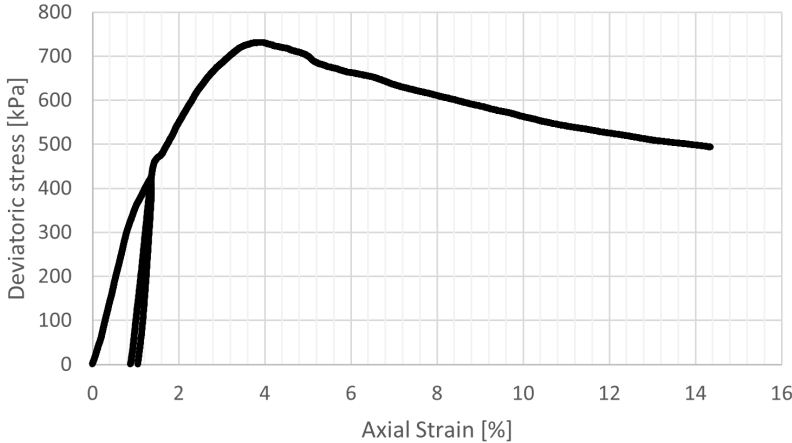


Figure G.29. Stage 4.

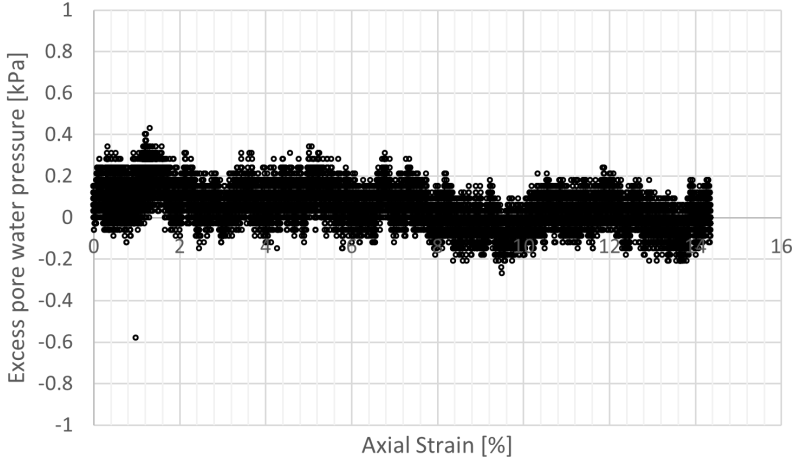


Figure G.30. Stage 4.

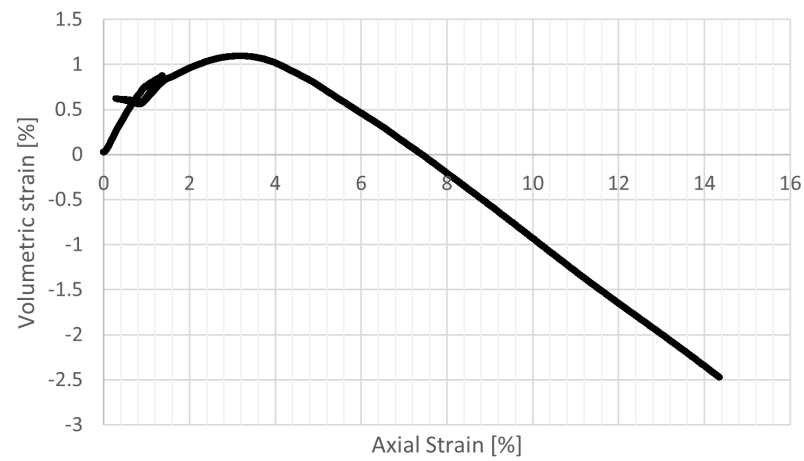


Figure G.31. Stage 4.

G.8 Triaxial21: Cyclic curing for 28 days at 20 °C

This cyclic test was performed on a gyttja-cement specimen that cured for 28 days.

Test description:

The test was performed using a GDS advanced dynamic triaxial cell using GDSLab v2.5.4.28 software.

Cement amount:	150 kg/m ³		Before	After
Curing period:	28 days ¹⁾	Water content, w:	87.9 %	78.9 %
Curing temp.:	19 to 20.5 °C	Saturation, S:	108.6 %	-
Diameter, d:	70 mm	Height, h:	70 mm	-
Pore water:	Demineralised	Void ratio, e:	2.15	-
Test type:	Cyclic ($\sigma' = 30$ kPa)	Unit weight, γ	15.5 kN/m ³	-
Frequency:	0.1 Hz		Remoulded²⁾	Cement added²⁾
Test data:	01/05 to 04/05/2023	Water content, w:	58.1 %	55.8 %

Primary results:

See Figure 4.27

- 1) The last ≈ 24 hours of curing were performed in the triaxial cell during consolidation
- 2) Water contents when mixing the specimen before curing

Stage	Description of triaxial test stages
1	Ramp up to a cell pressure of 530 kPa and back pressure of 500 kPa.
2	Consolidation.
3	B-check to verify saturation level.
4	Execution of cyclic test.

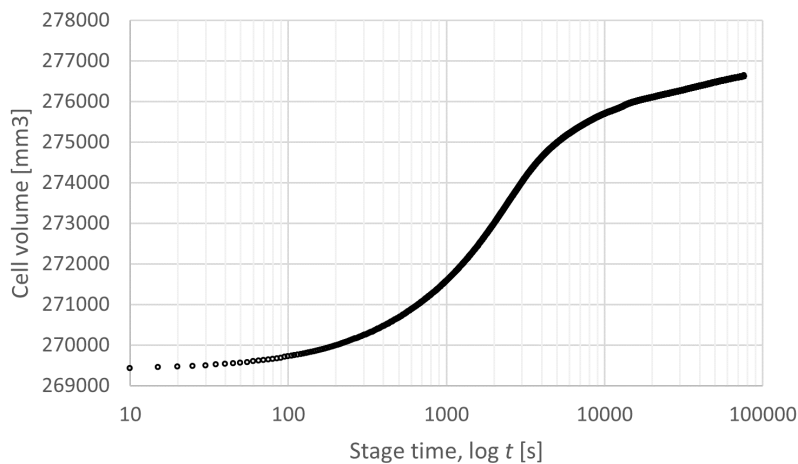


Figure G.32. Stage 2.

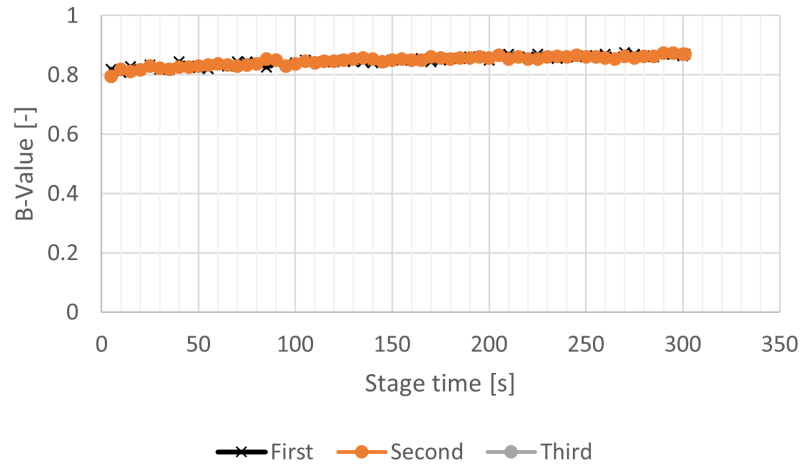


Figure G.33. Stage 3.

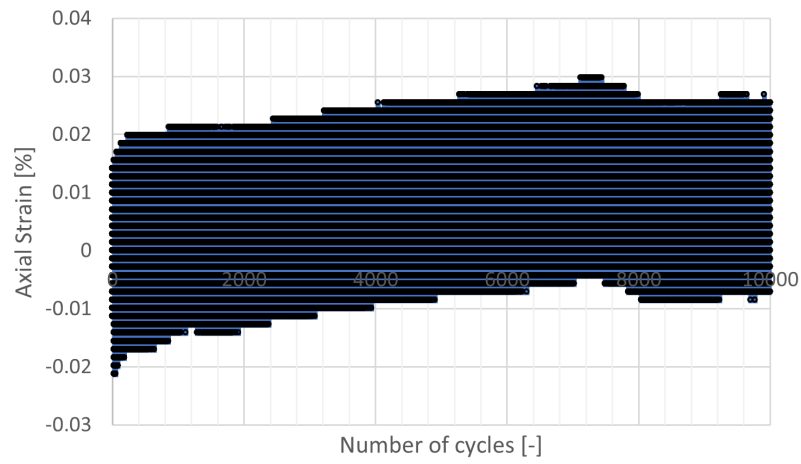


Figure G.34. Stage 4.

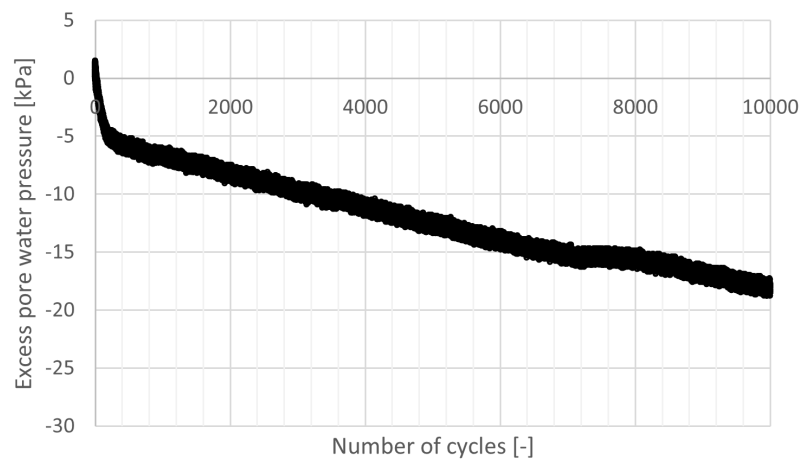


Figure G.35. Stage 4.

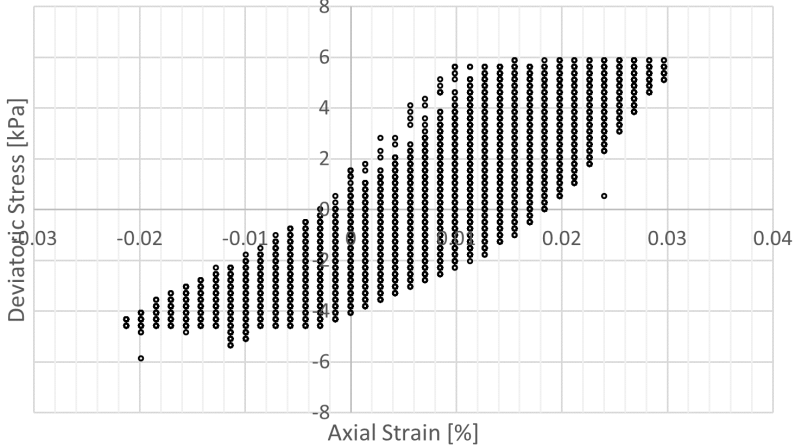


Figure G.36. Stage 4.

G.9 Oedometer03: Curing for 28 days at 20 °C (Swell log)

This test was performed on a gyttja-cement specimen that cured inside the oedometer ring for 28 days.

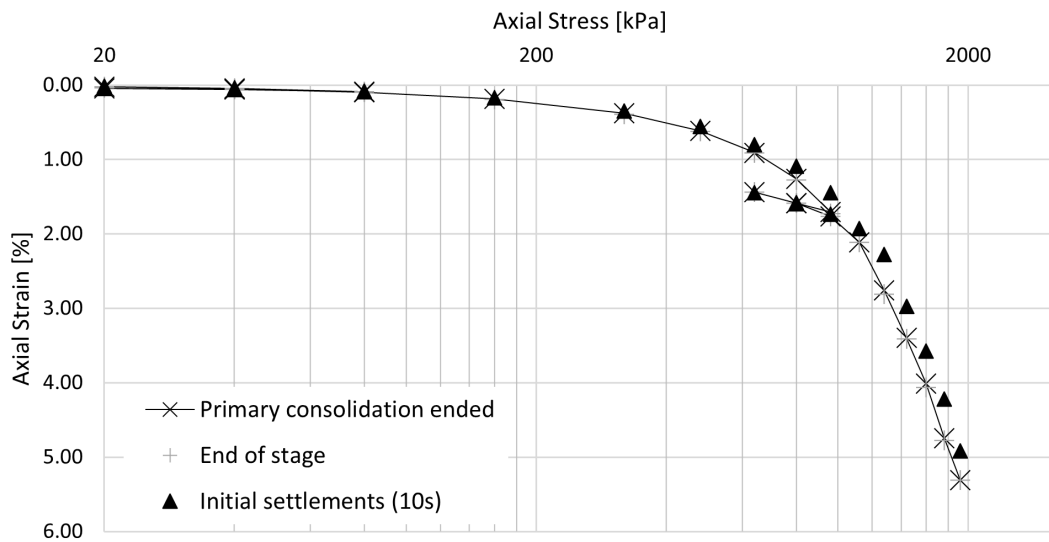


Figure G.37. Stress strain curve.

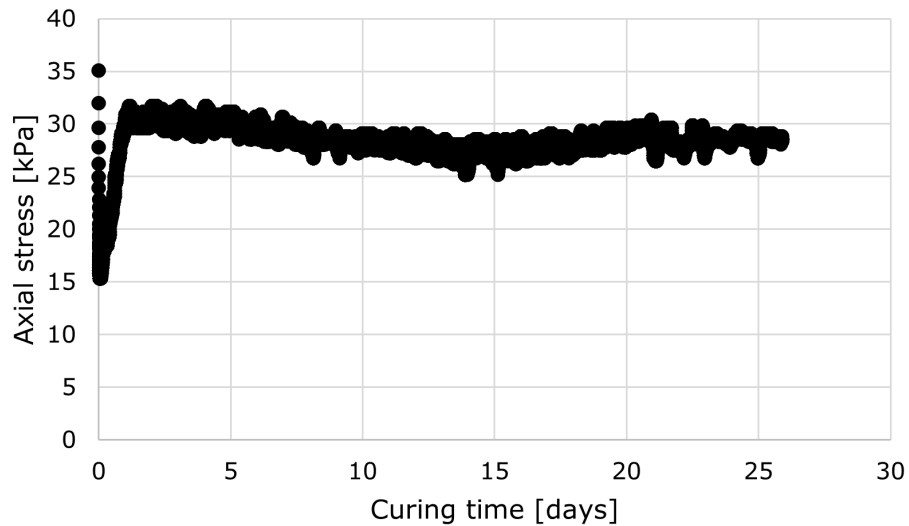


Figure G.38. Swelling log while curing.

Test description:

The test was performed using a GDSAOS with GDSLlab v2.5.4.28 software.

Cement amount:	150 kg/m ³		Before	After
Cement type:	FutureCem	Water content, w:	53.9 %	50.5 %
Temp. lab:	19 to 20.5 °C	Saturation, S:	94.1 %	101.3
Diameter, d:	70 mm	Void ratio, e:	1.52	1.33
Pore water:	Demineralised	Height, h:	35 mm	33 mm
Test data:	27/02 to 27/04/2023	Unit weight, γ	15.9 kN/m ³	16.9 kN/m ³
			Remoulded¹⁾	Cement added¹⁾
		Water content, w:	67.2 %	53.9 %

Results:

See Table G.1

1) Water contents when mixing the specimen prior to curing

Table G.1. Results from oedometer test.

σ_v [kPa]	t_{end} [min]	ε_{100} [%]	ε_{end} [%]	ε_{int} [%]	$C_{\varepsilon C}$ [%]	E_{oed} [MPa]
20	720	0.02	0.02	0	-	-
40	720	0.04	0.04	0.02	0.08	80.91
80	720	0.09	0.09	0.04	0.15	86.69
40	720	0.06	0.06	0.09	0.11	123.34
20	720	0.04	0.04	0.06	0.05	123.92
40	720	0.06	0.06	0.04	0.05	144.30
80	720	0.10	0.10	0.06	0.13	99.30
160	720	0.18	0.19	0.10	0.29	90.17
320	720	0.38	0.39	0.19	0.65	81.63
480	720	0.62	0.63	0.39	1.34	67.59
640	720	0.91	0.91	0.63	2.34	54.82
800	720	1.26	1.27	0.91	3.60	45.83
960	720	1.70	1.73	1.27	5.64	35.82
800	720	1.59	1.59	1.73	1.46	138.77
640	720	1.44	1.44	1.59	1.55	106.67
800	720	1.58	1.59	1.44	1.50	110.42
960	720	1.76	1.76	1.59	2.25	89.89
1120.0	720	2.11	2.11	1.76	5.27	45.34
1280	720	2.76	2.81	2.11	11.06	24.94
1440	720	3.39	3.41	2.81	12.47	25.09
1600	720	4.01	4.07	3.41	13.45	25.99
1760	720	4.75	4.77	4.07	17.80	21.72
1920	720	5.31	5.31	4.77	14.86	28.50

On the following pages, the oedometer data for each load step are presented. The lines used for interpreting the end of primary consolidation are kept.

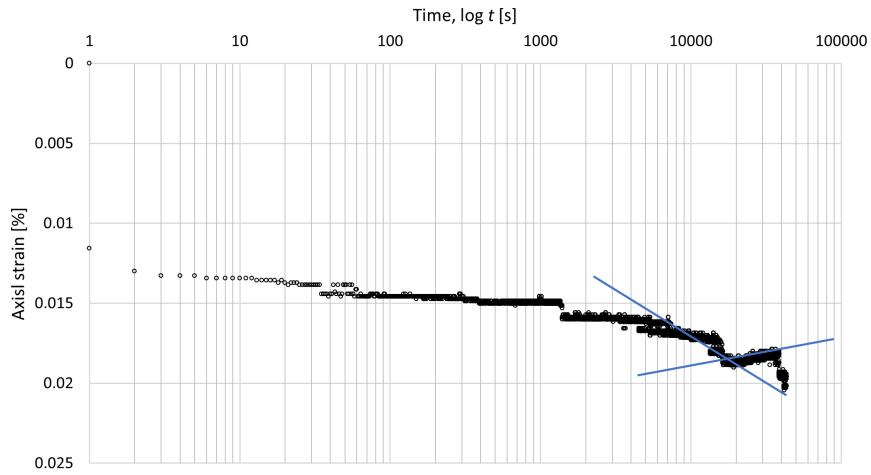


Figure G.39. Load step 1.

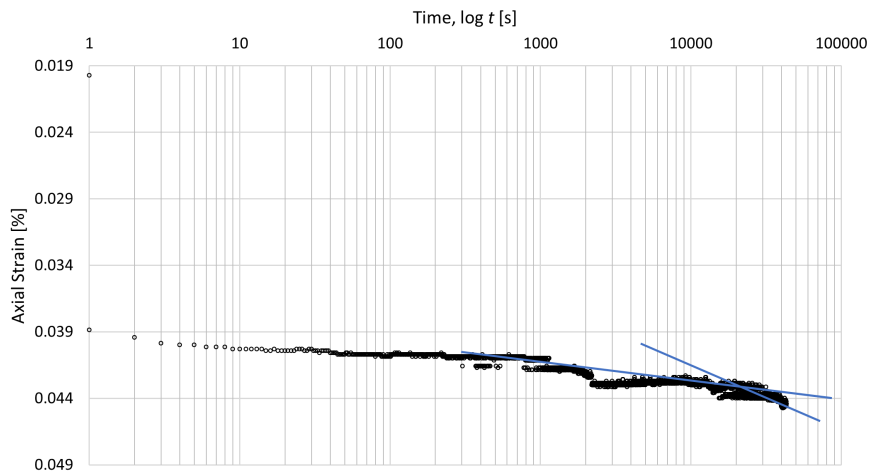


Figure G.40. Load step 2.

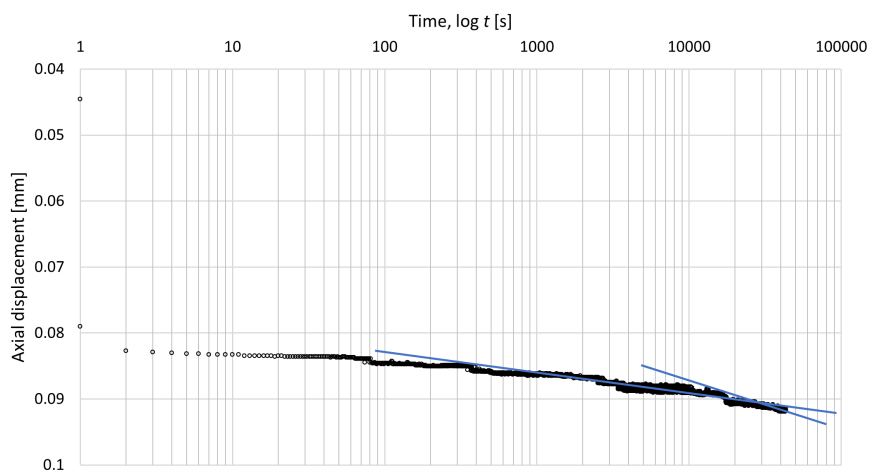


Figure G.41. Load step 3.

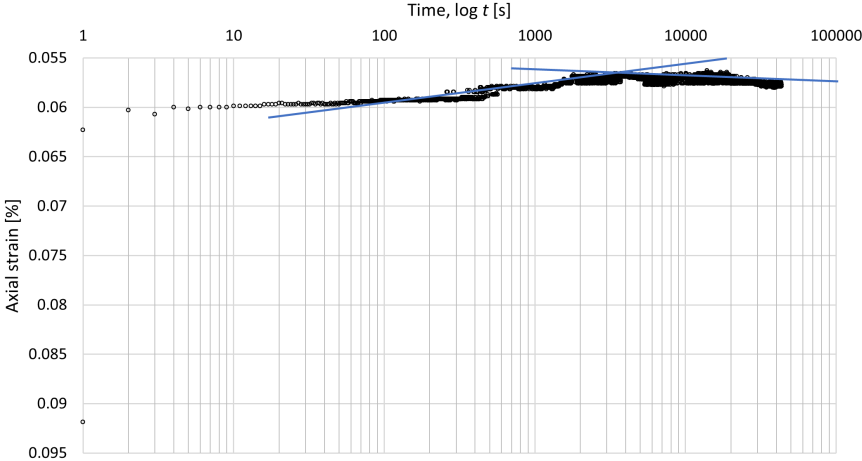


Figure G.42. Load step 4.

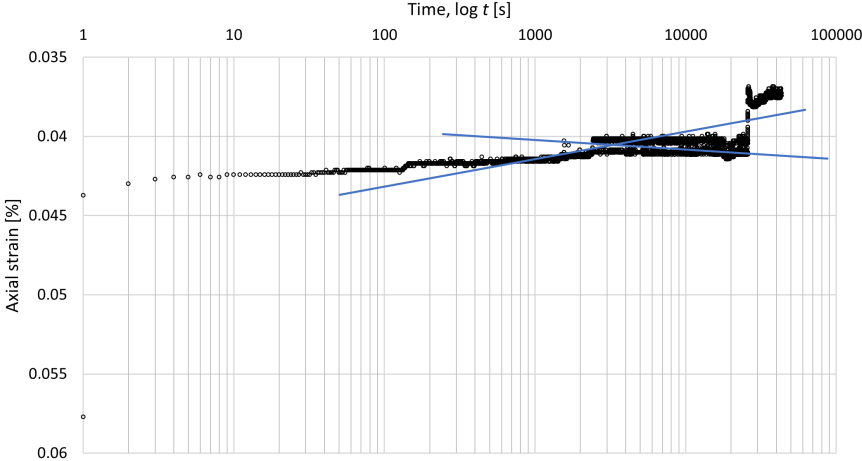


Figure G.43. Load step 5.

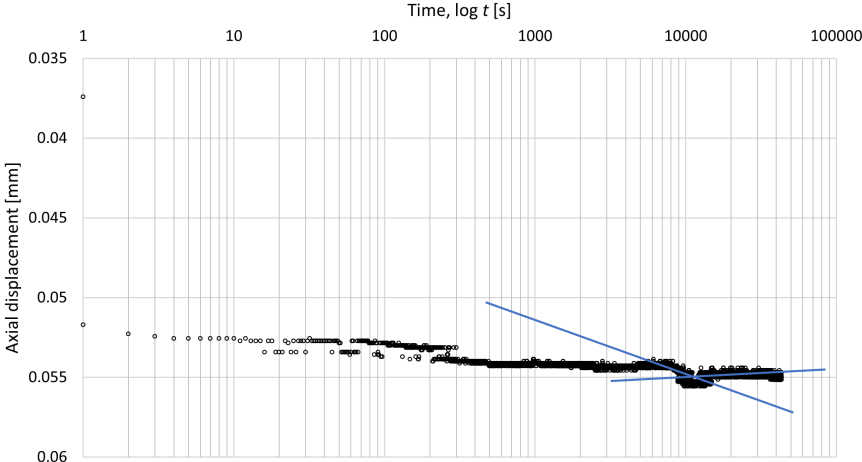


Figure G.44. Load step 6.

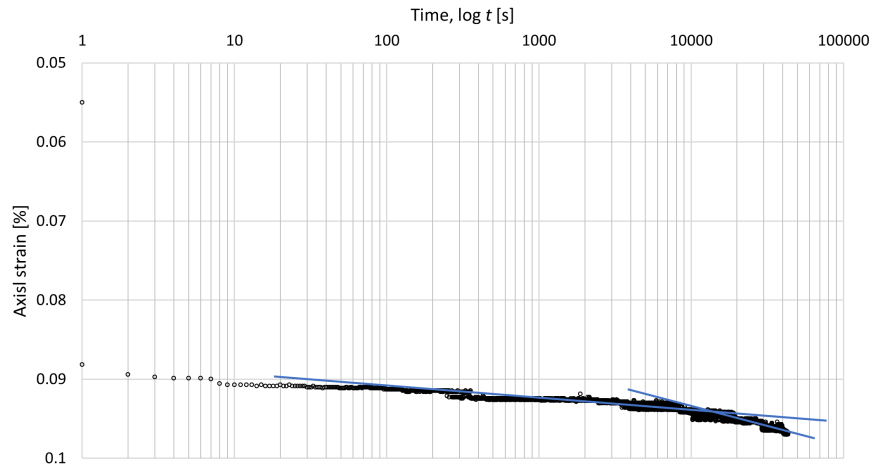


Figure G.45. Load step 7.

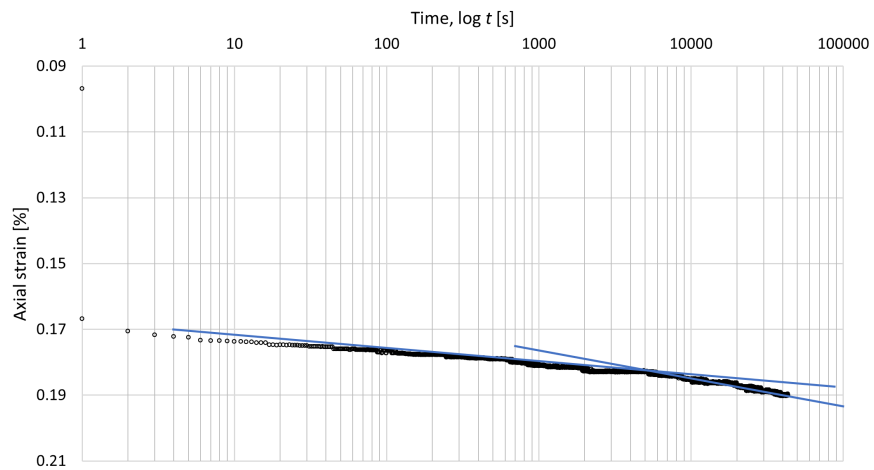


Figure G.46. Load step 8.

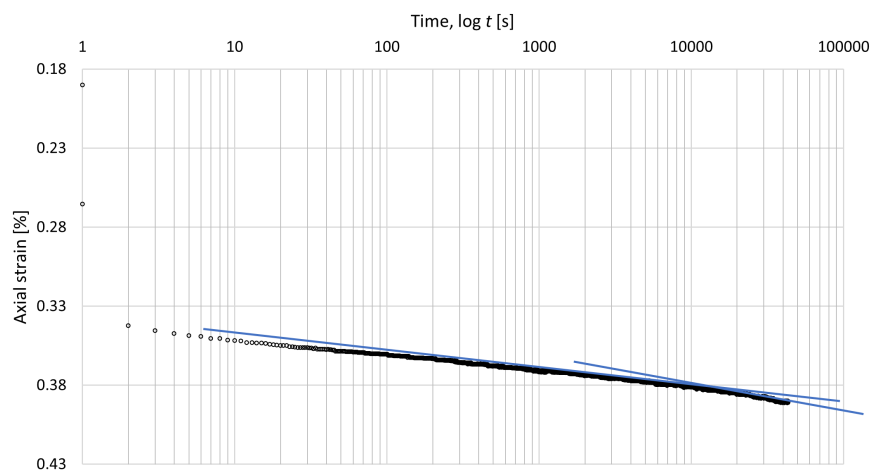


Figure G.47. Load step 9.

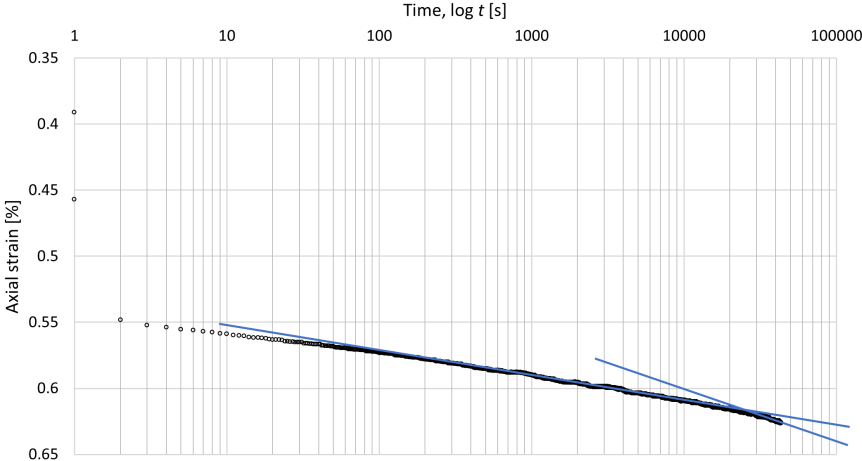


Figure G.48. Load step 10.

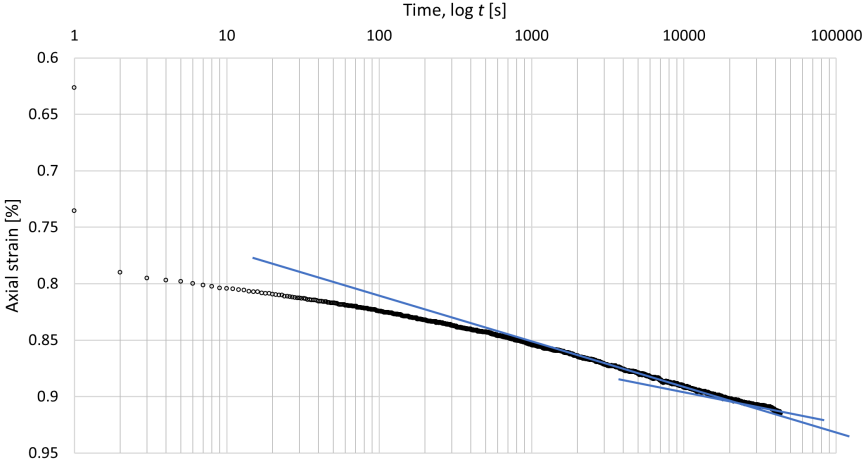


Figure G.49. Load step 11.

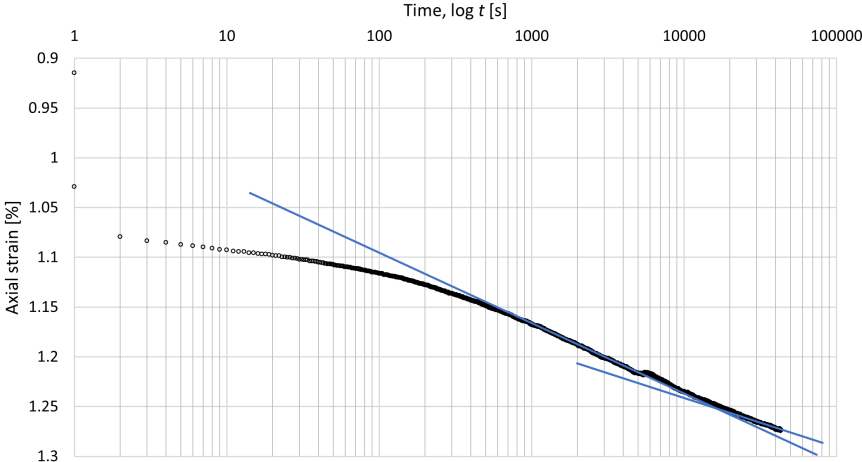


Figure G.50. Load step 12.

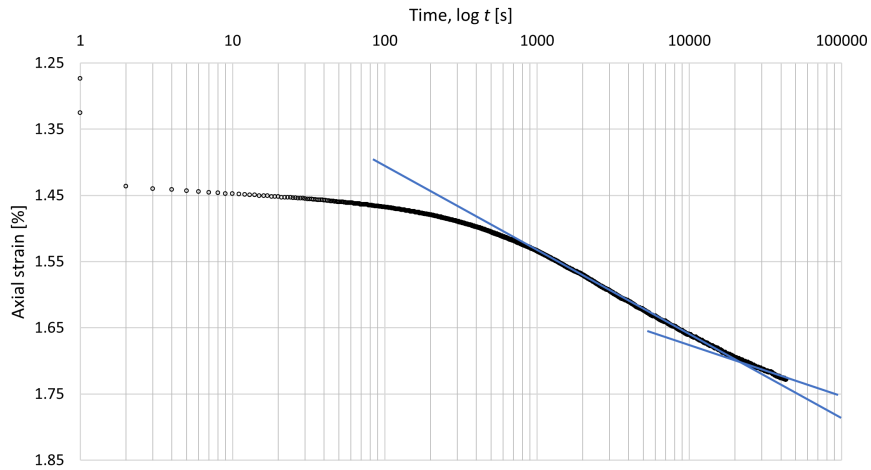


Figure G.51. Load step 13.

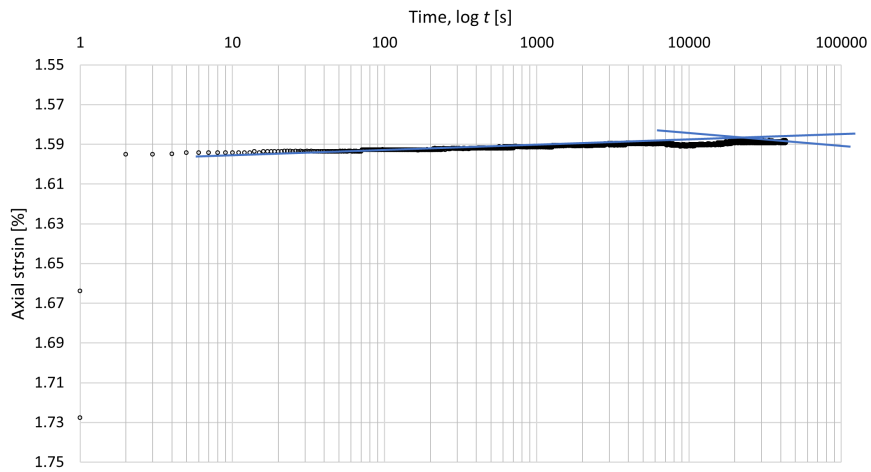


Figure G.52. Load step 14.

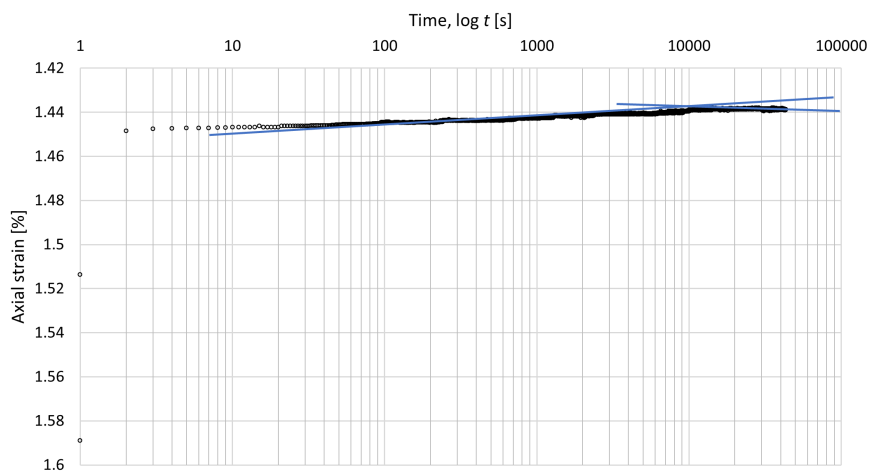


Figure G.53. Load step 15.

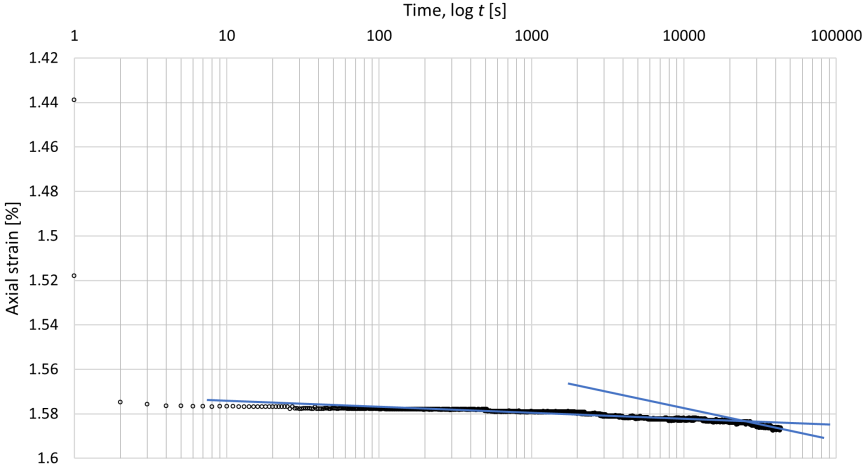


Figure G.54. Load step 16.

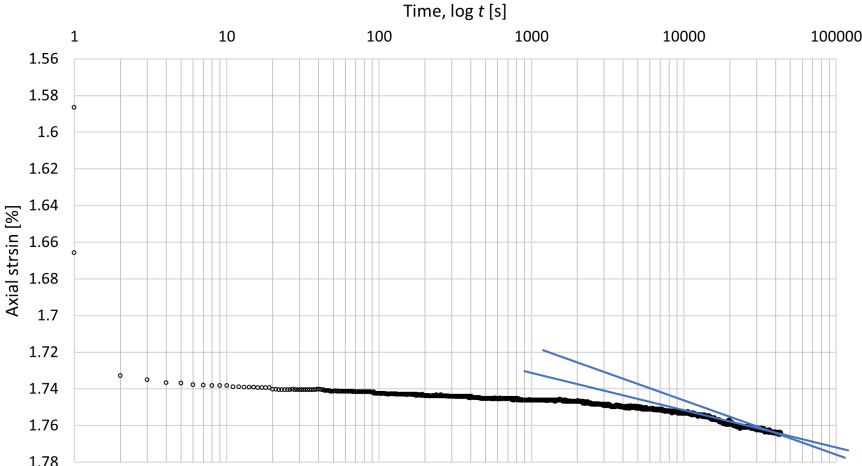


Figure G.55. Load step 17.

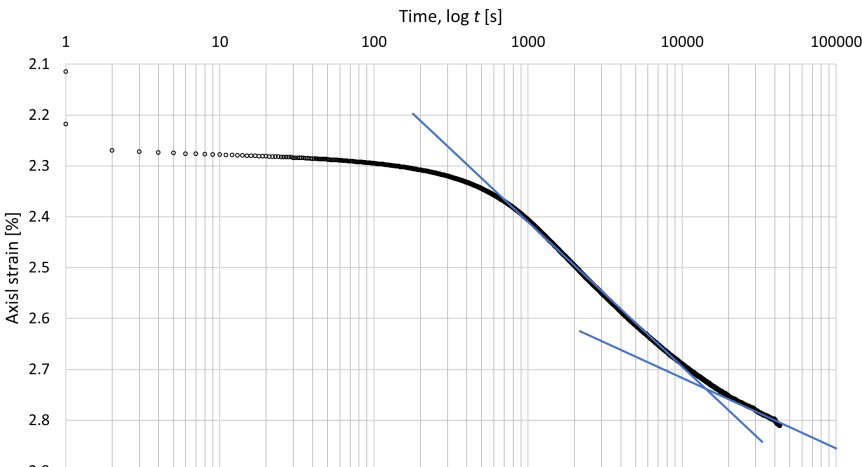


Figure G.56. Load step 18.

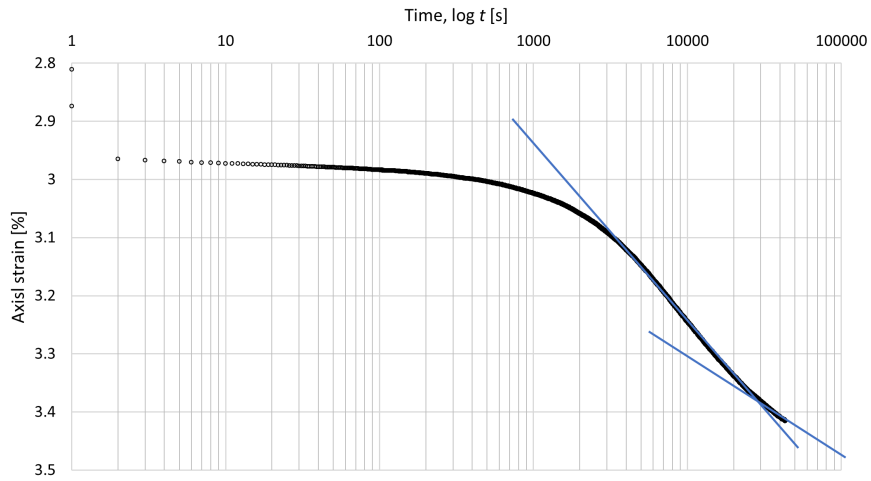


Figure G.57. Load step 19.

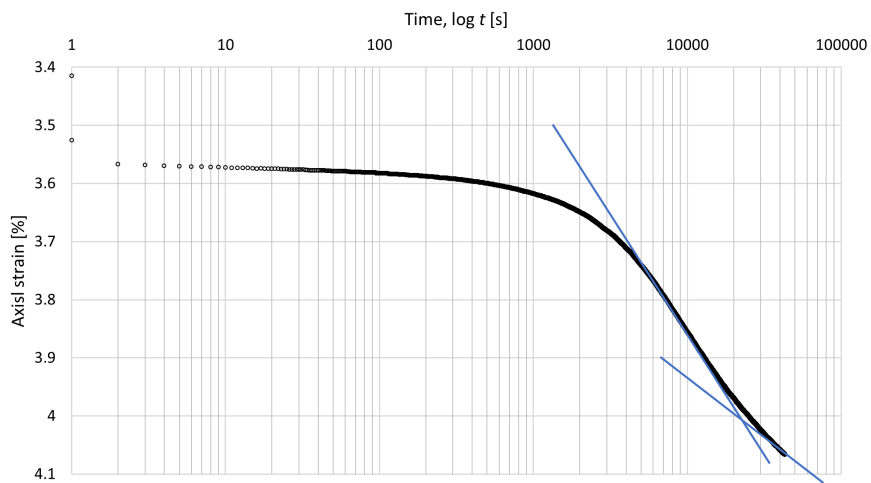


Figure G.58. Load step 20.

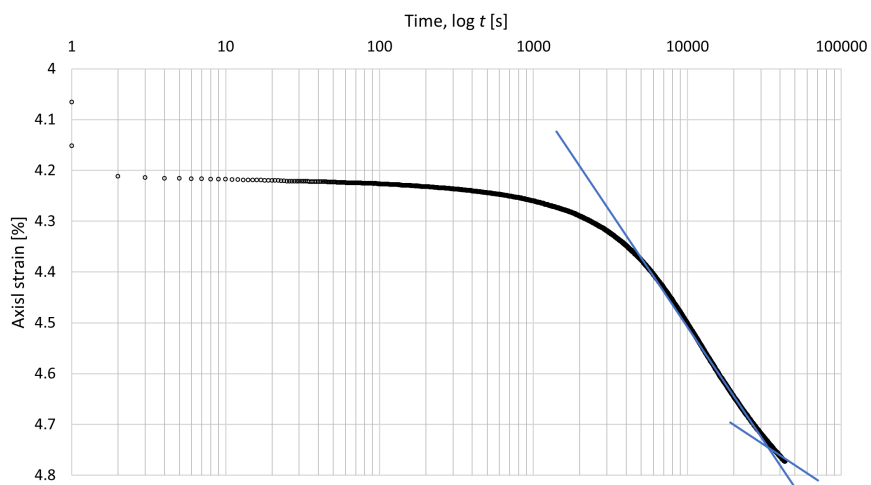


Figure G.59. Load step 21.

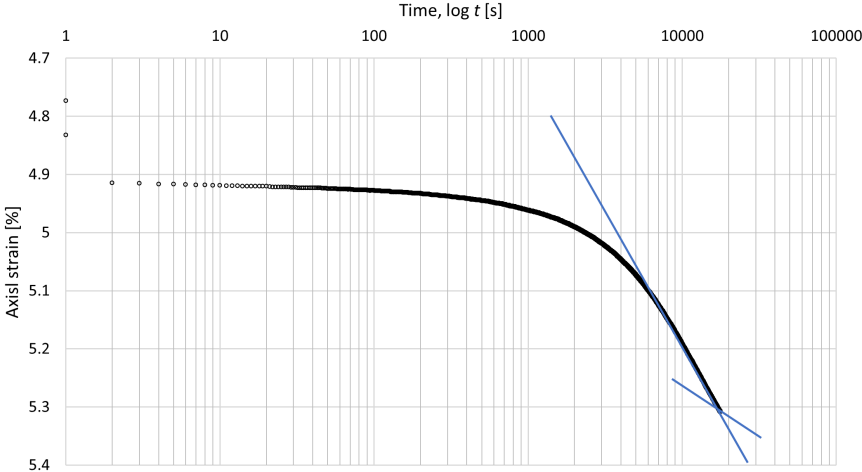


Figure G.60. Load step 22.

G.10 BenderElement03: Curing for 28 days at 20 °C (V_s log)

This test was performed on a gyttja-cement specimen that cured inside the triaxial cell until 28 days.

Test description:

The test was performed using the GDS bender element system using GDS BES v2.2.13 software.

Cement amount:	150 kg/m ³		Before	After
Temp. lab:	19 to 20.5 °C	Water content, w:	85.6 %	67.6 %
Diameter, d:	70 mm	Saturation, S:	-	-
Wavetype:	Sine	Void ratio, e:	-	-
Wave period:	0.2 ms	Height, h ¹⁾ :	63 mm	-
Test date:	18/04/ to 13/05/2022	Unit weight, γ	15.6 kN/m ³	-
			Remoulded²⁾	Cement added²⁾
		Water content, w:	89.4 %	76.3 %

Results:

V_s (7 days):	245.6 m/s
V_s (14 days):	278.2 m/s
V_s (21 days):	305.1 m/s
V_s (28 days):	320.6 m/s

1) Subtracted the transmitter height of 7 mm

2) Water contents when mixing the specimen prior to curing

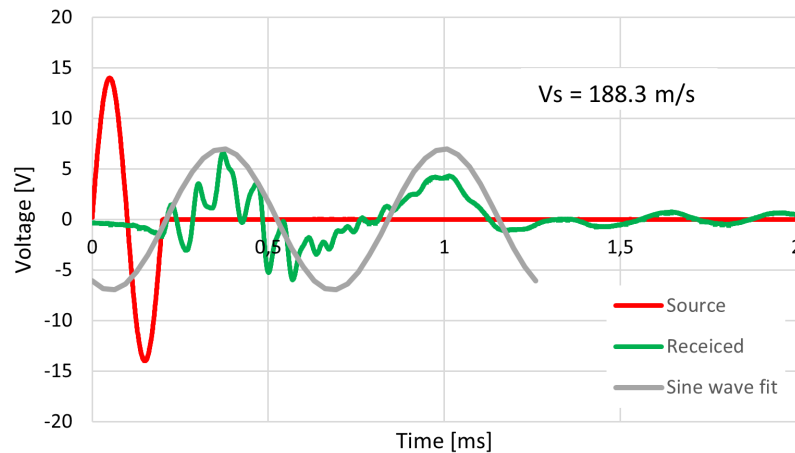


Figure G.61. Day 2.

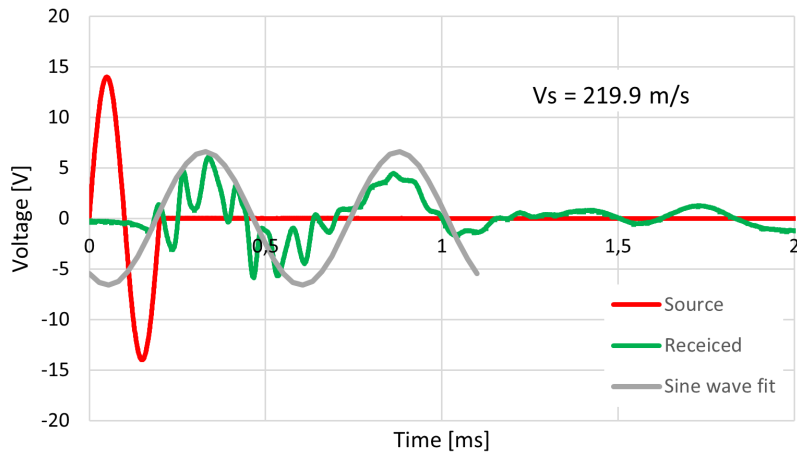


Figure G.62. Day 4.

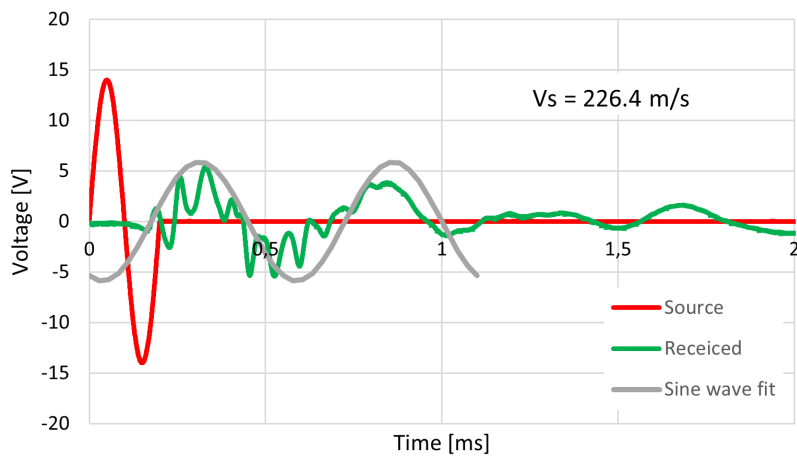


Figure G.63. Day 5.

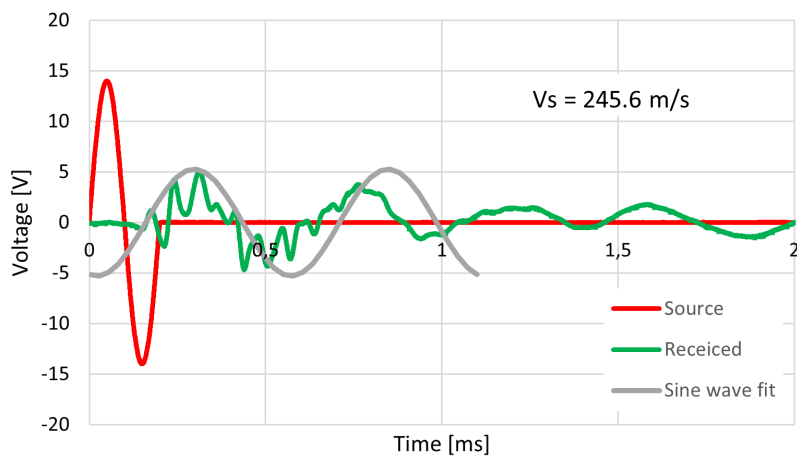


Figure G.64. Day 7.

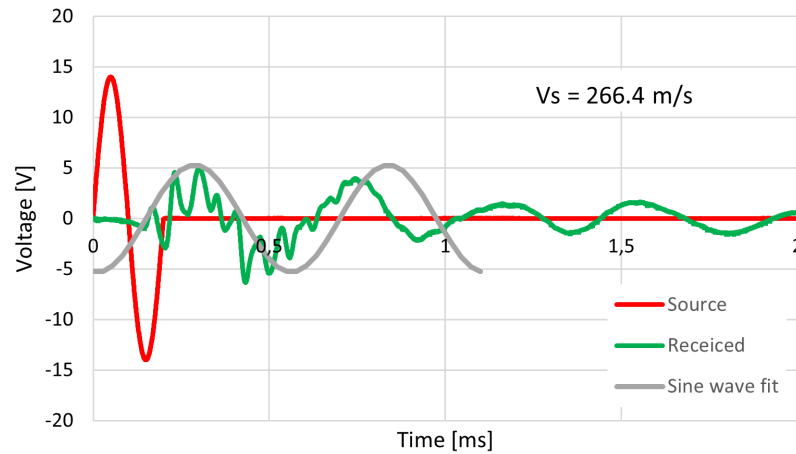


Figure G.65. Day 9.

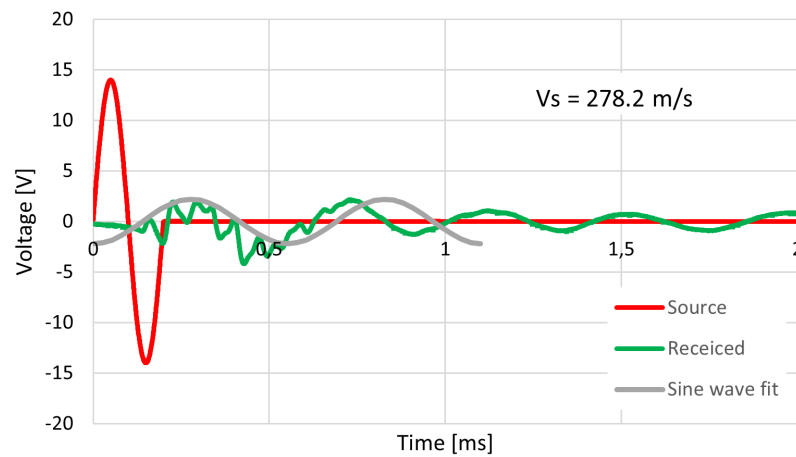


Figure G.66. Day 12.



Figure G.67. Day 14.

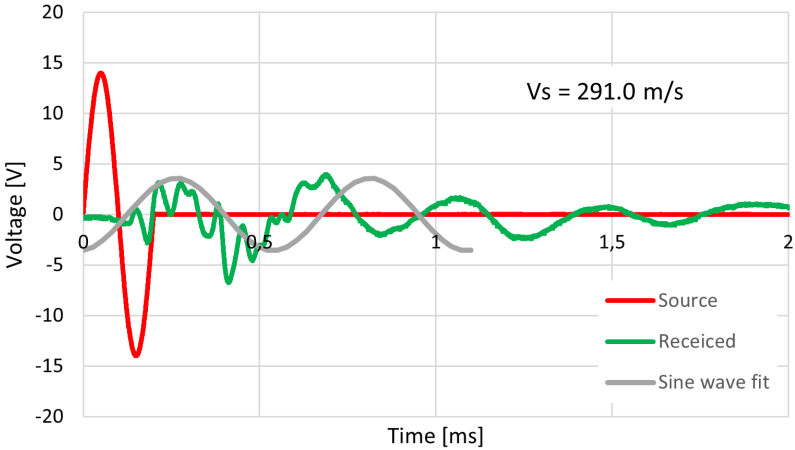


Figure G.68. Day 18.

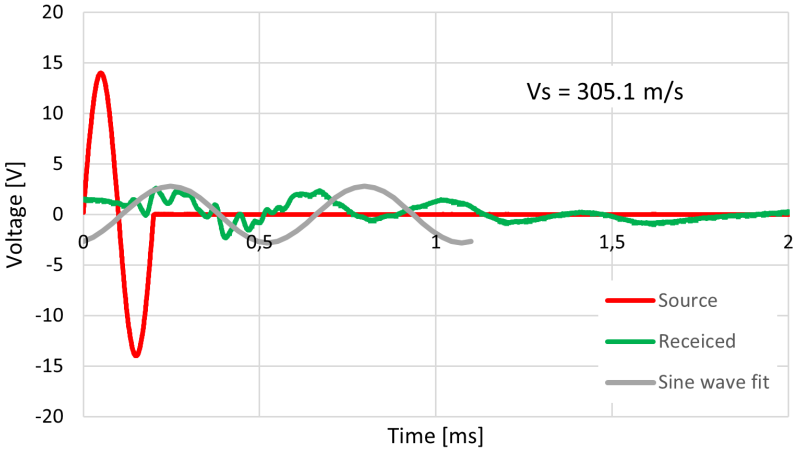


Figure G.69. Day 21.

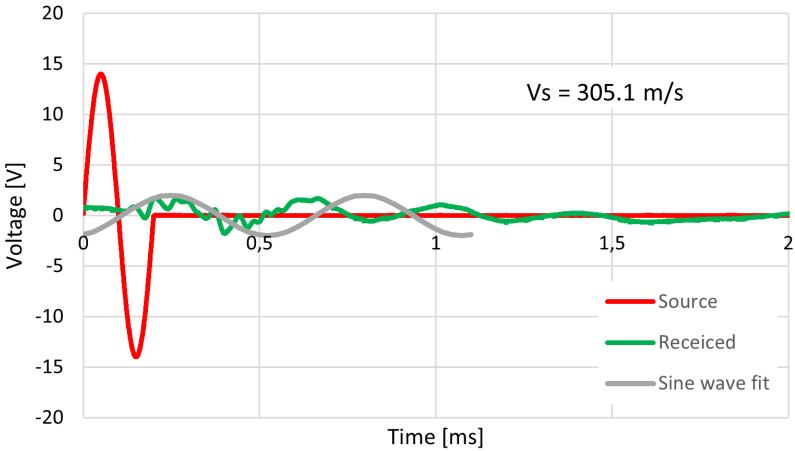


Figure G.70. Day 23.

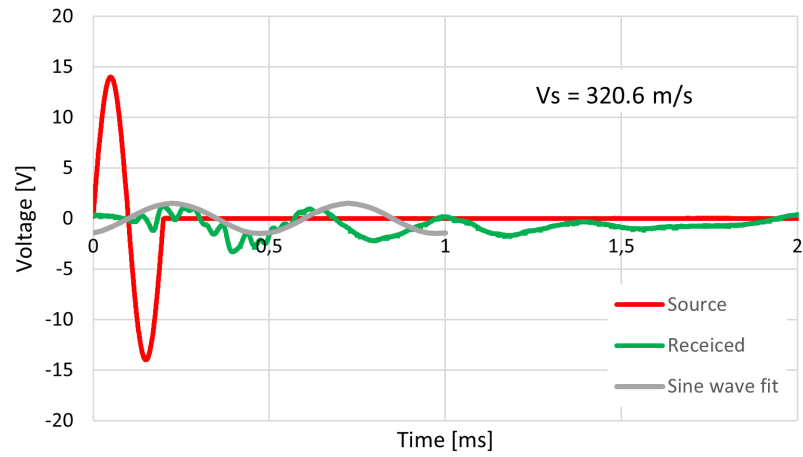


Figure G.71. Day 27.

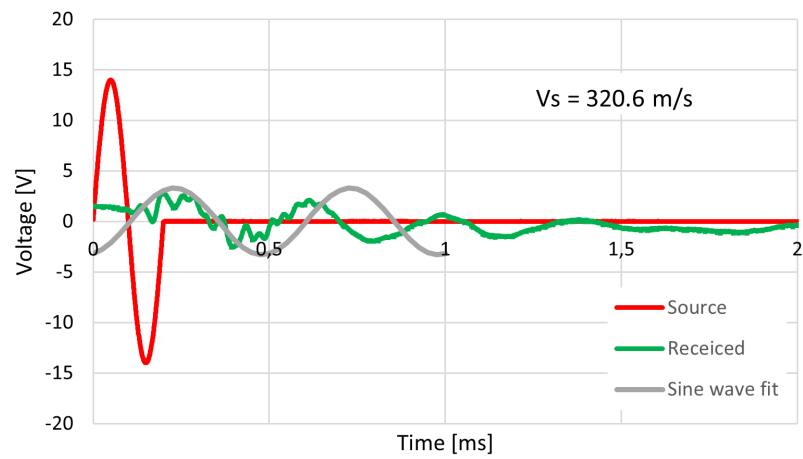


Figure G.72. Day 28.

Bibliography

- Aalborg Portland, 2023a.** Aalborg Portland. *Environmental Product Declaration for Basis cement*. Aalborg Portland, 2023a.
- Aalborg Portland, 2023b.** Aalborg Portland. *FUTURECEM CEMENT*, 2023b. URL <https://www.aalborgportland.dk/produkter/futurecem-cement/>. Accessed: 20-02-2023.
- Aalborg Portland, 2020.** Aalborg Portland. *FutureCem - Ny Miljøvenlig Cement Fra Aalborg Portland*. Aalborg Portland, 2020.
- Aalborg Portland, 2019.** Aalborg Portland. *Environmental Product Declaration for FutureCem cement*. Aalborg Portland, 2019.
- Aalborg Portland, 1999.** Aalborg Portland. *Portlandcementer*. Aalborg Portland, 1999.
- Al-Jabban, 2019.** Wathiq Jasim Al-Jabban. *Soil Modification by Adding Small Amounts of Binder - A Laboratory Study*. Luleå University of Technology, 2019.
- Arkil, 2023.** Arkil. *Cementstabilisering ved Gubsø*, 2023. URL <https://www.arkil.dk/cases/6-miljoeteknik/cementstabilisering-ved-gubsoe>. Accessed: 2023-05-02.
- Aslmand et al., 2022.** Mojtaba Aslmand et al. *Evaluation of Field Shear Wave Velocity in Deep Soil Mixing Based on Laboratory Studies*. Teknik Dergi, 2022.
- Axelsson et al., 2000.** Karin Axelsson et al. *Stabilisering av organisk jord med cement- och puzzolanreaktioner - Förstudie*. Svensk Djupstabilisering, 2000.
- Bentley Systems, 2023.** Bentley Systems. *PLAXIS Material Models CONNECT Edition V20.02*. PLAXIS, 2023.
- Bentley Systems, 2020.** Bentley Systems. *PLAXIS 2D-Reference Manual*. PLAXIS, 2020.
- Boral, 2022.** Boral. *Boral Cement - Lime and Limestone Products EPD*, 2022.
- Budhu, 2021.** Muni Budhu. *Soil Mechanics and Foundations*. Wiley, 2021.

- Building Seismic Safety Council, 1994.** Building Seismic Safety Council. *NEHRP Recommended Provisions For Seismic Regulations For New Buildings*. Federal Emergency Management Agency, 1994.
- Castro et al., 2019.** Rodrigo Castro et al. *How to design buildings with Life Cycle Assessment by accounting for the material flows in refurbishment*. In: IOP Conference Series: Earth and Environmental Science, 2019.
- Centrumpæle, 2021.** Centrumpæle. *EPD for 1 m steel-reinforced concrete pile*. EPD Danmark, 2021.
- Chaiprakaikeow et al., 2017.** Susit Chaiprakaikeow et al. *Development of a Quality Control Index of Cement Stabilized Road Structures Using Shear Wave Velocity*. In: World Congress on Civil, Structural, and Environmental Engineering, 2017.
- COWI, 2011.** COWI. *Forstærkning af slamdepot ved Cementstabilisering*. Miljøstyrelsen, 2011.
- Energi Styrelsen, 2013.** Energi Styrelsen. *DS/EN 1991-1-1 DK NA:2013*. Dansk Standard, 2013.
- GDS Instruments, 2014.** GDS Instruments. *Bender Elements. The GDS Bender Elements System Hardware Handbook for Vertical and Horizontal Elements*. GDS Instruments, 2014.
- GDS Instruments, 2023.** GDS Instruments. *GDS Bender Element System (Website video)*, 2023. URL <https://www.gdsinstruments.com/gds-products/gds-bender-element-system>. Accessed: 08-06-2023.
- GDS Instruments, 2016.** GDS Instruments. *GDSLAB v.2.5.4. The GDS Laboratory User Handbook*. GDS Instruments, 2016.
- GDS Instruments, 2017.** GDS Instruments. *GDSTAS. The GDS Triaxial Automated System Hardware Handbook*. GDS Instruments, 2017.
- Gebretsadik, 2014.** Alex Gezahegn Gebretsadik. *Shear resistance degradation of lime-cement stabilized soil during cyclic loading*. KTH Royal Institute of Technology, 2014.
- Helle et al., 2021.** Tonje Eide Helle et al. *Ny laboratorieprosedyre for innblandingsforsøk av bindemiddelstabilisert leire*. In: Fjellsprengningsteknikk bergmekanikk/geoteknikk, 2021.

- Ibsen et al., 2012.** Lars Bo Ibsen et al. *Manual for Cyclic Triaxial Test*. Aalborg university, 2012.
- Karl Terzaghi and others, 1996.** Karl Terzaghi and others. *Soil Mechanics in Engineering Practice, 3rd Edition*. Wiley, 1996.
- Keller, 2023a.** Keller. *Dry soil mixing*, 2023a. URL <https://www.keller-na.com/expertise/techniques/dry-soil-mixing>. Accessed: 18-02-2023.
- Keller, 2023b.** Keller. *Mass mixing*, 2023b. URL <https://www.keller.com.pl/en/expertise/techniques/mass-mixing>. Accessed: 18-02-2023.
- Keller, 2018.** Keller. *Soil mixing - An efficient and flexible technology to overcome a variety of soil problems*, 2018.
- Koch et al., 2013.** E. Koch et al. *Laboratory tests and numerical modeling for embankment foundation on soft chalky silt using deep-mixing*. In: International Conference on Soil Mechanics and Geotechnical Engineering, 2013.
- Lang et al., 2020.** Lei Lang et al. *Small-strain dynamic properties of silty clay stabilized by cement and fly ash*. In: Construction and Building Materials, 2020.
- Larsen et al., 2019.** Gunnar Larsen et al. *Hvornår er det slut med grus i Danmark?* Aktuel naturvidenskab, 2019.
- Larsson, 2006.** Rolf Larsson. *Djupstabilisering med bindemedelsstabiliserade pelare och masstabilisering - En vägledning*. Swedish Deep Stabilization Research Centre, 2006.
- Mirshekari, 2017.** Morteza Mirshekari. *Cyclic Triaxial Test to Measure Strain-Dependent Shear Modulus for Unsaturated Sand*. In: International Journal of Geomechanics, 2017.
- Norwegian Geotechnical Society, 2012.** Norwegian Geotechnical Society. *Veiledning for grunnforsterkning med kalksementpeler*. Norwegian Geotechnical Society, 2012.
- Pacheco-Torgal et al., 2014.** Fernando Pacheco-Torgal et al. *Handbook of Alkali-Activated Cements, Mortars and Concretes*. Woodhead Publishing, 2014.

- Tanderup, 2022.** Martin Tanderup. *Sustainability of cement stabilization for The Third Limfjords Connection*. Aalborg University, 2022.
- TenCate Geosynthetics, 2012.** TenCate Geosynthetics. *NGS Product Certificate (Miragrid GX 110/30)*. NorGeoSpec, 2012.
- The Danish Road Directorate, 2023.** The Danish Road Directorate. *InfraCLA*, 2023. URL <https://www.vejdirektoratet.dk/infralca>. Accessed: 10-05-2023.
- The Danish Standard Association, 2018.** The Danish Standard Association. *Geotechnical investigation and testing - Laboratory testing of soil - Part 9: Consolidated triaxial compression tests on water saturated soils*. European standard, 2018.
- The European Committee For Standardization, 2012.** The European Committee For Standardization. *Sustainability of construction works - Assessment of environmental performance of buildings - Calculation method (DS/EN 15978)*. Dansk Standard, 2012.
- The European Committee For Standardization, 2017.** The European Committee For Standardization. *Geotechnical investigation and testing - Laboratory testing of soil - Part 5: Incremental loading oedometer test*. European Standard, 2017.
- Torres et al., 2017.** Aurora Torres et al. *A looming tragedy of the sand commons*. In: Science, 2017.
- Trafik, Bygge- og Boligstyrelsen, 2021.** Trafik, Bygge- og Boligstyrelsen. *DS/EN 1997-1 DK NA:2021*. Dansk Standard, 2021.
- United Nations, 2022.** United Nations. *The Sustainable Development Goals Report 2022*. United Nations, 2022.
- United Nations Development Programme, 2023.** United Nations Development Programme. *What are the Sustainable Development Goals?*, 2023. URL <https://www.undp.org/sustainable-development-goals>. Accessed: 10-04-2023.
- Zhu et al., 2008.** Fanya Zhu et al. *Field measurements of shear wave velocities of soils*. In: GeoEdmonton, 2008.

Åhnberg, 2006. Helen Åhnberg. *Strength of stabilised soils - A laboratory study on clays and organic soils stabilised with different types of binder*. Swedish Deep Stabilization Research Centre, 2006.